Lecture note on **Magnetism (1)**

6th April (2022) Shingo Katsumoto, Institute for Solid State Physics, University of Tokyo

Chapter 1
Basic Notions of Magnetism

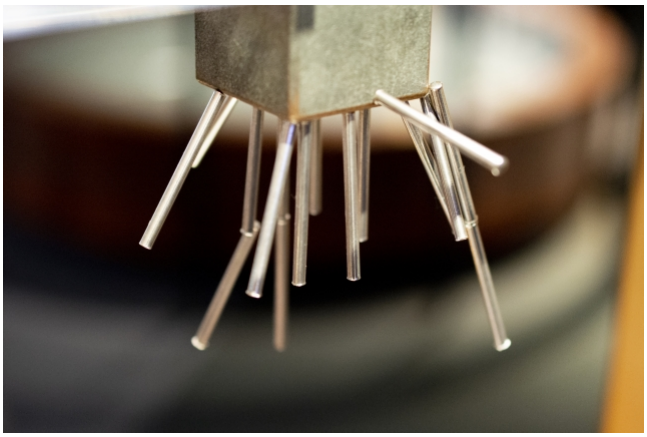

Magnetic fields are well known as "fields" that generate remote (but actually proximity) forces as well as magnetic fields or gravitational fields. Materials respond to magnetic fields on one hand, create magnetic fields on the other. Such properties are called "magnetism." Perhaps the most prominent "magnetism" for us is spontaneous magnetization represented by permanent magnets. On the other hand, every material has some magnetic properties. Then what do we call magnetism? What is the origin of magnetism? We will consider these problems in this half-year lecture. I do not think I can give you sufficient answers though I would like to try to give you some usuful hints to consider the problems.

In this chapter, we will have a short look at very basic notions in magnetism. I may skip some of the contents in the lecture notes in the real lectures due to the time limitations.

1.1 Electromagnetic fields in the vacuum and those with materials

We skip the very elementary electromagnetism, with which all of you are already familiar. First, we consider the magnetic properties of matter phenomenologically.

1.1.1 The Maxwell equaitons and magnetic moment

In classical theory, the electromagnetic field in a vacuum is described by the Maxwell equations

$$\nabla \cdot \boldsymbol{E} = \frac{\rho}{\epsilon_0}, \tag{1.1a}$$

$$\nabla \times \boldsymbol{E} = -\frac{\partial \boldsymbol{B}}{\partial t}, \tag{1.1b}$$

$$\nabla \cdot \boldsymbol{B} = 0, \tag{1.1c}$$

$$\nabla \times \boldsymbol{B} = \mu_0 \left(\boldsymbol{j} + \epsilon_0 \frac{\partial \boldsymbol{E}}{\partial t} \right). \tag{1.1d}$$

We adopt MKSA (SI) unit of system (Appendix 1A). The annotations of symbols may be skipped, but for confirmation, $\boldsymbol{B}$ is the magnetic flux density with unit of [T] (Tesla) in SI. The unit [T] is the same as [Wb/m^2], where we consider the number of magnetic flux [Wb] (Weber). The unit of magnetic field intensity is [A/m], and we usually use symbol $\boldsymbol{H}$ the quantity measured in this unit. In the vacuum, they are in a linear relation $\boldsymbol{B} = \mu_0 \boldsymbol{H}$ with the coefficient μ_0 (permeability of vacuum). Because μ_0 μ_0 has a physical dimension in MKSA unit system, thus $\boldsymbol{B}$ is a different quantity from $\boldsymbol{H}$ to be strict. However $\mu_0 = 4\pi \times 10^{-7}$ [H/m] is a universal scalar and we often call $\boldsymbol{B}$ as "magnetic field", as well as $\boldsymbol{H}$ in the vacuum. In materials, the situation changes.

In eq. (1.1c), $\boldsymbol{E}$ and $\boldsymbol{B}$ are not symmetrical even after tunings of coefficients. The origin is ρ (charge density) in the rhs of eq. (1.1a), and $\boldsymbol{j}$ (current density) in the rhs of eq. (1.1d). These come from the fact that the electric monopole exsits. Though the possibility of the existence of magnetic monopole is not completely eliminated, there has been no convincing report on the finding of magnetic monopole. At present, as in eqs. (1.1), we do not consider the existence of magnetic monopole. In eqs. (1.1), hence, magnetic fields are created by electric currents and time-derivatives of electric field as in eq. (1.1d). However, as we see later, electrons and some of nuclei have spin angular monments and associated magnetic dipole moments. These produce dipole magnetic fields around them.

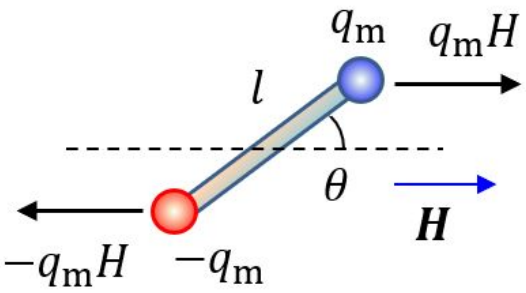

Fig. 1.1 Pair of force moment on a magnetic dipole in a magnetic field.

The concept of dipole magnetic field can be introduced as the shrinkage limit of a circular current(1B.2). On the other hand, in correspondence with the electric dipole, introduction of fictitious magnetic charges which always appear as a pair with the same amplitude and the opposite sign, and the limit of shrinkage under the condition of keeping the product (magnetic charge)×(distance) constant. Then let us define magnetic moment as follows. We use [Wb] (weber) as the unit of "magnetic charge" in MKSA system in parallel with the unit of electric charge ([C]) = that of electric flux due to the Gauss theorem. We consider a magnetic dipole (before taking the shrinkage limit), which has magnetic charges $\pm q_\mathrm{m}$ with distance l. Let the dipole be placed in a uniform magnetic field H and has an angle θ to the field (Fig. 1.1). The magnetic charges get the force $q_\mathrm{m}H$ from the field and the dipole get the pair of force

$$L = -q_\mathrm{m} l H \sin\theta = -(q_\mathrm{m} l/\mu_0) B \sin\theta. \tag{1.2}$$

The quantities that depend q_m and l only in the form of their product $q_\mathrm{m} l$, do not change with taking the limit. Hence we write

$$\mu \equiv q_\mathrm{m} l/\mu_0, \tag{1.3}$$

and call μ **magentic moment**.

Because the couple coment in eq. (1.2) drives a rotation of the magnetic moment to the direction of $\theta = 0$, it can be expressed by a static magnetic potential ϕ_m as follows.

$$\phi_\mathrm{m} = -\mu B \cos\theta. \tag{1.4}$$

By generalizing the above to a vector representation, we get

$$\boldsymbol{L} = \boldsymbol{\mu} \times \boldsymbol{B}, \quad \phi_\mathrm{m} = -\boldsymbol{\mu} \cdot \boldsymbol{B}. \tag{1.5}$$

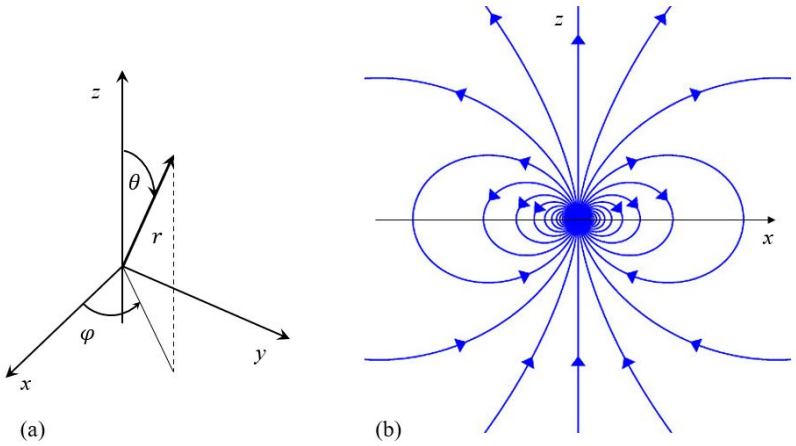

Fig. 1.2 (a) Schematic view of polar coordinate (r, θ, φ). (b) Schematic diagram of magnetic power force lines from magnetic dipole.

1.1.2 Dipole interaction

Let a magnetic moment along z-axis be at the origin. We use the polar coordinate (r, θ, φ) in Fig. 1.2(a).

From the spherical fields that the magnetic charges create, it is easy to see that the magnetic field has no component along φ. It is well known that the magnetic flux density (B_r, B_θ) along (r, θ) are

$$\left.\begin{aligned} B_r &= \frac{|\boldsymbol{\mu}|}{4\pi\mu_0}\frac{2\cos\theta}{r^3}, \\ B_\theta &= \frac{|\boldsymbol{\mu}|}{4\pi\mu_0}\frac{\sin\theta}{r^3}. \end{aligned}\right\} \tag{1.6}$$

We see they are inverse proportional to the cube of distance. The derivation can be fined in Appendix 1B1. We can draw the magnetic force line by connecting tangent lines of magnetic field vectors and obtain, e.g., that in Fig. 1.2(b)[*1] .

Next we consider two such magnetic moments $\boldsymbol{\mu}_1$, $\boldsymbol{\mu}_2$. As in Fig. 1.3, the vector going from $\boldsymbol{\mu}_1$ to $\boldsymbol{\mu}_2$ is written as $\boldsymbol{r}$. $\boldsymbol{\mu}_1$ and $\boldsymbol{\mu}_2$ form the potential in eq. (1.4) in the magnetic fields of eq. (1.6). Then the total potential of the two magnetic moments is

$$U = \frac{1}{4\pi\mu_0 r^3}\left\{\boldsymbol{\mu}_1\cdot\boldsymbol{\mu}_2 - \frac{3}{r^2}(\boldsymbol{\mu}_1\cdot\boldsymbol{r})(\boldsymbol{\mu}_2\cdot\boldsymbol{r})\right\}. \tag{1.7}$$

The derivation is given in Appendix 1B2. The interaction between the moments expressed by eq. (1.7) is called **dipole-dipole interation**. In the potential of eq. (1.7), the stable configuration can be obtained by maximizing the amplitude of the second term because the sign is minus and the coefficient is larger than the first one. $|r|$ is canceled by the denominator

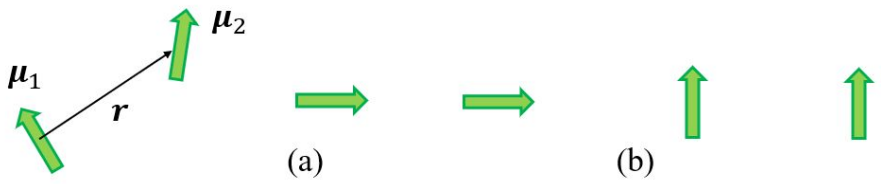

Fig. 1.3 Classical interaction of two magnetic dipoles. (a) Stable configuration. (b) Unstable configuration.

[*1] In this figure, it is not taken into consideration that the magnetic field line density is proportional to the magnetic field.

and the numerator, hence the stable configuration is obtained as in Fig. 1.3(a). On the ohter hand the configuration in Fig. 1.3(b) has a higher energy and is unstable. The effect of classical dipole-dipole interaction is generally much smaller than the quantum mechanical exchange interaction. However, in some characteristic phenomena, it plays important roles.

A more fundamental problem of multiple magnetic moments is how we can view a set of magnetic moments from a far distance. The problem of taking a limt of moment-moment approach with a constant moment-distance product, is the problem of **multipole**. However, simply looking from a distance, the problem is the same as that a set of various charges from a distance can be treated as a point charge with the sum of the charges. This from the linearity of the Maxwell equations. Then let $\{\boldsymbol{\mu}_0, \boldsymbol{\mu}_1, \cdots\}$ be the magnetic moments under consideration and we see the set as a moment which is the sum

$$\boldsymbol{\mu} = \sum_i \boldsymbol{\mu}_i. \tag{1.8}$$

1.1.3 Magnetization of materials

Generally a magnetic field induces a magnetic moment in materials. This phenomenon is called magnetization of a material. Assuming a uniform distribution of induced magnetic moments, the moment per unit volume is called **magnetization** or **magnetic polarization**. Now, we write the magnetization as $\boldsymbol{M}$. Then from definition (1.3), we express the induced magnetic moment as the sum of equal descrete moment $\boldsymbol{\mu} = q_{\mathrm{m}}\boldsymbol{l}/\mu_0$ of concentration N (per unit cell) as

$$\boldsymbol{M} = \sum_{\text{unitvol.}} \boldsymbol{\mu} = Nq_{\mathrm{m}}\boldsymbol{l}/\mu_0 \equiv \rho\boldsymbol{l}/\mu_0. \tag{1.9}$$

Here, $\rho \equiv Nq_{\mathrm{m}}$ is like a density of magnetic charges. In the naive model described in Fig. 1.4, small bar magnets with length $l = |\boldsymbol{l}|$ are aligned. The magnetic charges of neighboring magnets cancel each other due to the zero distance and no magnetic charge exists inside the material naturally. The magnetic charges then appear just at the ends of the material.

When the end surfaces are taken perpendicular to the magnetic polarization, the surface magnetic charge density is q_{m} times s, the areal density of "rods" which are the serieses of bar magnets. We consider a slab with unit area and height l, which should contain just one moment along the height, then the total number inside should be s. On the other hand from the definition the number should be Nl, which means $s = Nl$. Therefore the areal density of magnetic charge σ at the ends is given by

$$\sigma = q_{\mathrm{m}}s = q_{\mathrm{m}}Nl = \mu_0|\boldsymbol{M}|, \tag{1.10}$$

that is, the magnetic polarization is the same as the areal density of magnetic charges.

As considered above, the magnetic moment induced in the material (there is also spontaneous magnetization that occurs without an external magnetic field), that is, the magnetization generates a magnetic field around the material. The field is in a far distance, that of the magnetic moment of $LS|\boldsymbol{I}| = V|\boldsymbol{M}|$, where S is the area of ends of the material, L is the length. Thereofre, measurement of outer magnetic field originated from the material can give $\boldsymbol{M}$. In the discussion

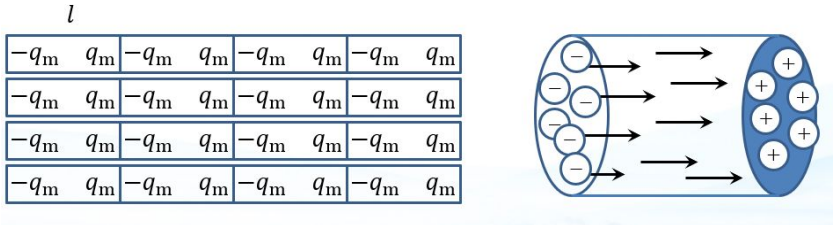

Fig. 1.4 A naive model of magnetization of a material which is composed of many small magnets with length l and magnetic charges $\pm q_{\mathrm{m}}$.

of magnetism, i.e., magnetic properties of materials, (apart from how far the above simple model can be used) what we should consider in the first place is **how magnetic moments are induced in the material ?**

1.1.4 Electromagnetic field in the presence of materials

Since the magnetic moment is expressed as a circular current, the effect of the magnetic moment in a substance can also be expressed as a current. As illustrated in Fig. 1.5, we take the coordinate $\boldsymbol{r}'$ inside the material and sum up the effect of local moments to give

$$\begin{aligned}\boldsymbol{A} &= \frac{\mu_0}{4\pi}\int_{\text{mat}} dv' \frac{\boldsymbol{M}'\times\boldsymbol{r}}{r^3} = -\frac{\mu_0}{4\pi}\int_{\text{mat}} dv' \left(\boldsymbol{M}'\times\nabla\frac{1}{r}\right) \\ &= \frac{\mu_0}{4\pi}\int_{\text{mat}} dv' \left(\boldsymbol{M}'\times\nabla'\frac{1}{r}\right). \end{aligned} \tag{1.11}$$

Here the integration volume is taken inside the material. The symbols with prime as $\boldsymbol{M}'$ means they are expressed as a function of the coordinate (x', y', z'). Further partial integration gives

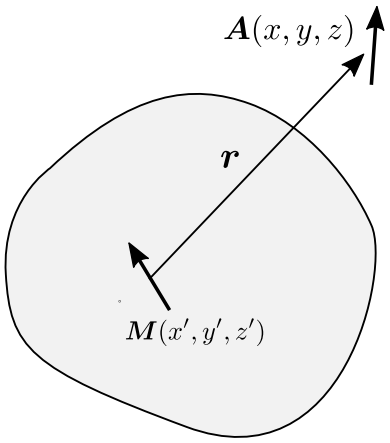

Fig. 1.5 Illustration of vector potential formed by magnetic moments inside a material

$$\boldsymbol{A} = \frac{\mu_0}{4\pi}\int_{\text{mat}} dv' \frac{\nabla'\times\boldsymbol{M}'}{r}. \tag{1.12}$$

Then if we write

$$\boldsymbol{j_M} \equiv \nabla\times\boldsymbol{M}, \tag{1.13}$$

from $\nabla\cdot\boldsymbol{j_M} = 0$, we can view $\boldsymbol{j_M}$ as a kind of electric current.

We add the true current of real charge $\boldsymbol{j}$ to the above "equivalent current" to obtain the vector potentioal as

$$\boldsymbol{A} = \frac{\mu_0}{4\pi}\int dv' \frac{\boldsymbol{j}' + \boldsymbol{j}'_{\boldsymbol{M}}}{r}. \tag{1.14}$$

Then if we write

$$\boldsymbol{B} = \nabla\times\boldsymbol{A} = \frac{\mu_0}{4\pi}\int dv' \frac{(\boldsymbol{j}' + \boldsymbol{j}'_{\boldsymbol{M}})\times\boldsymbol{r}}{r^3}, \tag{1.15}$$

we obtain the relation

$$\nabla\times\boldsymbol{B} = \mu_0(\boldsymbol{j} + \boldsymbol{j_M}) = \mu_0\boldsymbol{j} + \mu_0\nabla\times\boldsymbol{M}. \tag{1.16}$$

Defining magnetic field as

$$\boldsymbol{H} \equiv \boldsymbol{B}/\mu_0 - \boldsymbol{M}, \tag{1.17}$$

we find

$$\nabla\times\boldsymbol{H} = \boldsymbol{j}, \tag{1.18}$$

namely $\boldsymbol{H}$ does not depend on the equivalent current of magnetic moment.

Now we consider the electromagnetic field in the presence of a material. Electric flux density $\boldsymbol{D}$, and magnetic flux density $\boldsymbol{B}$ is given by

$$\boldsymbol{D} = \epsilon_0\boldsymbol{E} + \boldsymbol{P} \tag{1.19a}$$

$$\boldsymbol{B} = \mu_0(\boldsymbol{H} + \boldsymbol{M}), \tag{1.19b}$$

where $\boldsymbol{P}$ is electric polarization. In the case of electric charge, true charge ρ_{t} exists other than the polarization charge ρ_{p}. From $\rho_{\text{p}} = -\nabla\cdot\boldsymbol{P}$ we can write

$$\nabla\cdot\boldsymbol{D} = \rho_{\text{t}}, \tag{1.20}$$

which means the effect of polarization in taken into $\boldsymbol{D}$. Further, if we express $\nabla\times\boldsymbol{H}$ with $\boldsymbol{D}$, we obtain the formula

$$\nabla\times\boldsymbol{H} = \boldsymbol{j} + \frac{\partial\boldsymbol{D}}{\partial t}, \tag{1.21}$$

which is in the same form as (1.1d) and the effect of magnetization is included into $\boldsymbol{H}$.

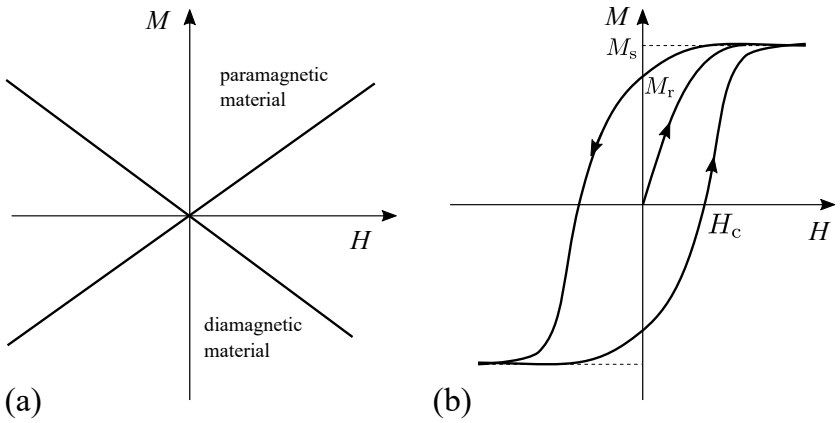

Fig. 1.6 (a) Schematic diagrams of M-H curves in paramagnetic ad diamagnetic materials. (b) Schematic diagram of M-H curve in ferromagnetic material. H_c: coercive force, M_r: remanent magnetization, M_s: saturation magnetization.

1.1.5 M(B)-H curve

As above, the response of materials to magnetc field $\boldsymbol{H}$ appears as magnetization $\boldsymbol{M}$. When $\boldsymbol{M}$ is proportional to $\boldsymbol{H}$, we write

$$\boldsymbol{M} = \chi \boldsymbol{H}, \tag{1.22}$$

where the coefficient χ is called **magnetic susceptibility**. Then we write

$$\boldsymbol{B} = (\chi + \mu_0)\boldsymbol{H} \equiv \mu^* \boldsymbol{H}, \tag{1.23}$$

and call $\mu^* \equiv \chi + \mu_0$ **magnetic permeability**. $\bar{\mu} \equiv \mu^*/\mu_0 = \bar{\chi} + 1 = \chi/\mu_0 + 1$ is called **relative permiability**.

Among such materials with linear response, we call **paramagnetic** material for those with $\chi > 0$ and **diamagnetic** material for those with $\chi < 0$. And there are many materials such as **ferromagnetic** materials in which the linear relation in eq. (1.22) does not hold. These materials are very important particularly in the field of magnetics – field of application. In such cases, behavior of magnetization is often presented in the form of **M-H curve**, in which magnetization M is plotted versus H. Figure 1.6 shows a schematic of M-H curve. In the case of linear response in eq. (1.22), the M-H curve should be linear as shown in Fig. 1.6(a). On the other hand, Fig. 1.6(b) shows a schematic of ferromagnetic response. With up-down sweeps of H, the response of M is strongly non-linear, and different behavior is observed for the direction of the sweeps, which phenomenon is called **hysteresis**. B-H curves are also adopted for giving the same information.

1.2 Measurement of magnetization

Here we introduce some of experimental methods for the measurement of magnetization before going into the theories. Also we touch on the problem of demagnetizing field, which is important for measurement.

1.2.1 Methods of magnetization measurement

Below we list some representative methods. There are two major ways for the measurement: (a) Measurement of magnetic field caused by magnetization; (b) Variation in magnetization is detected as voltage caused by electromagnetic induction. Examples of (a) are, vibrating sample magnetometer (VSM), superconducting quantum interference device (SQUID) magnetometer. An example of (b) is a pick-up coil type magnetometer.

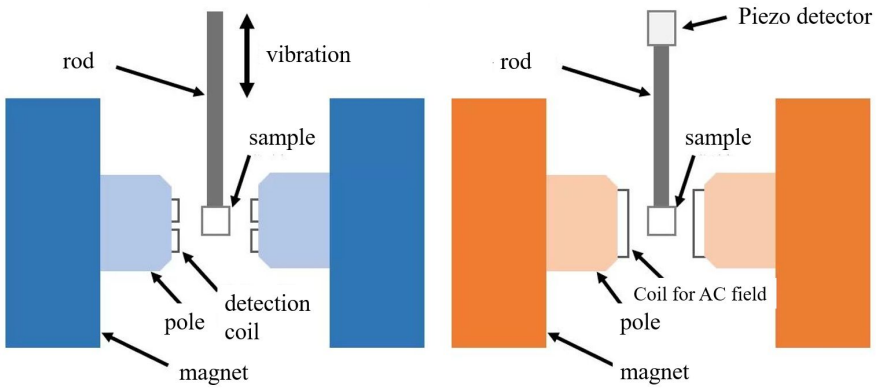

(a) (b)

Fig. 1.7 (a) Principle of magnetization measurement in VSM. (b) Principle of magnetization measurement in AGM. From https://www.toyo.co.jp/material/casestudy/detail/id=7003

(a1) **Vibrating sample magnetometer**: Figure 1.7(a) shows the principle of magnetization measurement by VSM. When a magnetized substance is spatially vibrated, the magnetic field generated by the magnetization is not spatially uniform, so it vibrates with time when viewed at a fixed point in space. Then in a detection coil placed at the point the vibrating field procuces an alternating voltage though electromagnetic induction. In VSM the ditection of the AC voltage gives measurement of magnetization.

In actual use of VSM, as annotated in the figure, the sample, in addition to the vibration, moves slowly through two inversely-wound detection coils to produce a signal peak and dip, which are mirrored to each other. With this devicing, the signal offset can be eliminated.

(a2) **Alternating-gradient magnetometer**: AGM[1] utilizes the fact that a magnetic moment gets force in magnetic field gradient. As shown in Fig. 1.7(b), alternative current in coils attached to an external magnet provide a vibration in field gradient. Then the vibration in the force on the suspender is detected to give the magnetization. Force detection has become extremely sensitive by the method using a laser and a cantilever, which is familiar with atomic force microscopes (AFM) (the piezo element is used in the figure), so extremely high sensitivity can be obtained.

(a3) **SQUID magnetometer**: Magnetic flux piercing a superconducting ring is quantized by the unit of quantum flux $\Phi_0 \equiv h/2e \approx 2.07 \times 10^{-15}$ Wb. A superconducting quantum interference device (SQUID) is a superconducting ring

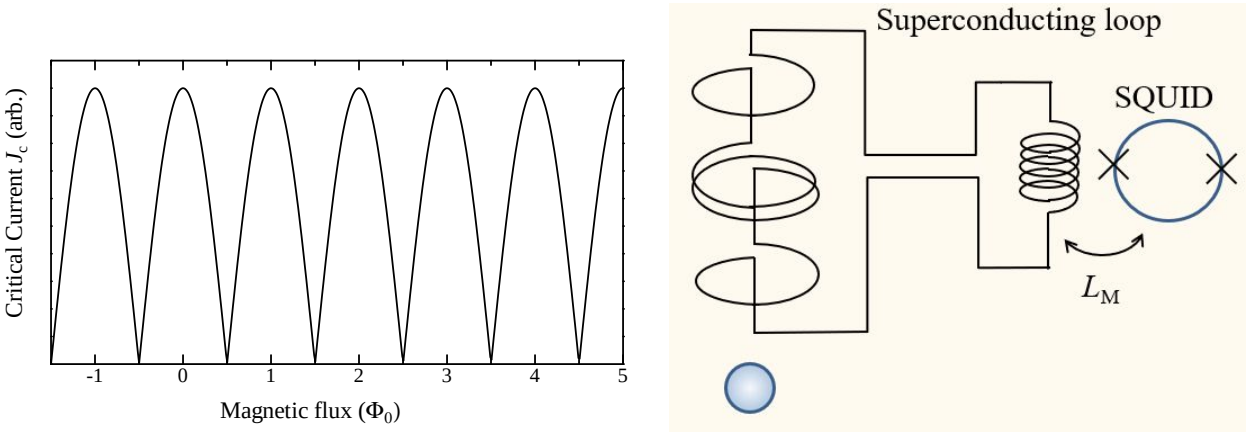

(a) (b)

Fig. 1.8 (a) Schematic diagram of critical current in a SQUID device as a function of magnetic field. (b) Superconducting circuit diagram of a SQUID magnetometer.

with some (in the case of dc-SQUID, two) weak links. The superconducting critical current J_c through it largely oscillates with magnetic flux with the period of Φ_0 as illustrated in Fig. 1.8(a). The unit Φ_0 itself is already very small and the output of a SQUID is strongly non-linear as shown in Fig. 1.8(a), which fact enables us to measure orders of smaller change in the magnetic flux.

Because SQUID sensors should be placed in weak magnetic fields, a closed loop of superconductor is used as shown in Fig. 1.8(b). One end of the loop is magnetically coupled to a SQUID sensor through a coil. As in VSMs, a specimen moves in counter-wound superconducting coil (in the figure the winding is $-++-$), which form the closed loop. The function fitting to the lineshape gives precise value of magnetization. To get high S/N, the specimen should be suspended by a uniform substance with small magnetic susceptibility. The upper limit of the field is determined by superconducting critical field of the pick-up coil. Because the SQUID magnetometers have very high sensitivity, they are applied for measurement of environmental magnetic field or magnetic field leakage from brains (magnetoencephalograph).

(a4) **NV center magnetometer**: Lattice defects formed as complex of a nitrogen (N) impurity and a vacancy (V) in diamonds have quantum states in the bandgap. Combination of optical excitation/detection and electron spin resonance with microwave provides highly sensitive detection of very local magnetic field. S/N can be highly enhanced by, e.g., combination of spin-rotation pulse sequences. In some cases, the sensitivity is as high as the replacement of SQUID magnetometers.

(b1) **Pick-up coil method**: It is used that the response of the coil changes depending on the magnetic permeability inside the coil. A specimen is inserted into a coil. When an AC magnetic field is appled, a voltage is induced on the coil due to the flux variation. Integration of the signal gives the variation of magnetic flux and thus the magnetization.

1.2.2 Effect of demagnetizing field

One thing to note when measuring magnetization is the effect of demagnetizing field. This appears as shape dependence, especially when measuring the magnetization of ferromagnets. In the magnetic charge model, when a material with a finite size is placed in a magnetic field and magnetized, magnetic charges (magnetic poles) appear at both ends of the sample, which creates a magnetic field inside the sample in the opposite direction to the external field. This is the **demagnetizing field** (Fig. 1.9(a)). The demagnetizing field H_d is proportional to the magnetization M as

$$H_d = N\frac{M}{\mu_0}, \tag{1.24}$$

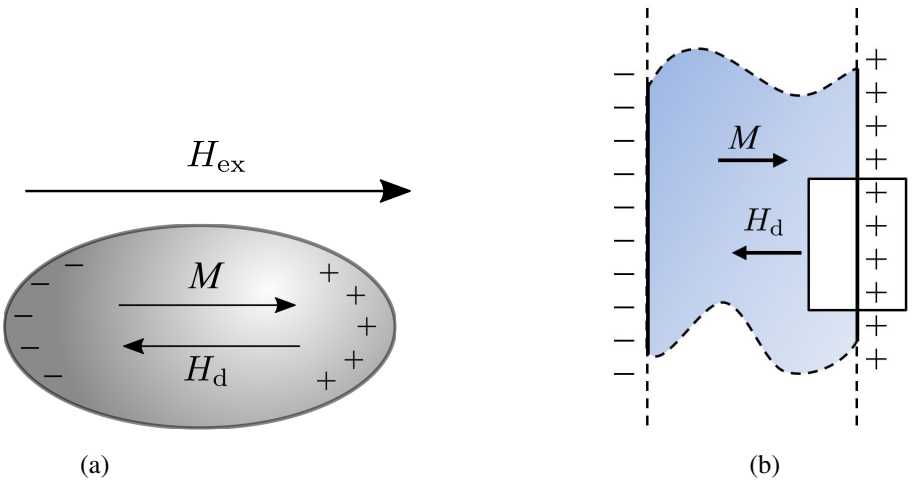

Fig. 1.9 (a) Conceptual diagram of demagnetic field. (b) Calculation of demagnetic field coefficient of plate-shaped sample.

where N is called **demagnetizing factor**. The demagnetizing factor depends on the shape of specimen. For needle-like thin specimen, it is almost zero while large for thick and short ones.

As the simplest case, we consider the case of plate-like sample in Fig. 1.9(b). For magnetization M, the areal densities of surface magnetic charge is $\pm M$. From the symmetry, the magnetic force lines are perpendicular to the plane. Applying the Gauss theorem to a cylinder containing both front and back of the plate, we know that no magnetic flux comes out because the total magnetic charge in the cylinder is zero. Here we again apply the Gauss theorem to another cylinder which contains just one of the surface with a bottom of unit area to obtain

$$\int_{\text{surface}} H_{\text{n}} ds = H_{\text{d}} = \frac{M}{\mu_0},$$

which gives the demagnetizing factor $N = 1$. Demagnetizing factors for various shapes have been calculated.

When there is large demagnetizing field, e.g., hysteretic M-H curve as in Fig. 1.6(b) is largely distorted. The following example is introduced in ref. [2]. Permalloy (an alloy of Fe and Ni, symbol Py) has a very small coercive force 2 A/m ($\approx$ 0.025 Oe), and under usual condition, the magnetization saturates at very small external fields. However, if we make a sphere with Py, becase the saturation field of Py is about 9.23×10^5 A/m and the demagnetizing factor of sphere is 1/3, the demagnetizing field amounts to 3.08×10^5 A/m (=3860 Oe). That is, saturation magnetization cannot be obtained unless a magnetic field of about 100,000 times that without a demagnetizing field is applied. Normally, when submitting data as an M-H curve to a scientific paper, etc., it is necessary to correct the demagnetizing field or to state that it has not been corrected.

1.3 Classical theory of magnetization

Let us go into the physical mechanism of magnetic properties. Though magnetism still has many unsolved problems the present understandings have been obtained with quantum mechanics. Within the classical theory, even elementary understanding is difficult. We see that in this section. Here we refer to "classical theory" that inside materials exists a group of electrons which are classical particles with charge $-e$ and mass m. And they create the equivalent current (1.13).

1.3.1 Classical treatment of paramagnetic moment

Before digging into how to deal with magnetism in classical mechanics and statistics, let us assume that there is already a magnetic moment in matter that has a degree of freedom to change direction, and see the consequence. Matter is composed of atoms, and we will consider a model in which the electrons around the nucleus originally have a magnetic moment due to orbital motion.

Let us consider a set of molecules in a magnetic field along z-axis with flux density $\boldsymbol{B}$. Each molecule has independent magnetic moment μ. The magnetic energy of a moment is $U = -\boldsymbol{\mu}\cdot\boldsymbol{B} = -\mu B\cos\theta$. In classical statistics, the average of z-component in the moment over the is given by

$$\begin{aligned}
\langle \mu_z | \mu_z \rangle &= \int \exp\left(-\frac{U}{k_{\text{B}}T}\right)\mu_z d\Omega \Big/ \int \exp\left(-\frac{U}{k_{\text{B}}T}\right) d\Omega \\
&= \int \exp\left(\frac{\mu B\cos\theta}{k_{\text{B}}T}\right)\mu\cos\theta d\Omega \Big/ \int \exp\left(\frac{\mu B\cos\theta}{k_{\text{B}}T}\right) d\Omega \\
&= k_{\text{B}}T\frac{\partial}{\partial B}\log\left[2\pi\int_0^\pi \exp\left(\frac{\mu B\cos\theta}{k_{\text{B}}T}\right)\sin\theta d\theta\right] \\
&= \mu\left[\coth\left(\frac{\mu B}{k_{\text{B}}T}\right) - \frac{k_{\text{B}}T}{\mu B}\right],
\end{aligned} \tag{1.25}$$

where Ω is the solid angle. In high temperature approximation $\mu B \ll k_{\mathrm{B}}T$, the average is

$$\frac{\langle \mu_z | \mu_z \rangle}{B} \sim \frac{\mu^2}{3k_{\mathrm{B}}} \frac{1}{T}. \tag{1.26}$$

This indicates **Curie law**, that is the magnetic susceptibility is inversely proportional to temperature.

1.3.2 Classical theory of diamagnetism

We consider an electron moving along a circle with radius r in xy plane. We write the circle as Γ and the area as S, and write down the integral form of the Maxwell equation (1.1b) as

$$\oint_{\Gamma} \boldsymbol{E} \cdot d\boldsymbol{l} = -\frac{\partial}{\partial t} \int_{\mathrm{S}} \boldsymbol{B} \cdot d\boldsymbol{\sigma}. \tag{1.27}$$

From this, the induced electromotive force for variation of magnetic flux B is given as

$$2\pi r E = -\frac{\partial}{\partial t}\left(B\pi r^2\right) \quad \therefore E = -\frac{r}{2}\frac{dB}{dt}. \tag{1.28}$$

The electron is accelerated by $-eE$ to the tangential direction and the time derivative of angular momentum L is

$$\frac{dL}{dt} = r \times (-eE) = e\frac{r^2}{2}\frac{dB}{dt}. \tag{1.29}$$

Then the shift $0 \to B$ creates the angular momentum $L = e\frac{r^2}{2}B$. The velocity of electron also increases from 0 to v then $v = L/mr$. As describe in Appendix 1B.2, the magnetic moment of this circular current is (the area of circle)$\times$(crrent). Then it is

$$\mu = SJ = \pi r^2 \frac{ev}{2\pi r} = \pi r^2 \frac{L}{mr}\frac{e}{\pi r} = \frac{e}{2m} e \frac{r^2}{2} B. \tag{1.30}$$

If we replace r, the distance between nucleous and electron, with the average $\left\langle x^2 + y^2 \middle| x^2 + y^2 \right\rangle_{\mathrm{av}}$,

$$\mu = -\frac{e^2}{4m} \left\langle x^2 + y^2 \middle| x^2 + y^2 \right\rangle_{\mathrm{av}} B. \tag{1.31}$$

1.3.3 Breakdown of classical theory of magnetism

In the above, seemingly reasonable results have been obtained even within classical mechanics. However, below, we see the theory is actually broken down in a simple discussion. We introduce electromagnetic field to simple single-particle hamiltonian $\mathcal{H} = \boldsymbol{p}^2/2m$ by changing energy $\mathcal{E}$ and momentu $\boldsymbol{p}$ as

$$\mathcal{E} \to \mathcal{E} + e\phi, \quad \boldsymbol{p} \to \boldsymbol{p} + e\boldsymbol{A}. \tag{1.32}$$

That is the hamiltonian is written as

$$\mathcal{H} = \frac{1}{2m}(\boldsymbol{p} + e\boldsymbol{A})^2 - e\phi. \tag{1.33}$$

This way of introduction is justified by the derivation of canonical equation

$$m\frac{d\boldsymbol{v}}{dt} = -e[\boldsymbol{E} + \boldsymbol{v} \times \boldsymbol{B}],$$

which reproduces the Lorentz force.

We take symmetric gauge $\boldsymbol{A} = (\boldsymbol{B} \times \boldsymbol{r})/2$. Then (1.33) is calculated as follows.

$$\mathcal{H} = \frac{\boldsymbol{p}^2}{2m} + \frac{e}{2m}(\boldsymbol{r} \times \boldsymbol{p}) \cdot \boldsymbol{B} + \frac{e^2}{8m}(\boldsymbol{B} \times \boldsymbol{r})^2. \tag{1.34}$$

From this, the magnetic dipole moment $\mu_{\rm m}$ originates from the motion of electrom is calculated as

$$\mu_{\rm m} = -\frac{\partial \mathcal{H}}{\partial B} = -\frac{e}{2m}(\boldsymbol{r}\times\boldsymbol{p}) - \frac{e^2}{4m}(\boldsymbol{r}\times(\boldsymbol{B}\times\boldsymbol{r})). \tag{1.35}$$

Here, the first term in rhs is called **paramagnetic term**, which is proportional to the angular momentum $\boldsymbol{r}\times\boldsymbol{p}$. On the other hand, the second term is proportional to magnetic flux density $|\boldsymbol{B}|$, which indicates that the inductive electric field accelerates the electron and that this comes form the eddy current-like motion to cancel the external field. Hence this is called **diamagnetic term**.

Let us move on to an N-particle electron system. The hamiltonian is written with writing electron-electron interaction as V as

$$\mathcal{H}_N = \sum_{n=1}^{N}\left[\frac{1}{2m}\left(\boldsymbol{p}_n + e\boldsymbol{A}(\boldsymbol{r}_n)\right)^2 - e\phi(\boldsymbol{r}_n)\right] + V(\boldsymbol{r}_1,\boldsymbol{r}_2,\cdots,\boldsymbol{r}_N). \tag{1.36}$$

The partition function Z at temperature T is

$$Z = \prod_{n=1}^{N}\int \frac{d\boldsymbol{r}_n d\boldsymbol{p}_n}{h^3} e^{-\mathcal{H}/k_{\rm B}T}. \tag{1.37}$$

Though it is classical, it has the Planck constant h because we need to calculate the number of states and that should be based on a unit space in the $\boldsymbol{r}$-$\boldsymbol{p}$ phase space.

Here we write $\boldsymbol{\pi}_n = \boldsymbol{p}_n + e\boldsymbol{A}(\boldsymbol{r})$, then

$$\begin{aligned} Z &= \prod_{n=1}^{N}\int \frac{d\boldsymbol{r}_n d\boldsymbol{\pi}_n}{h^3} e^{-\mathcal{H}'/k_{\rm B}T}, \\ \mathcal{H}' &= \sum_{n=1}^{N}\left[\frac{\boldsymbol{\pi}_n^2}{2m} - e\phi(\boldsymbol{r}_n)\right] + V(\boldsymbol{r}_1,\boldsymbol{r}_2,\cdots,\boldsymbol{r}_N), \end{aligned} \tag{1.38}$$

which has no $\boldsymbol{A}$ in the expression. Hence the statistical average of the magnetic moment is naturally

$$\langle\boldsymbol{\mu}_{\rm m}|\boldsymbol{\mu}_{\rm m}\rangle = -\frac{1}{N}\frac{\partial F}{\partial \boldsymbol{B}} = \frac{1}{Nk_{\rm B}T}\frac{\partial \ln Z}{\partial \boldsymbol{B}} = \langle\boldsymbol{\mu}_{\rm para}|\boldsymbol{\mu}_{\rm para}\rangle + \langle\boldsymbol{\mu}_{\rm dia}|\boldsymbol{\mu}_{\rm dia}\rangle = 0. \tag{1.39}$$

That is, within the classical picture of electrons and classical statistics, the pramagnetic and diamagnetic terms cancel each other and there shuold be no magnetism in this system. This is called **Bohr-van Leeuwen theorem**.

1.4 Spin and magnetic moment of electron

There are several factors that cause magnetism in quantum theory, one of which is that in quantum theory, an electron has a spin and a spin magnetic moment. The question why a point charge like an electron can have an internal freedom called spin and that also has a magnetic moment can be answered clearly by relativistic quantum mechanics. All of you should have already learned about this in the undergraduate course. However we would like review here the beautiful logics how this is derived[3].

1.4.1 Dirac equation

We consider quantum mechanics in the form of wavefunction and try to find out a form which stands with the special relativity. Schrödinger equation is a non-relativistic approximation and for the above purpose, we need to find out the form which is invariant for Lorentz transformations.

The one-dimensional Schrödinger equation is obtained by replacing the energy and the momentum as

$$E \to i\hbar\frac{\partial}{\partial t}, \quad p \to -i\hbar\frac{\partial}{\partial x}, \tag{1.40}$$

in the energy-momentum relation $E = p^2/2m$ in Newtonian mechanics. Furthermore, the wavefunction in the wave mechanics should have the meaning of probability amplitude and hence the differential equation for the wavefunction should be that of single-derivtive in time[4].

First the relativistic energy-momentum relation is

$$E^2 = (pc)^2 + (mc^2)^2. \tag{1.41}$$

If the transformation (1.40) is applied directly to the above we obtain Klein-Gordon equation but this is in the second order in time and does not fulfil the condition for the wavefunction. If the differential equation is first order in time and the orders for time and space should be the same, the derivative on the space also should be the first order. Then we write

$$E = \sum_{k=1,2,3} \alpha_k p_k c + \beta mc^2, \tag{1.42}$$

and try to compromise the above with eq. (1.41). Taking the square of the lhs and the equation to be eq. (1.41), the conditions are

$$\begin{cases} \alpha_k^2 = 1, \quad \beta^2 = 1, & \text{(1.43a)} \\ \alpha_k \alpha_j + \alpha_j \alpha_k = 0 \ (k \neq j), & \text{(1.43b)} \\ \alpha_k \beta + \beta \alpha_k = 0. & \text{(1.43c)} \end{cases}$$

In order to satisfy the above, we consider matrices for α_k, β and the dimension should be at least 4×4.

Then the wavefunction should have four components. The equation for the 4-component wavefunction $\boldsymbol{\psi} = {}^t(\psi_1, \psi_2, \psi_3, \psi_4)$ (^{t} means transpose) should be

$$i\hbar \frac{\partial \boldsymbol{\psi}}{\partial t} = \left[-i\hbar c \sum_{k=x,y,z} \alpha_k \frac{\partial}{\partial x_k} + \beta mc^2 \right] \boldsymbol{\psi} \tag{1.44a}$$

$$\equiv \mathcal{H}_{\mathrm{D}} \boldsymbol{\psi}, \quad \mathcal{H}_{\mathrm{D}} = c\boldsymbol{\alpha}\boldsymbol{p} + mc^2\beta. \tag{1.44b}$$

To obtain a specific form of α_k, β, we introduce the following **Pauli matrices**:

$$\sigma_x = \begin{pmatrix} 0 & 1 \\ 1 & 0 \end{pmatrix}, \quad \sigma_y = \begin{pmatrix} 0 & -i \\ i & 0 \end{pmatrix}, \quad \sigma_z = \begin{pmatrix} 1 & 0 \\ 0 & -1 \end{pmatrix}, \quad I = \begin{pmatrix} 1 & 0 \\ 0 & 1 \end{pmatrix}. \tag{1.45}$$

These matrices have the following relations

$$\sigma_i \sigma_j = -\sigma_j \sigma_i = i\sigma_k, \quad \sigma_x^2 = \sigma_y^2 = \sigma_z^2 = I. \tag{1.46}$$

Here for (i, j, k), (x, y, z) are assigned with cyclic rotations. From the above we reach a specific representation (Pauli representation) as follows.

$$\alpha_k = \begin{pmatrix} 0 & \sigma_k \\ \sigma_k & 0 \end{pmatrix}, \quad \beta = \begin{pmatrix} I & 0 \\ 0 & -I \end{pmatrix}. \tag{1.47}$$

Pauli representaion is one of the possible representations and we can find infinite numbers of representation with unitary transformation. Calculated results for the observables should be the same for all the representations. The four dimensions correspond to the spin degree of freedom and the freedom of particle-antiparticle (isospin). These four freedoms exist on the spatially point charge of electron-positron. In conclustion, this is the equation for the particle with spin 1/2 and with a finite mass.

1.4.2 Spin angular momentum

We consider a centeral force potential $V(\boldsymbol{r})$ and write

$$\mathcal{H} = \mathcal{H}_{\mathrm{D}} + V(\boldsymbol{r}). \tag{1.48}$$

The angular momentum

$$\boldsymbol{L} = \boldsymbol{r} \times \boldsymbol{p} \tag{1.49}$$

does not commute with the hamiltonian (1.48) as

$$[\boldsymbol{L}, \mathcal{H}] = i\boldsymbol{\alpha} \times \boldsymbol{p}. \tag{1.50}$$

$\boldsymbol{\alpha}$ is a vector of components α_k. We expand Pauli matrices to 4×4 dimension as

$$\sigma_k^{(4)} = \begin{pmatrix} \sigma_k & 0 \\ 0 & \sigma_k \end{pmatrix},$$

and write the vector of elements $\sigma_{x,y,z}^{(4)}$ as $\boldsymbol{\sigma}$. Then from the relation

$$[\boldsymbol{\sigma}, \mathcal{H}] = -2i\boldsymbol{\alpha} \times \boldsymbol{p}/\hbar, \tag{1.51}$$

we define the total angular momentum $\boldsymbol{J}$ as

Total angular momentum

$$\boldsymbol{J} = \boldsymbol{L} + \frac{\hbar}{2}\boldsymbol{\sigma} \equiv \boldsymbol{L} + \boldsymbol{s}, \tag{1.52}$$

then we obtain

$$[\boldsymbol{J}, \mathcal{H}] = 0, \tag{1.53}$$

that means $\boldsymbol{J}$ is a constant of motion. Namely $\boldsymbol{s} \equiv (\hbar/2)\boldsymbol{\sigma}$ is an observable which has characteristics of angular momentum. This is the **spin angular momentum**. We reach the conclusion that though an electron is a point in the space, it has an angular momentum as if it has a rotation.

1.4.3 Magnetic moment

We consider the Dirac equation in the presence of static electromagnetic fields. Just like eq. (1.32), we introduce a scalar and a vector potential to obtain

$$i\hbar\frac{\partial\psi}{\partial t} = [c\boldsymbol{\alpha}(\boldsymbol{p} + e\boldsymbol{A}) + \beta m - e\phi]\,\psi. \tag{1.54}$$

Now we rewrite it to

$$\left[\left(i\hbar\frac{\partial}{\partial t} + e\phi\right) - c\sum_{j=x,y,z}\alpha_j\left(-i\hbar\frac{\partial}{\partial r_j} + eA_j\right) - \beta mc^2\right]\psi = 0. \tag{1.55}$$

Then operate

$$i\hbar\frac{\partial}{\partial t} + e\phi + c\sum_{j=x,y,z}\alpha_j\left(-i\hbar\frac{\partial}{\partial r_j} + eA_j\right) + \beta mc^2 \tag{1.56}$$

from the left. After some algebra by using the commutation relations of α_j, β, we reach

$$\left[\left(i\hbar\frac{\partial}{\partial t} + e\phi\right)^2 - c^2(\boldsymbol{p} + e\boldsymbol{A})^2 - m^2c^4 + ic\hbar e(\boldsymbol{\alpha}\cdot\boldsymbol{E}) + i\hbar c^2 e(\alpha_x\alpha_y B_z + \alpha_y\alpha_z B_x + \alpha_z\alpha_x B_y)\right]\psi = 0. \tag{1.57}$$

Here from

$$\alpha_x\alpha_y = i\sigma_z^{(4)}, \quad \alpha_y\alpha_z = i\sigma_x^{(4)}, \quad \alpha_z\alpha_x = i\sigma_y^{(4)} \tag{1.58}$$

we can write (1.57) as

$$\left[\left(i\hbar\frac{\partial}{\partial t} + e\phi\right)^2 - c^2(\boldsymbol{p} + e\boldsymbol{A})^2 - m^2c^4 + ic\hbar e(\boldsymbol{\alpha}\cdot\boldsymbol{E}) - \hbar c^2 e\boldsymbol{\sigma}\cdot\boldsymbol{B}\right]\psi = 0. \tag{1.59}$$

To obtain steady state we write

$$\psi(\boldsymbol{r},t) = \exp(-i\epsilon t/\hbar)\varphi(\boldsymbol{r}) \tag{1.60}$$

and obtain

$$\left[(\epsilon + e\phi)^2 - c^2(\boldsymbol{p} + e\boldsymbol{A})^2 - m^2c^4 + ic\hbar e(\boldsymbol{\alpha}\cdot\boldsymbol{E}) - \hbar c^2 e\boldsymbol{\sigma}\cdot\boldsymbol{B}\right]\varphi = 0. \tag{1.61}$$

Here we put $\phi = 0$, $\boldsymbol{E} = 0$. In non-relativistic approximation $p \ll mc$, i.e., $\epsilon \approx mc^2$, hence we write $\epsilon = mc^2 + \delta$ and ignore the power of δ/mc^2 higher than the second order to obtain[*2]

$$\left[\frac{1}{2m}(\boldsymbol{p} + e\boldsymbol{A})^2 + \frac{e\hbar}{2m}\boldsymbol{\sigma}\cdot\boldsymbol{B}\right]\varphi = \delta\varphi. \tag{1.62}$$

Here we define the quantity called **Bohr magneton** as

Bohr magneton

$$\mu_{\mathrm{B}} \equiv \frac{e\hbar}{2m} \approx 9.274\times10^{-24}\ \mathrm{JT}^{-1}, \tag{1.63}$$

then in eq. (1.62) the term related to the magnetic field is

$$\frac{e\hbar}{2m}\boldsymbol{\sigma}\cdot\boldsymbol{B} = \mu_{\mathrm{B}}\boldsymbol{\sigma}\cdot\boldsymbol{B} = \frac{2}{\hbar}\mu_{\mathrm{B}}\boldsymbol{s}\cdot\boldsymbol{B}. \tag{1.64}$$

This means that an electron has, with the spin angular momentum $\boldsymbol{s}$, a magnetic moment $-2\mu_{\mathrm{B}}\boldsymbol{s}/\hbar$

Appendix 1A Unit systems of electromagnetism

The unit system, or metrology is extremely important for human life even beyond the boundaries of science or the framework of scholarship. In usual systems, at first place a small number of basic units are determined by some way, and then other units are determined through universal laws of physics. Naturally, there are many possible ways to constitute unit systems. We should choose a unit system convenient for the problem that we need to tackle from many possible ones, particularly in the case of electromagnetism. Many researchers, even among non-expert in unit, have their own opinions for unit systems. Hence it is impossible to force everyone to choose one. In spite of such tendency, the SI (Système International) unit system is defined as an international standard in consideration of practicality, logical consistency, and historical continuity. I would like to adopt the SI unit system as far as I can, but here, I introduce major systems of unit in electromagnetism in very short. If you are interested in the metrology, I would like to recommend Ref. [5]. Care should be taken, though, that the committee meeing of the SI unit is held annually, and the unit may have big changes as did in 2019. It is necessary to refer to the web etc. for the latest definition. Here I summarize CGS-esu (electrostatic system of unit) and MKSA (SI) system of unit very briefly.

1A.1 CGS-esu

The Coulomb's law should be written in the form

$$F = k_{\mathrm{q}}\frac{q_1 q_2}{r^2}. \tag{1A.1}$$

In CGS electrostaticunit, k_{q} is just 1 and with no physical dimension. Then the electric charge can be expressed by [L], [M], [T] as

$$[Q] = [M^{1/2}L^{3/2}T^{-1}].$$

[*2] This φ has four components and then we need to reduce the dimension to two with the non-relativistic approximation. But here we skip the procedure for simplicity. The result here is the same for this but to derive spin-orbit interaction, this is indispensable.

When the force between electric charges with the same amount at the distance of 1 cm is 1 dyn, the charge is 1 esu (CGS esu). There are three basic quantities and there is no factor of $(4\pi)^{-1}$ in the Coulomb's law (this means 4π appears in the Maxwell equation). Hence this unit system is classified to three components irrational unit system.

1A.2 MKSA unit system

Until a while ago, the current was introduced as the fourth basic quantity, the unit of the current was A (ampere), and 1 A was defined from the force acting between the parallel conductors separated by 1 m in a vacuum with a length of 1 m as to be 2×10^{-7} N. However in the redefinition in 2019, the fourth basic quantity becomes the charge, which is introduced by determining the elementary charge e as $1.602176634\times10^{-19}$ C (coulomb). Then the current is introduce by the charge and the time (A·s =C). Because the number of basic quantities is four and $k_{\rm q}$ has the factor $(4\pi)^{-1}$, the unit system is classified to four components rational unit system.

Appendix 1B: Dipole field and dipole inteaction

1B.1 Magnetic field created by magnetic dipole

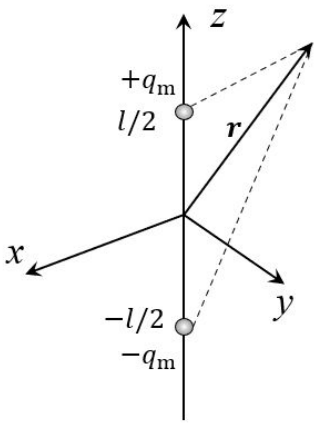

Fig. 1B.1 Magnetic charge model of magnetic dipole.

From eq. (1.1d), when there is no true current and no time-derivative of electric field, the rotation of magnetic field $\nabla\times\boldsymbol{B}$ is zero. In such a case, we can define magnetostatic potential $\phi_{\rm m}$ as a scalar function of spatial coordinage $\boldsymbol{r}$. The magnetic field is given by

$$\boldsymbol{H}=-\nabla\phi_{\rm m}. \tag{1B.1}$$

We consider the magnetostatic potential $\phi_{\rm m}$ for the situation that magnetic charges of $\pm q_{\rm m}$ are placed at $\pm\boldsymbol{p}=(0,0,\pm l/2)$ respectively.

$$\phi_{\rm m}(\boldsymbol{r})=\frac{1}{4\pi\mu_0}\left(\frac{q_{\rm m}}{|\boldsymbol{r}-\boldsymbol{p}|}-\frac{q_{\rm m}}{|\boldsymbol{r}+\boldsymbol{p}|}\right). \tag{1B.2}$$

We assume that l is sufficiently smaller than $|\boldsymbol{r}|$ ($|\boldsymbol{r}|\gg l$), and expand $\phi_{\rm m}$ with the power of l and take the first order term to obtain

$$\phi_{\rm m}(\boldsymbol{r})=\frac{q_{\rm m}}{4\pi\mu_0}\frac{lz}{r^3}=\frac{q_{\rm m}l}{4\pi\mu_0}\frac{\cos\theta}{r^2}. \tag{1B.3}$$

The last expression is on the polar coordinate (r,θ,φ).

We write $\boldsymbol{l}=(0,0,l)$, and the magnetic moment as $\boldsymbol{\mu}=q_{\rm m}\boldsymbol{l}/\mu_0$, the magnetic field originates from the magnetic dipole is

$$\boldsymbol{B}=-\frac{1}{4\pi\mu_0}\nabla\left(\frac{\boldsymbol{\mu}\cdot\boldsymbol{r}}{r^3}\right). \tag{1B.4}$$

We apply the polar coordinate representation of ∇

$$\nabla=\frac{\partial}{\partial r}\boldsymbol{e}_r+\frac{1}{r}\frac{\partial}{\partial\theta}\boldsymbol{e}_\theta+\frac{1}{r\sin\theta}\frac{\partial}{\partial\varphi}\boldsymbol{e}_\varphi \tag{1B.5}$$

to eq. (1B.3), and we reach

$$B_r=\frac{|\boldsymbol{\mu}|}{4\pi\mu_0}\frac{2\cos\theta}{r^3},\quad B_\theta=\frac{|\boldsymbol{\mu}|}{4\pi\mu_0}\frac{\sin\theta}{r^3}, \tag{1B.6}$$

which is nothing but eq. (1.6).

1B.2 Dipole field as shrink limit of circular current

In the text, we considered the fictitious "magnetic charge" to make the physical picture simpler. The experiments so far have shown that there is no isolated magnetic monopole like electric monopole. Then there is an opinion that we should not use the magnetic charge even as a mathematical concept. On the other hand, there are researchers who positively use the magnetic charge as an established physical concept [2], because there are many such physically established concepts like the vector potential which is not an observable but a mathematical method.

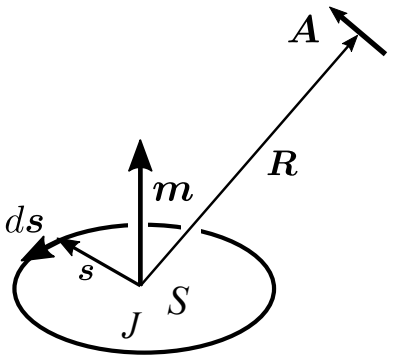

Fig. 1B.2 Definition of magnetic dipole by circular current.

This problem also relates to the view of electric-magnetic symmetry in the Maxwell equation (1.1). That is, so called the problem whether $\boldsymbol{E}$-$\boldsymbol{B}$ formulation or $\boldsymbol{E}$-$\boldsymbol{H}$ formulation. In the former, the magnetic field is introduced along the Viot-Savart law as formed by a current on a wire element while in the latter the field is formed by magnetic charges through the Coulomb law. In CGS unit system, these two ways of introduction do not give significant difference. However in MKSA unit system, this leads to the difference in the unit of magnetization. The same problem appears when we introduce magnetic dipole through magnetic charges. When we consider a pair of moment (1.2), the selection of $\boldsymbol{E}$-$\boldsymbol{H}$ correspondence or $\boldsymbol{E}$-$\boldsymbol{B}$ correspondence results in the difference whether eq. (1.3) gets μ_0 or not. In this lecture we do not go into the problem to construct electromagnetic theory though we adopt $\boldsymbol{E}$-$\boldsymbol{B}$ formulation for the unit of magnetization.

Now we consider a circular current J surrounding the area S in xy-plane as in Fig. 1B.2. The vector potential $\boldsymbol{A}$ is

$$\begin{aligned}\boldsymbol{A} &= \frac{\mu_0}{4\pi}\iiint \frac{\boldsymbol{j}}{r}dv = \frac{\mu_0 J}{4\pi}\oint \frac{d\boldsymbol{s}}{r} = \frac{\mu_0 J}{4\pi}\frac{1}{R}\oint\left\{1+\frac{1}{R^2}(\boldsymbol{R}\cdot\boldsymbol{s})+\cdots\right\} \\ &\simeq \frac{\mu_0 J}{4\pi}\frac{1}{R^3}\oint(\boldsymbol{R}\cdot\boldsymbol{s})d\boldsymbol{s}. \end{aligned} \tag{1B.7}$$

s_x component of the integration over $d\boldsymbol{s}$ is

$$\oint(\boldsymbol{R}\cdot\boldsymbol{s})ds_x = \oint\sum_{i=x,y,z} R_i s_i ds_x = \sum_{i=y,z} R_i \oint s_i ds_x,$$

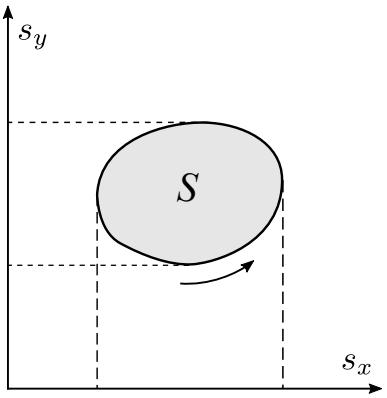

and the term of $R_x s_x$ vanishes because s_x goes back and forth over the integral interval. On the other hand for $s_y ds_x$, $s_x ds_y$, as in the right figure

$$\oint s_y ds_x = -\oint s_x ds_y = -S.$$

This gives

$$\oint(\boldsymbol{R}\cdot\boldsymbol{s})d\boldsymbol{s} = -\oint(\boldsymbol{R}\cdot d\boldsymbol{s})\boldsymbol{s},$$

and from the identities of vector analysis we get

$$\oint(\boldsymbol{R}\cdot\boldsymbol{s})d\boldsymbol{s} = \frac{1}{2}\oint\{(\boldsymbol{R}\cdot\boldsymbol{s})d\boldsymbol{s} - (\boldsymbol{R}\cdot d\boldsymbol{s})\boldsymbol{s}\} = \frac{1}{2}\oint(\boldsymbol{s}\times d\boldsymbol{s})\times\boldsymbol{R}, \tag{1B.8}$$

where

$$\frac{1}{2}\oint \boldsymbol{s}\times d\boldsymbol{s}$$

is the vector perpendicular to the current plane and with the size of the area (S) of the circular current. Then we define a vector $\boldsymbol{\mu}$ as

$$\boldsymbol{\mu} = J\left(\frac{1}{2}\oint \boldsymbol{s}\times d\boldsymbol{s}\right), \tag{1B.9}$$

then we can write

$$\boldsymbol{A} = \frac{\mu_0}{4\pi}\frac{\boldsymbol{\mu}\times\boldsymbol{R}}{R^3}. \tag{1B.10}$$

By using this equation and after some algebra, we obtain, e.g., x-component of $\boldsymbol{B}$ as

$$B_x = \frac{\partial A_z}{\partial y} - \frac{\partial A_y}{\partial z} = -\frac{\mu_0}{4\pi}\left(\nabla\frac{\boldsymbol{\mu}\cdot\boldsymbol{r}}{r^3}\right)_x. \tag{1B.11}$$

Then the magnetic field created by the circular current is given by

$$\boldsymbol{B} = -\frac{\mu_0}{4\pi}\nabla\frac{\boldsymbol{\mu}\cdot\boldsymbol{r}}{r^3}. \tag{1B.12}$$

This is in accordance with eq. (1B.4), and now we know that the circular current is working as a magnetic dipole.

1B.3 Dipole interaction

(Under construction)

References

[1] P. J. Flanders. An alternating-gradient magnetometer (invited). *Journal of Applied Physics*, Vol. 63, No. 8, pp. 3940–3945, April 1988.

[2] S. Chikazumi and S. H. Charap. *Physics of Magnetism (Wiley Series on the Science and Technology of Materials)*. Wiley, 1 1964.

[3] Shinichiro Tomonaga. *The Story of Spin*. University of Chicago Press, 10 1998.

[4] J. J. Sakurai and Jim Napolitano. *Modern Quantum Mechanics*. Cambridge University Press, 9 2020.

[5] N. V. Raghavendra and L. Krishnamurthy. *Engineering Metrology and Measurements*. Oxford Univ Pr, 10 2016.

1.4.4 Spin-orbit interaction

Another important effect stems from the Dirac equation is **spin-orbit interaction** (SOI). We have already seen that the four components in the solution of the Dirac equation correspond to (freedom of particle-antiparticle)×(spin freedom). In the Pauli representation (1.44b), (1.47), within non-relativistic limit of $p \ll mc$, the upper two rows correspond to the solution with positive energy, the lower two correspond to that with negative energy. However with growing p, the shifts from the free particle become large and some mixing appears between the upper two and the lower. For example, we consider a free dirac particle propagating along z-direction with up-spin for quantization axis of z-axis. Let $\tan 2\theta$ be

$$\tan 2\theta = \frac{p}{mc}, \tag{1.65}$$

then the four component wavefunction is

$$\psi_\uparrow = e^{i(kz-\omega t)} \begin{pmatrix} \cos\theta \\ 0 \\ \sin\theta \\ 0 \end{pmatrix}, \tag{1.66}$$

which indicates the increase of negative energy component with p. Inclusion of this leakage into the picture of particle with two-component of spin creates the SOI as the correction.

The equation for stationary solution obtained from the treatment in (1.60) is given by

$$(c\boldsymbol{\alpha}\cdot\boldsymbol{p} + \beta mc^2 + V)\varphi = \epsilon\varphi, \tag{1.67}$$

where σ_j are Pauli matrices defined in eq. (1.45), $\boldsymbol{\alpha}$ is a vector of elements α_k defined in eq. (1.47), β is defined in eq. (1.47). We write φ as a two-component vector of φ_A and φ_B as $\varphi = {}^t(\varphi_\mathrm{A}\ \varphi_\mathrm{B})$. Then eq. (1.67) is written in a simultaneous equation as follows.

$$\boldsymbol{\sigma}\cdot\boldsymbol{p}\varphi_\mathrm{B} = c^{-1}(\delta - V)\varphi_\mathrm{A}, \tag{1.68a}$$
$$\boldsymbol{\sigma}\cdot\boldsymbol{p}\varphi_\mathrm{A} = c^{-1}(\delta - V + 2mc^2)\varphi_\mathrm{B}, \tag{1.68b}$$

where $\delta = \epsilon - mc^2$ and $\boldsymbol{\sigma}$ is a vector of Pauli matrices as elements. φ_B can be erased virtually as

$$c^{-2}\boldsymbol{\sigma}\cdot\boldsymbol{p}(\delta - V + 2mc^2)^{-1}\boldsymbol{\sigma}\cdot\boldsymbol{p}\varphi_\mathrm{A} = (\delta - V)\varphi_\mathrm{A}. \tag{1.69}$$

We apply low energy expansion, in which we assume the kinetic energy of electron is sufficiently smaller than the rest energy mc^2.

$$c^2(\delta - V + 2mc^2)^{-1} \approx \frac{1}{2m}\left[1 - \frac{\delta - V}{2mc^2} + \cdots\right]. \tag{1.70}$$

The second term in rhs corresponds to $(v/c)^2$, where v is the electron velocity and we take up to this term. Substituting this to eq. (1.69) leads to the equation of ψ_A. However, the normalization condition is $\langle\varphi|\varphi\rangle = \langle\varphi_\mathrm{A}|\varphi_\mathrm{A}\rangle + \langle\varphi_\mathrm{B}|\varphi_\mathrm{B}\rangle = 1$, which should be considered in solving eq. (1.68) for φ_A. The first order perturbative mixing in wavefunction is on the second order in the normalization and in eq. (1.70). Hence in eq. (1.70), we take the first term in rhs. We use the commutation of σ_j and p_i, $\sigma_j^\dagger = \sigma_j$ and the following identity

$$(\boldsymbol{\sigma}\cdot\boldsymbol{a})(\boldsymbol{\sigma}\cdot\boldsymbol{b}) = (\boldsymbol{a}\cdot\boldsymbol{b}) + i[\boldsymbol{\sigma}\cdot(\boldsymbol{a}\times\boldsymbol{b})],$$

In the presence of magnetic field $\boldsymbol{B} = \nabla \times \boldsymbol{A}$, we replace $\boldsymbol{p}$ with $\boldsymbol{p} + e\boldsymbol{A}$ to get

$$\langle \varphi_{\rm B} | \varphi_{\rm B} \rangle = \langle \varphi_{\rm A} | \left[\frac{p^2 + e\hbar \boldsymbol{\sigma} \cdot \boldsymbol{B}}{4m^2c^2} \right] | \varphi_{\rm A} \rangle = O\left(\frac{v^2}{c^2} \right).$$

Then as the wavefunction

$$\varphi_a = \left(1 + \frac{p^2 + e\hbar \boldsymbol{\sigma} \cdot \boldsymbol{B}}{8m^2c^2} \right) \varphi_{\rm A} \tag{1.71}$$

is enough for the approximation to order of $(v/c)^2$. From eq. (1.69), we reach the Pauli equation (approximation to order of $(v/c)^2$) as

$$\left[\frac{p^2}{2m} + V + \frac{e\hbar}{2m} \boldsymbol{\sigma} \cdot \boldsymbol{B} - \frac{e\hbar \boldsymbol{\sigma} \cdot \boldsymbol{p} \times \boldsymbol{E}}{4m^2c^2} - \frac{e\hbar^2}{8m^2c^2} \nabla \cdot \boldsymbol{E} - \frac{p^4}{8m^3c^2} - \frac{e\hbar p^2}{4m^3c^2} \boldsymbol{\sigma} \cdot \boldsymbol{B} - \frac{(e\hbar B)^2}{8m^3c^2} \right] \varphi_a = \delta \varphi_a, \tag{1.72}$$

where $\boldsymbol{E} = \nabla V/e$ is the electric field. In the lhs of eq. (1.72), the third term is the Zeeman energy, the fourth is the spin-orbit interaction.

If we write $\boldsymbol{B}_{\rm so} \equiv \boldsymbol{p} \times \boldsymbol{E}/2mc^2$, the fourth SOI term looks like in the same form as the third term. Namely the spin feels an effective magnetic field of $\boldsymbol{B}_{\rm so}$, which is sometimes called a spin-orbit effective field.

1.5 Magetism in quantum theory

In Sec. 1.3.3, we saw that the magnetism cannot be explained within the framework of classical theory. On the other hand in Sec. 1.4, in the Dirac theory, which considers both quantum theory and relativity, an electron, though it is a point charge, has a spin angular momentum and an associated magnetic moment. We will see, throughout this lecture for a semester, how the difficulty in the classical theory is solved. But here we see quickly how this spin angular momentum produces magnetism in a simple model of the classical framework plus spin.

A Hamiltonian with magnetic field $\boldsymbol{B}$ is given by

$$\mathcal{H} = \sum_n \left[\frac{1}{2m} (\boldsymbol{p}_n + e\boldsymbol{A}(\boldsymbol{r}_n))^2 + U(\boldsymbol{r}_n) + g\mu_{\rm B} \boldsymbol{s}_n \cdot \boldsymbol{B} \right] + V(\boldsymbol{r}_1, \boldsymbol{r}_2, \cdots), \tag{1.73}$$

where a nucleus potential is written as $U(\boldsymbol{r}_n)$. In (1.52), we define $\boldsymbol{s}$ as to have the dimension of angular momentum and then $(\hbar/2)\boldsymbol{\sigma}$ is $\boldsymbol{s}$. But here we redefine $\boldsymbol{s}$ to fit the ordinary definition:

$$\boldsymbol{s}: \ \frac{\hbar \boldsymbol{\sigma}}{2} \to \frac{\boldsymbol{\sigma}}{2}, \tag{1.74}$$

which has the difference of a factor $\hbar$. The third term in the summation is the Zeeman term mentioned in Sec. 1.4. g is called **g-factor**, which is just t within the approximation of eq. (1.72) In the quantum electrodynamics, this is a bit larger than 2, due to the effect of electromagnetic field. As we will see later, in some cases we need to include orbital angular momentum into the form of g-factor (Landé g-factor). Here we do not include the spin-orbit interaction.

Just as before, we take symmetric gauge $\boldsymbol{A}(\boldsymbol{r}_n) = (\boldsymbol{B} \times \boldsymbol{r}_n)/2$ to obtain

$$\mathcal{H} = \sum_n \left[\frac{\boldsymbol{p}_n^2}{2m} + U(\boldsymbol{r}_n) \right] + V(\boldsymbol{r}_1, \boldsymbol{r}_2, \cdots) \qquad \mathcal{H}_0 \tag{1.75a}$$

$$+ \mu_{\rm B} \sum_n (\boldsymbol{l}_n + g\boldsymbol{s}_n) \cdot \boldsymbol{B} \qquad \mathcal{H}_1 \tag{1.75b}$$

$$+ \frac{e^2}{8m} \sum_n \{ r_n^2 B^2 - (\boldsymbol{B} \cdot \boldsymbol{r}_n)^2 \} \qquad \mathcal{H}_2, \tag{1.75c}$$

where we write the orbital angular momentum in unit of $\hbar$ as

$$\hbar \boldsymbol{l}_n \equiv \boldsymbol{r}_n \times \boldsymbol{p}_n. \tag{1.76}$$

And $\mathcal{H}_0$, $\mathcal{H}_1$, $\mathcal{H}_2$ are the terms of order zero-th, 1st, 2nd order of B respectively.

There are commutation relations between the coordinate and momentum operators:

$$[r_{n\alpha}, p_{n\beta}] = r_{n\alpha}p_{n\beta} - p_{n\beta}r_{n\alpha} = i\hbar\delta_{\alpha\beta} \quad (\alpha, \beta = x, y, z). \tag{1.77}$$

And from the redifinition of eq. (1.74),

$$[s_{n\alpha}, s_{n\beta}] = is_{n\gamma} \quad (\alpha, \beta, \gamma = x, y, z \text{ (cyclic)}). \tag{1.78}$$

The same for the orbital angular momentum as

$$[l_{n\alpha}, l_{n\beta}] = il_{n\gamma} \quad (\alpha, \beta, \gamma = x, y, z \text{ (cyclic)}). \tag{1.79}$$

The magnetic moment is given as in eq. (1.35) by

$$\begin{aligned} \mu = -\frac{\partial \mathcal{H}}{\partial \boldsymbol{B}} &= -\mu_{\mathrm{B}} \sum_n (\boldsymbol{l}_n + g\boldsymbol{s}_n) - \frac{e^2}{4m} \sum_n \{r_n^2 \boldsymbol{B} - \boldsymbol{r}_n(\boldsymbol{r}_n \cdot \boldsymbol{B})\} \\ &= -\mu_{\mathrm{B}} \sum_n (\boldsymbol{l}_n + g\boldsymbol{s}_n) - \frac{e^2}{4m} \sum_n (\boldsymbol{r}_n \times (\boldsymbol{B} \times \boldsymbol{r}_n)\}. \end{aligned} \tag{1.80}$$

In comparison with (1.35), naturally the term $\boldsymbol{s}_n$ is the difference in this mathematical form.

In a naive thought, the relativistic quantum mechanics brings in the spin-angular momentum and magnetic moment, and that leads to the explanation of the magnetism. It is true that the spin magnetic moment plays an important role but the above is too naive of course. In quantum theory, the quantization in orbital angular moments, spatial distribution of particles, and also statistics of particles give big differences both in paramagnetic and diamagnetic terms, which lead to the appearance of magnetic moment. What we have seen are the minimum knowledges to consider the magnetism. In the next chapter let us first have a look on the magnetism of atoms and ions, in which the quantization gives crutial effects.

I have a little comment on the spin of particles, that is the **nuclear magnetism**. Representative nucleons are proton and neutron, which both are known to have spin 1/2 (the histry of finding these facts is described in Ref. [1]). Though the concept of spin was naturally introduced by the Dirac equation, proton and neutron belong to hadron and are not described by the Dirac equation. Actually the g-factors are very different from 2 that is the value in the Dirac equation. Proton has a charge of $+e$ and the magnetic moment can be naturally understood. On the other hand, neutron does not have total charge and still has a magnetic moment. This is due to the inner structure, that is the inner charge distribution. The spins of neucleons have opened up a huge field of magnetic detection of various phenomena. A representative is magnetic resonance imaging (MRI), which is now an important inspection device for the protection of lives. And the neutron diffraction is widely used to explore magnetic structures taking advantage of electrical neutrality.

Chapter 2

Magnetism of Localized Electrons

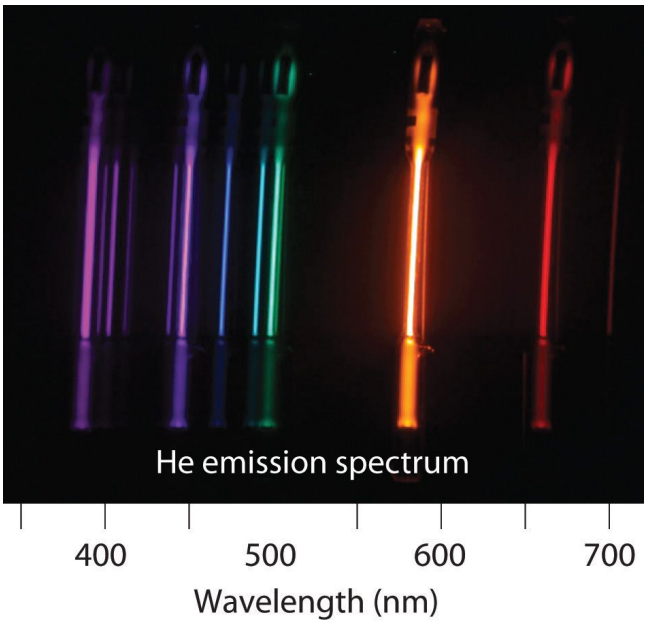

The goal of elementary quantum mechanics is the derivation of hydrogen atomic spectrum, that is the quantum confinement by spherical Coulomb potential. But the goal is at the same as the starting point of atomic/molecular spectroscopy as well as magnetism. The problem of localized electrons as the basics of magnetism is, in other words, the many-body problem in localized potentials. The subject of this chapter is how the magnetic moments arise from many-body systems.

2.1 Localized many-body problem

Let us consider the magnetism in localized electron systems like atoms and ions. When they are placed inside crystals, we need to consider the effect of surrounding lattices. Then we write the hamiltonian as

$$\mathcal{H}_{\rm L} = \mathcal{H}_{\rm L0} + \mathcal{H}_{\rm C} + \mathcal{H}_{\rm SOI} + \mathcal{H}_{\rm CF}, \tag{2.1}$$

where $\mathcal{H}_{\rm L0}$ is an ordinary spherical potential hamiltonian, $\mathcal{H}_{\rm C}$ is the Coulomb interaction among electrons, $\mathcal{H}_{\rm SOI}$ is the SOI, and $\mathcal{H}_{\rm CF}$ is the **crystal field** caused by surrounding lattices. The amplitude of $\mathcal{H}_{\rm CF}$ greatly depends on the situation. When it is large, sometimes we need to go back to the single-electron problem in the potential under the effect of ligands[2]. There is no that term in the case of gases.

2.1.1 Problem of spherical potential

$\mathcal{H}_{\rm L0}$ is the sum of kinetic energy and the spherical potential $V_{\rm sp}(r)$ created by nucleus as

$$\mathcal{H}_{\rm L0} = \sum_j \left[\frac{\boldsymbol{p}_j^2}{2m} + V_{\rm sp}(r_j) \right], \tag{2.2}$$

which has basically the same form as hydrogen atom problem. Then the energy eigenvalue is indexed with (main quantum number, azimuthal quantum number, magnetic quantum number)=(n, l, m). A specific form of wavefunction in the polar coordinate representation is

$$\psi_{nlm}(\boldsymbol{r}) = R_{nl}(r)Y_{lm}(\theta, \varphi), \tag{2.3}$$

where $R_{nl}(r)$ is a radial wavefunction, $Y_{lm}(\theta, \varphi)$ is the spherical harmonic function. In the case that $V_{\rm sp}(r)$ is the Coulomb potential, which is proportional to r^{-1},

$$R_{nl}(r) = b_{nl}\rho^l e^{-\rho/2} L_{n+1}^{2l+1}(\rho), \quad \rho \equiv \frac{2}{n}\frac{r}{a_0}, \tag{2.4}$$

where b_{nl} is the normalization constant, L_{n+1}^{2l+1}, an associated Laguerre polynomial, is a polynomial of $n+l-(2l+1) = n-l-1$-th order, a_0 is a quantity of length dimension, the Bohr radius in the case of Hydrogen atom[3]. The eigenenergies are degenerated for l, m and written as the function of main quantum number n as

$$\epsilon_{nl} = -\frac{R_\infty}{n^2}, \quad R_\infty = \frac{me^4}{8\epsilon_0 h^3 c}. \tag{2.5}$$

In the above, the spin-degree of freedom is dropped. Hence here, as in many non-relativistic approximation, we take the spin degree of freedom σ into account by taking the direct product. $\mathcal{H}_{\rm L0}$ can be written in the form of second quantization as

$$\mathcal{H}_{\rm L0} = \sum_{nl} \epsilon_{nl} \sum_{m\sigma} a^\dagger_{nlm\sigma} a_{nlm\sigma}. \tag{2.6}$$

2.1.2 Larmor precession

To see the effect of quantization on the magnetic moment caused by the orbital angular moment, we consider the Coulomb potential of atomic number Z,

$$V_{\rm sp}(r_j) = -\frac{Ze^2}{4\pi\epsilon_0}\frac{1}{r_j}. \tag{2.7}$$

The total orbital angular momentum $\hbar\boldsymbol{L}$ is written as the sum of each orbital contributions:

$$\hbar\boldsymbol{L} = \hbar\sum_i \boldsymbol{l}_i. \tag{2.8}$$

To concentrate ourselves on the effect of orbitals, we tentatively drop the spin ($\boldsymbol{s}$) term and write the term in (1.75b) as

$$\mathcal{H}_1 = \mu_{\rm B}\boldsymbol{L}\cdot\boldsymbol{B} = \mu_{\rm B}L_z B. \tag{2.9}$$

$\boldsymbol{B}$ is taken to be parallel to z-axis. L_z is azimuthally quantized by

$$L_z = M : -L,\ -L+1, \cdots, L-1,\ L.$$

The electron energy in the magnetic field is

$$E = E_0 + \mu_{\rm B}MB \equiv E_0 + \hbar\omega_{\rm L}M, \quad \omega_{\rm L} \equiv \frac{\mu_{\rm B}B}{\hbar} = \frac{eB}{2m}\ (\text{Larmor frequency}), \tag{2.10}$$

where E_0 is the value for zero magnetic field.

We will have a look at a motion of angular momentum $\boldsymbol{L}$ in magnetic field $\boldsymbol{B}$ along z-axis. Heisenberg equation of motion for $\boldsymbol{L}$ is given by

$$\frac{{\rm d}\boldsymbol{L}}{{\rm d}t} = \frac{1}{i\hbar}[\boldsymbol{L}, \mathcal{H}_0 + \mathcal{H}_1 + \mathcal{H}_2], \tag{2.11}$$

with the hamiltonian in eq. (1.75). In the hamiltonian, the term $\mathcal{H}_0$ in zero-th order of B is $\mathcal{H}_{\rm L0}$ in eq. (2.2) in this problem. The terms of higher order in B than 2 are ignored here and we drop $\mathcal{H}_2$.

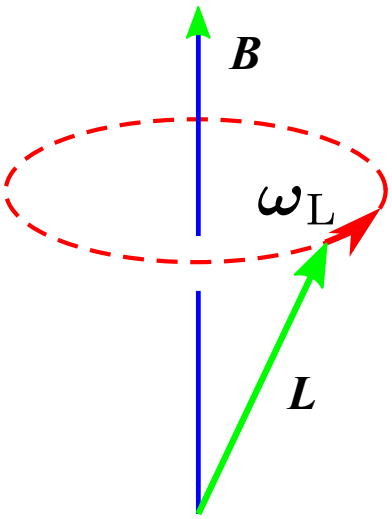

Fig. 2.1 Schematics of Larmor precession. The electron angular momentum L precesses around the axis of magnetic field $\boldsymbol{B}$ with angular frequency ω_{L}.

From the axial symmetry of magnetic field $\boldsymbol{B}$ and the spherical symmetry of potential, L_z is a constant of motion, which commutes with the hamiltonian. For the residual L_x, L_y, from

$$\frac{\mathrm{d}L_x}{\mathrm{d}t} = -\omega_{\mathrm{L}} L_y, \quad \frac{\mathrm{d}L_y}{\mathrm{d}t} = \omega_{\mathrm{L}} L_x \tag{2.12}$$

we obtain

$$L_x(t) = L_0 \cos(\omega_{\mathrm{L}} t + \theta_0), \quad L_y(t) = L_0 \sin(\omega_{\mathrm{L}} t + \theta_0), \tag{2.13}$$

which means L_x, L_y undergo a circular motion with angular frequency ω_{L}, and the total momentum precesses as illustrated in Fig. 2.1. This is called **Larmor precession**.

This is generalized into **Larmor theorem**[4], which tells that the motion of electronic systems in magnetic field $\boldsymbol{B}$ is the same as that in the zero-magnetic field if we see that on the coordinate system rotating with angular frequency ω_{L} under the condition (i) the central force potential sits still, (ii) the axial symmetry around the magnetic field $\boldsymbol{B}$, (iii) the phenomenon up to the first order of magnetic field.

The above is for the orbital angular momentum. In the case of spin angular momentum, the expression of the magnetic moment has g-factor, then the Larmor frequency has the g-factor as

$$\omega_{\mathrm{L}} = g\frac{eB}{2m} \approx \frac{eB}{m}. \tag{2.14}$$

Further, the expression ω_{L} is also used for nuclear magnetic moment etc. The coefficient of B for ω_{L} is often written as γ (that is $\omega_{\mathrm{L}} = \gamma B$), where γ is called **gyromagnetic ratio**. These are the basis of magnetic resonance experiment, and we revisit the magnetic resonance experiments afterwords.

2.2 Magnetism of inert gas atoms and closed shell ion cores

At the beginning of chapter 1, I wrote that what we feel the magnetism is from the permanent magnet. In comparison with that, it may be a bit hard to feel that the gases also have the magnetism. However, if the isolated atoms or molecules have the magnetism, the gases of those particles naturally have magnetic moments. An example of important role played by the gas magnetism, is the birth of stars, in which the interstellar magnetic field ($\sim 10^{-10}$ T) is said to work for the integration of gases as well as the gravitational force[*1]. Another example is the trapping and cooling of laser cooled gases

[*1] However, according to recent observation by Alma telescope, it is deduced that the effect of magnetic field may be weaker than that of gravitation[5]

Z	Element	Susceptibility
2	He	-1.9×10^{-6}
10	Ne	-7.2×10^{-6}
18	Ar	-19.4×10^{-6}
36	Kr	-28×10^{-6}
54	Xe	-43×10^{-6}

Tab. 2.1 Measured mole magnetic susceptibility of inert gases.

of neutral atoms. By adding a spatial distribution to the Zeeman split due to the magnetic moment by the magnetic field gradient, atoms with the magnetic moment can be collected near one point in space (magnetic trap). Atoms with higher kinetic energies tends to distribute positions far from the center of trap and the radio frequency wave rotates spins around there and selectively expels out the high energy atoms, which leads to the cooling (evaporation cooling).

We consider the case, in which the orbitals (n, l) are important. The orbital angular momentum $\boldsymbol{L}$, the spin angular momentum $\boldsymbol{S}$, and the total angular momentum $\boldsymbol{J}$ are written as

$$\boldsymbol{L} = \sum_j \boldsymbol{l}_j = \sum_\sigma \sum_{mm'} \langle m|\boldsymbol{l}|m'\rangle_{nl} a^\dagger_{m\sigma} a_{m'\sigma}, \tag{2.15a}$$

$$\boldsymbol{S} = \sum_j \boldsymbol{s}_j = \sum_m \sum_{\sigma\sigma'} \left(\frac{\sigma}{2}\right)_{\sigma\sigma'} a^\dagger_{m\sigma} a_{m\sigma'}, \tag{2.15b}$$

$$\boldsymbol{J} = \sum_j \boldsymbol{j}_j = \boldsymbol{L} + \boldsymbol{S}. \tag{2.15c}$$

In inert gases like He, Ne, Ar, or in ion cores like Ag^+, which have closed shell structures, the total orbital and spin angular momentums are zero ($L = S = 0$) due to the cancelling between electrons. Then the paramagnetic term is zero in these cases. This is, of course, an important information and this leads to the survival of the diamagnetic term (second term) in eq. (1.80). The magnetic moment due to this term is

$$\boldsymbol{\mu}_{\rm dia} = -\frac{e^2}{4m} \sum_n [\boldsymbol{r}_n \times (\boldsymbol{B} \times \boldsymbol{r}_n)] = -\frac{e}{2} \sum_n [\boldsymbol{r}_n \times (\boldsymbol{\omega}_{\rm L} \times \boldsymbol{r}_n)] = -\frac{\mu_{\rm B}}{\hbar} \sum_n [\boldsymbol{r}_n \times (m\boldsymbol{v}_n)], \tag{2.16}$$

where $\boldsymbol{\omega}_{\rm L}$ is a vector of the Larmor frequency produced with replacing B in eq. (2.10) with the vector $\boldsymbol{B}$. Equation (2.16) indicates that the diamagnetism arises from the outer product of momentum and coordinate created by the Larmor precession, that is, the angular momentum of the Larmor precession. Hence we call the diamagnetism as **Larmor diamagnetism**. We have calculated classically the magnetic moment induced by the magnetic field in zero-field and without angular moment ($L = 0$) in Sec. 1.3.2. The quantum mechanical calculation of eq. (2.16) gives the same results as

$$\mu_{\rm d} = -\frac{e^2}{4m} \langle x^2 + y^2 \rangle B = -\frac{e^2}{6m} \langle r^2 \rangle B, \tag{2.17}$$

where we have used the fact that $\langle x^2 + y^2 \rangle = (2/3) \langle r^2 \rangle$ in the radial wavefunction in eq. (2.4). The molar susceptibility of inert gases of atomic number Z is then

$$\chi = -\frac{N_{\rm A} Z e^2 \langle r^2 \rangle}{6m}. \tag{2.18}$$

This leads to the estimation of radius of atoms (ions) from the susceptibility measurement[6]. The experimental values in Tab. 2.1 tells that

$$\langle r^2 \rangle \sim a_{\rm B}^2. \tag{2.19}$$

2.3 Electronic state of magnetic ions

Next we proceed the most important example of the appearance of paramagnetic term, which is zero in inert gases. That is, the **magnetic ions**, which have open shells and really big effects on the magnetism like ferromagnetism, etc.

2.3.1 Ground multiplex – Hund's rule –

The orbital with angular momentum l can take the eigenvalue m of z-component as $m = -l, -l+1, \cdots, l$ and with the spin degree of freedom, the number of possible states is $2(2l+1)$. The many-body state accommodating multiple electrons can be indexed with L and S in eq. (2.15), which can be written as (L, S).

These are degenerated for $\mathcal{H}_{\rm L0}$ in eq. (2.1) though the Coulomb interaction $\mathcal{H}_{\rm C}$ causes splitting in (L, S) state. Each of them is degenerated by $(2L+1)(2S+1)$ folds. These are called LS multiplex.

To consider which state is the ground state, we represent the Coulomb interaction as

$$\mathcal{H}_{\rm C} = \frac{1}{2} \sum_{m_1,\cdots,m_4} \sum_{\sigma_1\sigma_2} \left\langle m_1 m_2 \left| \frac{e^2}{4\pi\epsilon_0 r} \right| m_3 m_4 \right\rangle a^\dagger_{m_1\sigma_1} a^\dagger_{m_2\sigma_2} a_{m_3\sigma_3} a_{m_4\sigma_4}, \tag{2.20}$$

where l is not written. The bracket term in the coordinate representation is

$$\left\langle m_1 m_2 \left| \frac{e^2}{4\pi\epsilon_0 r} \right| m_3 m_4 \right\rangle = \int d\boldsymbol{r}_1 d\boldsymbol{r}_2 u^*_{m_1}(\boldsymbol{r}_1) u^*_{m_2}(\boldsymbol{r}_2) \frac{e^2}{4\pi\epsilon_0 |\boldsymbol{r}_1 - \boldsymbol{r}_2|} u_{m_3}(\boldsymbol{r}_2) u_{m_4}(\boldsymbol{r}_1). \tag{2.21}$$

The number of this combination of $(m_1, \cdots, m_4)$ is $5^4 = 625$ for d-orbital and much more for f-orbital. Then we need to consider the contribution of dominant terms. From eq. (2.21), the term of $m_1 = m_2 = m_3 = m_4$ is the largest and

$$\left\langle m_1 m_1 \left| \frac{e^2}{4\pi\epsilon_0 r} \right| m_1 m_1 \right\rangle a^\dagger_{m_1\uparrow} a^\dagger_{m_1\downarrow} a_{m_1\uparrow} a_{m_1\downarrow} = U_0 \sum_m \hat{n}_{m\uparrow} \hat{n}_{m\downarrow} \quad (\hat{n}_{m\sigma} = a^\dagger_{m\sigma} a_{m\sigma}). \tag{2.22}$$

In the rhs, the spin state is $(\uparrow, \downarrow)$ due to the Fermi statistics (the Pauli principle) on the spin-term in eq. (2.20). In consequence, the above represents the effect of the Coulomb repulsion between the electrons with spin $(\uparrow\downarrow)$ accommodated in the same orbital.

The next is the term of $m_1 = m_4 \neq m_2 = m_3$, given as

$$\frac{1}{2} \sum_{m_1 \neq m_2} U(m_1, m_2) \hat{n}_{m1} \hat{n}_{m2} \quad \left(\hat{n}_m = \sum_\sigma n_{m\sigma} \right). \tag{2.23}$$

This represents the Coulomb repulsion between the electrons in different orbitals.

And the next is the case of $m_1 = m_3 \neq m_2 = m_4$. The contribution is written as

$$\frac{1}{2} \sum_{m_1 \neq m_2} \sum_{\sigma_1\sigma_2} J(m_1, m_2) a^\dagger_{m_1\sigma_1} a^\dagger_{m_2\sigma_2} a_{m_1\sigma_2} a_{m_2\sigma_1} = -\frac{1}{2} \sum_{m_1 \neq m_2} J(m_1, m_2) \left(\frac{1}{2} \hat{n}_{m_1} \hat{n}_{m_2} + 2 \boldsymbol{s}_{m_1} \cdot \boldsymbol{s}_{m_2} \right). \tag{2.24}$$

Element	Configuration	Ion	Configuration	L	S
Sc	$3d^1 4s^2$				
Ti	$3d^2 4s^2$	Ti^{3+}, V^{4+}	$3d^1$	2	1/2
V	$3d^3 4s^2$	V^{3+}	$3d^2$	3	1
Cr	$3d^5 4s^1$	Cr^{3+}, V^{2+}	$3d^3$	3	3/2
Mn	$3d^5 4s^2$	Mn^{3+}, Cr^{2+}	$3d^4$	2	2
Fe	$3d^6 4s^2$	Fe^{3+}, Mn^{2+}	$3d^5$	0	5/2
Co	$3d^7 4s^2$	Co^{3+}, Fe^{2+}	$3d^6$	2	2
Ni	$3d^8 4s^2$	Co^{2+}	$3d^7$	3	3/2
Cu	$3d^{10} 4s^1$	Ni^{2+}	$3d^8$	3	1
Zn	$3d^{10} 4s^2$	Cu^{2+}	$3d^9$	2	1/2

Tab. 2.2 Electronic configurations of $3d$metal ions, ground state L and S derived from Hund's rule.

Here, $\boldsymbol{s}_m$ is the spin operator of orbital m, which is already defined in eq. (2.15b). We here write down it again as

$$\boldsymbol{s}_m = \sum_{\sigma_1\sigma_2} \left(\frac{\boldsymbol{\sigma}}{2}\right)_{\sigma_1\sigma_2} a^\dagger_{m\sigma_1} a_{m\sigma_2}. \tag{2.25}$$

In eq. (2.24), the term $2\boldsymbol{s}_{m_1} \cdot \boldsymbol{s}_{m_2}$ appears. At the first sight this is a bit strange. However, if we write the matrix representation for two-electron spin space (2×2=4 dimensional), the lhs and the rhs are the same. Which means this representation is possible.

The matrix element $J(m_1, m_2)$ is called **exchange integral**. By using Fourier transformation of Coulomb potential, we obtain

$$J(m_1, m_2) = \int d\boldsymbol{r}_1 d\boldsymbol{r}_2 u^*_{m_1}(\boldsymbol{r}_1) u_{m_2} \frac{e^2}{4\pi\epsilon_0 |\boldsymbol{r}_1 - \boldsymbol{r}_2|} u_{m_1}(\boldsymbol{r_2}) u^*_{m_2}(\boldsymbol{r_2}) \tag{2.26a}$$

$$= \int d\boldsymbol{r}_1 d\boldsymbol{r}_2 u^*_{m_1}(\boldsymbol{r}_1) u_{m_2} \left[\int d\boldsymbol{q} \frac{e^2}{\epsilon_0 q^2} e^{i\boldsymbol{q}\cdot(\boldsymbol{r}_1 - \boldsymbol{r}_2)}\right] u_{m_1}(\boldsymbol{r_2}) u^*_{m_2}(\boldsymbol{r_2}) \tag{2.26b}$$

$$= \int d\boldsymbol{q} \frac{e^2}{\epsilon_0 q^2} \left| \int d\boldsymbol{r}_1 u^*_{m_1}(\boldsymbol{r}_1) u_{m_2}(\boldsymbol{r}_1) e^{i\boldsymbol{q}\cdot\boldsymbol{r}_1} \right|^2 > 0. \tag{2.26c}$$

That is $J(m_1, m_2)$ is always positive. Hence the two spins in two orbitals tend to be parallel. Most naive explanation is that the electrons in the same state try to avoid each other and as a result the Coulomb energy is lowered.

From the above, the ground multiplex can be determined from the following **Hund's rule**.

Hund's rule

1. Multiplex with maximum S
2. Multiplex with maximum L among those have maximum S

The LS multiplexes in Tab. 2.2 are determined from the Hund's rule.

Appendix 2A: Second quantization method

We hve short review of second quantzation method, which will be frequently used. For the knowledges of the physical meanings, the mathematical proofs, you are recommended to refer to famous textbooks like Ref. [7, 8]. The explanation of the physical meaning in Ref. [1] also has good reputation.

2A.1 Creation and annihilation operators

In **number representation** of a homogeneous multi-particle system, a many-body state is represented by the numbers of particles $\{n_j\}$, where $j = 1, 2, \cdots$ are the indices of single particle states. Let $\boldsymbol{n}$ be the vector of elements $\{n_j\}$ and we write the state in number representation as

$$|\boldsymbol{n}\rangle = |n_1, n_2, \cdots\rangle. \tag{2A.1}$$

When every single-particle state is empty, we call the many-particle state "vacuum" and write it as $|0\rangle$. We consider an operator that add a particle to the j-th state and call it a **creation operator**. Writing a creation operator as $a^\dagger_j$, the definition is given by

$$a^\dagger_j |0\rangle = |1_j\rangle. \tag{2A.2}$$

a_j, the hermitian conjugate of $a^\dagger_j$, decreases the number of particles at j-th state by one. The operation of a_j on the vacuum produces zero. a_j is called an **annihilation operator**.

Henceforth we need to specify the statistics of homogeneous particles. In the case of fermions, a single state can only be occupied with a single particle and the number cannot be increased with repetitive operation of $a_j^\dagger$. Namely, $(a_j^\dagger)^2 = (a_j)^2 = 0$. Similar thought gives $a_j a_j^\dagger|0\rangle = |0\rangle$, $a_j^\dagger a_j|1_j\rangle = |1_j\rangle$. In consequence, the creation and annihilation operators of fermionic particles satisfy the following anti-commutation relations.

$$[a_i, a_j]_+ = [a_i^\dagger, a_i^\dagger]_+ = 0, \quad [a_i, a_j^\dagger]_+ = \delta_{ij}, \tag{2A.3}$$

where $[A, B]_+ = AB + BA$. Then applying the operator $\hat{n}_j \equiv a_j^\dagger a_j$ on the state $|\boldsymbol{n}\rangle$ gives

$$\hat{n}_j|\boldsymbol{n}\rangle = n_j|\boldsymbol{n}\rangle. \tag{2A.4}$$

This is understood by considering the cases of $n_j = 0, 1$. This tells that $\hat{n}_j$ is a **number operator** that has the eigenstates of particle numbers in j-th state.

For bosons, creation and annihilation operators $b_j^\dagger$, b_j satisfy the following commutation relation

$$[b_i, b_j] = [b_i^\dagger, b_i^\dagger] = 0, \quad [b_i, b_j^\dagger] = \delta_{ij}. \tag{2A.5}$$

$b_j|0\rangle = 0$ is the same as fermions. Also the same for number operators.

$$\hat{n}_j|\boldsymbol{n}\rangle = b_j^\dagger b_j|\boldsymbol{n}\rangle = n_j|\boldsymbol{n}\rangle. \tag{2A.6}$$

We can obtain the expression of $|n_j\rangle$ by the creation operator and the vacuum as

$$|n_j\rangle = \frac{1}{\sqrt{n_j!}}(a_j^\dagger)^{n_j}|0\rangle \tag{2A.7}$$

after some algebra to calculate the normalization constant.

2A.2 Expression of operators

In the expression of second quantization, the particle statistics can be represented by the (anti-)commutation relations between creation and annihilation operators. Hence for human, the second quantization expression is generally simpler than the direct treatment of many-body wavefunctions like the Slater determinant. Thus in the discussion of many-body problem, the second quantization is mostly used.

We consider the simplest case, in which a many-body operator is actually written as a sum of single-particle operators. That can be expressed in the coordinate representation as

$$\mathcal{F}(\boldsymbol{r}_1, \boldsymbol{r}_2, \cdots) = \sum_i f(\boldsymbol{r}_i). \tag{2A.8}$$

For fermions, by letting the Slater determinant be $|\psi_{1,2,\cdots}\rangle$, a matrix element is expressed as

$$\langle\psi_{m_1,m_2,\cdots}|\mathcal{F}|\psi_{n_1,n_2,\cdots}\rangle = \sum_i \langle\psi_{m_1,m_2,\cdots}|f(\boldsymbol{r}_i)|\psi_{n_1,n_2,\cdots}\rangle, \tag{2A.9}$$

which contains many complicated terms.

In second quantization, defining an operator

$$\begin{aligned} F &= \sum_{mn} \langle m|f|n\rangle \, a_m^\dagger a_n \\ \langle m|f|n\rangle &= \int d\boldsymbol{r}\phi_m^*(\boldsymbol{r})f(\boldsymbol{r})\psi_n(\boldsymbol{r}), \end{aligned} \tag{2A.10}$$

we can write the matrix element as

$$\langle\psi_{m_1,m_2,\cdots}|\mathcal{F}|\psi_{n_1,n_2,\cdots}\rangle = \langle\boldsymbol{m}|F|\boldsymbol{n}\rangle\,, \tag{2A.11}$$

where $|\boldsymbol{m}\rangle$ are the number representation of corresponding states. The matrix elements and the operators representing the statistics can be treated separately. This gives a better view of the calculation.

For multiparticle operators the same approach is possible. For example in the case of a two-particle operator $g(\boldsymbol{r}_1, \boldsymbol{r}_2)$ we can write

$$G = \frac{1}{2} \sum_{klmn} \langle kl|g|mn\rangle \, a_k^\dagger a_l^\dagger a_n a_m. \tag{2A.12}$$

References

[1] Shinichiro Tomonaga. *The Story of Spin*. University of Chicago Press, 10 1998.

[2] Hans L. Schlafer and Gunter Gliemann. *Basic Principles of Ligand Field Theory*. John Wiley & Sons Ltd, 1 1969.

[3] Walter Greiner. *Quantum Mechanics: An Introduction*. Springer, 2 2009.

[4] Leon Brillouin. A theorem of larmor and its importance for electrons in magnetic fields. *Phys. Rev.*, Vol. 67, pp. 260–266, Apr 1945.

[5] Patricio Sanhueza, Josep Miquel Girart, Marco Padovani, Daniele Galli, Charles L. H. Hull, Qizhou Zhang, Paulo Cortes, Ian W. Stephens, Manuel Fernández-López, James M. Jackson, Pau Frau, Patrick M. Koch, Benjamin Wu, Luis A. Zapata, Fernando Olguin, Xing Lu, Andrea Silva, Ya-Wen Tang, Takeshi Sakai, Andrés E. Guzmán, Ken'ichi Tatematsu, Fumitaka Nakamura, and Huei-Ru Vivien Chen. Gravity-driven magnetic field at $\sim$1000 au scales in high-mass star formation. *The Astrophysical Journal Letters*, Vol. 915, No. 1, p. L10, June 2021.

[6] J. H. Van Vlek. *The Theory Of Electric And Magnetic Susceptibilities*. 08 2015.

[7] Richard P. Feynman. *Statistical Mechanics: A Set Of Lectures (Frontiers in Physics)*. CRC Press, 8 2019.

[8] L. D. Landau. *Quantum Mechanics (Non-Relativistic Theory) Course of Theoretical Physics , Volume 3, Third Edition*. Butterworth-Heinemann, 1 1981.

2.4 LS coupling

We explained Hund's rule through estimation of Coulomb mutual interaction. In addition to these two terms ($\mathcal{H}_0$, $\mathcal{H}_{\rm C}$), the hamiltonian (2.1) for localized electron system in solids, has $\mathcal{H}_{\rm SOI}$ and $\mathcal{H}_{\rm CF}$. It is difficult to treat these simultaneously and we need to treat the term with higher priority and to treat the other as perturbation. First, let us examine the case the effect of $\mathcal{H}_{\rm SOI}$ is stronger than that of $\mathcal{H}_{\rm CF}$. Within this framework, there are several approaches: (i) first the ground state LS multiplex is picked and examine how that is split into sub-levels with $\mathcal{H}_{\rm SOI}$ (**LS coupling** approach); (ii) Single-electron state with spin-orbit interaction is prepared firstly, then the Coulomb effect is taken into account via Hund's rule to find the ground state (**j-j coupling**). This and the next sections are devoted to these two approaches illustrated in Fig. 2.2.

2.4.1 Effect of spin-orbit interaction on single-electron states

Here we revisit the single electron Hamiltonian for relativistic electron. The third term in eq. (1.72) is

$$-\frac{e\hbar\boldsymbol{\sigma}\cdot\boldsymbol{p}\times\boldsymbol{E}}{4m^2c^2}=-\frac{e^2\hbar}{4m^2c^2}\boldsymbol{\sigma}\cdot(\boldsymbol{p}\times\nabla V)=\frac{e^2\hbar}{2m^2c^2}\zeta(r)\boldsymbol{s}\cdot\boldsymbol{l}\equiv\xi(r)\boldsymbol{l}\cdot\boldsymbol{s}, \tag{2.27}$$

where $V(\boldsymbol{r})$ is a potential with spherical symmetry. We first write it as $V(r)$ taking the origin at the center of the potential, then define $\zeta(r)$ as $\nabla V=(\boldsymbol{r}/r)(dV(r)/dr)\equiv\zeta(r)\boldsymbol{r}$, and apply $\boldsymbol{l}=\boldsymbol{r}\times\boldsymbol{p}$ for the above. Assuming it as the Coulomb potential $V(r)=-Ze^2/(4\pi\epsilon_0 r)$, ξ is given by

$$\xi(r)=\frac{Ze^2}{2m^2c^2}\frac{1}{(4\pi\epsilon_0)r^3}, \tag{2.28}$$

which tells that the spin-orbit interaction is important for the atoms with large atomic number Z and for the atomic orbitals with smaller r, namely the orbitals closer to the atomic core. As examples of representative atoms, ions that have

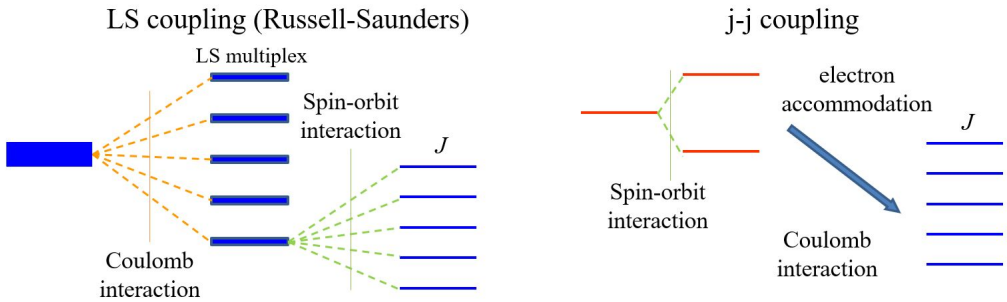

Fig. 2.2 Illustration of two representative approaches. In LS coupling (Russell-Saunders coupling) approach, the ground state LS multiplex split by the Coulomb interaction is further split into the levels with J as the quantum number by the spin-orbit interaction. In j-j coupling approach, spin-orbit interaction is considered at the single-electronic states, then the Coulomb interaction in multi-electron states is taken into account through Hund's rule.

open shells, we have listed $3d$ transition metals and Lanthanoid with $4f$ open shells. The above thought suggests that the approaches of "SOI-first" (both LS and j-j) are more appropriate for Lanthanoid than $3d$ transition metals.

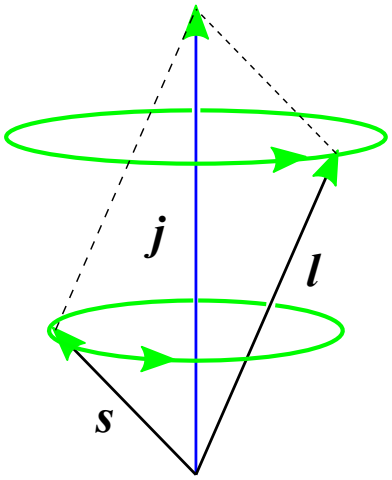

Fig. 2.3 Illustrates precessions of $\boldsymbol{l}$ and $\boldsymbol{s}$ around $\boldsymbol{j}$.

The single-electron Hamiltonian with the SOI is then given by

$$\mathcal{H} = \mathcal{H}_0 + \mathcal{H}_{\rm so} = \frac{\boldsymbol{p}^2}{2m} + V(\boldsymbol{r}) + \xi(r)\boldsymbol{l}\cdot\boldsymbol{s}. \tag{2.29}$$

The Hamiltonian (2.27) does not commute with $\boldsymbol{l}$, $\boldsymbol{s}$, which are no longer constants of motion. This can easily be confirmed from (1.78) and (1.79). On the other hand, commutation relations, e.g,

$$[\boldsymbol{l}\cdot\boldsymbol{s}, \hat{l}_z] = i\hbar(-l_y s_x + l_x s_y), \quad [\boldsymbol{l}\cdot\boldsymbol{s}, \hat{s}_z] = i\hbar(-l_x s_y + l_y s_x) = -[\boldsymbol{l}\cdot\boldsymbol{s}, \hat{l}_z],$$

tell that the total angular momentum

$$\boldsymbol{j} = \boldsymbol{l} + \boldsymbol{s} \tag{2.30}$$

commutes with Hamiltonian (2.27), and is a constant of motion. $\boldsymbol{j}$ satisfies the commutation relations in the same forms as (1.78) and (1.79). Hence it gets directional quantization, and the eigenfunction is indexed by (j, m) as $|j, m\rangle$ $(m = -j, -j+1, \cdots, j)$. $|j, m\rangle$ can be obtained, e.g., in the form of expansion with the eigenfunctions of $\mathcal{H}_0$.

On the other hand, $\boldsymbol{l}^2$, $\boldsymbol{s}^2$ commute with $\boldsymbol{l}\cdot\boldsymbol{s}$, thus with $\mathcal{H}$, making them as constants of motion. $\boldsymbol{l}\cdot\boldsymbol{s}$ is also written as

$$\boldsymbol{l}\cdot\boldsymbol{s} = (\boldsymbol{l}+\boldsymbol{s})\cdot\boldsymbol{s} - \boldsymbol{s}^2 = \boldsymbol{j}\cdot\boldsymbol{s} - \boldsymbol{s}^2.$$

This form tells that $\boldsymbol{s}$ and $\boldsymbol{l}$ have the Zeeman-like term with $\boldsymbol{j}$ (a constant of motion) as magnetic field in eq. (2.9). In a classical picture, $\boldsymbol{l}$ and $\boldsymbol{s}$ precess around $\boldsymbol{j}$ satisfying eq. (2.30) as illustrated in Fig. 2.3. The angular velocity of the precession is proportional to the spin-orbit coupling strength ξ.

The eigenvalues of $\boldsymbol{l}\cdot\boldsymbol{s}$ are obtained from

$$2\boldsymbol{l}\cdot\boldsymbol{s} = (\boldsymbol{l}+\boldsymbol{s})^2 - \boldsymbol{l}^2 - \boldsymbol{s}^2 = \boldsymbol{j}^2 - \boldsymbol{l}^2 - \boldsymbol{s}^2 \tag{2.31}$$

as

$$[j(j+1) - l(l+1) - s(s+1)]/2 = \frac{1}{2}\left[j(j+1) - l(l+1) - \frac{3}{4}\right]. \tag{2.32}$$

Then the energy eigenvalues are given by

$$\epsilon_{nlj} = \epsilon_{nl} + \frac{\eta_{nl}}{2}\left[j(j+1) - l(l+1) - \frac{3}{4}\right], \tag{2.33}$$

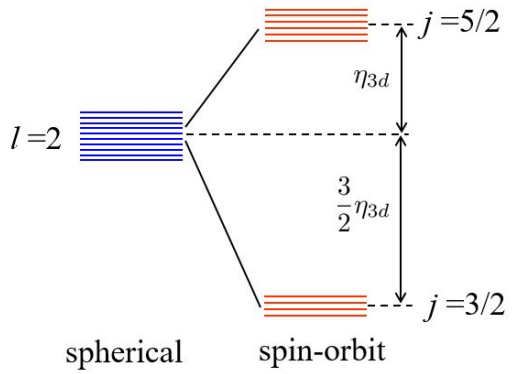

Fig. 2.4 Schematic diagram for splitting of $l = 2$ (i.e. $3d$ orbital) multiplet state with $(2l+1)(2s+1)$ =10 fold degeneracy by the SOI. η_{3d} is the integrated value of eq. (2.34) for $3d$-orbital.

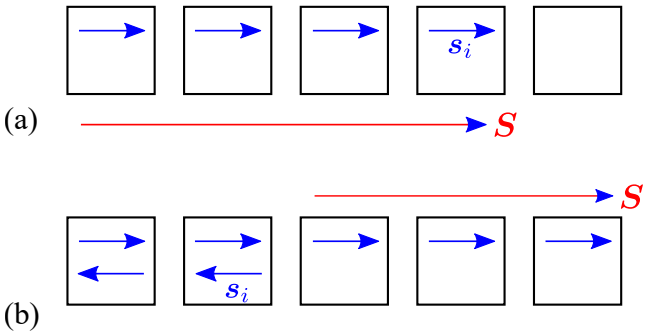

Fig. 2.5 Schematic diagrams of how electrons are packed according to Hund's rules into a degenerate state with the same angular momentum quantum number. (a) The number of electrons is less than or the same as the number of orbitals. (b) The number of electrons is more than that of orbitals. The sum of the orbital contributions corresponding to the spins represented by the arrows in the upper column is zero.

where η_{nl} is the integral of the radial wavefunction and $\xi(r)$, namely

$$\eta_{nl} = \int_0^\infty \xi(r) R_{nl}(r)^2 r^2 dt. \tag{2.34}$$

j can take values $|l \pm 1/2|$, splitting the energy level indicated by (n, l) into two levels. Figure 2.4 shows the case of $3d$ orbital.

2.4.2 Spin-orbit interaction in multi-electron states

The SOI Hamiltonian for a multi-electron system, then can be written as

$$\mathcal{H}_{\rm SOI} = \sum_i \xi(r_i) \boldsymbol{l}_i \cdot \boldsymbol{s}_i \ \rightarrow \ \sum_i \xi_i \boldsymbol{l}_i \cdot \boldsymbol{s}_i \ \rightarrow \ \xi \sum_i \boldsymbol{l}_i \cdot \boldsymbol{s}_i. \tag{2.35}$$

In the above we first replace $\xi(r_i) \rightarrow \xi_i$ because the radial part will be integrated out as in eq. (2.34). Next ξ_i comes out from the summation on i because in an LS-multiplet, the orbitals should have the same radial part. The Coulomb repulsion splits the degenerated levels in the single-electron problem into LS-multiplets. In the previous section, Hund's rule has been derived as a way to find the state in which the effect of Coulomb repulsion is minimized. An LS-multiplet (L, S) still has $(2L+1)(2S+1)$-fold degeneracy due to the freedom of orbital and spin angular momenta.

In the presence of $\mathcal{H}_{\rm SOI}$, just as in the single-electron problem, neither the total orbital angular momentum $\boldsymbol{L}$ nor the total spin angular momentum $\boldsymbol{S}$ (defined in (2.15)) commutes with the Hamiltonian, that is, they are not constants of motion. The total angular momentum defined as

$$\boldsymbol{J} = \boldsymbol{L} + \boldsymbol{S} \tag{2.36}$$

is a constant of motion.

The whole energy level structure is importtant in the discusstion of localized electron systems. For the magnetism, the ground state is particulary important. As noted, in the LS-coupling approach, we first consider the "ground state" LS-multiplet, and examine how this is split by $\mathcal{H}_{\rm SOI}$, find the ground state among them. When the number of electons n is smaller than that of degenerated orbitals $2l+1$ for the orbital angular momentum l, in the ground state every orbital accomodates 0 or 1 electron. Then according to Hund's rule, in the ground state all electron spins are in parallel. Namely a spin dose not depend on orbital index i:

$$\boldsymbol{s}_i = \frac{1}{n}\boldsymbol{S} = \frac{1}{2S}\boldsymbol{S} \quad (n \leq 2l+1). \tag{2.37}$$

Substituting the above into eq. (2.35), we can write

$$\mathcal{H}_{\rm SOI} = \xi \sum_i \boldsymbol{l}_i \cdot \boldsymbol{s}_i = \xi \left(\sum_i \boldsymbol{l}_i \right) \cdot \boldsymbol{s} = \frac{\xi}{2S} \boldsymbol{L} \cdot \boldsymbol{S} \equiv \lambda \boldsymbol{L} \cdot \boldsymbol{S}. \tag{2.38}$$

In the case of $n > 2l+1$, as shown in Fig. 2.5(b), though the electron spins are still in parallel for $2l+1$ electrons, the corresponding orbitals take all possible values of m_l, and the summation over $\boldsymbol{l}_i$ vanishes in (2.38). Hence the residual

Elements (Lanthanoid)	Electronic Configuration atom R	Electronic Configuration ion R^{3+}	L	S	J	Ground state multiplet	g_J
La	$5d6s^2$		0	0	0	$^1S_0$	0
Ce	$4f5d6s^2$	$4f^1$	3	1/2	5/2	$^2F_{5/2}$	6/7
Pr	$4f^36s^2$	$4f^2$	5	1	4	$^3H_4$	4/5
Nd	$4f^46s^2$	$4f^3$	6	3/2	9/2	$^4I_{9/2}$	8/11
Pm	$4f^56s^2$	$4f^4$	6	2	4	$^5I_4$	1/5
Sm	$4f^66s^2$	$4f^5$	5	5/2	5/2	$^6H_{5/2}$	2/7
Eu	$4f^76s^2$	$4f^6$	3	3	0	$^7F_0$	0
Gd	$4f^75d6s^2$	$4f^7$	0	7/2	7/2	$^8S_{7/2}$	2
Tb	$4f^96s^2$	$4f^8$	3	3	6	$^7F_6$	3/2
Dy	$4f^{10}6s^2$	$4f^9$	5	5/2	15/2	$^6H_{15/2}$	4/3
Ho	$4f^{11}6s^2$	$4f^{10}$	6	2	8	$^5I_8$	5/4
Er	$4f^{12}6s^2$	$4f^{11}$	6	3/2	15/2	$^4I_{15/2}$	6/5
Tm	$4f^{13}6s^2$	$4f^{12}$	5	1	6	$^3H_6$	7/6
Yb	$4f^{14}6s^2$	$4f^{13}$	3	1/2	7/2	$^2F_{7/2}$	8/7
Lu	$4f^{14}5d6s^2$	$4f^{14}$	0	0	0	$^1S_0$	0

Tab. 2.3 The electron configuration of the lanthanoid ion and the basis multiplex of the ion. Spectroscopic symbols are also listed for the ground state. A spectroscopic symbol $^{2S+1}L_J$ expresses a multielectron state indexed by $(L, S.J)$. $2S+1$ and J are given in Arabic numbers, and L is given from the correspondence $0, 1, 2, 3, \cdots$ with symbols $S, P, D, F, \cdots$.

$n-(2l+1)$ spins and orbitals actually contribute the SOI. Those effective spins are in anti-parallel states written as $-\boldsymbol{s}$, where $\boldsymbol{s}$ is defined in eq. (2.37). The above discussion is summarized in the following form [*1].

$$\mathcal{H}_{\rm SOI} = \xi \left[\left(\sum_{i=1}^{2l+1} \boldsymbol{l}_i \right) \cdot \boldsymbol{s} - \left(\sum_{i=2l+2}^{n} \boldsymbol{l}_i \right) \cdot \boldsymbol{s} \right] = -\frac{\xi}{2S} \boldsymbol{L} \cdot \boldsymbol{S} = -\lambda \boldsymbol{L} \cdot \boldsymbol{S}. \tag{2.39}$$

In the above we have found that the SOI on the ground state LS-multiplet found from Hund's rule can be expressed in the same form as that on a single-electron state by using $(\boldsymbol{L}, \boldsymbol{S}, \boldsymbol{J})$. Then as in the case of single electron problem, the split states of the ground LS-multiplet with $(2L+1)(2S+1)$-fold degeneracy can be indexed by J, the eigenvalue of $\boldsymbol{J}$. Possible value of J are from the definition,

$$J = |L-S|, |L-S|+1, \cdots, L+S. \tag{2.40}$$

The expectation value of $\boldsymbol{L} \cdot \boldsymbol{S}$ is obtained just as in (2.31) and (2.32). The result is

$$\boldsymbol{L} \cdot \boldsymbol{S} = \frac{1}{2}(\boldsymbol{J}^2 - \boldsymbol{L}^2 - \boldsymbol{S}^2) = \frac{1}{2}[J(J+1) - L(L+1) - S(S+1)]. \tag{2.41}$$

Then from eq. (2.38) and eq. (2.39), the ground state is the state for $J = |L-S|$ in the case of $n \leq 2l+1$, and that is the state for $J = |L-S|$ in the case of $n > 2l+1$.

The above is applied to obtain the multiplet ground states thus obtained for lanthanoid are listed in Tab. 2.3. These atoms often constitute (compound) ionic insulators. In many cases, $5d$, $6s$ electrons on the outer shells and also a $4f$ electron are emitted. In such ions, the outmost shell composed of $5s$, $5p$ electrons is closed just as Xe while $4f$ electrons on the open shell still exist *inside* the outmost shell. This situation is advantageous for localized electron system in

[*1] Such simplification of operator form can be generalized into the method of "operator equivalent" by Stevens[1].

spherical potential because the effect of $\mathcal{H}_{\rm CF}$ is comparatively weak[2]. The SOI has strong effect and the LS-coupling approach is a good approximation in most cases with some exceptions[3].

The eigenstates with quantum numbers J and M, composed of (L, S)-multiplet is formally written as

$$|J, M\rangle = \sum_{M_l M_s} \langle L, M_l; S, M_s | J, M\rangle \, |L, M_l; S, M_s\rangle, \tag{2.42}$$

where $\langle L, M_l; S, M_s | J, M\rangle$ are **Clebsch-Gordan** or **Wigner** coefficients.

So far we have assumed the second quantization formalism and estimated the matrix elements on the assumption of "independent calculation of matrix elements and particle statistics." We can write, e.g., the second quantization representation of $\mathcal{H}_{\rm SOI}$ on the orbital (n, l), as

$$\mathcal{H}_{\rm SOI} = \sum_{mm'\sigma\sigma'} \lambda_{nl}(m\sigma, m'\sigma') a^\dagger_{m\sigma} a_{m'\sigma'}, \tag{2.43a}$$

$$\lambda_{nl}(m\sigma, m'\sigma') \equiv \frac{Z_{\rm eff} e^2 \hbar^2 \langle r^3 \rangle}{2m^2 c^2 (4\pi\epsilon_0)} \langle m|\boldsymbol{l}|m'\rangle_{nl} \cdot \left(\frac{\boldsymbol{\sigma}}{2}\right)_{\sigma\sigma'}. \tag{2.43b}$$

Here for the spherical potential, we take the effect of screening by core electrons into account by changing Z into an effective atomic number $Z_{\rm eff}$ to get $V(r) = -Z_{\rm eff} e^2/(4\pi\epsilon_0 r)$.

2.5 j-j coupling

As mentioned in the beginning of the previous section, the j-j coupling approach starts from the single-electron states in which the SOI is already included as in Fig. 2.2. In the thought similar to the derivation of Hund's rule in Sec. 2.3.1, the ground state in which the effect of Coulomb interaction is taken into account, is obtained for the electron configuration that maximizes the quantum number J.

Let us see the case of Pr^{3+} ($(4f)^2$) as an example. f-electron has $l = 3$, then $j = 3 \pm 1/2 = 5/2, 7/2$. The single electron ground state is thus $j = 5/2$. The electron configuration with the maximum J is $j = 5/2, 3/2$ then $J_{\rm max} = 4$. This value of J agrees with that in the LS-coupling approach (Tab. 2.3). This state in number representation is obtained as

$$|J, M\rangle = |4, +4\rangle = a^\dagger_{+5/2} a^\dagger_{+3/2} |0\rangle. \tag{2.44}$$

From eq. (2.42), the creation operator of $j = 5/2$ and $j_z = m$ state, $a^\dagger_{j_z}$ can be represented by the creation operator $a^\dagger_{ms}$ of states $(l = 3, m, s)$ as

$$a^\dagger_{j_z} = \sum_{m,s} \langle 3, m; 1/2, s | 5/2, j_z\rangle \, a^\dagger_{ms} = \sqrt{\frac{7 + 2j_z}{14}} a^\dagger_{j_z+1/2\downarrow} - \sqrt{\frac{7 - 2j_z}{14}} a^\dagger_{j_z-\uparrow}. \tag{2.45}$$

The way of approximation is different for j-j coupling and LS-coupling. Hence they give different ground states. Although according to the report ref. [4], they have large overlaps to each other. Care should be taken for the following. As will be seen in the next section, in LS-coupling paramagnetic moment expressed as $\boldsymbol{\mu} = \mu_{\rm B}(\boldsymbol{L} + g\boldsymbol{S})$ is not parallel to $\boldsymbol{J} = \boldsymbol{L} + \boldsymbol{S}$ due to the g-factor. Hence $\boldsymbol{\mu}$ precesses around $\boldsymbol{J}$ and the coefficient is given as the average. In j-j coupling $\boldsymbol{\mu}$ is given as the sum of electronic magnetic moments. Therefore the g-factor is the same as that of single electron. Namely l in the discussion of LS-coupling is replaced with j, thus $(2j + 1)/2(j + 1)$ for $n \leq 2j + 1$ and $(2j + 1)/2J$ for $n > 2j + 1$.

2.6 Paramagnetism generated by magnetic ions

As mentioned, $\mathcal{H}_{\rm CF}$ is important for magnetic ions with an open-shell structure of $3d$ electrons, but before proceeding to the theoretical examination, we will apply the LS-coupling approach to paramagnetism and examine to what extent it can explain the experiements.

2.6.1 Free local moment and Curie law

The LS-coupling approach is a tool to find the ground state of magnetic ions in crystals. Hence we examine the behavior of magnetization in a simple model of magnetic moments free to each other.

The Hamiltonian in the first order of mgnetic field is from eq. (1.75b)

$$\mathcal{H}_1 = \mu_{\rm B}(\boldsymbol{L} + g\boldsymbol{S}) \cdot \boldsymbol{B}. \tag{2.46}$$

On the other hand, in the ground multiplet state in the LS-coupling, $\boldsymbol{J}$ is the angular momentum quantum number. The main term thus should be in the form of

$$\mathcal{H}_1 = g_j \mu_{\rm B} \boldsymbol{J} \cdot \boldsymbol{B}, \tag{2.47}$$

where the coefficient g_J includes various effects. Comparison of these two, $g_J\boldsymbol{J} = \boldsymbol{L} + g\boldsymbol{S}$, $\boldsymbol{J} = \boldsymbol{L} + \boldsymbol{S}$, we reach

Landé g-factor

$$g_J = \frac{1+g}{2} - \frac{g-1}{2}\frac{L(L+1) - S(S+1)}{J(J+1)}. \tag{2.48}$$

i This g_J is called **Landé g-factor**. g_J is listed in Tab. 2.3 for lanthanoid. As already noted, this expression is obtained within the narrow space of ground state in LS-coupling.

The expectation value of magnetic moment $-g_j\mu_{\rm B}\boldsymbol{J}$ is

$$M = \langle -g_j\mu_{\rm B}J_z\rangle = -\frac{\mathbf{Tr}[g_j\mu_{\rm B}J_z \exp(-g_j\mu_{\rm B}J_zB/k_{\rm B}T)]}{{\rm Tr}[\exp(-g_j\mu_{\rm B}J_zB/k_{\rm B}T)]} = k_{\rm B}T\frac{\partial}{\partial B}\log\left[{\rm Tr}\left(\exp\frac{-g_j\mu_{\rm B}J_zB}{k_{\rm B}T}\right)\right], \tag{2.49}$$

with taking the field along z-axis. The partition function is calculated as

$${\rm Tr}\left(\exp\frac{-g_j\mu_{\rm B}J_zB}{k_{\rm B}T}\right) = \frac{\sinh\left[\dfrac{1}{2k_{\rm B}T}g_J\mu_{\rm B}\left(J+\dfrac{1}{2}\right)B\right]}{\sinh(g_J\mu_{\rm B}B/2k_{\rm B}T)}. \tag{2.50}$$

From the above, the magnetization per a single ion M is obtained as

$$M = g_J\mu_{\rm B}JB_J\left(\frac{g_J\mu_{\rm B}JB}{k_{\rm B}T}\right), \tag{2.51}$$

where $B_J(x)$ is called **Brillouin function** given by

Brillouin function

$$B_J(x) = \frac{2J+1}{2J}\coth\frac{2J+1}{2J}x - \frac{1}{2J}\coth\frac{x}{2J}. \tag{2.52}$$

The functional behavior is drawn in Fig. 2.6.

In the case of $x \ll 1$ (weak field, high temperature), the Brillouin function can be approximated as $B_J(x) \sim (J+1)x/3J$, then we reach the **Curie law**:

$$\chi = \frac{dM}{dB} = (g_J\mu_{\rm B})^2\frac{J(J+1)}{3k_{\rm B}T}, \tag{2.53}$$

which is also obtained in the classical theory.

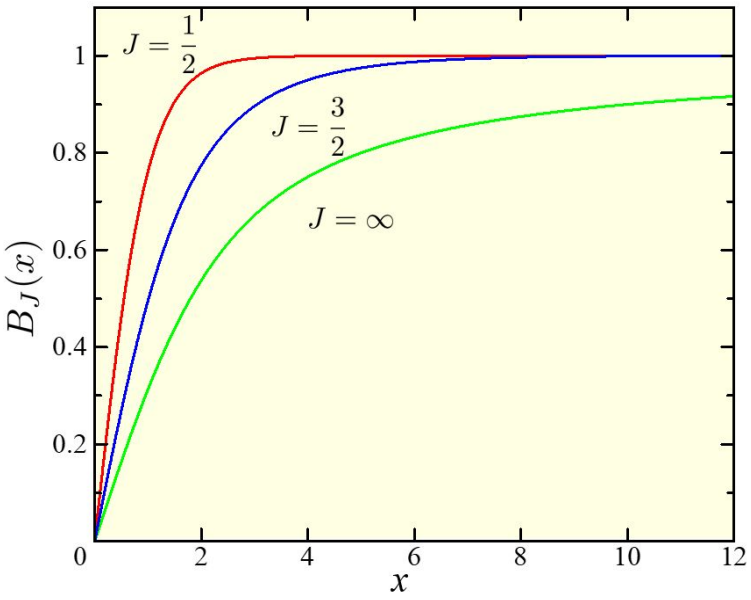

Fig. 2.6 Brillouin function(2.52) for $J = 1/2, 3/2, \infty$.

2.6.2 Comparison with experiments: magnetization curve

Figure 2.7 shows well-known experimental results, in which the magnetizations of alums (sulfate) with various magnetic ions are successfully fit to the Brillouin function. A systematic response to expected values of J is observed.

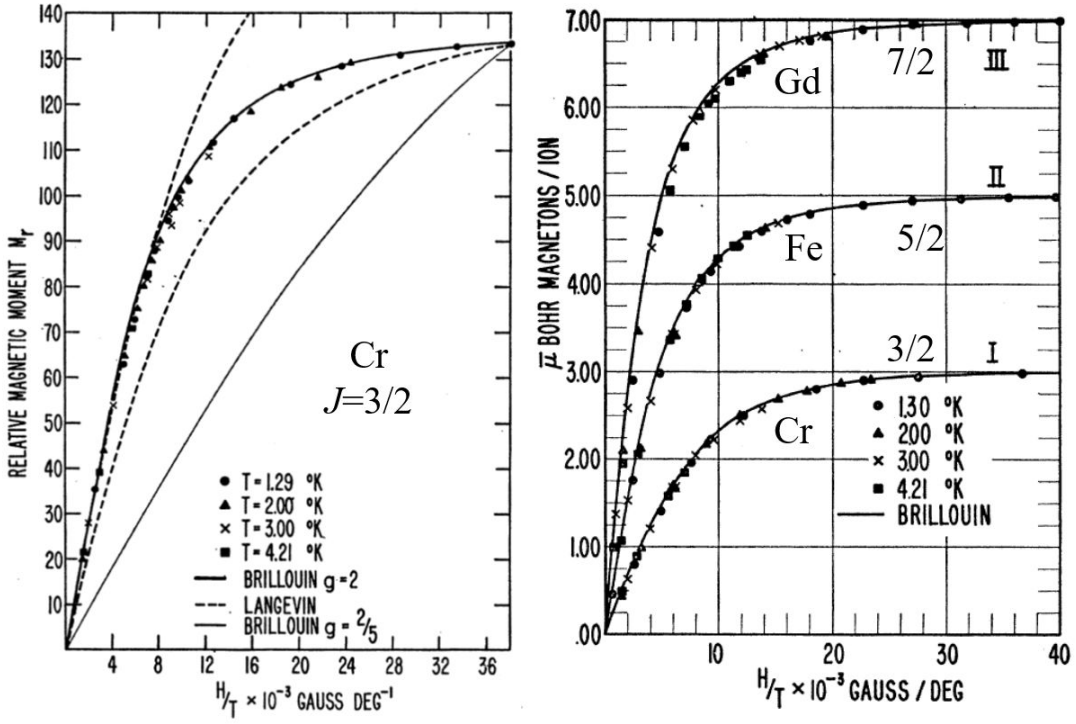

Fig. 2.7 Fittings of the Brillouin function to the magnetic field and temperature dependencies of magnetization of various paramagnetic salt (sulfates (alum) with various magnetic ions). Left: Cr ($J = 3/2$). Annotation of "Langevin" means the Langevin function corresponding to $J = \infty$ in the Brillouin function. Right: The same experiments for Cr ($J = 3/2$), Fe ($J = 5/2$), Gd ($J = 7/2$). From [5].

Configuration		ion	p (exp.)	$g_J[J(J+1)]^{1/2}$	$2[S(S+1)]^{1/2}$
$3d^1$	$^2D_{3/2}$	V^{4+}	1.8	1.55	1.73
$3d^2$	$^3F_2$	V^{3+}	2.8	1.63	2.83
$3d^3$	$^4F_{3/2}$	V^{2+}	3.8	0.77	3.87
		Cr^{3+}	3.7	0.77	3.87
		Mn^{4+}	4.0	0.77	3.87
$3d^4$	$^5D_0$	Cr^{2+}	4.8	0	4.90
		Mn^{3+}	5.0	0	4.90
$3d^5$	$^6S_{5/2}$	Mn^{2+}	5.9	5.92	5.92
		Fe^{3+}	5.9	5.92	5.92
$3d^6$	$^5D_4$	Fe^{2+}	5.4	6.7	4.90
$3d^7$	$^4F_{9/2}$	Co^{2+}	4.8	6.63	3.87
$3d^8$	$^3F_4$	Ni^{2+}	3.2	5.59	2.83
$3d^9$	$^2D_{5/2}$	Cu^{2+}	1.9	3.55	1.73

Tab. 2.4 Comparison of effective Bohr magneton number p (eq. (2.55)) obtained in experiments, that given by the LS-coupling approach (2.54), and that by "spin-only" model for $3d$ transition metal ions. The data are taken from [6], [7].

Configuration		ion	p (exp.)	$g_J[J(J+1)]^{1/2}$	$2[S(S+1)]^{1/2}$
$4f^1$	$^2F_{5/2}$	Ce^{3+}	2.5	2.54	2.56
$4f^2$	$^3H_4$	Pr^{3+}	3.6	3.58	3.62
$4f^3$	$^4I_{9/2}$	Nd^{3+}	3.8	3.62	3.68
$4f^5$	$^6H_{5/2}$	Sm^{3+}	1.5	0.84	1.53
$4f^6$	$^7F_0$	Eu^{3+}	3.6	0.00	3.40
$4f^7$	$^8S_{7/2}$	Gd^{3+}	7.9	7.94	7.94
$4f^8$	$^7F_0$	Tb^{3+}	9.7	9.72	9.7
$4f^9$	$^6H_{15/2}$	Dy^{3+}	10.5	10.65	10.6
$4f^{10}$	$^5I_8$	Ho^{3+}	10.5	10.61	10.6
$4f^{11}$	$^4I_{15/2}$	Er^{3+}	9.4	9.58	9.6
$4f^{12}$	$^3H_6$	Tm^{3+}	7.2	7.56	7.6
$4f^{13}$	$^2F_{7/2}$	Yb^{3+}	4.5	4.54	4.5

Tab. 2.5 Comparison of effective Bohr magneton number p (eq. (2.55)) obtained in experiments, that given by the LS-coupling approach (2.54), and that by "spin-only" model for $4f$ lanthanoid. The data are taken from [6], [7].

2.6.3 Effective Bohr magneton number

Another check of the theory is the effective Bohr magneton number p defined from the inverse proportionality constant C to temperature from the Curie law. In eq. (2.53) we write

$$p = g_j\sqrt{J(J+1)}, \tag{2.54}$$

then p in the theory is

$$p = \sqrt{3k_{\mathrm{B}}C}/\mu_{\mathrm{B}}. \tag{2.55}$$

In Tab. 2.4 and in Tab. 2.5, we compare effective Bohr magneton number p (eq. (2.55)) obtained in experiments, that given by the LS-coupling approach (2.54), and that by "spin-only" model for $3d$ transition metal ions and $4f$ lanthanoid respectively.

In the case of lanthanoid in Tab. 2.5, the experimental values of p is well explained by $g_J\sqrt{J(J+1)}$ obtained from the LS-coupling other than Eu^{3+}, Sm^{3+}. On the other hand, in the case of $3d$ transition metals, the experiments differ so much from $g_J\sqrt{J(J+1)}$, rather they are close to "spin-only" $2\sqrt{S(S+1)}$. That looks as if $L = 0$ and the phenomenon

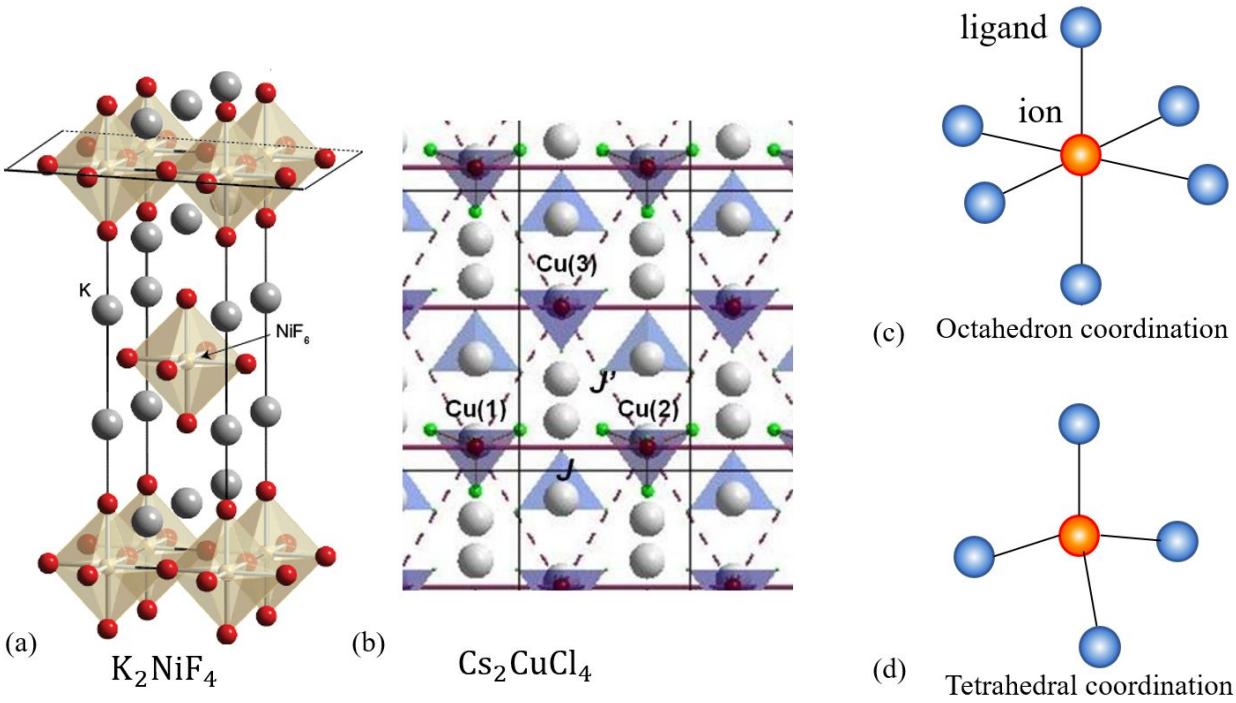

Fig. 2.8 (a) Crystal structure of K_2NiF_4, in which Ni ion has an octahedron coordination. (b) Crystal structure of Cs_2CuCl_4, in which Cu ion has a tetrahedron coordination. (c) Schematic view of octahedron coordination. (d) Schematic view of tetrahedron coordination.

is called "quenching of orbital angular moment." In $3d$ electron systems, the difference from the LS-coupling is so large that it is also difficult to explain with j-j coupling.

As mentioned above, the $4f$ electron system is relatively inside the atomic structure even though the shell is open, the influence of the surroundings is small, and the approximation of the lone electron system is relatively small. Accordingly, it is indicated that the breakdown of LS-coupling approach in $3d$ electron systems is considered to be due to the effect of $\mathcal{H}_{\rm CF}$. Therefore, next, let us consider incorporating the influence of the crystal field from the beginning.

2.7 Magnetic ions in crystal fields

Magnetic atoms (atoms of open electron shells) exist as positive ions in many insulators with strong paramagnetism. Such ions are surrounded by negative ions. An example in Fig. 2.8(a) is K_2NiF_4, in which structure Ni ion is surrounded by F ions in octahedron coordination. Figure 2.8(c) shows a schematic view. As annotated, the surrounding ions or molecules are called **ligand**. Another example in (b) is Cs_2CuCl_4, in which structure Cu ion is surrounded in tetrahedron coordination. These two are the representative coordination.

2.7.1 Level splitting by octahedron coordination

Let us consider the octahedron coordination in Fig. 2.8(c) in a simplest way. We take the coordinate origin at the ion, and ligand ions are at $(\pm R, 0, 0)$, $(0, \pm R, 0)$, $(0, 0, \pm R)$. The vectors pointing them are written as $\boldsymbol{R}_i = (R, \theta_i, \varphi_i)$ and the potential generated by the ligands is written as

$$v_{\rm c}(\boldsymbol{r}) = \sum_i \frac{Z_i e^2}{|\boldsymbol{r} - \boldsymbol{R}_i|} = \sum_i \frac{Ze^2}{\sqrt{r^2 + R^2 - 2Rr\cos\omega_i}}. \tag{2.56}$$

Here we take CGSesu for the simpler form of Coulomb potential. In the polar coordinate, (θ_i, φ_i) are

$$(\pi/2, 0),\ (\pi/2, \pi/2),\ (0, 0),\ (\pi/2, \pi),\ (\pi/2, 3\pi/2),\ (\pi, 0) \tag{2.57}$$

for $i = 1 \sim 6$.

We assume that the averaged distance of $3d$ electrons from the nucleus is sufficiently shorter than R. Then $v_{\rm c}$ can be expanded with r/R as

$$v_{\rm c}(\boldsymbol{r}) = \sum_i \frac{Ze^2}{R} \sum_{k=0}^{\infty} \left(\frac{r}{R}\right)^k P_k(\cos\omega_i), \tag{2.58}$$

where $P_k(\cos\omega_i)$ are Legendre functions defined as

$$P_n(x) = \frac{1}{2^n n!} \frac{d^n}{dx^n}[(x^2 - 1)]. \tag{2.59}$$

Apparently these are the expansion coefficients of

$$\frac{1}{\sqrt{1 - 2xt + t^2}} = \sum_{n=0}^{\infty} P_n(x) t^n. \tag{2.60}$$

From an identity of spherical harmonic function $Y_{km}(\theta, \varphi)$,

$$P_k(\cos\omega_i) = \frac{4\pi}{2k+1} \sum_{m=-k}^{k} Y_{km}(\theta, \varphi) Y^*_{km}(\theta_i, \varphi_i). \tag{2.61}$$

Note ω_i is a function of $\boldsymbol{r}$. This results in dropping of i from the argument in the first Y_{km}. Here we define two functions:

$$T_{km} \equiv \sqrt{\frac{4\pi}{2k+1}} \frac{Ze^2}{R^{k+1}} \sum_i Y_{km}(\theta_i, \varphi_i), \quad C_{km} \equiv \sqrt{\frac{4\pi}{2k+1}} Y_{km}(\theta, \varphi), \tag{2.62}$$

with which $v_c(\boldsymbol{r})$ is written as

$$v_c(\boldsymbol{r}) \sum_{k=0}^{\infty} \sum_{m=-k}^{k} r^k T_{km} C_{km}(\theta, \varphi). \tag{2.63}$$

From the symmetry of positions (2.57), $T_{km} = 0$ for odd m. Others are

$$T_{k0} = \sqrt{\frac{2}{2k+1}} \frac{Ze^2}{R^{k+1}} \left[\Theta_{k0}(0) + 4\Theta_{k0}\left(\frac{\pi}{2}\right) + \Theta_{k0}(\pi)\right], \tag{2.64a}$$

$$T_{km} = \sqrt{\frac{8}{2k+1}} \frac{Ze^2}{R^{k+1}} \Theta_{km}\left(\frac{\pi}{2}\right)\left(1 + \cos\frac{m\pi}{2}\right) \quad (m\text{: even}), \tag{2.64b}$$

where $\Theta(\theta)_{km}$ are defined as

$$Y_{km}(\theta, \varphi) = \Theta_{km}(\theta) e^{im\varphi}. \tag{2.65}$$

From the form of $\Theta(\theta)_{km}$, T_{km}'s are also zero for odd k.

From above, we reach the expression to the fourth order of k:

$$v_{\rm c}(\boldsymbol{r}) = \frac{6Ze^2}{R} + \frac{2}{5} Der^4 \left[C_{40}(\theta, \varphi) + \sqrt{\frac{5}{14}}(C_{44}(\theta, \varphi) + C_{4-4}(\theta, \varphi))\right], \tag{2.66}$$

where

$$D = \frac{35Ze}{4R^5}. \tag{2.67}$$

Let $v_c b(\boldsymbol{r})$ be the potential without the energy shift term (the first term in eq. (2.66)). We also restore $v_c b(\boldsymbol{r})$ into the expression in cartesian coordinate, then obtain

$$v_{\rm cb}(\boldsymbol{r}) = eD\left(x^4 + y^4 + z^4 - \frac{3}{5} r^4\right). \tag{2.68}$$

Appendix 3A: Isolated electron systems and point group

3A.1 Definition of group

When the operation $*$ is defined between any elements of a set A and the following conditions are satisfied, we call A a "group" with respect to $*$.

1. $\forall a_1,\ a_2 \in A\ \{a_1 * a_2 \in A\}$ (closed for the operation *)
2. $\forall a_1.\ a_2,\ a_3 \in A\ \{(a_1 * a_2) * a_3 = a_1 * (a_2 * a_3)\}$ (associative law).
3. $\exists E \in A\ \{\forall a_1 \in A\ \{a_1 E = E a_1 = a_1\}\}$ (existence of unit element).
4. $\exists a_1^{-1} \in A\ \{\forall a_1 \in A\ \{a_1 a_1^{-1} = a_1^{-1} a_1 = E\}\}$ (existence of the inverse element).

When elements a_i, a_j of a group A are written as $a_i = a a_j a^{-1}$, where a is also an element of A, we say a_i and a_j are conjugate to each other. Generally a group is classified into classes, which are sets of conjugate elements.

An element of a group a_i has a corresponding square matrix $D(a_i)$ and the operation $a * b = c$ is projected to $D(a)D(b) = D(c)$. We call $D(a_i)$ as a representation of group A. There are infinite number of representations. When a square matrix S transfers as $D'(a_i) = S^{-1} D(a_i) S$, we call $D'(a_i)$ an equivalent representation to $D(a_i)$. The direct sum of $D^{(1)}$ and $D^{(2)}$ is defined as

$$\forall a_i :\ D(a_i) = \begin{pmatrix} D^{(1)}(a_i) & 0 \\ 0 & D^{(2)}(a_i) \end{pmatrix},$$

which is expressed as $D = D^{(1)} \oplus D^{(2)}$. The above is summarized as "D is reduced to $D^{(1)}$ and $D^{(2)}$ by equivalent conversion with S." Expressions that cannot be further reduced are called irreducible expressions. Expression of an element a can be written as $D_{ij}(a) = \langle \chi_i | a | \chi_j \rangle$ by using a basis $|\chi_i\rangle$ of expression. Equivalent conversion matrix S is a basis transformation matrix. When a is an operator, the matrix representation with basis $|\chi_i\rangle$ is χ-expression of a.

3A.2 Symmetry operations of point group

A set of symmetry operations around a point in space is called a point group.

E	:	Identical operation
C_n	:	Rotation of $2\pi/n$
C_2'	:	π rotation around two-fold axis perpendicular to the principal axis. Written as C_2' or U_2 and called Umklappung.
I	:	Space inversion ($\boldsymbol{r} \to -\boldsymbol{r}$)
σ	:	Mirroring
IC_n	:	Circumference. Space inversion after rotation of $2\pi/n$.
S_n	:	Improper rotation. Mirroring after rotation of $2\pi/n$.

(Continue to next time)

Appendix 3B: Clebsch-Gordan coefficient

Students must have learned about coupling of angular momentum in elementary quantum mechanics. But here we have a short review. Even in classical mechanics, additive quantities should be summed up in the coupled system. In the case of angular momentum, they should be summed up as vectors. In quantum mechanics, the operator of total angular

momentum is written as the sum of angular momentum operators. However in quantum mechanics, due to the directional quantization, eigenfunctions and eigenvalues are not the sums of each eigenfunction and eigenvalue.

3B.1 General treatment

Let $\hat{\boldsymbol{j}}_1$, $\hat{\boldsymbol{j}}_2$ be independent angular momentums, and consider simultaneous eigenstates $|j_i^2, m_i\rangle$ of operators $\hat{\boldsymbol{j}}_1^2$, $\hat{j}_{iz}$ $(i = 1, 2)$. We write a wavefunction of the coupled system as

$$\psi = |j_1^2, m_1\rangle|j_2^2, m_2\rangle. \tag{3B.1}$$

The total angular momentum $\hat{\boldsymbol{J}}$ of the coupled system is

$$\hat{\boldsymbol{J}} = \hat{\boldsymbol{j}}_1 + \hat{\boldsymbol{j}}_2. \tag{3B.2}$$

However, ψ in eq. (3B.1) is not an eigenstate of, e.g., $\hat{\boldsymbol{J}}^2$ apparently. From the independence of $\hat{\boldsymbol{j}}_1$, $\hat{\boldsymbol{j}}_2$ (thus they commute each other), and from the general properties of angular momentum, $[\hat{\boldsymbol{J}}^2, \hat{J}_z]$, $[\hat{\boldsymbol{j}}_1^2, \hat{\boldsymbol{j}}_2^2]$ are apparently zero, and the following commutation relation can be proven.

$$[\hat{\boldsymbol{J}}^2, \hat{\boldsymbol{j}}_\alpha^2] = [\hat{J}_z, \hat{\boldsymbol{j}}_\alpha^2] = 0. \tag{3B.3}$$

Simultaneous eigenstates of $\hat{\boldsymbol{J}}^2$, $\hat{J}_z$, $\hat{\boldsymbol{j}}_1^2$, $\hat{\boldsymbol{j}}_2^2$ can be obtained from basis transformation from eq. (3B.1) as

$$|J^2, M, j_1^2, j_2^2\rangle = \sum_{m_1=-j_1}^{j_1} \sum_{m_2=-j_2}^{j_2} C^{JM}_{j_1 m_1 j_2 m_2} |j_1^2, m_1\rangle|j_2^2, m_2\rangle, \tag{3B.4}$$

where $C^{JM}_{j_1 m_1 j_2 m_2}$ are called **Clebsch–Gordan coefficients**.

3B.2 Coupling of two spins

For general way to find $C^{JM}_{j_1 m_1 j_2 m_2}$, refer to textbooks. Instead we obtain them for the simplest case of $j_1 = j_2 = 1/2$, namely two spins. We take $\hat{\boldsymbol{s}}_i$ $(i = 1, 2)$ for the two spin operators and write the total spin operator as

$$\hat{\boldsymbol{S}} = \hat{\boldsymbol{s}}_1 + \hat{\boldsymbol{s}}_2. \tag{3B.5}$$

Because $\hat{\boldsymbol{s}}_1$ commutes with $\hat{\boldsymbol{s}}_2$,

$$\hat{\boldsymbol{S}}^2 = \hat{\boldsymbol{s}}_1^2 + 2\hat{\boldsymbol{s}}_1 \cdot \hat{\boldsymbol{s}}_2 + \hat{\boldsymbol{s}}_2^2, \qquad \hat{S}_z = \hat{s}_{1z} + \hat{s}_{2z}. \tag{3B.6}$$

First, for $\hat{S}_z$ we see

$$\hat{S}_z \begin{pmatrix} |\uparrow_1\rangle|\uparrow_2\rangle & |\uparrow_1\rangle|\downarrow_2\rangle \\ |\downarrow_2\rangle|\uparrow_2\rangle & |\downarrow_1\rangle\downarrow_2\rangle \end{pmatrix} = \begin{pmatrix} |\uparrow_1\rangle|\uparrow_2\rangle & 0 \\ 0 & -|\downarrow_1\rangle|\downarrow_2\rangle \end{pmatrix}. \tag{3B.7}$$

Therefore the eigenvalues of $\hat{S}_z$ are ± 1, 0 with two-fold degeneracy. The "size" of $\boldsymbol{S}$, S is then 0 or 1. Next, generally for the operator $\hat{\boldsymbol{s}}$ of spin 1/2

$$\hat{\boldsymbol{s}}^2 = \hat{s}_x^2 + \hat{s}_y^2 + \hat{s}_0^2 = \frac{3}{4}\begin{pmatrix} 1 & 0 \\ 0 & 1 \end{pmatrix} \tag{3B.8}$$

holds. In $\hat{\boldsymbol{S}}^2$ $\hat{\boldsymbol{s}}_1^2 + \hat{\boldsymbol{s}}_2^2$ are 3/2

$\hat{\boldsymbol{s}}_1 \cdot \hat{\boldsymbol{s}}_2 \hat{\boldsymbol{s}}_1 \cdot \hat{\boldsymbol{s}}_2 \hat{\boldsymbol{s}}_1 \cdot \hat{\boldsymbol{s}}_2 \hat{\boldsymbol{s}}_1 \cdot \hat{\boldsymbol{s}}_2 \hat{\boldsymbol{s}}_1 \cdot \hat{\boldsymbol{s}}_2$, Residual $\hat{\boldsymbol{s}}_1 \cdot \hat{\boldsymbol{s}}_2$ are calculated as follows. For simplicity we use expression $|\uparrow_1\rangle|\downarrow_2\rangle = |\uparrow\downarrow\rangle$.

$$\hat{\boldsymbol{s}}_1 \cdot \hat{\boldsymbol{s}}_2 \begin{pmatrix} |\uparrow\uparrow\rangle & |\uparrow\downarrow\rangle \\ |\downarrow\uparrow\rangle & |\downarrow\downarrow\rangle \end{pmatrix} = \frac{1}{4}\begin{pmatrix} .|\uparrow\uparrow\rangle & -|\uparrow\downarrow\rangle + 2|\downarrow\uparrow\rangle \\ 2|\uparrow\downarrow\rangle - |\downarrow\uparrow\rangle & |\downarrow\downarrow\rangle \end{pmatrix}.$$

Because neither$|\uparrow\downarrow\rangle$ nor $|\downarrow\rangle|\uparrow\rangle$ is not eigenstates, this part should be diagonalized by transformation. The results are simply

$$\chi_{\pm} \equiv |\uparrow\downarrow\rangle \pm |\downarrow\uparrow\rangle. \tag{3B.9}$$

This is easily confirmed as

$$\hat{\boldsymbol{s}}_1 \cdot \hat{\boldsymbol{s}}_2 \chi_+ = (1/4)\chi_+, \qquad \hat{\boldsymbol{s}}_1 \cdot \hat{\boldsymbol{s}}_2 \chi_- = (3/4)\chi_-. \tag{3B.10}$$

From the above, the eigenvalues of $\hat{\boldsymbol{S}}^2$ are 0, 2, the eigenfunctions are

$$\begin{aligned} &|1,-1\rangle = |\downarrow\downarrow\rangle, \quad |1,0\rangle = \frac{1}{\sqrt{2}}(|\uparrow\downarrow\rangle + |\downarrow\uparrow\rangle), \quad |1,1\rangle = |\uparrow\uparrow\rangle, \\ &|0,0\rangle = \frac{1}{\sqrt{2}}(|\uparrow\downarrow\rangle - |\downarrow\uparrow\rangle) \end{aligned} \quad . \tag{3B.11}$$

Here we use S as index, not $S(S+1)$. The state of $S=1$ is called spin triplet state, $S=0$ is called spin singlet state. Then we obtain follows as Clebsch-Gordan coefficient in eq. (3B.4),

$$\begin{aligned} &C^{11}_{1/2,1/2,1/2,1/2} = C^{1-1}_{1/2,-1/2,1/2,-1/2} = 1, \\ &C^{10}_{1/2,1/2,1/2,-1/2} = C^{10}_{1/2,-1/2,1/2,1/2} = C^{00}_{1/2,1/2,1/2,-1/2} = 1/\sqrt{2}, \\ &C^{00}_{1/2,-1/2,1/2,1/2} = -1/\sqrt{2}. \end{aligned}$$

References

[1] K W H Stevens. Matrix elements and operator equivalents connected with the magnetic properties of rare earth ions. *Proceedings of the Physical Society. Section A*, Vol. 65, No. 3, pp. 209–215, March 1952.

[2] Yoshichika Ōnuki. *Physics of Heavy Fermions*. WORLD SCIENTIFIC, September 2017.

[3] J. H. Van Vleck. *The Theory Of Electric And Magnetic Susceptibilities*. 08 2015.

[4] Takashi Hotta. Microscopic approach to magnetism and superconductivity of f-electron systems with filled skutterudite structure. *Journal of the Physical Society of Japan*, Vol. 74, No. 4, pp. 1275–1288, 2005.

[5] Warren E. Henry. Spin paramagnetism of cr^{+++}, fe^{+++}, and gd^{+++} at liquid helium temperatures and in strong magnetic fields. *Phys. Rev.*, Vol. 88, pp. 559–562, Nov 1952.

[6] Figgis. *Introduction to Ligand Fields*. Krieger Pub Co, 6 1966.

[7] 上村洸, 菅野暁, 田辺行人. 配位子場理論とその応用 (物理科学選書). 裳華房, 6 1969.

Let us continue the discussion of octahedral ligand filed. We begin with the cartesian coordinate expression of the potential.

$$v_{\rm cb}(\boldsymbol{r}) = eD\left(x^4+y^4+z^4-\frac{3}{5}r^4.\right) \tag{2.68}$$

In eq. (2.1), the above potential should be $\mathcal{H}_{\rm CF}$, which now has more priority than $\mathcal{H}_{\rm SOI}$ for present. First we consider the single-electron problem in the central force plus octahedral potential. Since our problem is on the $3d$ electrons in an open shell, we restrict ourselves to the space generated on the basis of d-orbital wavefunctions. Also it can be known from the group theory, that will be introduced afterwards, the potential in (2.68) does not split s and p orbitals, as can be easily guessed by considering the symmetry of $p_{x,y,z}$.

In order to diagonalize this potential within d-orbitals ($l=2$) ϕ_{nlm}: $(n,l,m)=(n,2,m=2,1,0,-1,-2)$, in an orthodox way, we write down the secular equation and then obtain the eigenvalues and the eigenvectors[1]. But here, we deduce the functional forms of diagonalization basis functions from a simpler thought[2]. The radial part is common for d-orbitals (rather for principal quantum number n). The parts of spherical harmonic functions are

$$Y_{20}(\theta,\varphi) = \sqrt{\frac{5}{16\pi}}(3\cos^2\theta-1), \tag{2.69a}$$

$$Y_{2\pm1}(\theta,\varphi) = \mp\sqrt{\frac{15}{8\pi}}\cos\theta\sin\theta e^{\pm i\varphi}, \tag{2.69b}$$

$$Y_{2\pm2}(\theta,\varphi) = \sqrt{\frac{15}{32\pi}}\sin^2\theta e^{\pm 2i\varphi}. \tag{2.69c}$$

This directional dependences in cartesian coordinate are quadratic in (x,y,z) as $r\cos\theta = z$, $r\sin\theta\cos\varphi = x$, $r\sin\theta\sin\varphi = y$. Since the non-spherical part in the potential (2.68) is given as an even function of (x,y,z), off-diagonal elements of the matrix representation on the (partial) basis of the quadratic functions yz, zx, xy are zero by integrating out the odd functions. Residual quadratics are x^2, y^2, z^2. For vanishing off-diagonal terms in the matrix representation for $x^4+y^4+z^4$, we need to take differences between (x^2,y^2,z^2). Possible independent candidates are x^2-z^2, y^2-z^2 though they are not orthogonal. Hence with orthogonalization we reach $3z^2-r^2$, x^2-y^2.

These directional dependencies can be obtained in the linear combination of eq. (2.69) as

$$\phi_\xi = \frac{i}{\sqrt{2}}(\phi_{n21}+\phi_{n2-1}) = \sqrt{\frac{15}{4\pi}}\frac{yz}{r^2}R_{n2}(r), \tag{2.70a}$$

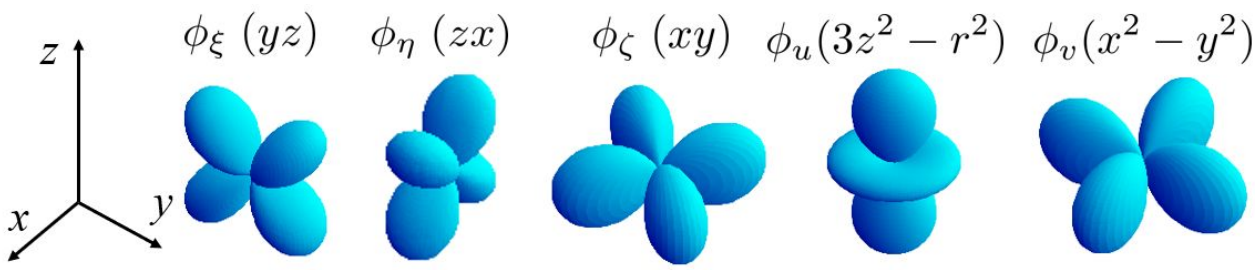

Fig. 2.9 Eigenstates of d-electron in an octahedral ligand field (eq. (2.70)). The surfaces of (absolute value of wavefunction)=(constant) are drawn with shading.

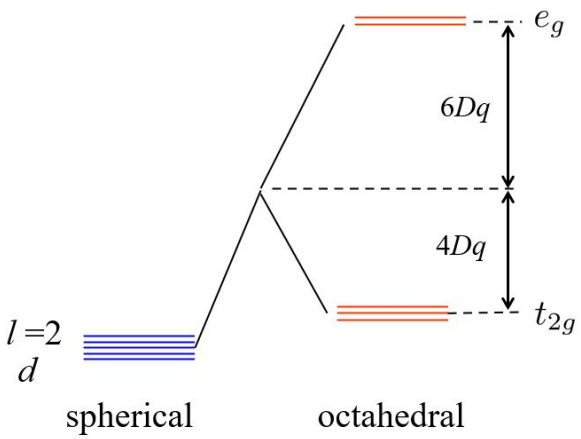

Fig. 2.10 Level splitting of d-orbital by an octahedral ligand potential. D, q are defined in eq. (2.67) and eq. (2.71) respectively. The uniform increase of levels by the constant term is also drawn.

$$\phi_\eta = -\frac{1}{\sqrt{2}}(\phi_{n21} - \phi_{n2-1}) = \sqrt{\frac{15}{4\pi}}\frac{zx}{r^2}R_{n2}(r), \tag{2.70b}$$

$$\phi_\zeta = -\frac{i}{\sqrt{2}}(\phi_{n22} - \phi_{n2-2}) = \sqrt{\frac{15}{4\pi}}\frac{xy}{r^2}R_{n2}(r). \tag{2.70c}$$

And

$$\phi_u = \phi_{320} = \sqrt{\frac{5}{16\pi}}\frac{3z^2 - r^2}{r^2}R_{n2}(r), \tag{2.70d}$$

$$\phi_v = -\frac{1}{\sqrt{2}}(\phi_{322} + \phi_{32-2}) = \sqrt{\frac{5}{16\pi}}\frac{x^2 - y^2}{r^2}R_{n2}(r). \tag{2.70e}$$

The "shapes" of these wavefunctions are expressed in Fig. 2.9 as shaded surfaces of (absolute value of direction-dependent part in the wavefunction)=(a constant).

We restrict ourselves to $3d$ electrons. Let q be

$$q = \frac{2e}{105}\langle r^4\rangle = \frac{2e}{105}\int |R_{32}(r)|^2 r^4 (r^2 dr), \tag{2.71}$$

and the group of three wavefunctions ϕ_ξ, ϕ_η, ϕ_ζ and the group of two wavefunctions ϕ_u, ϕ_v have the eigen energies

$$\epsilon_1 = -4Dq, \quad \epsilon_2 = 6Dq \tag{2.72}$$

respectively. The states corresponding to ϵ_1 and ϵ_2 are called T_{2g}, E_g respectively named after the point groups. The single-electron orbitals belonging to those are called t_{2g} (or $d\epsilon$) orbital and e_g (or $d\gamma$) orbital. The level splitting of d-orbital is illustrated in Fig. 2.10. The shift between t_{2g} and e_g is roughly explained from the shapes of wavefunctions drawn in Fig. 2.9 as follows. The three orbitals of t_{2g} have zero amplitude when one of (x, y, z) is zero, avoiding the positions of ligands, hence decrease the Coulomb energy. On the other hand, e_g orbitals elongate to the directions of ligand, enhancing the Coulomb energy.

The angular moments of these orbitals are zero. For example, $\langle\phi_\zeta|l_z|\phi_\zeta\rangle$ gets +2 from ϕ_{322}, -2 from ϕ_{32-2}, and the total is zero. Similarly $\langle \boldsymbol{l}^2\rangle = 0$. This is the result of linear combination, in which the sum of the orbital angular momentum vanishes. In other words, the eigenstates are the standing waves for the octahedral potential, naturally have zero angular momentum. Very important conclusion of this analysis is that the result explains the experimental results in Tab. 2.4, in which the effective number of Bohr magneton appears to be as if the orbital angular moment vanishes.

2.7.2 Ground states of multiple electrons

Next we should consider the electron configuration in these t_{2g}, e_g orbitals along with the Hund's rule. Here we need to compare the crystal (ligand) field splitting $10Dq$ and the energy gain of the exchange integral (eq. (2.20c)) by following

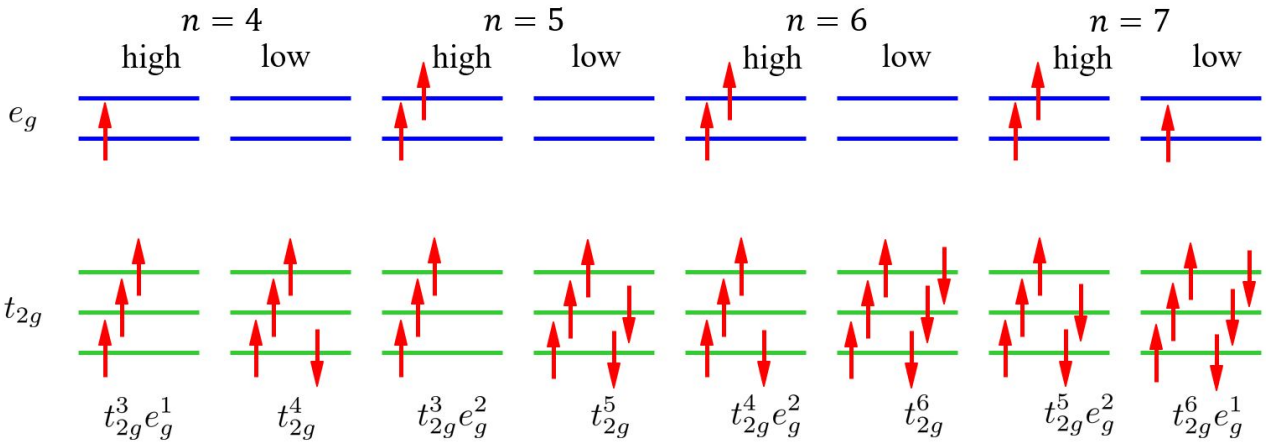

Fig. 2.11 Two possible electron accommodations of t_{2g} and e_g orbitals. There are high-spin states and low-spin states for electron numbers more than $n = 4$.

the Hund's rule. When the former surpasses the latter, the configuration of more accommodation in t_{2g} orbital with lower total spin is favored. Such a multiple-electron state is called low-spin state.

Figure 2.11 shows possible spin configurations (high- and low-spin states) for $n = 4 \sim 7$. For $n = 8, 9$, t_{2g} orbitals are fully occupied, and there is a single possible configuration. In the example of an iron ion Fe^{2+} in a hemoglobin, the existence of two possible (high, low) spin states brings about a dramatic effect. Four nitrogen atoms of porphyrin and imidazole nitrogen at the end of the globin protein polypeptide chain are coordinated to this iron ion, which is not a regular octahedron coordination. However we still take t_{2g}, e_g orbitals as the basis since the splitting due to the further lowering in the symmetry is not very large. When the complex structure does not have an oxygen atom, namely a five coordination state, the electrons are in a high-spin state ($t_{2g}^4 e_g^2$) while under the coordination of an oxygen atom (one of two in a molecule), the splitting $10Dq$ between t_{2g}-e_g becomes larger and the state transits to the low-spin state t_{2g}^6. The transition can be detected by, e.g., the electron spin resonance.

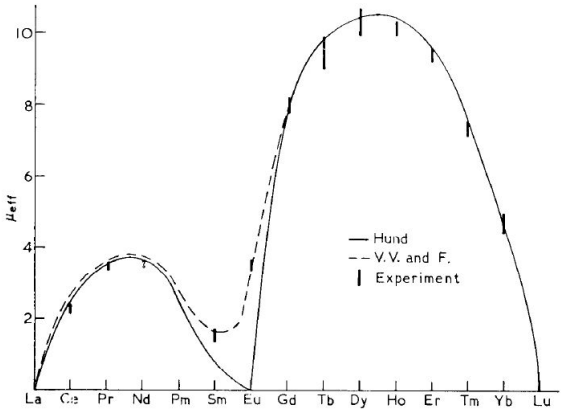

The ground state of t_{2g} or e_g still has 3-fold or 2-fold degeneracy. When the octahedral structure gets a distortion along z-axis, the degeneracy is lifted and generally the energy of ground state lowered. Hence when the energy lowering of the ground state surpasses the energy increase due to the lattice distortion, the lattice-distorted state is favored and the symmetry lowered. This phenomenon is called the **Jahn-Teller effect** and observed, e.g., in $CuSiF_6 6H_2O$ salt. Or in some cases, the crystal field effect is coupled to the lattice vibration yielding the effect called dynamic or vibronic Jahn-Teller effect.

2.7.3 Van Vleck paramagnetism

In the above, on the paramagnetism of $3d$ transition metals and $4f$ lanthanoid, we have seen that, the former can be understood by considering the effect of ligand field while the latter can be fairly understood by considering the SOI via LS coupling (or j-j coupling) approach. However we still have a problem in the latter. As we see in Tab. 2.5, there are big discrepancies between the theory and the experiment for Eu^{3+}, Sm^{3+}. The problem was theoretically solved by Van Vleck, and the phenomenon is called Van Vleck paramagnetism. The above figure is from the Nobel lecture[3] given by

Van Vleck, which demonstrates that his theory quantitatively explains the discrepancies in the simple theory.

Let us see how the theory works in the case of Eu^{3+}. The electron configuration is $4f^6$, the electron number is less than $2l+1=7$, then we see the coefficient of $\boldsymbol{L}\cdot\boldsymbol{S}$ is positive from eq. (2.38). Namely $\boldsymbol{L}$ and $\boldsymbol{S}$ couple as anti-parallel. The ground state is ${}^7F_0$, which means $J=0$. In the excited states, possible total angular momenta are $J=1,2,\cdots,6$. From eqs. (2.38),(2.41),

$$\mathcal{H}_{\rm SOI}=\lambda\boldsymbol{L}\cdot\boldsymbol{S}=\frac{\lambda}{2}[J(J+1)-S(S+1)-L(L+1)]. \tag{2.73}$$

The splitting width of LS-multiplet (L, S are fixed, J is the index of split states) is

$$\Delta E_{LS}=E_{LS}(J)-E_{LS}(J-1)=\lambda J. \tag{2.74}$$

The energy difference between the ground state with $J=0$ and the first excited state with $J-1$ is λ, which is as small as 200∼300 K. Hence even at low temperatures, when there is a finite external magnetic field, the term $\mathcal{H}_{\rm SOI}$ causes mixing of the state $J=1$ with the $J=0$ ground state, which gives rise to a finite magnetic moment.

2.8 Symmetry and degeneracy of quantum states

In the above we have solved a specific problem of d-electrons in an octahedral potential. In more general treatment, we should apply regular perturbation theory. However, the thoughts from the symmetry of the system is very helpful in the calculation since we can largely decrease the amount of calculation[4]. The symmetry of a system is defined by **symmetry operations**. A symmetry operation is a transformation in a space of some degrees of freedom. Examples are rotations, parallel transformations, mirror reflections, etc. in the coordinate space. When a system is invariant under a symmetry operation, the system has the symmetry for the operation. The total symmetry of a system is defined as a set of symmetries possessed by the system. In the following we will have a short look at a general method to know the degeneracy of quantum states from the symmetry of the system.

2.8.1 Symmetry operations in point groups

We use **group** theory for such discussions. In Appendix 3A, we have seen that symmetry operations constitute a group, an element of which has a corresponding matrix of representation. Thus the symmetry of a system can be specified by the corresponding group. The symmetry groups that have correspondence to spatially localized systems are called **point groups**. Particularly in crystals, the constraint of discrete translational symmetry restricts the number of possible point groups called “crystal point groups” to 32 listed in Tab. 2.6.

We won’t go deep into mathematics though the group theoretical knowledges of symmetry operation are indispensable for the researchers of crystallography, symmetry-sensitive properties like multi-ferroics. Embarrassing in symmetry group theories is that similar symbols are

The problem with handling a group of symmetric operations is that they are all confusing with similar symbols to various concepts, and the symbols are different and more confusing depending on the style of the mathematicians. In physics, Schönflies and Mulliken symbols have been used, and we also follow that here but recently “international standard” symbols are also frequently used. At present I cannot find the way to describe the expressions in a beautifully organized manner.

When a set of functions $\mathscr{A}_\varphi=\{\varphi_1,\varphi_2,\cdots\}$ is transformed back to itself by a symmetry operation R, that is, $\mathscr{A}\xrightarrow{R}\mathscr{A}'_\varphi=\{\varphi'_1,\varphi'_2,\cdots\}=\mathscr{A}$, $\mathscr{A}$ can be a representation basis of R and the corresponding matrix is given as

$$D_{ij}(R)=\langle\varphi_i|R|\varphi_j\rangle\,. \tag{2.75}$$

system	Schönflies	Hermann-Mauguin symbol		examples
	symbol	full	abbreviated	
triclinic	C_1	1	1	
	C_i, (S_2)	$\bar{1}$	$\bar{1}$	Al_2SiO_5
monoclinic	C_{1h}, (S_1)	m	m	KNO_2
	C_2	2	2	
	C_{2h}	2/m	2/m	
orthorhombic	C_{2v}	$2mm$	mm	
	D_2, (V)	222	222	
	D_{2h}, (V_h)	$2/m2/m2/m$	mmm	I, Ga
tetragonal	C_4	4	4	
	S_4	4	4	
	C_{4h}	4/m	4/m	$CaWO_4$
	D_{2d}, (V_d)	$\bar{4}2m$	$\bar{4}2m$	
	C_{4v}	$4mm$	$4mm$	
	D_4	422	42	
	D_{4h}	$4/m2/m2/m$	$4/mmm$	TiO_2, In, β-Sn
rhombohedral	C_3	3	3	AsI_3
	C_3, (S_6)	3	3	$FeTiO_3$
	C_{3v}	$3m$	$3m$	
	D_3	32	32	Se
	D_{3d}	$32/m$	$3m$	Bi, As, Sb, Al_2O_3
hexagonal	C_{3h}, (S_3)	6	6	
	C_6	6	6	
	C_{6h}	$6/m$	$6/m$	
	D_{3h}	$62m$	$62m$	
	C_{6v}	$6mm$	$6mm$	ZnO, NiAs
	D_6	622	62	CeF_3
	D_{6h}	$6/m2/m2/m$	$6/mmm$	Mg, Zn, graphite
cubic	T	23	23	$NaClO_3$
	T_h	$2/m3$	$m3$	FeS_2
	T_d	$43m$	$43m$	ZnS
	O	432	43	β-Mn
	O_h	$4/m32/m$	$m3m$	NaCl, diamond, Cu
icosahedral	C_5	5	5	
	C_{5i}, (S_{10})	10	10	
	C_{5v}	$5m$	$5m$	
	C_{5h}, S_5	5	5	
	D_5	52	52	
	D_{5d}	$52/m$	$5/m$	C_{80}
	D_{5h}	$10\bar{2}/m$	$10\bar{2}/m$	C_{70}
	I	532	532	
	I_h			C_{60}

Tab. 2.6 Crystal systems, Schönflies symbols, Hermann-Mauguin symbols and examples of materials of 32 crystal point groups. From Ref. [4].

	Symmetry operation	Rotation axis	Number of operation
E	Identical transformation		1
C_4	$\pi/2$ rotation around 4-fold axis	x, y, z	3
$C_2 = C_4^2$	π rotation around 4-fold axis	x, y, z	3
C_4^3	$3\pi/2$ rotation around 4-fold axis	x, y, z	3
C_2	π rotation around 2-fold axis	(0,1,1), (1,0,1), (1,1,0)	6
		(0,1,−1), (−1,0,1), (1,−1,0)	
C_3	$2\pi/3$ rotation around 3-fold axis	(1,1,1), (1,1,−1), (1,−1,1), (−1,1,1)	4
C_3^2	$4\pi/3$ rotation around 3-fold axis	(1,1,1), (1,1,−1), (1,−1,1), (−1,1,1)	4

Tab. 2.7 Symmetry operations octahedral group (O group).

Here, if $D(R)$ can get further block diagonalization by unitary matrix S (i.e., replacement of basis) as

$$SD(R)S^{-1} = \begin{pmatrix} D_1(R) & & 0 \\ & D_2(R) & \\ 0 & & \ddots \end{pmatrix}, \tag{2.76}$$

$D(R)$ is **reducible** and can be expressed as a **direct summation** of $D_1(R), D_2(R), \cdots$ as

$$D(R) = D_1(R) \oplus D_2(R) \oplus \cdots . \tag{2.77}$$

On the other hand, if such block diagonalization is impossible, the representation is **irreducible**. Expression of a reducible representation as a direct summation of irreducible representations, is called reduction.

Irreducible or reducible namely the possibility of block diagonalization cannot be judged from the simple diagonalizability of matrix. Often adopted is the use of **character** table. Character of representation is the trace of representation matrix, which is invariant for the changing of basis. Hence a character for reducible representation is the sum of characters for irreducible representations in the direct summation. From this the reduced form in the direct summation can be deduced.

Table 2.7 lists the symmetry operations that keep an octahedral system invariant. Those operations constitute a group called octahedral group, of which the symbol is O. As in Tab. 2.6, it belongs to the cubic symmetry. The octahedral complex systems with magnetic ions also have the space-inversion symmetry in addition to O. Hence to be strict, we need to consider O_h group. Although here for simplicity we consider O group and it is known that the level-splitting behavior is the same for O_h. Group O has 24 symmetry operations as the elements as listed in this table.

	O	E	$8C_3$	$3C_2 = 3C_4^2$	$6C_2'$	$6C_4$
$\Gamma_{l=0}$	A_1	1	1	1	1	1
$\Gamma_{l=1}$	T_1	3	0	−1	−1	1
$\Gamma_{l=2}$	$E + T_2$	5	−1	1	1	−1
$\Gamma_{l=3}$	$A_2 + T_1 + T_2$	7	1	−1	−1	−1
$\Gamma_{l=4}$	$A_1 + E + T_1 + T_2$	9	0	1	1	1
$\Gamma_{l=5}$	$E + 2T_1 + T_2$	11	−1	−1	−1	1
Γ_1	A_1	1	1	1	1	1
Γ_2	A_2	1	1	1	−1	−1
Γ_{12}	E	2	−1	2	0	0
Γ_{15}'	T_1	3	0	−1	−1	1
Γ_{25}'	T_2	3	0	−1	1	−1

Tab. 2.8 Symmetry operations in group O (topmost low), and characters. The representations in the upper low are on bases of eigenfunctions of orbital angular momentum. Those in the lower low display irreducible representations.

Next we consider the representations of these symmetry operations. A simple choice of representation basis is the eigenfunctions in a system of a spherical potential. They can have the orbital angular momentum as the quantum number, namely s, p, d, $f, \cdots$. The representations based on them are listed in the upper band in Tab. 2.8. The symbols $\Gamma_{l=0} \sim \Gamma_{l=5}$ are the representations on the orbital angular momentum l. However they are not generally irreducible. The symbols of irreducible representations are named in the following way. A, E, T are for 1, 2, and 3-dimensional representations. The suffices do not have strict rule, being numbered starting from O group. In the table, the irreducible representations A_1, A_2, E, T_1, T_2 of group O and the characters are listed in the lower band. From the comparison of these characters, we know that $\Gamma_{l=0}$, $\Gamma_{l=1}$ are irreducible. This fact indicates that s and p orbitals do not split in an octahedral potential. For $l \geq 2$, Γ_l are reduced as indicated in the table. When we consider the split of d-orbital, we added suffix g as T_{2g} and E_g. Actually we need to consider group O_h including the space-inversion operation i. The symmetry operations are the direct product with i and the number of i operations brings the difference between even number (gerade, g in Germany) and odd number (ungerade, u). The irreducible representation also needs the suffix of g (even).

2.8.2 Symmetry operation and degeneracy

Let R be one of such symmetry operation and a function φ transform as

$$\varphi' = R\varphi. \tag{2.78}$$

Assume an operator $\mathscr{O}$ is transformed by R to $\mathscr{O}'$, then the operation of $\mathscr{O}'$ on the transformed function $R\varphi$ should be the result of operation R on the $\mathscr{O}$-operated original φ. Therefore

$$\mathscr{O}' R\varphi = R\mathscr{O}\varphi = R\mathscr{O}R^{-1}R\varphi.$$

That is, $\mathscr{O}$ is transformed to $R\mathscr{O}R^{-1}$. Now assume $\mathscr{H}$ is invariant for the symmetry operation R.

$$R\mathscr{H}R^{-1} = \mathscr{H}, \quad \therefore [R, \mathscr{H}] = 0. \tag{2.79}$$

Let ϕ an eigenfunction of $\mathscr{H}$ with an eigenvalue of E, that is $\mathscr{H}\phi = E\phi$. Then

$$\mathscr{H}R\phi = R\mathscr{H}R^{-1}R\phi = RE\phi = ER\phi, \tag{2.80}$$

which indicates that $\phi' = R\phi$ is an eigenstate of $\mathscr{H}$ with the same eigenvalue E. If ϕ and ϕ' are independent to each other, they are degenerate eigenfunctions. This degeneracy is based on the symmetry of the system. Other kinds of degeneracy is called "accidental" and usually lifted by some factors in real systems.

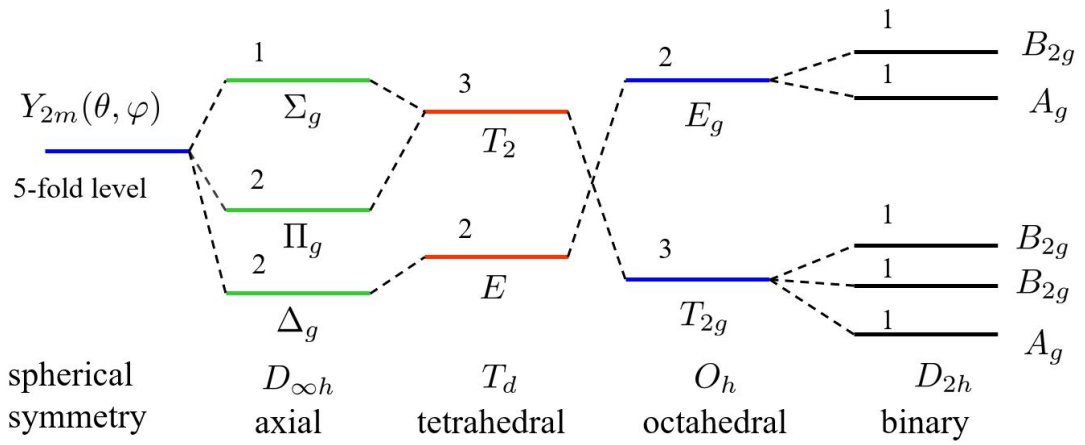

Fig. 2.12 Level splitting of 5-fold $l = 2$ states in various symmetries expressed by crystal point groups. The numbers attached to the levels indicate the degree of degeneracy. From Ref. [4].

Let $\{\phi_i\}$ be eigenfunctions with degree of degeneracy d with eigenvalue E of $\mathscr{H}$. The representation matrix of R in this space is given by

$$D_{ij}(R) = \langle \phi_i | R | \phi_j \rangle \,. \tag{2.81}$$

That is,

$$R\phi_\nu = \sum_{\mu=1}^{d} D_{\mu\nu}(R)\phi_\mu. \tag{2.82}$$

Here $D(R)$ must be irreducible. Otherwise, e.g., assume $D(R)$ is block diagonalized as

$$D(R) = D_1(R) \oplus D_2(R) = \begin{pmatrix} D_1(R) & 0 \\ 0 & D_2(R) \end{pmatrix}.$$

Then the basis is transformed by the transformation matrix for the reduction as $\{\phi_i\} \to \{\chi_i\}$. We can thus divide the basis $\{\phi_i\}$ into $\{\phi_i^{(1)}\}$ and $\{\phi_i^{(2)}\}$ which belong to $D_1(R)$ and $D_2(R)$ respectively. They are not transformed to each other by symmetry operation, hence the degeneracy is accidental.

From the above discussion and by the character tables of irreducible representation, we can deduce how the degenerate states under consideration split when the symmetry of the system changes. Further we can know the shape of wavefunction from the basis of representation, hence infer the order of energy levels. Thus obtained level splitting of d-orbitals in various ligand field potentials is illustrated in Fig. 2.12.

2.9 Experiments and applications of localized spins

We have studied magnetic atoms or ions, which have large localized magnetic moments based on the measurement of magnetic susceptibility and the crystal structures. Here we have a look at fundamentals of magnetic resonance – a very important experimental method for magnetism. As an application of paramagnetic salt, we have short visit to magnetic refrigeration.

2.9.1 Magnetic resonance

In Sec. 2.1.2, we have mentioned that the magnetic moment tilted in a static magnetic field causes Larmor precession. In the method of **magnetic resonance** (MR), by applying an oscillating magnetic field at the Larmor frequency and by observing the resonance, we obtain not only the information of the magnetic moment itself, but also that of the environment surrounding the moment. It is needless to say the academic and social importance.

Let $\boldsymbol{J}$ be the total angular momentum of an isolated electron system. The Zeeman term in a static magnetic field $\boldsymbol{B}_0$ along z axis is given by

$$\mathcal{H}_1 = g_J \mu_{\mathrm{B}} \boldsymbol{J} \cdot \boldsymbol{B}_0, \tag{2.47}$$

which is just the same as eq. (2.47). Heisenberg equation of motion is written as

$$\frac{d\boldsymbol{J}}{dt} = \frac{i}{\hbar}[g_J \mu_{\mathrm{B}} \boldsymbol{J} \cdot \boldsymbol{B}_0, \boldsymbol{J}], \tag{2.83}$$

to which the commutation relation

$$J_y J_z - J_z J_y = iJ_x, \quad J_z J_x - J_x J_z = iJ_y, \quad J_x J_y - J_y J_x = iJ_z \tag{2.84}$$

is applied to obtain

$$\frac{d\boldsymbol{J}}{dt} = \frac{g_J \mu_{\mathrm{B}}}{\hbar} \boldsymbol{B}_0 \times \boldsymbol{J}. \tag{2.85}$$

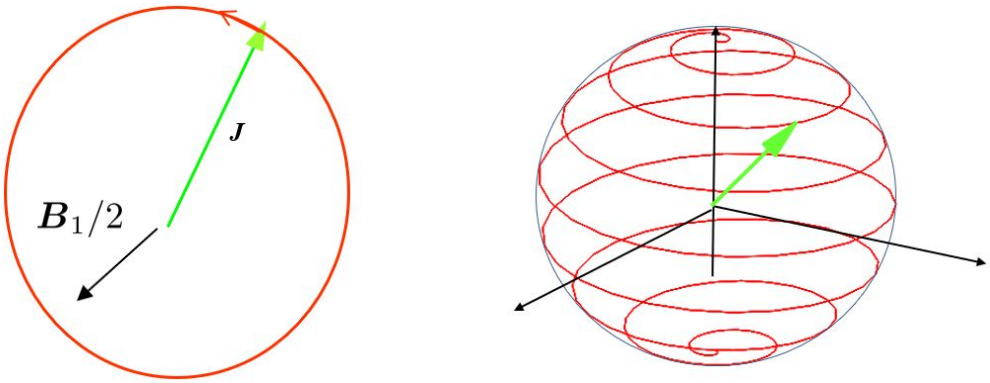

Fig. 2.13 Left: Precession of angular momentum $\boldsymbol{J}$ around the in-plane magnetic field $\boldsymbol{B}_1/2$ on the rotating coordinate. Right: Illustration of the total motion tracing the end-point of $\boldsymbol{J}$ from the static coordinate. Under realistic conditions, the rotation around z-axis is much faster.

This expresses the precession with Larmor frequency

$$\omega_{\mathrm{L}} = g_J \frac{eB_0}{2m}. \tag{2.86}$$

Now if we observe this precession from the coordinate rotating around z-axis with frequency ω_{L}, the precession is canceled out and the momentum looks as if it sits still. Namely in this coordinate, the effect of static field along z axis vanishes and virtually zero-field state is realized.

An oscillation magnetic field $\boldsymbol{B}(t) = \boldsymbol{B}_1 \cos(\omega t)$ (on the non-rotating coordinate) perpendicular to the static field $\boldsymbol{B}_0$ can be written as the sum of rotating field as

$$\boldsymbol{B}(t) = \frac{\boldsymbol{B}_1}{2}[\exp(i\omega t) + \exp(-i\omega t)]. \tag{2.87}$$

When $\omega \approx \omega_{\mathrm{L}}$, from the rotating coordinate the ω-component almost sits still while the $-\omega$-component is rotating with 2ω. We take **rotating wave approximation**, in which the latter is ignored. Now on the rotating coordinate, a static field of $B_1/2$ is applied in xy-plane and the angular momentum starts precession around this field with frequency

$$\omega_1 = g_J \frac{eB_1}{4m}. \tag{2.88}$$

This is the basic process of **magnetic resonance**.

Figure 2.13 illustrates the motion of angular momentum under a magnetic resonance, in which the end-point draws a spiral. Note that under realistic conditions, the rotation around z-axis is much faster.

References

[1] C.J. Ballhausen. *Introduction to Ligand Field Theory (Advanced Chemistry)*. McGraw-Hill Inc.,US, 12 1962.

[2] Joachim Stöhr and Hans Christoph Siegmann. *Magnetism: From Fundamentals to Nanoscale Dynamics (Springer Series in Solid-State Sciences, 152)*. Springer, 9 2006.

[3] J. H. Van Vleck. Quantum mechanics: The key to understanding magnetism. *Science*, Vol. 201, No. 4351, pp. 113–120, July 1978.

[4] Mildred S. S. Dresselhaus. *Group Theory: Application to the Physics of Condensed Matter*. Springer, 10 2010.

In the last lecture, for magnetic resonance, we introduced the concept of "observation from rotating coordinates" . The time evolution of the angular momentum was treated in the Heisenberg picture, and the results were the same as that obtained in the classical picture as in eq. (2.83). Then in the following, for simplicity, we consider classical equations of motion for macroscopic magnetic moment $\boldsymbol{M}$ and introduce energy and phase relaxations phenomenologically[1].

$$\frac{dM_z}{dt} = \gamma[\boldsymbol{M}\times\boldsymbol{H}]_z + \frac{M_0 - M_z}{T_1}, \tag{2.89a}$$

$$\frac{dM_{x,y}}{dt} = \gamma[\boldsymbol{M}\times\boldsymbol{H}]_{x,y} - \frac{M_{x,y}}{T_2}. \tag{2.89b}$$

T_1, T_2 are longitudinal and transverse relaxation times respectively, or energy and phase relaxation times. We here use $\boldsymbol{H}$ instead of $\boldsymbol{B}$ to avoid confusion due to the existence of $\boldsymbol{M}$ though the use of $\boldsymbol{B}$ is not the problem at all. The definition of gyromagnetic ratio should be changed from eq. (2.14) so as to have consistent dimension. We consider a static field $\boldsymbol{H}_0$ along z and a rotating field $\boldsymbol{H}_1/2$ in xy-plane with an angular frequency $(-)\omega$. The total field is

$$\boldsymbol{H} = (\frac{H_1}{2}\cos\omega t, -\frac{H_1}{2}\sin\omega t, H_0). \tag{2.90}$$

The magnetic moment derived from the angular momentum gets minus sign due to the sign of electric charge (eq. (1.80)). Hence the rotation is clockwise for positive magnetic moment $\boldsymbol{M}$. The equations of motion are thus,

$$\frac{dM_x}{dt} = \gamma[M_y H_0 + M_z\frac{H_1}{2}\sin\omega t] - \frac{M_x}{T_2}, \tag{2.91a}$$

$$\frac{dM_y}{dt} = \gamma[M_z\frac{H_1}{2}\cos\omega t - M_x H_0] - \frac{M_y}{T_2}, \tag{2.91b}$$

$$\frac{dM_z}{dt} = \gamma[-M_x H_1\sin\omega t - M_y\frac{H_1}{2}\cos\omega t] + \frac{M_0 - M_z}{T_1}. \tag{2.91c}$$

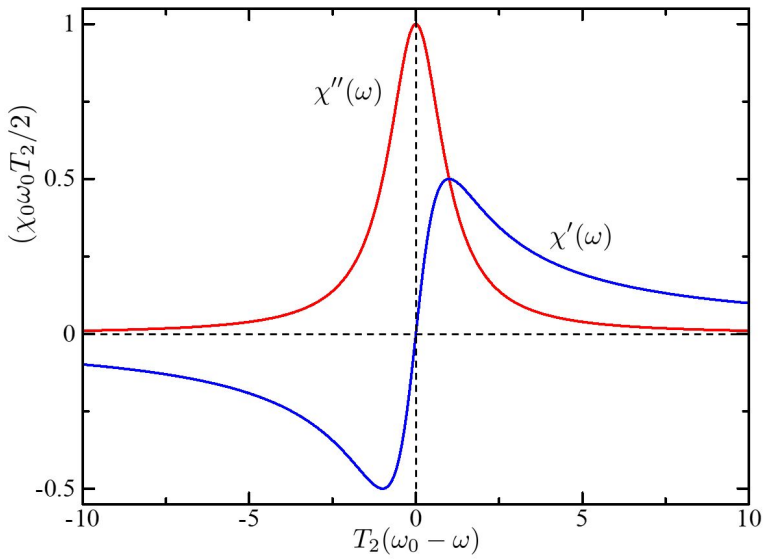

Fig. 2.14 The plot of eq. (2.96). The real part ($\chi'(\omega)$, blue line) and the imaginary part ($\chi''(\omega)$, red line) of the complex susceptibility around a magnetic resonance in the presence of relaxations.

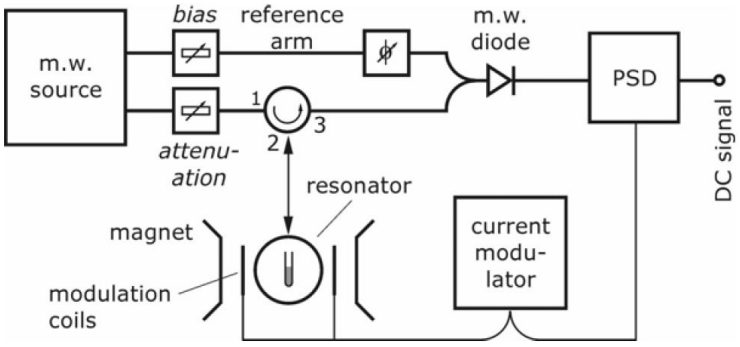

Fig. 2.15 Typical setup of electron paramagnetic resonance (electron spin resonance) experiment.The circle mark with numbering indicates a circulator of microwave. A microwave enters via terminal 1 through 2 to the cavity with a sample and the reflected wave propagates through 3 to a diode. The detected signal is sent to a phase sensitive detector (PSD). From [2].

We introduce the coordinate system (x', y', z') $(z' = z)$ rotating around z-axis clockwise with angular frequency ω to obtain

$$M_{x'} = M_x \cos\omega t - M_y \sin\omega t, \tag{2.92a}$$
$$M_{y'} = M_x \sin\omega t + M_y \cos\omega t. \tag{2.92b}$$

By using eq. (2.92), we rewrite eq. (2.91) into the kinetic equations of $(M_{x'}, M_{y'}, M_z)$. Under the conditions:

$$\begin{aligned} &\frac{dM_{x'}}{dt} = \frac{dM_{y'}}{dt} = 0 \quad \text{(stationary state)}, \\ &M_z \simeq M_0 = \chi_0 H_0 \quad \text{(oblique angle is small)}, \end{aligned} \tag{2.93}$$

we obtain the following solutions.

$$M_{x'} = \chi_0\omega_0 T_2 \frac{(\omega_0 - \omega)T_2 H_1/2}{1 + (\omega_0 - \omega)^2 T_2^2 + \gamma^2 (H_1/2)^2 T_1 T_2} \tag{2.94a}$$
$$M_{y'} = \chi_0\omega_0 T_2 \frac{H_1/2}{1 + (\omega_0 - \omega)^2 T_2^2 + \gamma^2 (H_1/2)^2 T_1 T_2}. \tag{2.94b}$$

ω_0 is Larmor frequency ω_{L} in eq. (2.86) with $B = \mu_0 H_0$.

The solution expresses a state with a comparatively large relaxation, thus the moment gets large friction in rotation around $\boldsymbol{H}_1$. Hence the stationary state has a small angle to z-axis. From the rest system,

$$M_x = \chi'(\omega) H_1 \cos\omega t + \chi''(\omega) H_1 \sin\omega t, \tag{2.95a}$$
$$M_y = -\chi'(\omega) H_1 \sin\omega t + \chi''(\omega) H_1 \cos\omega t. \tag{2.95b}$$

In case $\gamma^2 H_1^2 T_1 T_2 \ll 1$ (large relaxation), the real and imaginary parts of the susceptibility are given by

$$\chi'(\omega) = \frac{\chi_0\omega_0}{2} T_2 \frac{(\omega_0 - \omega)T_2}{1 + (\omega_0 - \omega)^2 T_2^2}, \tag{2.96a}$$
$$\chi''(\omega) = \frac{\chi_0\omega_0}{2} T_2 \frac{1}{1 + (\omega_0 - \omega)^2 T_2^2}, \tag{2.96b}$$

respectively, that is $\chi = \chi' - i\chi''$. They are plotted against $\omega_0 - \omega$ in Fig. 2.14.

In the experiments, the specimens are placed in coils or cavities of resonators and the variations of resonance characteristics are detected. An increase in energy dissipation in a resonator results in a widening and lowering of the resonance peak [*1]. Figure 2.15 illustrates a typical setup of experiments. A microwave enters via terminal 1 through 2 to the cavity with a sample and the reflected wave propagates through 3 to a three port connection for interference and then to a detector (diode). The signal is then sent to a phase sensitive detector (PSD). Variation of resonant frequency in microwave cavity is not so easy in most cases, so usually it is fixed. The frequency of input microwave is tuned to the resonance.

[*1] This can be understood, e.g, by inserting a resistor into an LC resonator circuit in a model for calculation.

Instead, the Larmor frequency $\omega_{\rm L}$ in eq. (2.86) of the sample is swept by the external magnetic field. In eq. (2.96), this corresponds to the variation of ω_0, and anyway the resonance curve is obtained. ω_0 in the coefficients of eq. (2.96) gives the first order slow variation while the resonance generally has a sharp lineshape and the distortion due to the coefficient is ignorable. The imaginary part in eq. (2.96), $\chi'(\omega)$ (eq. (2.96b)) represents the energy dissipation, which shows a peak structure as the red line in Fig. 2.14.

Coils for the field modulation is drawn in Fig. 2.15. In many experiments, field modulation with frequencies around 100 kHz is applied for improvement of signal to noise ratio by taking PSD signal. Such signals appear as frequency-derivative of eq. (2.96b).

2.9.2 Hyperfine structures in electron paramagnetic resonance

Owing to the large magnetic moment of electrons, electron spin resonance (ESR)or electron paramagnetic resonance (EPR)has high sensitivities among various magnetic resonance. Atomic wavefunctions of electron have finite amplitudes in the neighbors of nucleuses. When a nucleus has a finite spin, the exchange interaction (which will be introduced later) between the nuclear spin $\boldsymbol{I}$ and the electron total angular momentum $\boldsymbol{J}$ brings about **hyperfine interaction**, which can be expressed as

$$\mathcal{H}_{\rm HF} = A\boldsymbol{I}\cdot\boldsymbol{J}. \tag{2.97}$$

A is a parameter of the strength in the interaction. Since the Hamiltonian in eq. (2.97) has the same form as the spin-orbit interaction eqs. (2.38), (2.39), we consider the total angular momentum $\boldsymbol{F} = \boldsymbol{I}+\boldsymbol{J}$, and write the simultaneous eigenstate of $\mathcal{H}$, $\boldsymbol{F}^2$, F_z as $|F, M_F\rangle$. Then just as eq. (2.41), the eigenvalue of $\mathcal{H}_{\rm HF}$ is given by

$$\mathcal{H}_{\rm HF}|F,M_F\rangle = A\frac{\boldsymbol{F}^2-\boldsymbol{I}^2-\boldsymbol{J}^2}{2}|F,M_F\rangle = A\frac{F(F+1)-I(I+1)-J(J+1)}{2}|F,M_F\rangle. \tag{2.98}$$

The naming of "hyperfine" interaction comes from the further splitting of absorption levels, that already split by $\mathcal{H}_{\rm SOI}$. We do not have enough time to go into very important field and I recommend the readers who have strong interest in this field to refer to the journal "Hyperfine Interactions" [*2] .

2.9.3 Electron paramagnetic resonance in paramagnetic salts

EPRs are flourishing in the paramagnetic salts that have $3d$ transition metals or $4f$ lanthanoids as sources of magnetic moments. They have comparatively high moment densities (depending on the impurity concentrations), and importantly they are insulating that allows high frequency electromagnetic wave to go into the bulk in the absence of the skin effect.

Here we introduce an example of analyzing EPR data. Because EPR not only is sensitive but also has high resolution bringing rich information on the localized electronic states. For the actual analysis, we thus need a higher order approximation. In the case of $3d$ transition metals, we have discussed that the effect of orbital angular moment disappears due to the strong effect of ligand fields. Conversely, in $4f$ lanthanoid, we have given the priority to the spin-orbit interaction. However, these are the first order approximation and in the next step, we need to consider the SOI in the former, and the crystal field splitting in the latter. We skip the hyperfine interaction, which is not important for nucleus without spin, but consideration of the SOI on crystal field split levels is indispensable. For that we introduce the concept of effective spin Hamiltonian, which is common in this field. The effective spin Hamiltonian has no orbital operator but gives the same answer as the original one, if we restrict the problem to the effect of the SOI on the orbital levels that diagonalize the crystal field Hamiltonian[3].

[*2] https://www.springer.com/journal/10751

Let $\{\varphi_0, \varphi_1, \cdots, \}$ be an orbital basis that diagonalizes $\mathcal{H}_{\rm orb} = \mathcal{H}_0 + \mathcal{H}_{\rm CF}$, and in ket format $|n\rangle_{\rm o}$. We write the energy eigenvalues as ${}_{\rm o}\langle n|\mathcal{H}_{\rm orb}|n'\rangle_{\rm o} = E_n\delta_{nn'}$, the total spin of the basis as S, the spin wavefunction as $\{\phi_{-2S}, \phi_{-2S+1}, \cdots, \phi_{2S}\}$, ket-expression $|m\rangle_{\rm s}$.

The perturbation Hamiltonian of the SOI and the Zeeman effect is

$$\mathcal{H}' = \lambda \boldsymbol{L}\cdot\boldsymbol{S} + \mu_{\rm B}(\boldsymbol{L} + g_{\rm e}\boldsymbol{S})\cdot\boldsymbol{H}, \tag{2.99}$$

where $g_{\rm e}$ is g-factor of electron. We write a wavefunction in an expanded form as

$$\Psi = \sum_{nm} a_{nm}\varphi_n\phi_m = \sum_{nm} a_{nm}|n\rangle_{\rm o}|m\rangle_{\rm s}. \tag{2.100}$$

Then the eigenvalue equation of the total Hamiltonian is

$$\mathcal{H}\Psi = (\mathcal{H}_{\rm orb} + \mathcal{H}')\Psi = E\Psi. \tag{2.101}$$

Here e.g., the orbital part is integrated out in ${}_{\rm o}\langle l|\mathcal{H}'|n\rangle_{\rm o}$ but this still has the spin part as operator(s). Then we define a spin Hamiltonian as a second-order perturbation formula, in which the orbital part is integrated out. If the unperturbed ground state has degeneracy, we change the basis according to the perturbation theory, but there should be no confusion in using the symbols like $|n\rangle_{\rm o}$. We also restrict the transition matrix elements to the ones with the ground state $|0\rangle_{\rm o}$. Thus we obtain [*3]

$$\tilde{\mathcal{H}} = {}_{\rm o}\langle 0|\mathcal{H}'|0\rangle_{\rm o} + \sum_{n\neq 0}\frac{{}_{\rm o}\langle 0|\mathcal{H}'|n\rangle_{\rm o}\,{}_{\rm o}\langle n|\mathcal{H}'|0\rangle_{\rm o}}{E_0 - E_n}. \tag{2.102}$$

The introduction of ligand field quenches the orbital angular momentum. Namely the diagonal terms vanish ${}_{\rm o}|0|\boldsymbol{L}|0\rangle_{\rm o} = 0$ to give

$${}_{\rm o}\langle 0|\mathcal{H}'|0\rangle_{\rm o} = g_{\rm e}\mu_{\rm B}\boldsymbol{S}\cdot\boldsymbol{H}. \tag{2.103}$$

In the same way, from

$${}_{\rm o}\langle 0|\mathcal{H}'|n\rangle_{\rm o} = {}_{\rm o}|0|\boldsymbol{L}|n\rangle_{\rm o}\cdot(\lambda\boldsymbol{S} + \mu_{\rm B}\boldsymbol{H}), \tag{2.104}$$

we obtain

$$\tilde{\mathcal{H}} = g_{\rm e}\mu_{\rm B}\boldsymbol{S}\cdot\boldsymbol{H} - (\lambda\boldsymbol{S} + \mu_{\rm B}\boldsymbol{H})\Lambda(\lambda\boldsymbol{S} + \mu_{\rm B}\boldsymbol{H}), \tag{2.105}$$

where Λ is a tensor given by

$$\Lambda_{ij} = \sum_{n\neq 0}\frac{{}_{\rm o}\langle 0|L_i|n\rangle_{\rm o}\,{}_{\rm o}\langle n|L_j|0\rangle_{\rm o}}{E_n - E_0} \quad (i,j = x,y,z). \tag{2.106}$$

These elements are not necessarily zero and the effect of spin-orbit interaction appears in the second order perturbation. The same view is given by considering that the vanishing expectation value of orbital angular momentum comes from the way of superposition and the cancellation does not work for off-diagonal elements. Equation (2.105) is expanded as

$$\tilde{\mathcal{H}} = \mu_{\rm B}\boldsymbol{S}g_{\rm e}(\mathbf{1} - \lambda\Lambda)\boldsymbol{H} - \lambda^2\boldsymbol{S}\Lambda\boldsymbol{S} - \mu_{\rm B}^2\boldsymbol{H}\Lambda\boldsymbol{H}. \tag{2.107}$$

The first term is written in the Zeeman form as

$$\tilde{\boldsymbol{g}} = g_{\rm e}(\mathbf{1} - \lambda\Lambda). \tag{2.108}$$

This is an expansion of g-factor to a tensor form. Taking the principal axes of the tensor to x, y, z, we can write the second term in the following form.

$$-\lambda^2\boldsymbol{S}\Lambda\boldsymbol{S} = D\left[S_z^2 - \frac{S(S+1)}{3}\right] + E(S_x^2 - S_y^2), \tag{2.109}$$

[*3] You may not be satisfied with this treatment. In that case refer to a tutorial review [4]. A textbook in Japanese [5] gives rigorous treatment based on the projection operator method.

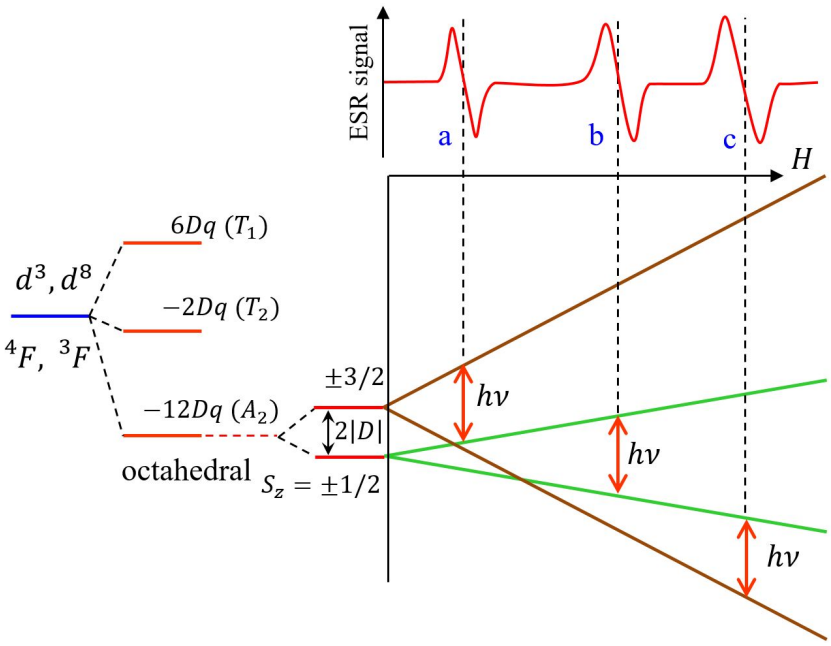

Fig. 2.16 Level splitting of $Cr^{3+}(3d^3$, S=3/2) in weak crystal field approximation and Zeeman splitting by external field. E=0 is assumed. Expected three ESR peak signals for microwave frequency ν corresponding to the red arrows are illustrated.

where Λ determines coefficients D and E in proportion to λ^2, called axial and orthorhombic coefficients respectively [*4]. The third term does not cause level-splitting being a small effect of orbital magnetic moment induced by external field. With dropping this term we reach

$$\tilde{\mathcal{H}} = \mu_{\mathrm{B}} \boldsymbol{S}\tilde{\boldsymbol{g}}\boldsymbol{H} + D\left[S_z^2 - \frac{S(S+1)}{3}\right] + E(S_x^2 - S_y^2). \tag{2.110}$$

As a simple example, let $\tilde{\boldsymbol{g}}$ be isotropic, $E = 0$, and $S = 3/2$. The spin states active for EPR are four states of $S_z = \pm 1/2, \pm 3/2$. At $H = 0$ they degenerate into two with the distance of $2|D|$ from eq. (2.110). Figure 2.16 illustrates such situation. The LS multiplet $(3d)^3$ is split as in the figure in weak field approximation given in App. 5A. The ground

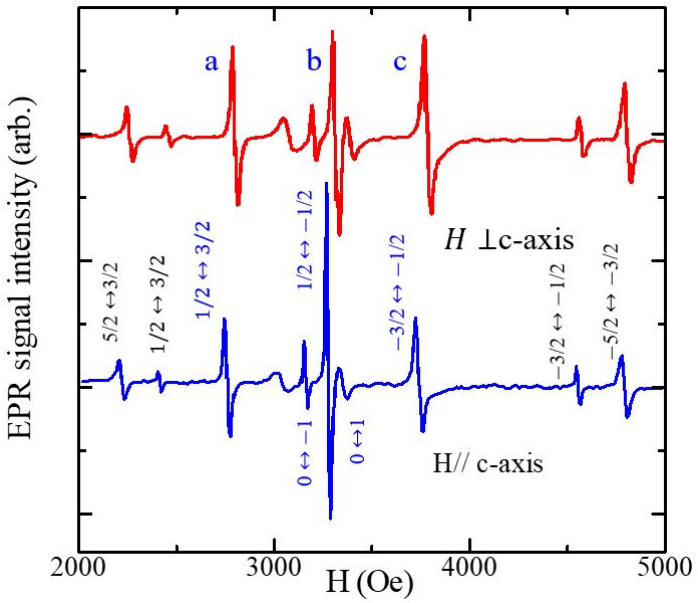

Fig. 2.17 EPR spectra of $BaTiO_3$ doped with 1% Cr^{3+} and Fe^{3+}. Blue and red lines are data for magnetic field parallel and perpendicular to c-axis respectively. The data are offset for clarity. Peaks (look like dissipation because of derivative taking in experiment) assigned as a, b, and c correspond to a, b, and c in Fig. 2.16. The microwave is in X-band (9-10 GHz), for which the value is not given. The annotations in blue letters indicate absorptions of S =3/2 state in Cr^{3+}, and S=1 state in Cr dimers. Those in black letters indicate absorptions of $S = 5/2$ in Fe^{3+}. From [6].

[*4] Repeated usage of D or E for different quantities inevitably causes confusion. These jargons are commonly used in many research papers and sometimes we find such symbols appear in a single diagram or table with different meanings. In this field we are often forced to express complicated concepts with simple and clear symbols, and at present we find no other better way. The readers are requested to judge from the context.

Ion	Crystal	g		$\lvert D\rvert$ (cm^{-1})	$\lvert E\rvert$ (cm^{-1})
Fe^{3+}	$BaTiO_3$	2.000		0.022	0.0079
another report		2.003		0.0987	
Cr^{3+}	$BaTiO_3$	1.975		0.046	0.0055
	h-$BaTiO_3$	H1 g_z=	1.9797	0.105	
		H1 $g_{x,y}$=	1.9857		
		H2 g_z=	1.9736	0.3220	
		H2 $g_{x,y}$=	1.9756		

Tab. 2.9 Values of g, $|D|$, $|E|$ for Fe^{3+} and Cr^{3+} in $BaTiO_3$ obtained from EPR lines in Fig. 2.17.

state is A_2 ($S = 3/2$). The external field split the two into four as in the figure. With microwave of frequency ν corresponding to the red arrows in the figure, absorptions at positions a, b, and c assuming equal populations of levels at high-enough temperatures.

Cr^{3+} (d^3, ^4F) often takes the states close to the above ideality. Figure 2.17 shows an EPR experiment on Cr^{3+}, in which they doped 1% Fe^{3+} and Cr^{3+} into cubic state of $BaTiO_3$. Three main peaks corresponding to a, b, and c in Fig. 2.16 are observed[6]. The lineshape did not change with the direction of magnetic field indicating that $\tilde{\boldsymbol{g}}$ is isotropic though finite E is deduced from the relative peak positions. The data indicate doped Cr^{3+} is in tetragonal state. The absorption peaks for $S = 1$ are from Cr dimers. The parameters are shown in Tab. 2.9.

$BaTiO_3$ also has hexiagonal phase h-$BaTiO_3$. Cr^{3+} impurities in h-$BaTiO_3$ show very different EPR absorption lines. Even this spectrum can be explained by the spin Hamiltonian of eq. (2.110) with an anisotropic $\tilde{\boldsymbol{g}}$ and parameters shown in the table[7].

2.9.4 Magnetic refrigeration

Magnetic refrigeration (MR) is a cooling method that can exert cooling ability in a wide temperature range by selecting a magnetic moment system (working substance) from room temperature to ultra-low temperature. The MR with paramagnetic salt was once main player in creating very low temperature till 1960's, then in the range from 0.01 to 1 K the position was replaced by the dilution refrigerators[8]. On the other hand, below few mK, once Pomeranchuk cooling was used, but then the main shifted to **nuclear demagnetization**.Even in regions other than low temperatures, the MR are now used for various purposes. Exploration of cooling substances spans not only paramagnetic materials but also

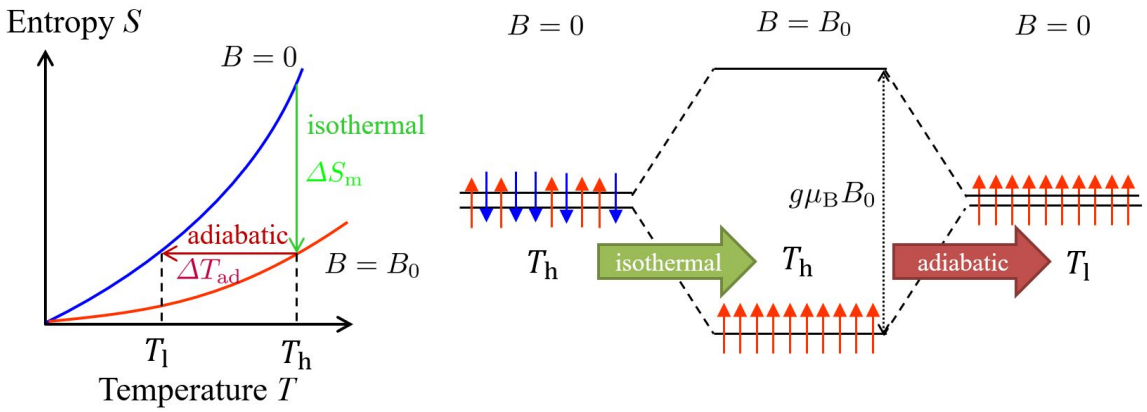

Fig. 2.18 Concept of magnetic refrigeration. Left: Illustration of temperature variation of entropy in a magnetic system in zero and finite magnetic fields. The green arrow indicates first isothermal application of magnetic field. The brown arrow shows adiabatic demagnetization. The right figure illustrates evolution of spin distribution in the sequence of isothermal field application and adiabatic demagnetization in a simple two-level spin system.

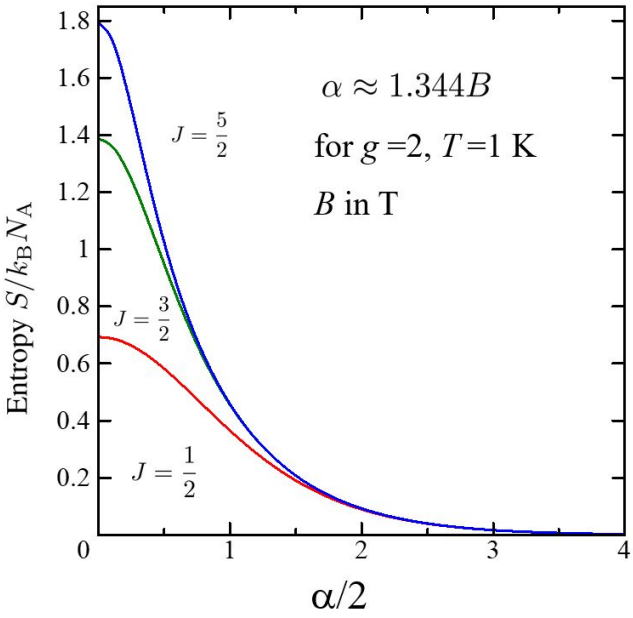

Fig. 2.19 Entropy in eq. (2.113) is expressed as a function of α for $J = 1/2, 3/2, 5/2$.

those have phase transitions caused by interactions between spins and magnetic field. In recent years, regardless of its pros and cons, the possibility of liquefying and transporting hydrogen has been explored, and development research using magnetic refrigeration for cooling is also being conducted[9].

The principle of MR is simple as follows. A free spin system has random directions in spin and the maximum entropy at zero field. With the isothermal magnetization, the spins are aligned along the magnetic field by the Zeeman effect. The process reduces the entropy. Hence a heat is discharged to the environment. Then during the adiabatic demagnetization, the entropy is kept constant. In the spin distribution, there is no increase in the population to excited states in spite of decrease in the distance between the ground and the excited states. This is a low temperature state. With connecting this coolant to a material to be cooled, a heat is transferred from this material to the coolant. The process is summarized in Fig. 2.18.

Let S be the entropy of system composed of paramagnetic ions with total angular momentum J. At zero field, $S = k_{\rm B}N_{\rm A}\ln(2J+1)$ for 1 mol. Let us write the variation in S with isothermal magnetization up to B as $\Delta S(B, T_{\rm i})$. Then with the final temperature $T_{\rm f}$ after the **adiabatic demagnetization**, $\Delta S(B, T_{\rm i})$ is given by

$$\Delta S(B, T_{\rm i}) = S(0, T_{\rm i}) - S(B, T_{\rm i}) = \int_{T_{\rm f}}^{T_{\rm i}} \frac{C_{\rm m}}{T} dT, \quad C_{\rm m} = T\left(\frac{\partial S}{\partial T}\right)_{B=0}. \tag{2.111}$$

C_m is the specific heat at zero field.

The magnetization M and the entropy S are calculated just as eq. (1.25) as

$$M = N_{\rm A} g \mu_{\rm B} \left[\frac{2J+1}{2}\coth\left(\frac{2J+1}{2}\alpha\right) - \frac{1}{2}\coth\frac{\alpha}{2}\right], \quad \alpha \equiv \frac{g\mu_{\rm B}B}{k_{\rm B}T}, \tag{2.112}$$

$$\frac{S}{N_{\rm A}k_{\rm B}} = \frac{\alpha}{2}\coth\frac{\alpha}{2} - \frac{2J+1}{2}\alpha\coth\left[\frac{2J+1}{2}\alpha\right] + \ln\left[\frac{\sinh[(2J+1)\alpha/2]}{\sinh\alpha/2}\right]. \tag{2.113}$$

Figure 2.19 shows the results for J =1/2, 3/2, 5/2. Since $\alpha \approx 1.344B$ (B in T) for $g = 2$, T =1 K, the most of entropy in a free spin system at T=1 K can be removed by cycling of B =2 T.

The spins in paramagnetic salts maintain a relatively large entropy even at low temperatures where other degrees of freedom are quenched, such as lattice vibration, so they are used to obtain extremely low temperatures based on low temperatures. However, e.g., if we choose a material with a phase transition induced by magnetic field, a large decrease in entropy is expected even at high temperatures. This can be understood by a Maxwell relation

$$\left(\frac{\partial S}{\partial B}\right)_T = \left(\frac{\partial M}{\partial T}\right)_B, \tag{2.114}$$

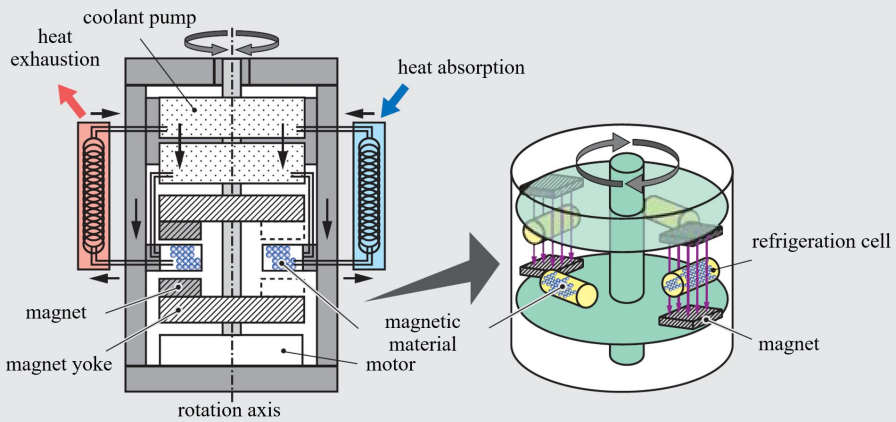

Fig. 2.20 Schematic diagram of active magnetic refrigeration (AMR). From Akiko Saito, Toshiba Review Vol.62, 78 (2007) (in Japanese).

in which magnetic field variation of entropy is proportional to temperature derivative of magnetization.

Gd (Curie temperature 289 K) is frequently used as a cooling material, which can have a cooling power at around room temperature.Further research and development of working materials and methods are underway with the aim of putting them into practical use near room temperature. For the use of MR under continuous inflow of heat, a continuous cooling method is active magnetic refrigeration (AMR) illustrated in Fig. 2.20. Magnetization/demagnetization is done by rotation of tables, to which permanent magnets are fixed. The turn table scheme realizes successive on/off of magnetic field and continuous flow of refrigerant realizes continuous cooling.

There are many proposals and exploration of cooling substance, e.g., nano-particles of ferromagnet that have giant magnetic moments, materials with meta magnetic transitions (first order transition from Pauli paramagnet to intinerant electron ferromagnet). If time permits we will revisit such transitions. They are already beginning to be used and some commercial machines are appearing.

Chapter 3

Magnetism of conduction electrons

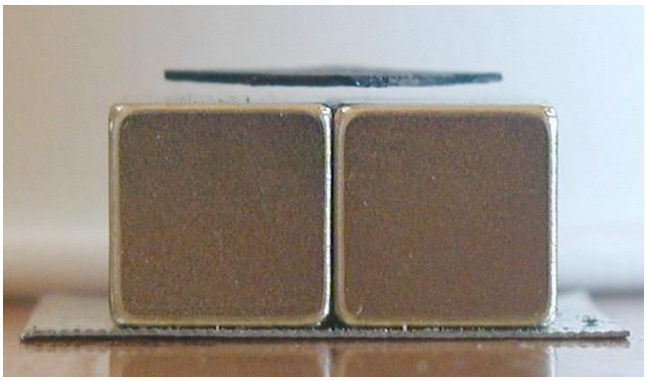

Magnetic levitation of graphite

https://sci-toys.com/scitoys/scitoys/magnets/pyrolytic_graphite.html

In the previous chapter, the focus has been on the paramagnetism of insulators including magnetic ions. The magnetism that appears due to the phase transition caused by the interaction between electron spins will be investigated in the following chapters. Here we have a short look on the magnetism of conduction electrons other than such cooperative phenomena.

3.1 Pauli paramagnetism

3.1.1 Conduction electrons

Electronic states in crystals are described by energy bands separated by energy gaps on the energy axis due to discrete spatial translational symmetry. In a system of free electrons, due to the fermionic constraint, there exists the Fermi level determined by the number of particles and the band structure. The orbital states described by Bloch functions have up-down spin degeneracy at zero field. In metals, the Fermi levels place inside energy bands (conduction bands), and we measure the Fermi energy E_{F} from the bottom of conduction band. At room temperatures $E_{\mathrm{F}} \gg k_{\mathrm{B}}T$, and the distribution is Fermi degenerated.

In many actual metals, the electronic structures are complicated due to, e.g., multiple bands in k-space, etc. However, here, to explore the essential properties, we assume a single band with single band in the center of k-space with a single effective mass. Further we ignore the mutual electron interactions, which must exist in real systems. Such a non-interacting model well describes behavior of electrons in actual metals in most cases. This gets theoretical support from Landau's **Fermi liquid theory**[10, 11].

3.1.2 Magnetic response by electron spins

To see the response of electron spins, we write the Hamiltonian in second-quantized form as

$$\mathscr{H} = \sum_{\boldsymbol{k}\sigma} E_{\boldsymbol{k}} c^{\dagger}_{\boldsymbol{k}\sigma} c_{\boldsymbol{k}\sigma} + \frac{1}{2} g\mu_{\mathrm{B}} B \sum_{\boldsymbol{k}\sigma} \sigma c^{\dagger}_{\boldsymbol{k}\sigma} c_{\boldsymbol{k}\sigma}. \tag{3.1}$$

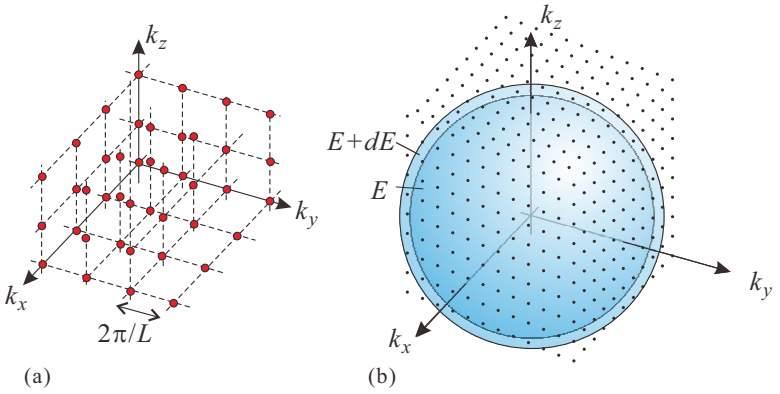

Fig. 3.1 (a) Red points represent eq. (3.2) in k-space. (b) To calculate the density of states, we count the numbe of possible points in the shell between E and $E + dE$.

$c^\dagger_{\boldsymbol{k}\sigma}$ is a creation operator of an electron with wavenumber $\boldsymbol{k}$, spin σ ($\sigma = \pm 1$ for $\uparrow\downarrow$). The first term is the kinetic energy, the second is the Zeeman energy.

We take periodic boundary condition in a cube with a side of L. $kL = 2n\pi$ (n: integer) along a side gives

$$\boldsymbol{k} = \frac{2\pi}{L}(n_x, n_y, n_z) \quad (n_x, n_y, n_z : \text{ integers}). \tag{3.2}$$

The discrete points in k-space are displayed in Fig. 3.1(a). The point density is $(L/2\pi)^3$. Let $\rho(E)$ the energy density of states per volume and per spin. ρ depends on the spin direction in ferromagnets but is common in paramagnets with time-reversal symmetry. In three dimensional free electron systems, $E_{\boldsymbol{k}} = \hbar^2 k^2/2m$ with the effective mass m. The wavenumbers which give a constant E for $E_{\boldsymbol{k}}$ are, in k-space, the points expressed in (3.2) and on the sphere with radius $k_E = \sqrt{2mE}/\hbar$. To obtain $\rho(E)$, we count such points within the shell between E and $E + dE$ and divide by dE as in Fig. 3.1(b). Thus we obtain

$$\rho(E) = \frac{1}{L^3}\left(\frac{L}{2\pi}\right)^3 4\pi k_E^2 \frac{dk_E}{dE} = \frac{1}{\pi^2\hbar^3}\sqrt{\frac{mE}{2}}. \tag{3.3}$$

The expectation value of the magnetic moment is given by

$$-\frac{g\mu_{\rm B}}{2}\sum_{\boldsymbol{k}\sigma}\sigma\left\langle c^\dagger_{\boldsymbol{k}\sigma}c_{\boldsymbol{k}\sigma}\right\rangle = \frac{g\mu_{\rm B}}{2}\sum_{\boldsymbol{k}}\left[f\left(E_{\boldsymbol{k}} - \frac{g\mu_{\rm B}B}{2}\right) - f\left(E_{\boldsymbol{k}} + \frac{g\mu_{\rm B}B}{2}\right)\right], \tag{3.4}$$

where

$$f(E) = \frac{1}{\exp[(E-\mu)/k_{\rm B}T] + 1} \tag{3.5}$$

is the Fermi distribution function with μ as the chemical potential. Then the magnetization M is given by

$$M = \frac{g\mu_{\rm B}}{2}\int_0^\infty dE\rho(E)\left[f\left(E_{\boldsymbol{k}} - \frac{g\mu_{\rm B}B}{2}\right) - f\left(E_{\boldsymbol{k}} + \frac{g\mu_{\rm B}B}{2}\right)\right]. \tag{3.6}$$

To determine μ, we write the electron concentration as $N_{\rm e}$ and use

$$N_{\rm e} = \int_0^\infty dE\rho(E)\left[f\left(E_{\boldsymbol{k}} - \frac{g\mu_{\rm B}B}{2}\right) + f\left(E_{\boldsymbol{k}} + \frac{g\mu_{\rm B}B}{2}\right)\right]. \tag{3.7}$$

Thus determined μ is the Fermi energy $E_{\rm F}$ described in Sec. 3.1.1.

We then obtain the spin magnetic susceptibility of conduction electrons at $T = 0$ as

Pauli paramagnetic susceptibility

$$\chi_{\rm Pauli} = \left(\frac{g\mu_{\rm B}}{2}\right)^2 [2\rho(E_{\rm F})]. \tag{3.8}$$

The spin susceptibility of Fermi-degenerated free electrons is constant and proportional to the density of states at the Fermi level. This is called **Pauli paramagnetism**. This result holds for general complicated band structures as long as the system can be treated as a Fermi liquid.

3.2 Landau diamagnetism

As we have seen as the Bohr-van Leeuwen theorem, that a classical system of charged particles cannot have magnetism. In real systems of charged particles, even without orbital quantization by local potentials or spins, the quantization causes magnetism. Let us have a look on that.

3.2.1 Landau quantization

Landau quantization is universally observed in the systems of free charged particles under magnetic field. Particularly in two-dimensional systems, it results in an extraordinary phenomenon called quantum Hall effect. Here we study its effect on orbital magnetism. We directly treat the orbital motions and write the Hamiltonian as

$$\mathscr{H} = \frac{1}{2m}\sum_i (\boldsymbol{p}_i + e\boldsymbol{A})^2. \tag{3.9}$$

We take Landau gauge $\boldsymbol{A} = (0, Bx, 0)$ to express the magnetic field B along z-axis. m is the electron rest mass. Schrödinger equation for a single electron is

$$-\frac{\hbar^2}{2m}\left[\frac{\partial^2}{\partial x^2} + \frac{\partial^2}{\partial z^2} + \left(\frac{\partial}{\partial y} - i\frac{eB}{\hbar}x\right)^2\right]\psi = E\psi. \tag{3.10}$$

The coordinate operator in the lhs of (3.10) is only x. Thus we assume plane wave along y and z, namely $\psi = \exp[i(k_y y + k_z z)]u(x)$. By substituting this to (3.10), we obtaine

$$-\frac{\hbar^2}{2m}\left[\frac{d^2u}{dx^2} + \left(k_y - \frac{eB}{\hbar}x\right)^2 u\right] = \left(E - \frac{\hbar^2 k_z^2}{2m}\right)u. \tag{3.11}$$

This is in the form of one-dimensional harmonic oscillator with the center coordinate

$$x_\mathrm{c} = \hbar k_y / eB. \tag{3.12}$$

The frequency of oscillator ω_c is

$$\frac{m\omega_\mathrm{c}^2}{2} = \frac{(eB)^2}{2m} \quad \therefore\ \omega_\mathrm{c} = \frac{eB}{m}. \tag{3.13}$$

This is called **cyclotron frequency**. The energy eigenvalues are

$$E(n, k_z) = \frac{\hbar^2 k_z^2}{2m} + \left(n + \frac{1}{2}\right)\hbar\omega_\mathrm{c} = \frac{\hbar^2 k_z^2}{2m} + (2n+1)\mu_\mathrm{B}B \quad (n = 0, 1, 2, \cdots). \tag{3.14}$$

The motion along z-axis is free-electron like but in xy-plane the kinetic energy is discretely quantized. This is called **Landau quantization**. The energy levels of harmonic oscillator indexed by n in (3.14) are called Landau levels.

It seems a bit strange that the solutions are strongly anisotropic although the system is uniform in xy-plane. This is the result of selection of Landau gauge to solve the equation. The symmetrically localized solutions can be obtained, e.g. by taking the symmetric gauge. These are degenerated for the same n, and with superpositions we can have eigenstates with various distributions in xy-plane. In semi-classical approach, the Landau quantization can be viewed as the quantization of cyclotron motion through the spatial localization. However there still exists the freedom in taking the center of cyclotron motion, that gives large degree of degeneracy and results in the eigenstates with various outlook.

3.2.2 Orbital diamagnetism

We consider the normalization of eigenstates in the form of $\exp[i(k_y y + k_z z)]u(x)$ in the cube with side length L. z-direction is the same as free electrons. From $k_z = (2\pi/L)n_z$ ($n_z = 0, \pm 1, \cdots$), $E_z = \hbar^2 k_z^2/2m$, possible number of k_z for kinetic energy along z-direction less than E_z is $2L\sqrt{2mE_z}/h$. Also for y, because the form is plane wave, from the periodic boundary condition

$$k_y = \frac{2\pi}{L} n_y \quad (n_y = 0, \pm 1, \pm 2, \cdots). \tag{3.15}$$

On the other hand, k_y relates with the center x_c of harmonic oscillator along x-direction as (3.12), then when x_c is in the region $[-L/2, L/2]$,

$$-\frac{L}{2} \le \frac{\hbar}{eB} k_y = \frac{\hbar}{eB}\frac{2\pi}{L} n_y \le \frac{L}{2} \quad \therefore\ |n_y| \le \frac{eBL^2}{4\pi\hbar}.$$

This means the degree of degeneracy of a single Landau level in xy-plane is eBL^2/h.

From the above, $\Omega(E)$, the number of states below the total energy E is

$$\Omega(E) = \frac{L^3}{\hbar^2}\sqrt{8m}eB \sum_{n=0}^{n_\mathrm{max}} \sqrt{E - (2n+1)\mu_\mathrm{B}B}, \tag{3.16}$$

where

$$n_\mathrm{max} = \mathrm{int}\left(\frac{E - \mu_\mathrm{B}B}{2}\right). \tag{3.17}$$

Because the density of states is given by $d\Omega/dE$, the Free energy of the system is

$$F = N\mu - 2k_\mathrm{B}T \int \frac{d\Omega}{dE} \ln\{1 + \exp[-(E-\mu)/k_\mathrm{B}T]\} dE, \tag{3.18}$$

where we consider the spin degree of freedom 2. The integral part is partially integrated as follows.

$$\begin{aligned}
\int \frac{d\Omega}{dE} \ln\{1 + \exp[-(E-\mu)/k_\mathrm{B}T]\} dE &= -\int \Omega(E) \left(-\frac{1}{k_\mathrm{B}T}\right) \frac{\exp[-(E-\mu)/k_\mathrm{B}T]}{1 + \exp[-(E-\mu)/k_\mathrm{B}T]} dE \\
&= \frac{1}{k_\mathrm{B}T} \int \left[\int \Omega(E) dE\right] \frac{d}{dE} \frac{1}{1 + \exp[(E-\mu)/k_\mathrm{B}T]} dE \\
&= \frac{1}{k_\mathrm{B}T} \frac{2\sqrt{8m}}{3} \frac{eBL^3}{h^2} \int \sum_{n=0}^{n_\mathrm{max}} [E - (2n+1)\mu_\mathrm{B}B]^{3/2} \frac{d}{dE} \frac{1}{1 + \exp[(E-\mu)/k_\mathrm{B}T]} dE.
\end{aligned}$$

From $\mu_\mathrm{B} = e\hbar/2m$ we can rewrite F as

$$F = N_\mathrm{e}\mu - A \int \phi(E) \frac{d}{dE} \frac{1}{1 + \exp[(E-\mu)/k_\mathrm{B}T]} dE, \tag{3.19a}$$

where

$$A = \frac{16L^3}{3\pi^2\hbar^3} m^{3/2} (\mu_\mathrm{B}B)^{5/2}, \tag{3.19b}$$

$$\phi(E) = \sum_{n=0}^{n_\mathrm{max}} \left[\frac{E}{2\mu_\mathrm{B}B} - \left(n + \frac{1}{2}\right)\right]^{3/2}. \tag{3.19c}$$

Taking the limit $B \to 0$, it becomes

$$F = N_\mathrm{e}E_\mathrm{F} - A\phi(E_\mathrm{F}). \tag{3.20}$$

Here we use the asymptotic form for $x \gg 1$

$$\sum_{n=0}^{n_\mathrm{max}} \left[x - \left(n + \frac{1}{2}\right)\right]^{3/2} \approx \frac{2}{5}x^{5/2} - \frac{1}{16}x^{1/2} + \cdots. \tag{3.21}$$

This is obtained by applying the Euler–Maclaurin formula to $F(y) = (x-y)^{3/2}$ as follows.

$$\sum_{n=0}^{n_0} F(n+1/2) \approx \int_0^{n_0+1} dy F(y) - \frac{1}{24}[F'(n_0+1) - F'(0)]$$
$$\approx \frac{2}{5}x^{5/2} - \frac{1}{16}x^{1/2}.$$

Hence we obtain the asymptotic expansion

$$\phi(E) = \frac{2}{5}\left(\frac{E}{2\mu_{\rm B}B}\right)^{5/2} + \frac{1}{16}\left(\frac{E}{2\mu_{\rm B}B}\right)^{1/2} + \cdots, \tag{3.22}$$

which gives the free energy as

$$F = \text{const.} - \frac{L^3}{3}\rho(E_{\rm F})(\mu_{\rm B}B)^2 + \cdots. \tag{3.23}$$

Then we obtain the orbital diamagnetic susceptibility of free electrons as

Landau diamagnetic susceptibility

$$\chi_{\rm Landau} = -\frac{2}{3}\rho(E_{\rm F})\mu_{\rm B}^2. \tag{3.24}$$

This is called **Landau diamagnetism**.

Taking the effective mass to the free electron rest mas, $\chi_{\rm Landau}$ has the opposite sign to $\chi_{\rm Pauli}$ and the magnitude is 1/3. The total susceptibility is then

$$\chi = \chi_{\rm Pauli} + \chi_{\rm Landau} = \frac{4}{3}\rho(E_{\rm F})\mu_{\rm B}^2. \tag{3.25}$$

Appendix 5A: Weak crystal field approximation

In the lecture on $3d$ transition metal ions, we consider the approximation of a strong crystal field (ligand field), that is, the one-electron states of $3d$ electron in the crystal field are considered first, and fill them with electrons to consider multi-electron states. On the other hand, there is also a method that first assumes the LS multiplex term as we did in the case of $4f$ lanthanoid ion, and then considers how this multi-electronic state splits in the crystal field using point group theory. This is called **weak crystal field approximation**. In Fig. 5A.1, we show how the state d^n splits in an octahedral potential.

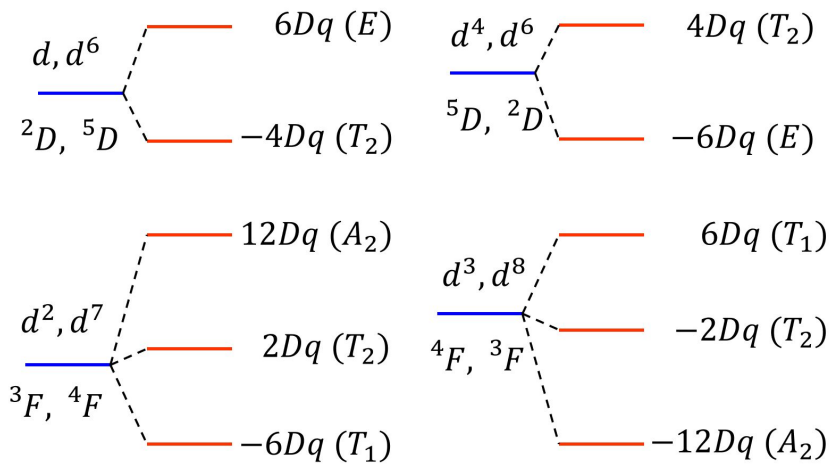

Fig. 5A.1 Split of d^n state in an octahedral crystal potential in weak crystal field approximation.

References

[1] Charles P. Slichter. *Principles of Magnetic Resonance (Springer Series in Solid-State Sciences) by Charles P. Slichter(2010-12-01)*. Springer, 1653.

[2] Marcus A. Hemminga and Lawrence Berliner. *ESR Spectroscopy in Membrane Biophysics (Biological Magnetic Resonance Book 27) (English Edition)*. Springer, 8 2007.

[3] M. H. L. Pryce. *Proc. Phys. Soc.*, Vol. A63, p. 25, 1950.

[4] Mohammad Mostafanejad. Basics of the spin hamiltonian formalism. *International Journal of Quantum Chemistry*, Vol. 114, No. 22, pp. 1495–1512, June 2014.

[5] 上村洸, 菅野暁, 田辺行人. 配位子場理論とその応用 (物理科学選書). 裳華房, 6 1969.

[6] Sundar R. Bairavarasu, Matthew E. Edwards, Medury D. Sastry, Tatiana Kukhtareva, Holger M. Jaenisch, Rastgo H. Hawrami, Dimitrios Lianos, and Manmohan D. Aggarwal. Photo-EPR studies of photorefractive batio$_3$ heavily doped with cr^{3+}: evidence of photo-induced dissociation of cr^{3+} dimers. In Ruyan Guo, Shizhuo S. Yin, and Francis T. S. Yu, editors, *Photonic Fiber and Crystal Devices: Advances in Materials and Innovations in Device Applications*. SPIE, September 2007.

[7] R Böttcher, E Erdem, H T Langhammer, T Müller, and H-P Abicht. Incorporation of chromium into hexagonal barium titanate: an electron paramagnetic resonance study. *Journal of Physics: Condensed Matter*, Vol. 17, No. 17, pp. 2763–2774, April 2005.

[8] O. V. Lounasmaa. *Experimental Principles and Methods Below 1K*. Academic Pr, 6 1974.

[9] Koji Kamiya, Koichi Matsumoto, Takenori Numazawa, Shinji Masuyama, Hiroyuki Takeya, Akiko T. Saito, Naoya Kumazawa, Kazumi Futatsuka, Keigo Matsunaga, Tsuyoshi Shirai, Suguru Takada, and Teruhito Iida. Active magnetic regenerative refrigeration using superconducting solenoid for hydrogen liquefaction. *Applied Physics Express*, Vol. 15, No. 5, p. 053001, January 2022.

[10] L. D. Landau. The theory of a fermi liquid. *Sov. Phys. JETP*, Vol. 3, pp. 920–925, 1957.

[11] Piers Coleman. *Introduction to Many-Body Physics*. Cambridge University Press, 11 2015.

3.2.3 de Haas-van Alphen effect

When we derived Landau orbital diamagnetic susceptibility, we took the small field limit, in that the Landau level splitting $\hbar\omega_c$ is much smaller than E_F and applied an asymptotic formula. When the magnetic field goes up to a comparatively large region [*1], the Landau quantization gives a dramatic effect on the magnetization. That is the oscillation of magnetization called the de Haas-van Alphen effect. In solids, the orbital diamagnetism strongly depends on the band structure particularly around the Fermi surface. This is in strong contrast to the spin paramagnetism. Hence the relation between the Pauli paramagnetism and the Landau diamagnetism shown in the previous subsection generally does not hold in solids. This sensitivity of diamagnetism to the band structure is applied for exploration of band structures.

We rewrite eq. (3.19) as

$$\frac{F}{n_e} = \mu - \frac{\hbar\omega_c}{E_F^{3/2}} \int_0^\infty dE \sum_{n=0} \left[E - \left(n + \frac{1}{2} \right) \hbar\omega_c \right]^{3/2} \left(-\frac{\partial f}{\partial E} \right), \tag{3.26}$$

where $n_e = N_e/L^3$. Also, the relation $2\mu_B B = \hbar\omega_c$ is used to restore $\hbar\omega_c$ in preparation for the change in the effective mass. The summation over n should be taken for positive arguments in the paretheses $(\cdots)$. On the other hand, the energy derivative of Fermi function $-\partial f \partial E$ approaches a delta function for $T \to 0$. We guess, therefore, the magnetization varies largely for the magnetic field where the Landau levels $(n+1/2)\hbar\omega_c$ coincide E_F. This oscillation of magnetization against the magnetic field is called **de Haas-van Alphen effect, dHvA effect**.

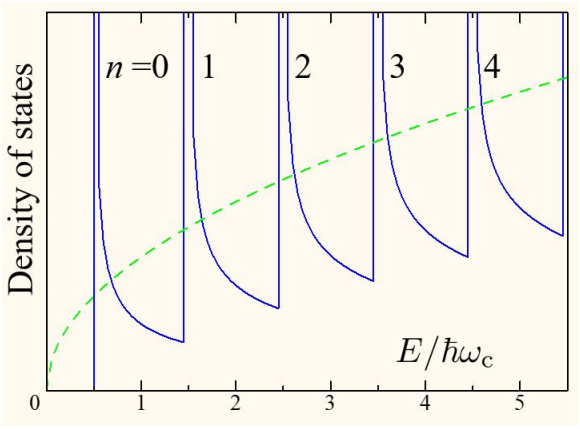

Fig. 3.2 Density of states is plotted against energy measured by Landau level spacing $\hbar\omega_c$.

The density of states of a one-dimensional system is given by

$$E_k = \frac{\hbar^2 k^2}{2m}, \quad \rho_{1d}(E) = \frac{1}{L}\frac{L}{2\pi}\left(\frac{\hbar^2 k}{m}\right)^{-1} = \frac{1}{2\pi\hbar}\sqrt{\frac{m}{2E}}.$$

By counting all these states, we get the total density of states per spin as

$$\rho(E) = \frac{1}{2\pi\hbar}\sqrt{\frac{m}{2}} \sum_{n=0} \frac{1}{\sqrt{(E-(n+1/2)\hbar\omega_c}}. \tag{3.27}$$

The summation over n should be taken for $E > (n+1/2)\hbar\omega_c$. The density of states in (3.27) is divergent at $E/\hbar\omega_c$ as shown in Fig. 3.2. With increasing magnetic field, the position of E_F decreases due to the increase in $\hbar\omega_c$. When E_F passes a position of divergence, a rapid rearrangement in electron population occurs and the thermodynamic functions including the magnetization get rapid changes.

To see how one can get the information of the Fermi surface, refer to Appendix 6B. In the lecture, I will introduce an example of experiment on Thallium-based high-Tc cuprate[1].

[*1] In usual metals, $\hbar\omega_c$ of "strong magnetic field" at an ordinary level does not go up to the level of Fermi energy. Hence even in this treatment, we still use the condition $\hbar\omega_c \ll E_F$

3.3 Orbital diamagnetism in graphene, graphite

What we have seen above is the magnetic response of the free electron system. The Pauli paramagnetism comes from a small shift of the spin bands on the energy axis. Hence we can guess that the same formula is applicable for band electrons in metals as long as the band has no anomaly at the Fermi level.

On the other hand, the orbital diamagnetism largely gets the effect of the band structure. Even in the low field limit, which is the constraint for the Landau diamagnetism, the magnetic response of Bloch electrons is a difficult problem. The theoretical frameworks from the viewpoint of linear response (Kubo formula)[2] and so forth have long been tried. The field is still active and there have been reports on theoretical developments aiming at application to graphene from this department[3, 4, 5]. Here I would like to introduce shortly a characteristic example of graphene and multilayer graphene (thin graphite). In the beginning of the present chapter, I have introduced the fact that a graphite has a very large negative orbital susceptibility. This is due to its characteristic band structure.

3.3.1 Orbital diamagnetism in graphene

We are familiar with **graphite**, e.g., as a material used in cores of pencils. It is said to be the most stable thermodynamically as elementally crystal of carbon. It's crystal structure is a stack of honeycomb planes as shown in Fig. 3.3. A single atomic layer of the graphite is called **graphene**, which can be extracted by exfoliation, grown by CVD, or thermalization of SiC.

Carbon atoms in a plane of graphene are strongly connected to the neighbors by covalent bonds with no buckling. Hence graphene conduction electrons in p_z orbitals can be treated as a complete two-dimensional orbital system. And just at $E_{\rm F}$ in pure graphenes, the linear dispersions form crossing points called **Dirac points** as shown in Appendix 6C. Hence the band is massless and gapless. The orbital susceptibility of graphene has long been calculated. In the simplest model[6], it is given by (in cgs unit)

$$\chi(E_{\rm F}) = -\frac{g_v g_s e^2}{6\pi}\left(\frac{e}{c}\right)^2 \delta(E_{\rm F}), \tag{3.28}$$

where $g_v = 2$ is the orbital degeneracy represented as K and K' points in k-space, $g_s = 2$ is the spin degeneracy, c is the speed of light. Here $E_{\rm F}$ is measured from the Dirac points, and the susceptibility in (3.28) is infinite when $E_{\rm F}$ is at the Dirac points, and is zero elsewhere.

This can be roughly interpreted as follows. Let an electron be in a cyclotron motion (thus not at Dirac points) under a magnetic field B. When B changes, an electric field E is created as in eq. (1.28). In sec. 1.3.2, E accelerates the electron resulting in the diamagnetism. In the present case, E gives an increase in the kinetic energy of the electron though that does not enhance the velocity due to the linear dispersion. Hence the diamagnetic susceptibility is zero. However, when

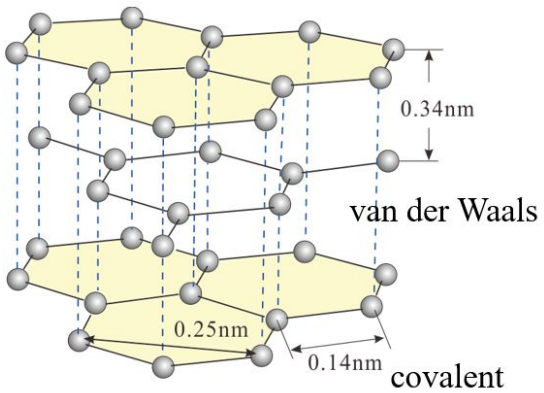

Fig. 3.3 Illustration of graphite crystal structure. Honeycomb sheets made of carbon covalent bonds are stacked with an in-plane half lattice constant shift by layer. That is, the same 2-dimensional lattice appears alternatively, which structure is called AB-stacking. The sheet-to-sheet is connected by the van der Waals coupling.

the increase in the energy goes over a Dirac point, the velocity jumps, e.g., from $-v_{\rm e}$ to $+v_{\rm e}$. The acceleration is infinite giving the divergence of the susceptibility at the Dirac point.

In the lecture I would like to introduce an experiment, in which the authors claim they have observed such peculiar orbital diamagnetic susceptibility of graphene.

3.3.2 Diamagnetic susceptibility of multi-layer graphene

The extraordinary diamagnetism that causes magnetic levitation, and the strong magneto-optical response have long been known, but clear interpretations have not been given yet. It has been said that we need to consider a more practical model, in which experimental details like inhomogeneity in the field[7].

In order to treat the space distribution of magnetic field, we consider the Fourier expansion in x: $B(\boldsymbol{r}) = B(q)\cos qx$, of the field along z-axis onto 2-dimensional system in xy-plane. The current distribution in response to $B(\boldsymbol{r})$ generally has the form of $j_y(\boldsymbol{r}) = j_y(q)\sin qx$[9]. The q-component of magnetization $m(\boldsymbol{r})$ is obtained from the two-dimensional current as この 2 次元電流から，磁化 $m(\boldsymbol{r})$ の q 成分は

$$j_y = -c\frac{\partial m}{\partial x} \to m(\boldsymbol{r}) = m(q)\cos qx \quad m(q) = -\frac{j_y(q)}{cq}.$$

The susceptibility $\chi(q)$ is defined as $m(q)/B(q)$. Then the response current of graphene to $B(\boldsymbol{r}) = B(q)\cos qx$ is

$$j_y(\boldsymbol{r}) = -\frac{g_v g_s e^2 v}{16\hbar c}B(q)\sin qx. \tag{3.29}$$

The diamagnetic inductive current by this responding current is from Amperé's law

$$B_{\rm ind}(\boldsymbol{r}) = -\alpha_g B(\boldsymbol{r}), \quad \alpha_g = \frac{2\pi g_v g_s e^2 v}{16\hbar c^2} \approx 4\times 10^{-5}, \tag{3.30}$$

which does not depend on the space distribution wavenumber q. Therefore any spatial distribution of magnetic field causes the inductive magnetic field of $-\alpha_g$ times the original field and the theorem of superposition leads to the total inductive field of $-\alpha_g$ times the total original field.

As an example, let us place a magnetic charge $q_{\rm m}$ in the region $z > 0$. The graphene at $z = 0$ partially screens the field to create the mirror charge $-\alpha_q q_{\rm m}$ seen from $z < 0$, namely the field caused by the mirror charge is superposed to the original field. The same for $z > 0$ and the field created by the mirror charge of $\alpha_q q_{\rm m}$ in $z < 0$ region is overlapped to the original field. The force, which the original magnetic charge in Fig. 3.4(a) gets from the graphene, is calculated from the mirror charge in Fig. 3.4(c).

Let us consider the case a permanent magnet approaches a graphene. The magnet is a half-infinite cylinder with a radius a having the edge magnetic charge density σ_m. When the edge reaches the graphene, $d = 0$, the force given to the magnet per area is $2\pi\alpha_g\sigma_m^2$. In the case of Neodymium magnet, σ_m can be around 1 T. The force is then 0.16 dyne, which is surprisingly large for a single atomic layer.

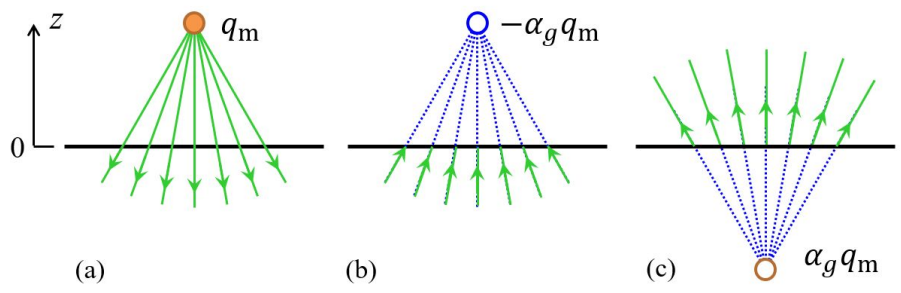

Fig. 3.4 Mirror magnetic charge caused by a graphene. The graphene is illustrated as the black line at $z = 0$. (a) Magnetic field by a magnetic charge. (b) Inducted field in $z < 0$, (c) and in $z > 0$. From [8].

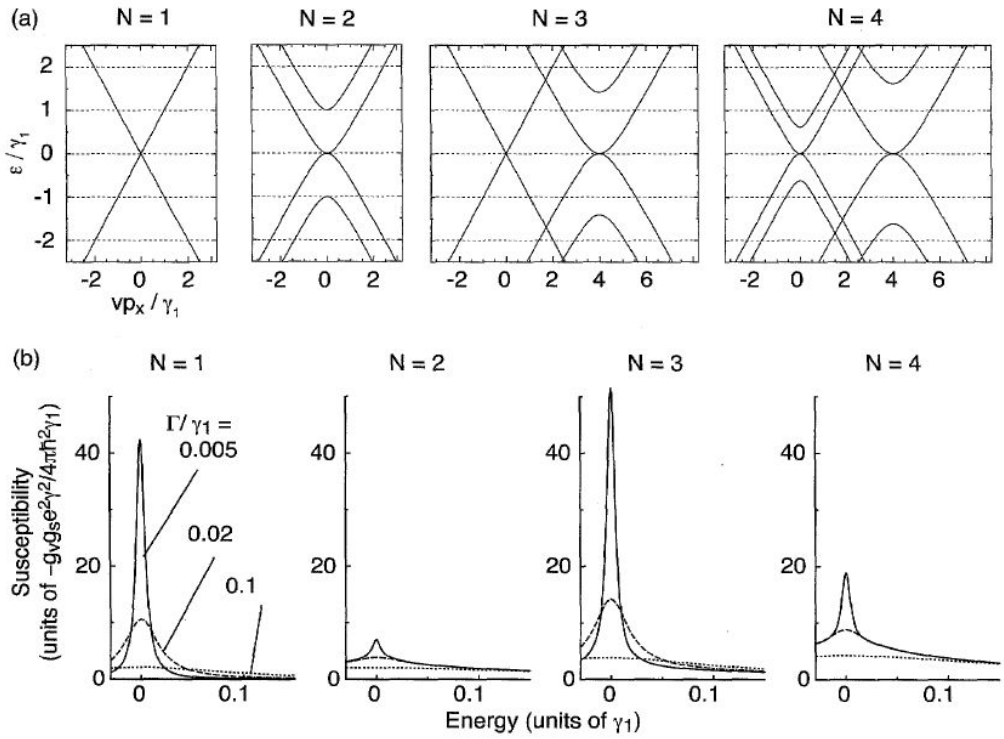

Fig. 3.5 (a) Band structures and (b) orbital diamagnetic susceptibilities $\chi(E_{\rm F})$ for single to four layer graphenes. Γ is the width of energy fluctuation caused by impurities. From [8, 10].

In an ordinary 2-dimensional metal with an effective mass m^*, the susceptibility is a constant $\chi_0 = -e^2/(24\pi m^* c^2)$ in the long wavelength limit. Let us take an example of GaAs 2-dimensional electrons with $m^* = 0.067 m_0$. Then the ratio of repulsive force f_c to that of graphene f_g is $f_g/f_c \approx a/(0.01\ \mathrm{nm})$. The radius is in cm order then the ratio goes up to 9-digits.

Next we go to multi-layer graphenes, which can be seen as thin films of graphite[10]. They have the AB stacking as in Fig. 3.3 with a weak interlayer coupling with the coupling energy of 0.4 eV. The structure with more layers than two, can be treated as a repetition of the AB stack and the calculation can be reduced to the case of the bilayer graphene. A single-layer graphene has gapless linear dispersion both at K and K'. Also in a bilayer graphene, a pair of bands has a zero-gap with finite effective masses, the other pair has a gap due to the inter-layer coupling. An $N = 2M$ layer graphene has M sets of bilayer-type bands. When $N = 2M + 1$, a set of single-layer bands is added.

Figure 3.5 shows such calculation of the band structures and the orbital diamagnetic susceptibilities for single to four layer graphenes. The band with a Dirac point appears for an odd number of N giving a large contribution to the diamagnetic susceptibility. For an even N, that contribution disappears. However the further increase in the number of layers results in the increase in the diamagnetic susceptibility. This increase is thought to lead to the large diamagnetism in graphite.

Chapter 4

Interaction between Spins

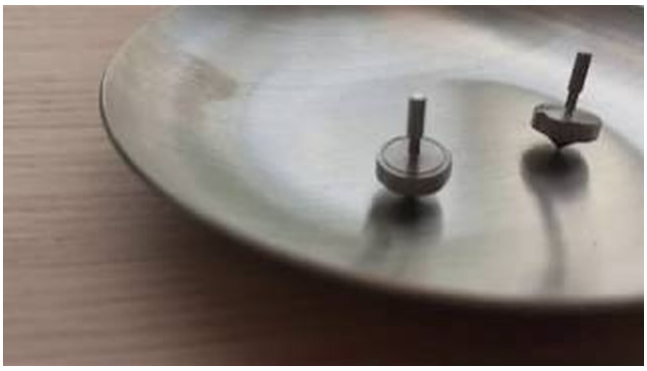

Fighting tops

https://www.youtube.com/watch?v=2WaU7NDOHLQ

We have looked for "entities" which work as magnetic dipoles in materials and found in the quantum theory, that the spins and the orbitals are working as magnetic dipoles namely magnetic moments in various forms. However the macroscopic moments never appear without applying external magnetic field due to the randomness in the direction of microscopic moments. In ferromagnetic materials the microscopic moments – let us call them spins – are aligned in the same direction at zero magnetic field and at finite temperatures. This fact indicates that, as we have seen in the magnetic refrigeration, the entropy is largely reduced and there should be a large decrease in the internal energy to compensate that. In other words, there should be some interaction that decreases the total energy. Let us examine such possibilities.

4.1 Exchange interaction

In chapter 1, we introduced the classical interaction between two magnetic dipoles (spins) $\boldsymbol{\mu}_1$, $\boldsymbol{\mu}_2$, namely the moments feel their magnetic field each other. Let $\boldsymbol{r}_{12}$ be the vector connecting the two moments, then the potential is given by [*2]

$$U(\boldsymbol{\mu}_1, \boldsymbol{\mu}_2, \boldsymbol{r}_{12}) = \frac{\mu_0}{4\pi}\left[\frac{\boldsymbol{\mu}_1 \cdot \boldsymbol{\mu}_2}{r_{12}^3} - 3\frac{(\boldsymbol{r}_1 \cdot \boldsymbol{r}_{12})(\boldsymbol{r}_2 \cdot \boldsymbol{r}_{12})}{r_{12}^5}\right]. \tag{4.1}$$

It is easy to guess from the analogy of bar magnets that the stable configuration is that the two spins are in-line. However this has the quantitative problem. Let $\boldsymbol{\mu}_{1,2}$ be $5\mu_\mathrm{B}$, r_{12} be 200 pm (typical lattice constant), then U is about 2 K. Hence this interaction cannot explain real ferromagnets, which keep alignments of spins above room temperature quantitatively.

Based on the quantum theory, Heisenberg showed the possibility of far-stronger mutual interaction between spins, that comes from a characteristic quantum effect[11]. It is now known through various researches that the direct exchange interaction, which Heisenberg claimed to be the source of ferromagnetism, cannot explain real ferromagnetism in materials. However, the concept of exchange interaction is still used in the present understandings. Here let us introduce the naive direct exchange interaction.

[*2] In eq. (1.7), we used E-H formulation. Here we restore it to E-B formulation (i.e., SI unit system).

4.1.1 Heitler-London approximation

In the ground state of Hydrogen molecule, two electrons with $\uparrow$ and $\downarrow$ are accommodated in the bonding orbital. Hence the spin is zero and the orbital diamagnetism appears (molecular orbital approximation, MO). However, here we consider the case that the inter-atom distance is larger and instead of considering bonding and anti-bonding orbitals, we consider atomic orbitals φ_a, φ_b and the two-body wavefunction is composed with keeping the Fermi statistics (**Heitler-London approximation**). In this approximation, the wavefunction of two electrons is written in the form of Slater determinant:

$$\Psi = \frac{1}{\sqrt{N}} \begin{vmatrix} \varphi_a(\boldsymbol{r}_1)\chi_a(s_1) & \varphi_b(\boldsymbol{r}_1)\chi_b(s_1) \\ \varphi_a(\boldsymbol{r}_2)\chi_a(s_2) & \varphi_b(\boldsymbol{r}_2)\chi_b(s_2) \end{vmatrix}, \tag{4.2}$$

where N is a normalization constant, $(\boldsymbol{r}_i, s_i)$ are space and spin coordinates of i-th electron. s_i corresponds to z-component of spin and can take one of two values $\pm 1/2$. We write the state of the spin pointing $+z$ as $\alpha(s)$, in which $\chi(s)$ is

$$\chi(1/2) = 1, \quad \chi(-1/2) = 0. \tag{4.3}$$

On the other hand, the $-z$ pointing state $\beta(s)$ is given as

$$\chi(1/2) = 0, \quad \chi(-1/2) = 1. \tag{4.4}$$

Pauli's exclusion principle is fulfilled as

$$\Psi(\boldsymbol{r}_1, s_1; \boldsymbol{r}_1, s_1) = 0, \quad \Psi(\boldsymbol{r}_1, s_1; \boldsymbol{r}_2, s_2) = -\Psi(\boldsymbol{r}_2, s_2; \boldsymbol{r}_1, s_1). \tag{4.5}$$

Ψ takes argument of spin functions (χ_a, χ_b), and we can classify Ψ by the spin states (α, β) as $\{\Psi_{\alpha\alpha}, \Psi_{\alpha\beta}, \Psi_{\beta\alpha}, \Psi_{\beta\beta}\}$. We take this as a basis and consider the expression of the interaction Hamiltonian $\mathscr{H}_{\rm int}$. As an example of the matrix elements, $\langle\alpha\alpha|\mathscr{H}_{\rm int}|\alpha\alpha\rangle$ has two terms:

$$\begin{aligned} \langle\alpha\alpha|\mathscr{H}_{\rm int}|\alpha\alpha\rangle &= \sum_{s_1,s_2} \int d\boldsymbol{r}_1 d\boldsymbol{r}_2 \Psi^*_{\alpha\alpha} \mathscr{H}_{\rm int} \Psi_{\alpha\alpha} \\ &= \int d\boldsymbol{r}_1 d\boldsymbol{r}_2 \varphi^*_a(\boldsymbol{r}_1)\varphi^*_b(\boldsymbol{r}_2)\mathscr{H}_{\rm int}\varphi_a(\boldsymbol{r}_1)\varphi_b(\boldsymbol{r}_2) - \int d\boldsymbol{r}_1 d\boldsymbol{r}_2 \varphi^*_a(\boldsymbol{r}_1)\varphi^*_b(\boldsymbol{r}_2)\mathscr{H}_{\rm int}\varphi_b(\boldsymbol{r}_1)\varphi_a(\boldsymbol{r}_2), \end{aligned} \tag{4.6}$$

where we take $N = 2$, $\langle\varphi_a|\varphi_b\rangle = 0$. The second term in rhs of (4.6) is a matrix element between the states in which the electrons are exchanged, and called **exchange integral**. This is essentially the same as $J(m_1, m_2)$ in eq. (2.26). In Ch.2, we derived Hund's rule from this integral. The direct exchange interaction is essentially the same. We write the first and the second term in rhs of eq. (4.6) as K_{ab} and J_{ab}. The 4×4 matrix elements are as follows.

	$\alpha\alpha$	$\alpha\beta$	$\beta\alpha$	$\beta\beta$
$\alpha\alpha$	$K_{ab} - J_{ab}$	0	0	0
$\alpha\beta$	0	K_{ab}	$-J_{ab}$	0
$\beta\alpha$	0	$-J_{ab}$	K_{ab}	0
$\beta\beta$	0	0	0	$K_{ab} - J_{ab}$

(4.7)

This can be easily diagonalized and the eigenfunctions are

$$\left.\begin{matrix} \Psi_{\alpha\alpha} \\ \frac{1}{\sqrt{2}}(\Psi_{\alpha\beta} + \Psi_{\beta\alpha}) \\ \Psi_{\beta\beta} \end{matrix}\right\} (s_1 + s_2 = 1), \quad \frac{1}{\sqrt{2}}(\Psi_{\alpha\beta} - \Psi_{\beta\alpha})\ (s_1 + s_2 = 0). \tag{4.8}$$

The three states for $s_1 + s_2 = 1$ are **spin triplet** and the one for $s_1 + s_2 = 0$ is **spin singlet**. The eigenenergy of the former is $K_{ab} - J_{ab}$ and that of the latter is $K_{ab} - J_{ab}$. The spin states thus give the difference in the energy. When

J_{ab} is positive, the spin parallel state has a lower energy giving ferromagnetic interaction while the interaction is anti-ferromagnetic when J_{ab} is negative. The situation can be viewed as the exchange integral creates the interaction between the spins and we call the interaction **exchange interaction**. Though J_{ab} appears from the integration of orbital states, the symmetry of the electronic states requires the interaction between spins.

Then we look for an effective Hamiltonian composed of spin operators just like the spin Hamiltonian introduced in Ch.2 to analyze EPR experiments. First we introduce spin operators $\boldsymbol{s}_a$ and $\boldsymbol{s}_b$, which operate on the states a and b respectively (don't get confused with s_1, s_2). Because they commute each other,

$$2\boldsymbol{s}_a \cdot \boldsymbol{s}_b = (\boldsymbol{s}_a + \boldsymbol{s}_b)^2 - \boldsymbol{s}_a^2 - \boldsymbol{s}_b^2 = \boldsymbol{S}^2 - \boldsymbol{s}_a^2 - \boldsymbol{s}_b^2. \tag{4.9}$$

Here we use

$$\langle\uparrow\uparrow|\boldsymbol{S}^2|\uparrow\uparrow\rangle = S(S+1) = 2, \quad \boldsymbol{S}^2|\uparrow\downarrow\rangle = 0, \tag{4.10}$$

$$\boldsymbol{s}_a^2 = \boldsymbol{s}_b^2 = \frac{1}{2}\left(\frac{1}{2}+1\right) = \frac{3}{4}, \tag{4.11}$$

and calculate the elements of operator $(1 + 4\boldsymbol{s}_a \cdot \boldsymbol{s}_b)/2$ to obtain

$$(\uparrow\uparrow) \to 2\boldsymbol{s}_a \cdot \boldsymbol{s}_b = 2 - 2 \times \frac{3}{4} = \frac{1}{2} \Longrightarrow \frac{1}{2}(1 + 4\boldsymbol{s}_a \cdot \boldsymbol{s}_b) = +1,$$
$$(\uparrow\downarrow) \to 2\boldsymbol{s}_a \cdot \boldsymbol{s}_b = 2 - 2 \times \frac{3}{4} = -\frac{3}{2} \Longrightarrow \frac{1}{2}(1 + 4\boldsymbol{s}_a \cdot \boldsymbol{s}_b) = -1.$$

Therefore we can adopt

$$\mathscr{H}_{\text{int}} = K_{ab} - \frac{1}{2}J_{ab}(1 + 4\boldsymbol{s}_a \cdot \boldsymbol{s}_b) \tag{4.12}$$

as an effective Hamiltonian.

Then we expand the above concept to the interaction between general spins $\boldsymbol{S}_i$ indexed by i and formally extract the spin part to obtain **Heisenberg Hamiltonian**

Heisenberg Hamiltonian

$$\mathscr{H} = -2\sum_{\langle i,j\rangle} J_{ij}\boldsymbol{S}_i \cdot \boldsymbol{S}_j. \tag{4.13}$$

This is an important basics for us to treat various phenomena originated from the interaction between spins.

For exchange integral, when the interaction is the Coulomb repulsion,

$$J_{ab} = \frac{e^2}{4\pi\epsilon_0}\int d\boldsymbol{r}_1 d\boldsymbol{r}_2 \varphi_a^*(\boldsymbol{r}_1)\varphi_b^*(\boldsymbol{r}_2)\frac{1}{r_{12}}\varphi_b(\boldsymbol{r}_1)\varphi_a(\boldsymbol{r}_2) \tag{4.14}$$

is always positive, which can be proven as eq. (2.26). And J_{ab} can go up to 0.1 eV depending on the way of estimation, hence might explain the room temperature ferromagnetism. In the above we see that the Coulomb repulsion causes a strong ferromagnetic interaction between spins in Heitler-London approximation. This is called **direct exchange interaction**. However, here we must notice that if we adopt the molecular orbital method, the interaction in the form of Heisenberg Hamiltonian can be derived with negative J, that is the anti-ferromagnetic interaction. This can be more easily understood from the general theory that in a general Schrödinger equation, the ground state has no degeneracy and the wavefunction has no node[12]. Hence the orbital part of wavefunction is symmetric resulting in the antisymmetric spin part.

4.1.2 Exchange interaction in the presence of tunneling

As an improvement of Heitler-London approximation, we consider the electronic state, in which two electrons are accommodated in a single atom as a possible configuration. In this treatment, a small amplitude of wavefunction

$$\Psi' = \frac{1}{\sqrt{N'}} \begin{vmatrix} \varphi_a(\boldsymbol{r}_1)\chi_a(s_1) & \varphi_a(\boldsymbol{r}_1)\chi'_a(s_1) \\ \varphi_a(\boldsymbol{r}_2)\chi_a(s_2) & \varphi_a(\boldsymbol{r}_2)\chi'_a(s_2) \end{vmatrix} \tag{4.15}$$

is overlapped to the one in (4.2). The transition of $\Psi \to \Psi'$ means tunneling of an electron $\varphi_b\chi_b \to \varphi_a\chi'_a$. Hence for such a superposition to occur, $\langle\Psi|\mathscr{H}|\Psi'\rangle \neq 0$. For that, due to Pauli's exclusion principle, χ_a and χ_b should be the spins opposite to each other. When $\boldsymbol{s}_a$ and $\boldsymbol{s}_b$ are anti-parallel, this hopping process leads to the energy decrease

$$W_{ab} = -\frac{1}{\Delta E} |\langle\Psi'|\mathscr{H}|\Psi\rangle|^2 \tag{4.16}$$

in the second order perturbation. For parallel spins, there is no such energy decrease. We thus write this part formally

$$\frac{1}{2}(1 - 4\boldsymbol{s}_a \cdot \boldsymbol{s}_b)W_{ab}, \tag{4.17}$$

which is in the same form as eq. (4.12). In summary we reach

$$\mathscr{H}'_{\rm int} = \frac{1}{2}(-J_{ab} + W_{ab}) - 2(J_{ab} + W_{ab})\boldsymbol{s}_a \cdot \boldsymbol{s}_b. \tag{4.18}$$

W_{ab} is negative and when $J_{ab} + W_{ab} < 0$ the total interaction becomes antiferromagnetic. We have confirmed Heitler-London approximation overestimates the ferromagnetic interaction.

Appendix 6A: Aharonov-Bohm phase and degeneracy of Landau levels

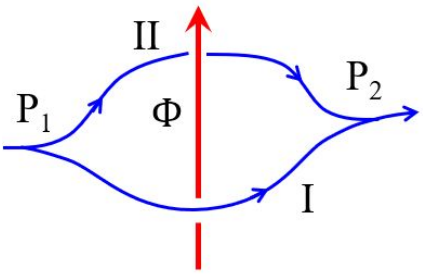

I would like to introduce the way to memorize the degree of Landau level degeneracy (the number of states per unit area). Of course this is just an example, and you can find your own way. In the existence of magnetic field, the momentum $\hbar\boldsymbol{k}$ is modified to

$$\hbar\boldsymbol{k} \ \to \ \hbar\boldsymbol{k} + e\boldsymbol{A} = \hbar\left(\boldsymbol{k} + \frac{e}{\hbar}\boldsymbol{A}\right).$$

This gives the phase evolution θ when a plane wave $\exp[i\boldsymbol{k}\cdot\boldsymbol{r}]$ propagates in space from a point P_1 to P_2 as

$$\theta_{12} = \int_{\mathrm{P}_1}^{\mathrm{P}_2} \left(\boldsymbol{k} + \frac{e}{\hbar}\boldsymbol{A}\right) \cdot d\boldsymbol{r}_{(\mathrm{I})} = \int_{\mathrm{P}_1}^{\mathrm{P}_2} \boldsymbol{k} \cdot d\boldsymbol{r}_{(\mathrm{I})} + \frac{e}{\hbar}\int_{\mathrm{P}_1}^{\mathrm{P}_2} \boldsymbol{A} \cdot d\boldsymbol{r}_{(\mathrm{I})} = \theta^{(k)}_{12(\mathrm{I})} + \theta^{(A)}_{12(\mathrm{I})}. \tag{6A.1}$$

The suffix I means the path signed as I in the figure. The first term in the rhs is the ordinary kinetic phase and the second term expresses the effect of magnetic field. The latter is called **Aharonov-Bohm** (AB) phase.

In path II, the kinetic phase differs from that in path I by the difference in the length. The AB phase in path II is also different from that in I. This can be understood by considering the route going back from P_2 to P_1 on path II. That is

$$\Delta\theta_{\rm AB} = \frac{e}{\hbar}\left[\int_{\mathrm{P}_1}^{\mathrm{P}_2} \boldsymbol{A} \cdot d\boldsymbol{r}_{(\mathrm{I})} + \int_{\mathrm{P}_1}^{\mathrm{P}_2} \boldsymbol{A} \cdot d\boldsymbol{r}_{(\mathrm{II})}\right] = \frac{e}{\hbar}\oint \boldsymbol{A} \cdot d\boldsymbol{r} = \frac{e}{\hbar}\int_S \mathrm{rot}\boldsymbol{A} d\boldsymbol{\sigma} = 2\pi\frac{\Phi}{\phi_0}, \quad \phi_0 = \frac{h}{e}. \tag{6A.2}$$

Here ϕ_0 is called **flux quantum**, which has the form of the ratio of h to e. This is an easy-to-memorize form. A physical meaning is that 2π of AB phase is given to an electron going around this amount of flux, and this is the condition of quantization in the electron loop.

The number of states in the magnetic field of magnetic flux density B in two-dimensional system is given by the flux per unit area (i.e. B) divided by the flux quantum. That is,

$$N(B) = \frac{B}{h/e} = \frac{eB}{h} = \frac{eBm}{hm} = \frac{m}{h^2}(h\omega_{\rm c}) = \frac{m}{2\pi\hbar^2}(\hbar\omega_{\rm c}). \tag{6A.3}$$

Hence we can see the number of states per Landau level eB/h and the two-dimensional density of states $m/2\pi\hbar^2$ in a very clear way.

Appendix 6B: Contribution of k-slab to the dHvA effect

There are various equivalent way to explain the principle of the dHvA effect. In the explanation from the density of states as in the text, it is rather difficult to see the effect contains the information of k-space. Hence here we explain the effect in the way given in Ref. [13]. Here we consider free electrons with an isotropic effective mass for simplicity. Electrons are free in z-direction (field direction) and Landau-quantized in xy plane as in eq. (3.14). Hence we define quasi-Fermi energy as the kinetic energy in xy-plane for a fixed k_z, that is

$$E'_{\rm F} \equiv E_{\rm F} - \frac{\hbar^2 k_z^2}{2m}. \tag{6B.1}$$

And we treat the system as a set of two-dimensional electrons with the Fermi energy of $E'_{\rm F}$ under Landau quantization. In k-space, each k_z is assigned to such a virtual two-dimensional system.

Then we consider a slab with thickness δk_z in k-space corresponding to a k_z. We call the region k-slab. The density of states in a k-slab "per magnetic flux density" ξ is given by

$$\xi = \frac{1}{L}\frac{L}{2\pi}\delta k_z \frac{eB}{h}\frac{1}{B} = \frac{e}{4\pi^2\hbar}\delta k_z \quad \left(= \frac{\delta k_z}{2\pi}\frac{1}{\phi_0}\right), \tag{6B.2}$$

where we also use things mentioned in App. 6A. I have put a comment on this quantity as a formula in the last parentheses. $\phi_0 \equiv h/e$ is **flux quantum** introduced in App. 6A. At absolute zero, the Landau levels corresponding to the integer q which satisfies $(q+1/2)\hbar\omega_{\rm c} \le E'_{\rm F}$ are occupied. Let us write the maximum integer in q as $q_{\rm max}$ and the number of occupied Landau levels is $q_{\rm max}+1$. Then the number of electrons belong to this k-slab is

$$n_{\rm e}(k_{\rm z}) = (q_{\rm max}+1)\xi B \tag{6B.3}$$

per unit area in the real space.

With increasing B, $n_{\rm e}$ increases linearly in accordance with (6B.3), and when B exceeds the value determined by the condition

$$q_{\rm max} + \frac{1}{2} = \frac{E'_{\rm F}}{\hbar\omega_{\rm c}} = \frac{mE'_{\rm F}}{\hbar e}\frac{1}{B}, \tag{6B.4}$$

$q_{\rm max}$ decreases by one and $n_{\rm e}$ discretely decreases. Namely, $n_{\rm e}(k_{\rm z})$ oscillates periodically against $1/B$ and the amplitude (the amount of dropping at the condition (6B.4)) increases with B as ξB though the center of the oscillation is the electron concentration of virtual 2-dimensional electrons (let us write it $n_{\rm e0}$) in the k-slab before the application of magnetic field. The behavior is drawn in Fig. 6B.1. As shown in the figure, the electronic states of number eB/h at zero field are assigned to a Landau level (App. 6A). In the oscillation, at the magnetic field $n_{\rm e}(B) = n_{\rm e0}$, where the electron concentration hits the center, $(q_{\rm max}+1)(eB/h)$ should be equal to $n_{\rm e0}$. We write $q_{\rm max}+1$ at such points as ν, the value of magnetic field as B_ν. Then they are in the relation

$$B_\nu = \frac{1}{\xi}\frac{n_{\rm e0}}{\nu} = \frac{2\pi}{\delta k_z}\phi_0\frac{n_{\rm e0}}{\nu} \quad (\nu = 1, 2, \cdots). \tag{6B.5}$$

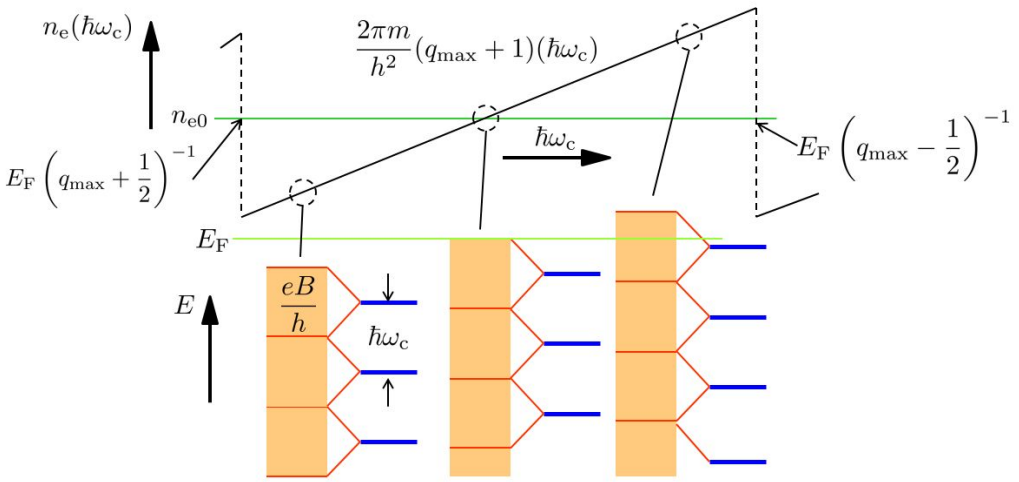

Fig. 6B.1 Illustration of relations between the Landau level distance $\hbar\omega_c$, the two dimensional electron concentration n_e, and jumping at which q_{max} changes. The lower shows corresponding energy diagrams (occupied energy levels in zero field is in orange color.

And the boundaries between different values of q_{max} are

$$B_{\nu\pm} = \frac{mE'_F}{\hbar e}\frac{1}{\nu \pm 1/2}. \tag{6B.6}$$

The energy $U_{\nu 0}$ of electrons in the k-slab corresponding to this B_ν is expressed as

$$U_{\nu 0} = \xi B_\nu \hbar\omega_c \sum_{q=0}^{\nu-1}\left(q+\frac{1}{2}\right) + n_e\frac{\hbar^2 k_z^2}{2m} = \frac{\xi B_\nu \hbar\omega_{c\nu}}{2}\nu^2 + n_e\frac{\hbar^2 k_z^2}{2m}$$
$$= \frac{\hbar\omega_{c\nu}}{2\xi B_\nu}n_{e0}^2 + \frac{\hbar^2 k_z^2}{2m}n_{e0} = \frac{h^2}{2m\delta k_z}n_{e0}^2 + \frac{\hbar^2 k_z^2}{2m}n_{e0}. \tag{6B.7}$$

This does not depend on the magnetic field and is the same as the sum of energies in k-slabs below E_F. In the region in the magnetic field $[B_{\nu+}, B_{\nu-}]$, this expression holds with replacing n_{e0} with n_e. We thus consider the quantity

$$U = \frac{h^2}{2m\delta k_z}n_e^2 + n_e\frac{\hbar^2 k_z^2}{2m} + (n_{e0}-n_e)E'_F. \tag{6B.8}$$

In the rhs, the first two terms are the extension of (6B.7) and the energy of electrons in k-slab. In the third term, the energies coming in/out the k-slab at E'_F. This term keeps U continuous even at the magnetic field of eq. (6B.6), where n_e gets a gap. Now we write E'_F as

$$E'_F = \hbar\omega_{c\nu}\nu = \hbar\frac{eB_\nu}{m}\frac{2\pi}{\delta k_z}\frac{h}{e}\frac{n_{e0}}{B_\nu} = \frac{h^2}{m}\frac{n_{e0}}{\delta k_z}. \tag{6B.9}$$

Then the variation in U is

$$\delta U = U - U_{\nu 0} = \frac{h^2}{2m\delta k_z}(n_e^2 - n_{e0}^2) + E'_F(n_{e0}-n_e) = \frac{h^2}{2m\delta k_z}(n_e - n_{e0})^2, \tag{6B.10}$$

which is more than or equal to zero.

The contribution of electrons in this k-slab to the magnetization is

$$\delta M = -\frac{\partial U}{\partial B} = -\frac{h^2}{m\delta k_z}(n_e - n_{e0})\frac{dn_e}{dB}. \tag{6B.11}$$

dn_e/dB is from eq. (6B.3)

$$\frac{dn_e}{dB} = \nu\xi \simeq \frac{E'_F}{\hbar\omega_c}\xi. \tag{6B.12}$$

Then the contribution is obtained as

$$\delta M \simeq -\frac{E'_{\rm F}}{B}(n_{\rm e} - n_{\rm e0}). \tag{6B.13}$$

While B in the denominator increases linearly, $n_{\rm e} - n_{\rm e0}$ strongly oscillates resulting in the oscillation of magnetic susceptibility.

In order to see the behavior of the total magnetization, the contribution in eq. (6B.13) should be summed up over k_z. For that, first δM is expanded in a Fourier series against the axis of B^{-1} as follows.

$$\delta M = \delta k_z \sum_{p=1}^{\infty} A_p \sin px, \quad x = 2\pi \frac{E'_{\rm F}}{\hbar\omega_{\rm c}}. \tag{6B.14}$$

We apply a mathematical identity for $-\pi < x < \pi$

$$x = e \sum_{n=1}^{\infty} \frac{(-1)^{n-1}}{n} \sin nx, \tag{6B.15}$$

and rewrite

$$\delta M = -\frac{1}{2\pi}\xi E'_{\rm F} x = \frac{1}{\pi} E'_{\rm F} \sum_p (-1)^p \frac{\sin px}{p}. \tag{6B.16}$$

Therefore the expansion coefficients are obtained as

$$A_p = \frac{1}{p\pi} E'_{\rm F} (-1)^p \frac{\xi}{\delta k_z} = (-1)^p \frac{e E'_{\rm F}}{4p\pi^3}. \tag{6B.17}$$

From the above, the summation over k_z can be written in the form of integration:

$$M = \frac{e}{4\pi^3} \sum_p \frac{(-1)^p}{p} \int_{-k_{\rm F}}^{k_{\rm F}} dk_z \cdot E'_{\rm F} \sin\left[\frac{p\pi}{\hbar\omega_{\rm c}}\left(E_{\rm F} - \frac{\hbar^2 k_z^2}{2m}\right)\right]. \tag{6B.18}$$

Here, though the magnetic field is comparatively strong, we assume the condition $\hbar\omega_{\rm c} \ll E_{\rm F}$ still holds. Then in the integrand in eq. (6B.18), $E'_{\rm F}$ varies in the section $[-k_{\rm F}, k_{\rm F}]$ as a parabola with the maximum at $k_z = 0$. On the other hand, the sine function rapidly oscillates against k_z. As a result the integration cancels out other than the region around $k_z = 0$, where $dE'_{\rm F}/dk_z \sim 0$. Hence $E'_{\rm F}$ outside the sine function can be replaced with $E_{\rm F}$. Further, applying the identity

$$\int_0^{\infty} \cos\frac{\pi}{2}x^2 dx = \int_0^{\infty} \sin\frac{\pi}{2}x^2 dx = \frac{1}{2}, \tag{6B.19}$$

the integration in (6B.18) is calculated to be

$$E_{\rm F}\left(\frac{\hbar\omega_{\rm c} m}{2p}\right)^{1/2} \sin\left(\frac{2\pi p E_{\rm F}}{\hbar\omega_{\rm c}} - \frac{\pi}{4}\right). \tag{6B.20}$$

Then we can write down the magnetization as

$$M = \frac{E_{\rm F} e^{3/2} (\hbar B)^{1/2}}{4\pi^3} \sum_p \frac{(-1)^p}{p^{3/2}} \sin\left(p\frac{2\pi E_{\rm F}}{\hbar\omega_{\rm c}} - \frac{\pi}{4}\right). \tag{6B.21}$$

The above discussion is for an ideal metal with a spherical Fermi surface. But this can be extended to general Fermi surfaces. Even in the general case, the dHvA oscillation is dominated by the region where $dE'_{\rm F}/k_z \approx 0$. Hence the magnetic field angle dependence of the dHvA oscillation (amplitude, period, etc.) gives detailed information on the Fermi surface.

Appendix 6C: Band structure of graphene

One of the ways to form a two dimensional electron system is to utilize two-dimensional crystals (two-dimensional materials). Graphene is the representative two-dimensional material. Graphene provides a good expample for the application of tight-binding calculation and we would like to see how the things go in a practical (though simplest) example.

The crystal structure of single-layer graphene is show in Fig. 6C.1(a), which is a simple honeycomb structure of carbon atoms. The diamond drawn in the figure is the unit cell and the primitive lattice vectors and the primitive reciprocal lattice vectors are written as

$$\boldsymbol{a}_1 = \begin{pmatrix} \sqrt{3}a/2 \\ a/2 \end{pmatrix}, \quad \boldsymbol{a}_2 = \begin{pmatrix} 0 \\ a \end{pmatrix}, \quad \boldsymbol{b}_1 = \begin{pmatrix} 4\pi/\sqrt{3}a \\ 0 \end{pmatrix}, \quad \boldsymbol{b}_2 = \begin{pmatrix} -2\pi/\sqrt{3}a \\ 2\pi/a \end{pmatrix}. \tag{6C.1}$$

Henceforce we calculate the electronic states of graphene under simplest approximation. Because the approximation is rough, quantitative comparison with experiments is difficult. However, the results help understanding properties of graphene, *e.g.* the Dirac points appear at the Fermi level in pure graphene. Carbon belongs to group-IV and the outmost electrons exist in the orbitals $2s$, $2p_x$, $2p_y$, $2p_z$. It is easy to see that these orbitals form sp^2-hybrids and the electronic states separate to σ-electrons (sp^2) and π-electrons (p_z). σ-electrons form the honeycome through covalent bonding and the energy bands lie at low energy region. Then the electronic states placed around the Fermi level are π-electrons. Hence we consider Schrödinger equation on π-electrons on the honeycomb lattice.

We write the equation as

$$\psi = \mathscr{H}\psi, \tag{6C.2}$$

and as Fig. 6C.1(a), we separate the lattice sites to A-sites and B-sites on different sub-lattices. We consider a kind of

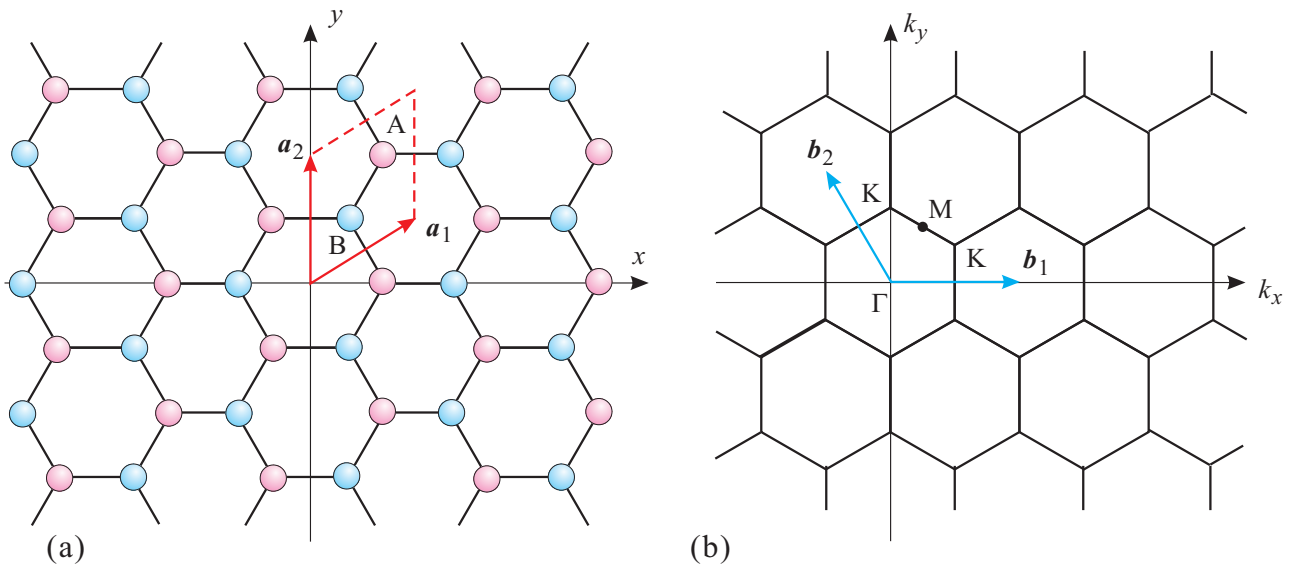

Fig. 6C.1 (a) Two dimensional cryatal structure of graphene. Carbon atoms form a honeycomb lattice. It can be also viewed as an overlap of two face-centered square lattices placed at A and B positions. (b) Reciprocal lattice of (a). $\boldsymbol{b}_1$, $\boldsymbol{b}_2$ are the primitive reciprocal lattice vector corresponding to $\boldsymbol{a}_1$, $\boldsymbol{a}_2$. The centtral point of the first Brillouin zone is Γ-point and as other points with high symmetries, K-point and M-point are indicated in the figure.

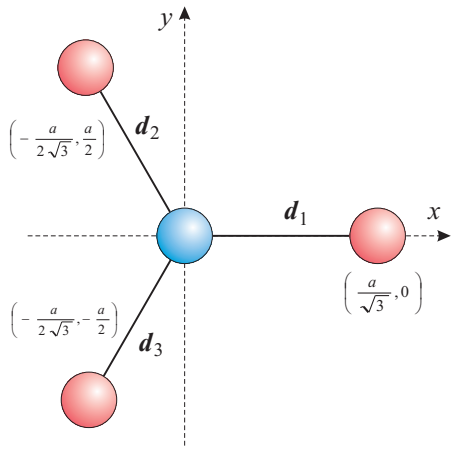

Fig. 6C.2 Vectors indicating three directional couplings between nearest neighbor carbon atoms.

tight-binding approximation between the two-sites. That is

$$\psi = \zeta_{\mathrm{A}}\psi_{\mathrm{A}} + \zeta_{\mathrm{B}}\psi_{\mathrm{B}}, \tag{6C.3}$$

$$\psi_{\mathrm{A}} = \sum_{j\in A} \exp(i\boldsymbol{k}\boldsymbol{r}_j)\phi(\boldsymbol{r}-\boldsymbol{r}_j), \tag{6C.4a}$$

$$\psi_{\mathrm{B}} = \sum_{j\in B} \exp(i\boldsymbol{k}\boldsymbol{r}_j)\phi(\boldsymbol{r}-\boldsymbol{r}_j), \tag{6C.4b}$$

where $\phi(\boldsymbol{r})$ is atomic wavefunction of π-electrons, $\boldsymbol{r}_j$ are the lattice points. Here we write the matrix elements of the Hamiltonian between the each sub-lattice wavefunctions as

$$H_{\mathrm{AA}} = \langle\psi_{\mathrm{A}}|\mathscr{H}|\psi_{\mathrm{A}}\rangle, \quad H_{\mathrm{BB}} = \langle\psi_{\mathrm{B}}|\mathscr{H}|\psi_{\mathrm{B}}\rangle, \quad H_{\mathrm{AB}} = H^*_{\mathrm{BA}} = \langle\psi_{\mathrm{A}}|\mathscr{H}|\psi_{\mathrm{B}}\rangle. \tag{6C.5}$$

And the number of atoms in the system is $2N$, that is

$$\langle\psi_{\mathrm{A}}|\psi_{\mathrm{A}}\rangle = \langle\psi_{\mathrm{B}}|\psi_{\mathrm{B}}\rangle = N. \tag{6C.6}$$

Let $\langle\psi_{\mathrm{A}}|\psi_{\mathrm{B}}\rangle$ be zero. We substitute (6C.3) to (6C.2). The condition of have non-trivial $(\zeta_{\mathrm{A}}, \zeta_{\mathrm{B}})$ givies the cecular equation

$$\begin{vmatrix} H_{\mathrm{AA}} - NE & H_{\mathrm{AB}} \\ H_{\mathrm{BA}} & H_{\mathrm{BB}} - NE \end{vmatrix} = 0. \tag{6C.7}$$

Lastly

$$E = (2N)^{-1}\left(H_{\mathrm{AA}} + H_{\mathrm{BB}} \pm \sqrt{(H_{\mathrm{AA}} - H_{\mathrm{BB}})^2 + 4|H_{\mathrm{AB}}|^2}\right) \equiv h_{\mathrm{AA}} \pm |h_{\mathrm{AB}}|, \tag{6C.8}$$

where we have used $H_{\mathrm{AA}} = H_{\mathrm{BB}}$, which comes from the symmetry, and we use lower cases for the quantities per atom with being devided by $(2N)^{-1}$.

$$H_{\mathrm{AB}} = \sum_{l\in\mathrm{A}, j\in\mathrm{B}} \exp\left[i\boldsymbol{k}(\boldsymbol{r}_j - \boldsymbol{r}_l)\right] \langle\phi(\boldsymbol{r}-\boldsymbol{r}_l)|\mathscr{H}|\phi(\boldsymbol{r}-\boldsymbol{r}_j)\rangle_{\boldsymbol{r}}. \tag{6C.9}$$

We further approximate that the off-diagonal matrix elements of $\mathscr{H}$ just exist between the nearest neighbor sites. For the calculation we take the atom indicated as A in Fig. 6C.1(a) as the center atom. The vectors from A to the nearest neighbor atoms 1, 2, 3 are $\boldsymbol{d}_i (i = 1, 2, 3)$ respectively. As is apparent from the figure,

$$\boldsymbol{k}\cdot\boldsymbol{d}_1 = \frac{k_x a}{\sqrt{3}}, \quad \boldsymbol{k}\cdot\boldsymbol{d}_2 = \left(-\frac{k_x}{2\sqrt{3}} + \frac{k_y}{2}\right)a, \quad \boldsymbol{k}\cdot\boldsymbol{d}_3 = \left(-\frac{k_x}{2\sqrt{3}} - \frac{k_y}{2}\right)a, \tag{6C.10}$$

where $a = |\boldsymbol{a}_1| = |\boldsymbol{a}_2|$. The terms $\langle\phi(\boldsymbol{r}-\boldsymbol{r}_l)|\mathscr{H}|\phi(\boldsymbol{r}-\boldsymbol{r}_j)\rangle_{\boldsymbol{r}}$ should be equal due to the symmetry and we write it as ξ. Consequently the residual resonant integral from the crystal structure is the repetition of the above and

$$h_{\mathrm{AB}} = \left(\sum_{j=1}^{3} \exp(i\boldsymbol{k}\cdot\boldsymbol{d}_j)\right)\xi. \tag{6C.11}$$

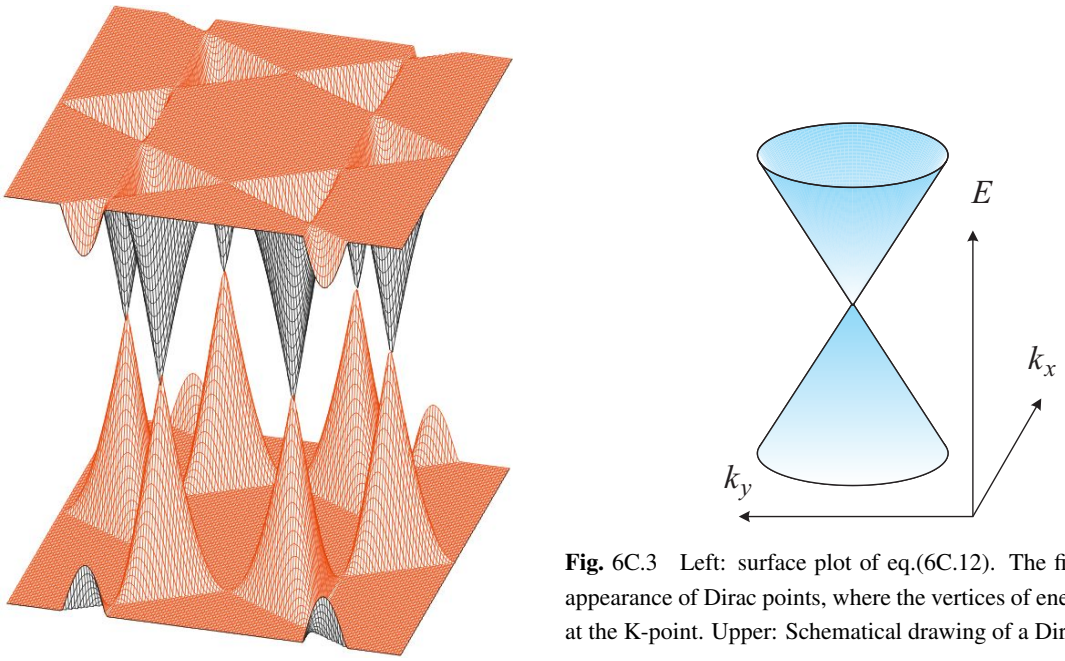

Fig. 6C.3 Left: surface plot of eq.(6C.12). The figure shows the appearance of Dirac points, where the vertices of energy corns crash at the K-point. Upper: Schematical drawing of a Dirac point.

Substituting eqs.(6C.10), (6C.11) into eq.(6C.8), we get the following expressio for the energy.

$$E = h_{\mathrm{AA}} \pm \xi \sqrt{1 + 4\cos\frac{\sqrt{3}k_x a}{2}\cos\frac{k_y a}{2} + 4\cos^2\frac{k_y a}{2}}. \tag{6C.12}$$

The second term is the perturbation from the nearest neighbor resonant integral, which vanishes at K-point in the reciprocal space

$$(k_x, k_y) = \left(0, \pm\frac{4\pi}{3a}\right), \quad \left(\frac{2\pi}{\sqrt{3}a}, \pm\frac{2\pi}{3a}\right), \quad \left(-\frac{2\pi}{\sqrt{3}a}, \pm\frac{2\pi}{3a}\right). \tag{6C.13}$$

We write $k_y = 4\pi/3a$ and around $k_x = 0$(one of the K-points), eq. (6C.12) can be approximated as

$$E\left(k_x, \frac{4\pi}{3a}\right) \approx h_{\mathrm{AA}} + \frac{\sqrt{3}\xi a}{2}|k_x|. \tag{6C.14}$$

Namely, at the K-point the upper band has a lower pointed shape. Because the same for the lower band and as a result, at the K-point, as shown in Fig. 6C.3, the band structure called **Dirac point**, which has no energy gap, no effective mass, appears.

Equation (6C.12) is for a very simplified model. Just like a cosine band appeared in the tight-binding model in one-dimension, the model itself does not have realistic meaning. However the model tells that the reason why we have the Dirac points at K-points is that the exsittence of three equivalent resonant integrals in eq. (6C.11). The inference holds for the band calculation with any level precision since it is based on the symmetry. That meas the K-points in real graphene are really Dirac points.

References

[1] P M C Rourke, A F Bangura, T M Benseman, M Matusiak, J R Cooper, A Carrington, and N E Hussey. A detailed de haas-van alphen effect study of the overdoped cuprate $\mathrm{tl_2ba_2cuo_{6+\delta}}$. *New Journal of Physics*, Vol. 12, No. 10, p. 105009, October 2010.

[2] Hidetoshi Fukuyama. Theory of orbital magnetism of bloch electrons: Coulomb interactions. *Progress of Theoretical Physics*, Vol. 45, No. 3, pp. 704–729, March 1971.

[3] Masao Ogata and Hidetoshi Fukuyama. Orbital magnetism of bloch electrons i. general formula. *Journal of the Physical Society of Japan*, Vol. 84, No. 12, p. 124708, December 2015.

[4] Masao Ogata. Orbital magnetism of bloch electrons: II. application to single-band models and corrections to landau–peierls susceptibility. *Journal of the Physical Society of Japan*, Vol. 85, No. 6, p. 064709, June 2016.

[5] Masao Ogata. Orbital magnetism of bloch electrons: III. application to graphene. *Journal of the Physical Society of Japan*, Vol. 85, No. 10, p. 104708, October 2016.

[6] J. W. McClure. Diamagnetism of graphite. *Phys. Rev.*, Vol. 104, pp. 666–671, Nov 1956.

[7] Bogdan Semenenko and Pablo Esquinazi. Diamagnetism of bulk graphite revised. *Magnetochemistry*, Vol. 4, No. 4, p. 52, November 2018.

[8] 越野幹人. グラフェンにおける巨大な軌道反磁性 (最近の研究から). 日本物理学会誌, Vol. 65, No. 1, pp. 21–25, 2010.

[9] Mikito Koshino, Yasunori Arimura, and Tsuneya Ando. Magnetic field screening and mirroring in graphene. *Phys. Rev. Lett.*, Vol. 102, p. 177203, Apr 2009.

[10] Mikito Koshino and Tsuneya Ando. Orbital diamagnetism in multilayer graphenes: Systematic study with the effective mass approximation. *Phys. Rev. B*, Vol. 76, p. 085425, Aug 2007.

[11] W. Heisenberg. Mehrkörperproblem und resonanz in der quantenmechanik. *Zeitschrift für Physik*, Vol. 38, No. 6-7, pp. 411–426, June 1926.

[12] L D Landau and E. M. Lifshitz. *Quantum Mechanics: Non-Relativistic Theory (English Edition)*. Butterworth-Heinemann, 12 1981.

[13] Charles Kittel. *Quantum Theory of Solids 2E Rev P*. WILEY, 3 1987.

Lat week, we show that a ferromagnetic exchange interaction appears in Heitler-London approximation though a hopping of electrons between the sites cases anti-ferromagnetic exchange interaction. The exchange interaction due to the transfer of electrons is a kind of **kinetic exchange interaction**, which often gives anti-ferromagnetic interaction though not always [*1]. Also, we found that the spin-spin interaction is always anti-ferromagnetic in a pure two-atom-model [*2]. From the numerical simulations so far, they have found no realistic example in which the direct exchange interaction causes ferromagnetism. However we extracted the concept of direct exchange interaction from the HL approximation and inferred that some "exchange interaction" is working in any magnetic materials. We thus introduced Heisenberg Hamiltonian (Heisenberg model). You may wonder why this kind of change in the related freedoms is possible. This can be understood in the context of quantum entanglement as stated in Appendix 7A. In the appendix, it is shown that the quantum entanglement is not a pure mathematical notion but a real physical phenomenon, useful in the experiment.

4.1.3 Hubbard model

The mechanism of anti-ferromagnetic exchange interaction in electron transfer can also be seen in the following simple model. Let us consider two sites (i, j) and write the electronic states as $|n; m\rangle$ (";" separates the parameters of two states). Electron hopping between the two sites is taken into account and the hopping operator is written as $t(a^\dagger_{i\sigma}a_{j\sigma} + \text{h.c.})$. Due to the Pauli's exclusion principle, two electrons occupying a single site are limited to spin up-down pair. Such states have higher energy due to the on-site repulsion and can exist as intermediate states during hopping process. We write this increase in the energy in the intermediate states as U, namely

$$U = E(|0; \sigma, -\sigma\rangle) - E(|\sigma; -\sigma\rangle). \tag{4.19}$$

The hopping process, however decreases the energy in the second perturbation and the amplitude of decrease is about $|t|^2/U$. The above simple model is called **Hubbard model**, in which the hopping amplitude with the nearest neighbor is t and the electron gets on-site repulsion U for double occupation. Here we introduce the simplest two-site model but extended ones are one of the most important model in exploration of magnetism. With the notation $n_{i\sigma} = a^\dagger_{i\sigma}a_{i\sigma}$, the model can be expressed in Hamiltonian form as

$$\mathscr{H} = t\sum_{\sigma=\uparrow\downarrow}(a^\dagger_{1\sigma}a_{2\sigma} + a^\dagger_{2\sigma}a_{1\sigma}) + U(n_{1\uparrow}n_{1\downarrow} + n_{2\uparrow}n_{2\downarrow}). \tag{4.20}$$

We limit the electron number as $n_\mathrm{e} = 2$ then the available states are

$$|\uparrow\downarrow; 0\rangle\,,\ |0; \uparrow\downarrow\rangle\,,\ |\uparrow; \uparrow\rangle\,,\ \frac{1}{\sqrt{2}}(|\uparrow; \downarrow\rangle + |\downarrow; \uparrow\rangle),\ |\downarrow; \downarrow\rangle\,,\ \frac{1}{\sqrt{2}}(|\uparrow; \downarrow\rangle - |\downarrow; \uparrow\rangle). \tag{4.21}$$

The operators of spin at each site, total spin, and total electron number, are defined as

$$\boldsymbol{s}_i = \sum_{\sigma\sigma'} a^\dagger_{i\sigma}\left(\frac{\boldsymbol{\sigma}}{2}\right)_{\sigma\sigma'} a_{i\sigma'}, \quad \boldsymbol{S} = \sum_{i=1,2}\boldsymbol{s}_i, \quad N = \sum_{i,\sigma} n_{i\sigma}, \tag{4.22}$$

[*1] Superexchange interaction, which we will see in the next section, is also a kind of kinetic exchange interaction. But sometimes it gives ferromagnetic interaction[1, 2].

[*2] Then you might ask how about the Hund's rule? This is a natural question long been addressed. Actually many textbooks on the physical chemistry say that "Hund's rule is empirical rules that cannot be mathematically proved." In large scale numerical calculations, it turned out that the disturbance of nuclear-potential screening by core electrons has larger effect than the Pauli exclusion principle. This is an example and there are various new findings[3, 4]. Anyway we need more study in this field.

No.	S	S_z	E	Eigenstate
1	0	0	U	$\frac{1}{\sqrt{2}}(\|\uparrow\downarrow;0\rangle - \|0;\uparrow\downarrow\rangle)$
2			$\left(1+\frac{1}{a}\right)\frac{U}{2}$	$\frac{\sqrt{1+a}}{2}(\|\uparrow\downarrow;0\rangle + \|0;\uparrow\downarrow\rangle) + \sqrt{\frac{1-a}{2}}\|0,0\rangle$
3			$\left(1-\frac{1}{a}\right)\frac{U}{2}$	$\sqrt{\frac{1+a}{2}}\|0,0\rangle - \frac{\sqrt{1-a}}{2}(\|\uparrow\downarrow;0\rangle + \|0;\uparrow\downarrow\rangle)$
4	1	+1	0	$\|1,+1\rangle$
5		0		$\|1,0\rangle$
6		-1		$\|1,-1\rangle$

Tab. 4.1 Eigenenergies of two-electron, two-site Hubbard model eq. (4.20). a is defined as $a^{-2} = 1 + (4t/U)^2$.

which commute with $\mathscr{H}$ and $\boldsymbol{S}^2$, S_z, N can be good quantum numbers. For $N = 2$, we can compose 6 eigenstates common for these operators from (4.21). The eigenergies of them are listed in Tab. 4.1 with definition of $a^{-2} = 1 + (4t/U)^2$. When the Coulomb repulsion is sufficiently larger than the hopping effect $t/U \ll 1$, from this table and from calculation similar to that for the direct exchange interaction, the effective spin Hamiltonian is obtained as

$$\mathscr{H}_{\text{eff}} = -J\left(\boldsymbol{s}_1 \cdot \boldsymbol{s}_2 - \frac{1}{4}\right), \quad J = -\frac{4t^2}{U}, \tag{4.23}$$

which again gives an anti-ferromagnetic exchange interaction.

4.2 Superexchange interaction

There are many magnetic materials, in which negative ions (anions) with closed shell electronic structures exists between magnetic positive ions. Figure 4.1(a) shows the crystal structure of perovskite-type $KFeF_3$, which is an anti-ferromagnet with the Néel temperature (explained later) 173 K. In the structure, F^{-1}'s exist between Fe^{2+}'s The interaction mechanism between such magnetic ions was proposed long time ago as **superexchange interaction**. As named, it is a kind of exchange interaction. In the starting point, the negative ions do not have spin and the exchange effect first causes spins in negative ions and then the created spins have interactions with magnetic ions. Hence the effect should be second order perturbation. Figure 4.1(b) shows the model, in which a part of electrons shift from a negative ion to neighboring magnetic ions. The transfer results in the appearance of a little spin on the negative ion that has the exchange interactions with neighboring magnetic ions.

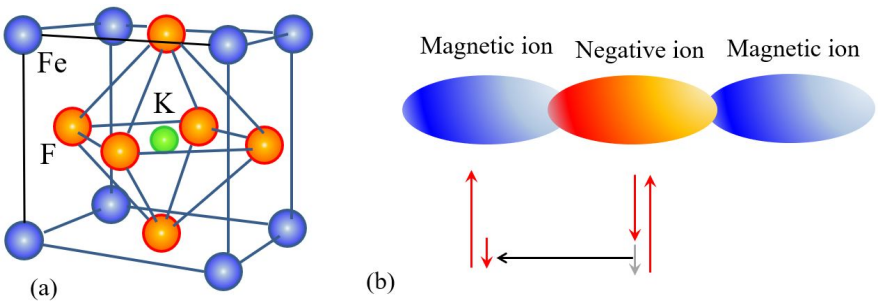

Fig. 4.1 (a) Cristal structure of anti-ferromagnet $KFeF_4$ in perovskite structure. (b) Schematic diagram of superexchange interaction.

The unperturbed state of negative ions is symmetric for spins, but the hopping to the magnetic ions is asymmetric due to the asymmetry of the magnetic ions. Hence a spin created on a negative ion reflects the direction of spin on the magnetic ion. The exchange interaction of this created spin with another magnetic ion thus results in the effective exchange interaction between magnetic ions. The above exchange interaction mechanism mediated by non-magnetic negative ions is called superexchange interaction[5].

4.2.1 Conditional change in sign and amplitude

Though the superexchange is a kind of kinetic exchange interaction, it is not necessarily anti-ferromagnetic because it is a three site problem[*3]. The sign and the amplitude of the superexchange interaction depend on the conditions such as coupling angle of magnetic ion-negative ion-magnetic ion. The dependence was half-empirically summarized as **Goodenough-Kanamori's rules**.

Consider the combination of d-orbital (i, j), and write the interaction as

$$-\sum_{i,j} 2J_{\text{eff}}(i,j)\boldsymbol{s}_i \cdot \boldsymbol{s}_j. \tag{4.24}$$

For simplicity, we assume Hund's rule on each magnetic ion, namely the total spin $\boldsymbol{S}_1 = \sum_i \boldsymbol{s}_{1i},\ \boldsymbol{S}_2 = \sum_j \boldsymbol{s}_{2j}$ is maximized. Let n be the number of electrons in the open shell of each ion, then $\boldsymbol{s}_i = \boldsymbol{S}/n$. The interaction is written again as in the form

$$-2J_{12}\boldsymbol{S}_1 \cdot \boldsymbol{S}_2. \tag{4.25}$$

The half empirical rules on the amplitude and the sign are called Goodenough-Kanamori's rules[6, 7]. Here I just quote what Kanamori himself describe: (after telling the difficulty in the calculation of J_{12}) "However, about the amplitude and the sign of J_{12}, rather vague rules exist, which can be theoretically explained and show good agreements with experiments[8]."

For example, when two magnetic ions and an anion line up in a straight line, the interaction between magnetic ions of the same species is anti-ferromagnetic ($J < 0$). When one of d orbitals has electrons more than 5 and less than 5

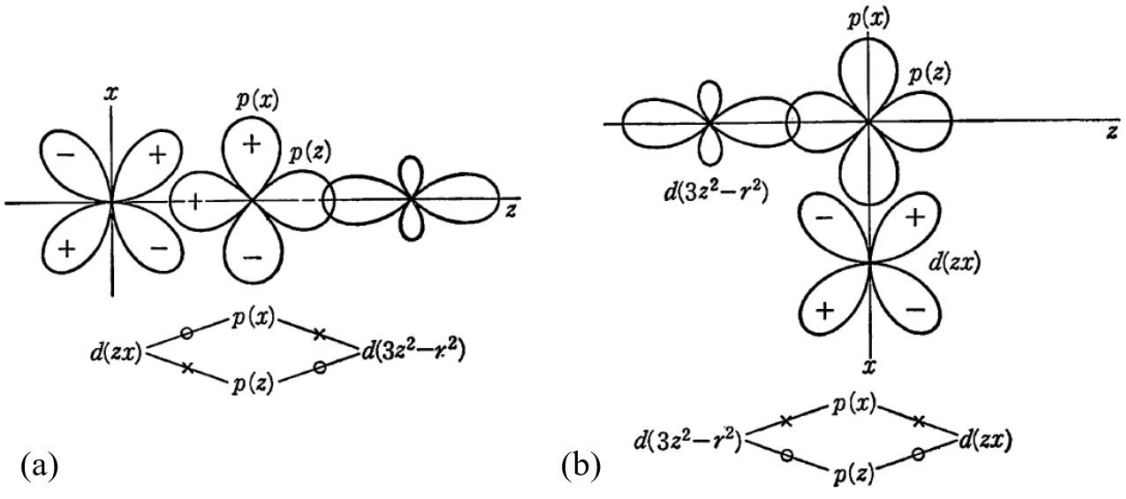

Fig. 4.2 Examples of Goodenough-Kanamori's rules. (a) Magnetic ions and an anion line up in a straight line (180°). (b) Bonding bends at an anion by 90°. +. − represent the signs of orbitals (phases). The line diagrams below the orbital drawings show electron hoppings between the orbitals. ○'s and ×'s represent possibilities of hoppings. From [8].

[*3] Conversely, the two involved interaction is anti-ferromagnetic, the total interaction should be ferromagnetic.

in the other, the interaction is ferromagnetic ($J > 0$). When the arrangement has a 90° bending at an anion as in (b), the tendency is inverse to (a), namely the interaction is ferromagnetic for the same species magnetic ions but the case of d^5. However there are various cases and exceptions. For details, refer to the original paper by Kanamori[7], or review articles[5].

4.3 s-d exchange interaction

In the superexchange interaction, we have considered insulating crystals without conduction electrons. Here on the contrary, consider the case of metallic crystals with many conduction electrons which interact with the spins on magnetic ions. Such situation occurs, e.g., small amount of magnetic ions like Fe or Mn are doped as impurities into non-magnetic metals.

4.3.1 Conduction electrons around local moments

Let $\boldsymbol{S}$ be the total spin operator of a magnetic impurity, $\boldsymbol{s}$ be the spin operators of conduction electrons. We write the matrix element of electron scattering by the local moment as

$$\mathscr{H}_{\rm scatt} = -2J_{\boldsymbol{k}\boldsymbol{k}'}\boldsymbol{S}\cdot\boldsymbol{s}. \tag{4.26}$$

In the long wavelength approximation ($2\pi/k$ is longer than the radius of scattering center), $J_{\boldsymbol{k}\boldsymbol{k}'} = J$ (const.). In other words, the interaction is δ-function (point-contact) type and with taking the position of impurity at the origin $\boldsymbol{r} = \boldsymbol{0}$ the above is approximated by

$$\mathscr{H}_{\rm scatt} = -2J\delta(\boldsymbol{r})\boldsymbol{S}\cdot\boldsymbol{s}. \tag{4.27}$$

We represent the conduction electrons as s, localized electrons at magnetic ion as d and call the interaction **s-d exchange interaction**. I hope we can have time to go into a many body effect caused by this interaction later. From the conduction electrons, the interaction in eq. (4.27) is equivalent to the δ-function like effective magnetic field $2J\boldsymbol{S}\delta(\boldsymbol{r})/(g_{\rm e}\mu_{\rm B})$ at the origin with the direction of $\boldsymbol{S}$. The Fourier transform of the field is

$$\boldsymbol{B}_{\rm eff}(\boldsymbol{r}) = \frac{2J\delta(\boldsymbol{r})}{g_{\rm e}\mu_{\boldsymbol{B}}}\cdot\boldsymbol{S} = \int\frac{d\boldsymbol{q}}{(2\pi)^3\sqrt{V}}\boldsymbol{B}_{\boldsymbol{q}}e^{i\boldsymbol{q}\cdot\boldsymbol{r}}. \tag{4.28}$$

We write the magnetization of conduction electrons as $\boldsymbol{m}(\boldsymbol{r})$ and the susceptibility $\chi(\boldsymbol{q})$ in the wavenumber space is defined by

$$\boldsymbol{m}(\boldsymbol{r}) = \int\chi(\boldsymbol{q})\boldsymbol{B}_{\boldsymbol{q}}\frac{d\boldsymbol{q}}{(2\pi)^3\sqrt{V}}. \tag{4.29}$$

For simplicity we consider the free electron model. We treat eq. (4.27) as a perturbation to the plane wave to obtain

$$\varphi_{\boldsymbol{k}}(\boldsymbol{r}) = \frac{e^{i\boldsymbol{k}\cdot\boldsymbol{r}}}{\sqrt{V}} \pm \frac{JS}{V}\int\frac{e^{i\boldsymbol{k}\cdot\boldsymbol{r}}}{E(\boldsymbol{k}+\boldsymbol{q})-E(\boldsymbol{k})}\frac{d\boldsymbol{q}}{(2\pi)^3\sqrt{V}}, \tag{4.30}$$

where the double sign $\pm$ reflects the sign of the inner product of $\boldsymbol{S}$ and $\boldsymbol{s}$. Then we can write

$$\boldsymbol{m}_{\boldsymbol{k}}(\boldsymbol{r}) = \frac{g_{\rm e}\mu_{\rm B}}{2}(\varphi^*_{\boldsymbol{k}-}\varphi_{\boldsymbol{k}-} - \varphi^*_{\boldsymbol{k}+}\varphi_{\boldsymbol{k}+}) = -\frac{g_{\rm e}\mu_{\rm B}JS}{V^2}\int\left(\frac{1}{E(\boldsymbol{k}+\boldsymbol{q})-E(\boldsymbol{k})}+\frac{1}{E(\boldsymbol{k}-\boldsymbol{q})-E(\boldsymbol{k})}\right)e^{i\boldsymbol{q}\cdot\boldsymbol{r}}\frac{d\boldsymbol{q}}{(2\pi)^3}. \tag{4.31}$$

With summing up the above over $\boldsymbol{k}$ and from eq. (4.28), (4.28), we reach the expression

$$\begin{aligned}\chi(\boldsymbol{q}) &= \frac{g_{\rm e}^2\mu_{\rm B}^2}{2V}\int_{k\le k_{\rm F}}\left(\frac{1}{E(\boldsymbol{k}+\boldsymbol{q})-E(\boldsymbol{k})}+\frac{1}{E(\boldsymbol{k}-\boldsymbol{q})-E(\boldsymbol{k})}\right)\frac{d\boldsymbol{k}}{(2\pi)^3}\\ &= \frac{3N}{8}\frac{(g_{\rm e}\mu_{\rm B})^2}{E_{\rm F}}\frac{1}{2}\left(1+\frac{4k_{\rm F}^2-q^2}{4qk_{\rm F}}\log\left|\frac{2k_{\rm F}+q}{2k_{\rm F}-q}\right|\right).\end{aligned} \tag{4.32}$$

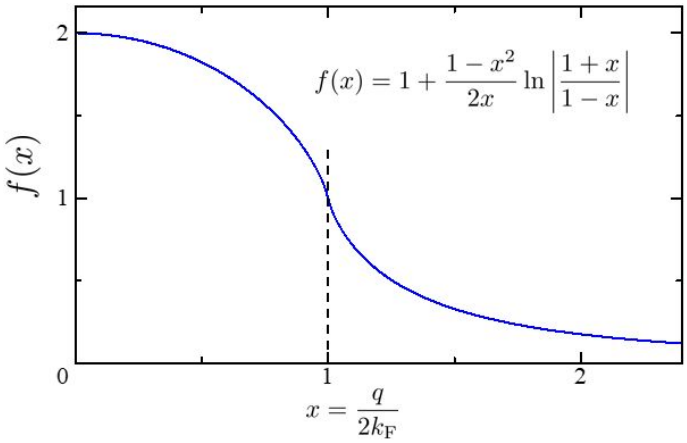

Fig. 4.3 Plot of $f(x)$ in eq. (4.33). The region is limited to $x > 0$ as $f(x)$ is an even function.

The last part in the parenthesis $(\cdots)$ is written as

$$f(x) = 1 + \frac{1-x^2}{2x} \log\left|\frac{1+x}{1-x}\right|, \tag{4.33}$$

where $x = q/2k_\mathrm{F}$ [*4]. The function is plotted in Fig. 4.3.

To calculate $\boldsymbol{m}(\boldsymbol{r})$ from eq. (4.29) and $\chi\boldsymbol{q}$ in eq. (4.32), we need the integral

$$\begin{aligned} F(r) &= \frac{1}{2\pi}\int d\boldsymbol{q} e^{i\boldsymbol{q}\cdot\boldsymbol{r}} f\left(\frac{q}{2k_\mathrm{F}}\right) = \frac{2}{r}\int_0^\infty q\sin(qr) f\left(\frac{q}{2k_\mathrm{F}}\right) dq \\ &= \frac{1}{r}\int_{-\infty}^\infty q\sin(qr) f\left(\frac{q}{2k_\mathrm{F}}\right) dq. \end{aligned} \tag{4.34}$$

In the application of partial integral, we need to apply Cauchy's principal value since df/dx diverges at $x = 1$ as shown in Fig. 4.3. We also use the identities

$$\int_{-\infty}^\infty \frac{\sin[2k_\mathrm{F}r(1\pm x)]}{1\pm x} dx = \pi, \quad \int_{-\infty}^\infty \frac{\cos[2k_\mathrm{F}r(1\pm x)]}{1\pm x} dx = 0, \tag{4.35}$$

to obtain

$$F(r) = -16\pi k_\mathrm{F}^3 \frac{2k_\mathrm{F}r\cos(2k_\mathrm{F}r) - \sin(2k_\mathrm{F}r)}{(2k_\mathrm{F}r)^4}. \tag{4.36}$$

Then we finally reach the expression of the local magnetization $\boldsymbol{m}(\boldsymbol{r})$:

$$\boldsymbol{m}(\boldsymbol{r}) = -\frac{3}{32\pi^2}\frac{Ng_\mathrm{e}\mu_\mathrm{B}F(r)J}{E_\mathrm{F}} S_z, \tag{4.37}$$

where we take z-direction to that of $\boldsymbol{S}$ and the expectation value S_z is used.

4.3.2 RKKY interaction

In eq. (4.37), the dependence on r is from $F(r)$ in eq. (4.36), the r-dependent part of which is plotted in Fig. 4.4. The decay with r is associated with an oscillation.

If we have another magnetic ion within the decay length, the conduction electrons interact with it by s-d exchange interaction and as a result, a kind of exchange interaction between the magnetic ions is established. This is called **RKKY interaction** [*5]. The interaction is estimated as

$$-\int \boldsymbol{m}(\boldsymbol{r})\boldsymbol{B}_\mathrm{eff}(\boldsymbol{r}-\boldsymbol{R})d\boldsymbol{r} = \frac{3N}{16\pi^2}\frac{J^2}{E_\mathrm{F}} F(R) S_{1z}S_{2z}, \tag{4.38}$$

[*4] The notation is confusing with the Fermi distribution function (the function itself is close!). But we do not have so many good symbols and this is a custom notation.

[*5] Capital letters of Ruderman-Kittel-Kasuya-Yosida [9, 10, 11].

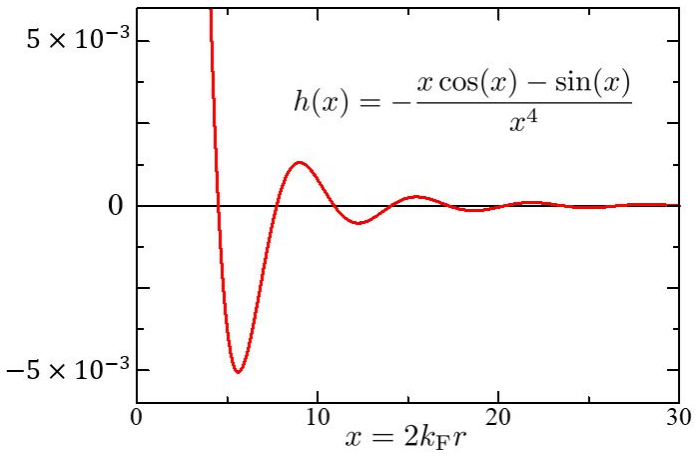

Fig. 4.4 Plot of r-dependent part of eq. (4.36), that is $-(x\cos x - \sin x)x^4$ ($x = 2k_{\mathrm{F}}r$). It decays with r to zero with an oscillation.

where $\boldsymbol{R}$ is the vector connecting the two magnetic ions, and the spins of them are written as $\boldsymbol{S}_1$ and $\boldsymbol{S}_2$. This equation is obtained from the expectation value $\boldsymbol{m}(\boldsymbol{r})$ and thus expressed in the product of expectation values along z-axis. It is an exchange interaction and we can replace $S_{1z}S_{2z}$ with $\boldsymbol{S}_1 \cdot \boldsymbol{S}_2$ to modify it to an RKKY Hamiltonian for quantum mechanical calculations.

As in eq. (4.38), the RKKY interaction oscillates with the period about $(2k_{\mathrm{F}})^{-1}$ and decays as R^{-3}. However when the distance between the ions is short, namely the second ion is close to the origin in Fig. 4.4, the interaction between the ions is always ferromagnetic because the s-d interaction works twice. De Gennes pointed out the possibility of ferromagnetism in diluted magnetic alloys[12] via this RKKY ferromagnetic interaction. However it is still unclear weather such systems really exist or not.

4.4 Double exchange interaction

The **double exchange interaction** mechanism was proposed by Zener[13] for the explanation of ferromagnetism in Mn perovskite type compound magnets. A typical example is aMnO_3, which is an insulating anti-ferromagnet due to the superexchange interaction. However, with replacing a part of La with Ca, the material $La_{1-x}Ca_xMnO_3$ ($0.2< x <0.4$) shows metallic conduction and transits to a ferromagnet.

Such a system can be modelized as Fig. 4.5. $3d$ electron levels are split by the octahedral potential of perovskite to t_{2g} orbitals and e_g orbitals. t_{2g} orbitals have lower energy and strongly localized while e_g orbitals spread over the neighbors, being hybridized with $2s$, $2p$ orbitals to form a band. In $LaMnO_3$, each Mn ion is 3+ and in the high spin state with a single electron in an e_g orbital. In spite of the formation of a band, the system is an insulator because of the on-site Coulomb repulsion U for the hopping to the neighboring e_g orbitals (due to the anti-ferromagnetic order, the electron spins do not disturb the hopping). The situation is close to the Hubbard model introduced in Sec. 4.1.3, and such insulators caused by the electron correlation are called **Mott insulators**.

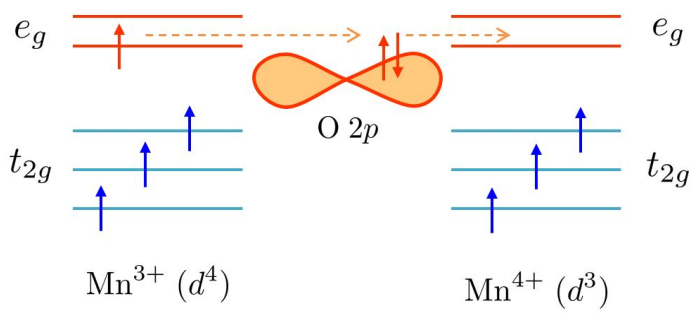

Fig. 4.5 Schematic diagram of double exchange interaction.

With replacing a part of La(3+) with Ca(2+), a part of electrons in Mn is transferred to Ca resulting in the appearance of Mn^{4+}. In Mn^{4+}, the e_g orbital is empty making the transfer of electrons via oxygen atoms possible (sometimes described as "hole doping" in the vocabulary of semiconductor physics). This leads to the breaking of electron correlation that sustains the insulating manner and the metallic conduction appears. In the metallic state, when an e_g electron shifts to the next Mn ion, the energy is lower for aligned spins of t_{2g} electrons due to Hund's rule in ions. And the higher transfer of electrons causes lowering of the kinetic energy resulting in the ferromagnetism. As can be seen in the above scenario, this can also be viewed as a kinetic exchange interaction.

So far we have seen superexchange, RKKY, and double exchange interactions. At the first glance they are so different, but it is difficult to say weather they are essentially different. The naming of the interactions comes from the human wish to understand the complicated behavior of spins in simple views. It is at a higher level than the fundamental law of physics and sticking to the classification of interactions is not a meaningful idea. Particularly in the case of spins, the interaction is due to the magic of entanglement as in Appendix 7A. We must keep in mind that sometimes the magic goes away.

4.5 Anisotropic exchange interaction

In many cases actual electrons in crystals have anisotropy reflecting complicated band structures. Such anisotropies in orbitals are reflected to spins through the spin-orbit interactions. Hence in treating the exchange interactions, we should take into account the anisotropy. We thus express the exchange interaction between sites i and j with a tensor $\boldsymbol{J}_{ij}$. Then the Hamiltonian of the spin system is given by

$$\mathscr{H} = \sum_j \mathscr{H}_{\rm A}(\boldsymbol{S}_j) - \frac{1}{2}\sum_{i\neq j} {}^t\boldsymbol{S}_i \boldsymbol{J}_{ij} \boldsymbol{S}_j, \tag{4.39}$$

where ${}^t\boldsymbol{a}$ is the transpose of $\boldsymbol{a}$. The anisotropic energy on site is written as $\mathscr{H}_{\rm A}$. We write the tensor elements indices as $J_{ij}^{\mu\nu}$ and separate (μ,ν) to symmetric and anti-symmetric parts as

$$J^{\mu\nu} = \frac{1}{2}[(J^{\mu\nu}+J^{\nu\mu}) + (J^{\mu\nu}-J^{\nu\mu})] \equiv K^{\mu\nu} + \sum_{\xi=x,y,z} \epsilon_{\mu\nu\xi} D^{\xi}. \tag{4.40}$$

$\epsilon_{\mu\nu\xi}$ is the complete anti-symmetric tensor (Levi=Chivita symbol). The site indices (i,j) are omitted. The second term in the rhs, the anti-symmetric part of eq. (4.39) is expressed as

$$\mathscr{H}_{ij}^{(\rm DM)} = {}^t\boldsymbol{S}_i \left\{ \sum_\xi \epsilon_{\mu\nu\xi} D_{ij}^{\xi} \right\} \boldsymbol{S}_j = \boldsymbol{D}_{ij}\cdot(\boldsymbol{S}_i \times \boldsymbol{S}_j). \tag{4.41}$$

$\boldsymbol{D}_{ij} = -\boldsymbol{D}_{ji}$ and this anti-symmetric exchange interaction $\mathscr{H}_{ij}^{(\rm DM)}$ is called **Dzyaloshinskii-Moriya** (DM) interaction[14, 15].

The DM interaction is important in the discussion of magnetic anisotropy of anti-ferromagnets, weak ferromagnets. In resent researches, the DM interaction is important in the magnetic interaction between thin films and in other spintronics field.

Chapter 5

Theories of magnetic insulators

Ferrite core transformer

There are many magnetic insulators as **ferrites** (AFe_2O_4, A=Mn, Co, Ni, Cu, Zn, $\cdots$). They are very advantageous for the high frequency use in the absence of eddy current and of skin effect. Now they are indispensable in high frequency techniques. Also since they do not deteriorate such as rust, the ferrites are mostly used for the magnets on blackboards etc., the magnetic sheets that can be used with cut [*6]

In the previous chapter we have introduced the Heisenberg model, which is one of the human-friendly models for dealing with magnetism. In insulators, superexchange interactions work between localized spins, and a situation close to the Heisenberg model may be realized in essence. Here we will see what kind of phenomena the model includes.

5.1 Molecular field theory

We consider **mean field theory**, which is the most basic approach in many body problems. In the field of magnetism, the approach is also called **molecular field approximation**.

5.1.1 Ferromagnetic Heisenberg model

We consider the Heisenberg model in eq. (4.13) with the magnetic field of magnetic flux density $\boldsymbol{B}$:

$$\mathscr{H} = -2J \sum_{\langle i,j \rangle} \boldsymbol{S}_i \cdot \boldsymbol{S}_j - \mu \sum_i \boldsymbol{B} \cdot \boldsymbol{S}_i, \tag{5.1}$$

where the sum on $\langle i, j \rangle$ is taken for the nearest neighbors. The interaction is ferromagnetic, i.e., $J > 0$, μ is taken as positive. In the mean field approximation for site i, the surrounding spins are replaced with averaged magnetic moments.

$$\mathscr{H}_{\text{eff}}(i) = -2J \sum_{\delta} \langle \boldsymbol{S}_{i+\delta} \rangle \cdot \boldsymbol{S}_i - \mu \boldsymbol{B} \cdot \boldsymbol{S}_i = -\mu \boldsymbol{B}_{\text{eff}} \cdot \boldsymbol{S}_i. \tag{5.2}$$

δ is for nearest neighbors. The effective field $\boldsymbol{B}_{\text{eff}}$ in eq. (5.2):

$$\mu \boldsymbol{B}_{\text{eff}} = 2J \sum_{\delta} \langle \boldsymbol{S}_{i+\delta} \rangle + \mu \boldsymbol{B}, \tag{5.3}$$

which is also called molecular field.

[*6] Long time ago, the ferrites were also used in magnetic tapes.

Here we use the expression (2.51) for magnetization M per single ion with replacing $g_J\mu_{\rm B} \to \mu$, $J \to S$, Brillouin function $B_J \to B_S$ to obtain

$$M = \mu S B_S \left[\frac{\mu S}{k_{\rm B}T} \left(B + \frac{2\alpha_z J}{\mu^2} M \right) \right]. \tag{5.4}$$

α_z is the number of neighboring sites and the direction of $\boldsymbol{B}$ is taken to z-direction. Equation (5.4) is a self-consistent equation for M.

We use the expansion of coth in Brillouin function B_S and obtain

$$B_S(x) = \frac{S+1}{3S}x - \frac{1}{90}\frac{[(S+1)^2+S^2](S+1)}{S^3}x^3 + \cdots. \tag{5.5}$$

Then eq. (5.4) is expanded as

$$\left(1 - \frac{2\alpha_z J}{\mu^2}\chi_0\right) M + \frac{1}{90}[(S+1)^2+S^2]\frac{1}{(k_{\rm B}T)^3}\left(\frac{2\alpha_z J}{\mu^2}\right)^2 M^3 = \chi_0 B. \tag{5.6}$$

$\chi_0 = \mu^2 S(S+1)/3k_{\rm B}T$ represents the Curie law in eq. (2.53).

When (5.6) has a non-zero solution of M (spontaneous magnetization) for $B = 0$, the system can have a ferromagnetic state. The condition is the coefficient of the first order in M in the lhs of (5.6) becomes zero. This gives the ferromagnetic transition temperature (**Curie temperature**) $T_{\rm C}$ as

$$k_{\rm B}T_{\rm C} = \frac{2}{3}S(S+1)\alpha_z J. \tag{5.7}$$

The susceptibility for $T > T_{\rm C}$ is obtained from eq. (5.6) by considering the first order term as

$$\chi = \chi_0 \left(1 - \frac{2\alpha_z J}{\mu^2}\chi_0\right)^{-1} = \mu^2 \frac{S(S+1)}{3k_{\rm B}(T - T_{\rm C})}, \tag{5.8}$$

which diverges as $(T - T_{\rm C})^{-1}$. This behavior is called **Curie-Weiss law**.

Appendix 7A: Quantum entanglement and quantum dot experiments

Although the magnetic-mediated spin-to-spin interaction is very weak, we found that a strong spin-to-spin interaction occurs due to the relationship with the orbit. Then the spin Hamiltonian model is introduced. As above, in quantum theory, the freedoms in an interaction model can be exchanged under some conditions. This is on the concept of **quantum entanglement**, which is widely used in the quantum information field.

7A.1 Quantum entanglement and effective Hamiltonian

The readers are already familiar with the concept and here a brief introduction is given. Let us consider two systems with two-dimensional orthogonal basis $\{|1\rangle, |2\rangle\}$ and $\{|p\rangle, |q\rangle\}$. We write the wavefunctions in the systems as $|\psi\rangle = a_1|1\rangle + a_2|2\rangle$, $|\phi\rangle = a_p|p\rangle + a_q|q\rangle$. When these two have no relation between them, a state of the combined system (of course the combined system can be considered even if there are no relation) is written as a direct product of the two wavefunctions:

$$|\Psi_{\rm n}\rangle = |\psi\rangle \otimes |\phi\rangle = a_1 a_p |1\rangle|p\rangle + a_1 a_q |1\rangle|q\rangle + a_2 a_p |2\rangle|p\rangle + a_2 a_q |2\rangle|q\rangle. \tag{7A.1}$$

On the other hand, we consider the case when the wavefunction of combined system is written in the form

$$|\xi\rangle = (|1\rangle\,|p\rangle + |2\rangle\,|q\rangle)/\sqrt{2}. \tag{7A.2}$$

In this state, assume we perform measurement on $|\psi\rangle$ and obtain e.g. the result 1. Then without observation on $|\phi\rangle$ and without direct interaction between the two systems, the state of $|\phi\rangle$ is determined to p by the above measurement. This situation is described as $|\psi\rangle$ and $|\phi\rangle$ are **entangled**. This was clearly pointed out in the famous EPR paper[16, 17]. In particular the state in eq. (7A.2) is called a maximally entangled state and the operations on the systems are unseparable.

Further, we write another maximally entangled state

$$|\zeta\rangle = (|1\rangle\,|q\rangle + |2\rangle\,|p\rangle)/\sqrt{2}, \tag{7A.3}$$

and consider the case the basis space is limited to $\{|\xi\rangle\,, |\zeta\rangle\}$. We assume the Hamiltonian in the system $\{|1\rangle\,, |2\rangle\}$

$$\mathscr{H}_{\rm n} = \begin{pmatrix} h_{11} & h_{12} \\ h_{21} & h_{22} \end{pmatrix}. \tag{7A.4}$$

Then

$$\langle\xi|\mathscr{H}_{\rm n}|\xi\rangle = h_{11} + h_{22}, \quad \langle\xi|\mathscr{H}_{\rm n}|\zeta\rangle = h_{12} + h_{21}, \quad \langle\zeta|\mathscr{H}_{\rm n}|\zeta\rangle = h_{11} + h_{22}. \tag{7A.5}$$

Hence if we can prepare an operator $\mathscr{H}_{\rm a}$ working on $\{|p\rangle\,, |q\rangle\}$ and gives the same matrix as $\mathscr{H}_{\rm n}$

$$\mathscr{H}_{\rm a} = \begin{pmatrix} h_{11} & h_{12} \\ h_{21} & h_{22} \end{pmatrix}, \tag{7A.6}$$

$\mathscr{H}_{\rm n}$ and $\mathscr{H}_{\rm a}$ give the same results in the basis space $\{|\xi\rangle\,, |\zeta\rangle\}$.

As seen above, the concept of "effective Hamiltonian" works when the basis space is limited to entangled states of two freedoms. In such states, operations on one system is equivalent to those on the other system. Hence they are working as "operators" very differently but equivalent. In quantum physics, though not always explicitly, the concept of quantum entanglement is used in various situations.

7A.2 Quantum entanglement and observation

Quantum entanglement is not only a tool for theory, but also used widely in experiments, confirming that the EPR paradox is not a mere thought experiment.

The electron paramagnetic resonance is introduced as an experiment to observe the Larmor precession of spins in magnetic field. The traditional way to detect the resonance is to detect the lowering in the Q-value of resonator due to the absorption of energy in electromagnetic wave by the spin system at the resonance. To give a change in the characteristics of a macroscopic resonator, an ordinary experiment in microwave needs at least 10^{10} spins[18]. In this method, in other words, the magnetic field caused by the magnetic dipoles of spins are detected though the interaction in eq. (4.1). The signal is naturally tiny and it is hopeless to detect single spin precession.

Let us consider "what is measurement." A possible answer is that a measurement is to create an entanglement between the freedoms of an object and those of something human can directly distinguish. As a system for measurement we consider $\{|\uparrow\rangle\,, |\downarrow\rangle\}$ and $\{|A\rangle\,, |B\rangle\}$ as another system which human can directly distinguish. Then the measurement is to create a maximally entangled state

$$\Psi = \frac{1}{\sqrt{2}}[|\uparrow\rangle\,|A\rangle + |\downarrow\rangle\,|B\rangle]. \tag{7A.7}$$

The system $\{|A\rangle\,, |B\rangle\}$ is readily integrated out and the measurement is accomplished when this Ψ is created [*7].

Now, then, in the case of a spin, instead of entanglement of spin with a photon through the magnetic moment, entanglement with other freedom with much larger effect might make the detection of single spin possible.

(to be continued).

[*7] In the terms of Schrödinger's cat problem, dead/alive of the cat is determined before the box is opened.

References

[1] Høgni Weihe and Hans U. Güdel. Quantitative interpretation of the goodenough-kanamori rules: a critical analysis. *Inorganic Chemistry*, Vol. 36, No. 17, pp. 3632–3639, August 1997.

[2] Zhishuo Huang, Dan Liu, Akseli Mansikkamäki, Veacheslav Vieru, Naoya Iwahara, and Liviu F. Chibotaru. Ferromagnetic kinetic exchange interaction in magnetic insulators. *Phys. Rev. Research*, Vol. 2, p. 033430, Sep 2020.

[3] 本郷研太, 小山田隆行, 川添良幸, 安原洋. フント則の起源は何か?(最近の研究から). 日本物理学会誌, Vol. 60, No. 10, pp. 799–803, 2005.

[4] 佐甲徳栄. ヘリウム様原子におけるフントの第一規則の起源 （解説）. 日本物理学会誌, Vol. 68, No. 6, pp. 358–365, 2013.

[5] Jacques Curély. The microscopic mechanisms involved in superexchange. *Magnetochemistry*, Vol. 8, No. 1, p. 6, December 2021.

[6] John B. Goodenough. Theory of the role of covalence in the perovskite-type manganites $[\mathrm{La}, m(\mathrm{II})]\mathrm{Mno}_3$. *Phys. Rev.*, Vol. 100, pp. 564–573, Oct 1955.

[7] Junjiro Kanamori. Superexchange interaction and symmetry properties of electron orbitals. *Journal of Physics and Chemistry of Solids*, Vol. 10, No. 2-3, pp. 87–98, July 1959.

[8] 金森順次郎. 磁性 (新物理学シリーズ 7). 培風館, 1969.

[9] M. A. Ruderman and C. Kittel. Indirect exchange coupling of nuclear magnetic moments by conduction electrons. *Phys. Rev.*, Vol. 96, pp. 99–102, Oct 1954.

[10] Tadao Kasuya. A theory of metallic ferro- and antiferromagnetism on zener's model. *Progress of Theoretical Physics*, Vol. 16, No. 1, pp. 45–57, July 1956.

[11] Kei Yosida. Magnetic properties of cu-mn alloys. *Phys. Rev.*, Vol. 106, pp. 893–898, Jun 1957.

[12] P.G. De Gennes. Polarisation de charge (ou de spin) au voisinage dúne impureté dans un alliage. *Journal de Physique et le Radium*, Vol. 23, No. 10, pp. 630–636, 1962.

[13] Clarence Zener. Interaction between the d-shells in the transition metals. ii. ferromagnetic compounds of manganese with perovskite structure. *Phys. Rev.*, Vol. 82, pp. 403–405, May 1951.

[14] Igor Dzyaloshinsky. A thermodynamic theory of "weak" ferromagnetism of antiferromagnetics. *Journal of physics and chemistry of solids*, Vol. 4, No. 4, pp. 241–255, 1958.

[15] Tôru Moriya. Anisotropic superexchange interaction and weak ferromagnetism. *Physical review*, Vol. 120, No. 1, p. 91, 1960.

[16] A. Einstein, B. Podolsky, and N. Rosen. Can quantum-mechanical description of physical reality be considered complete? *Phys. Rev.*, Vol. 47, pp. 777–780, May 1935.

[17] Giuliano Benenti, Giulio Casati, Davide Rossini, and Giuliano Strini. *Principles of Quantum Computation and Information: A Comprehensive Textbook*. World Scientific Publishing Company, 1 2019.

[18] Patrick Bertrand. *Electron Paramagnetic Resonance Spectroscopy: Fundamentals*. Springer, 2 2020.

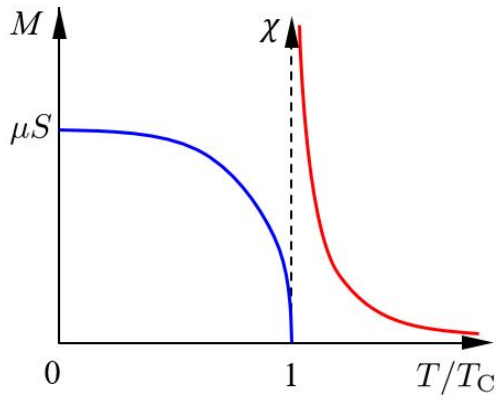

Fig. 5.1 Schematic drawing of susceptibility χ above $T_{\rm C}$ and spontaneous magnetization M below $T_{\rm C}$ for a ferromagnet.

Last week we introduced the Heisenberg model for magnetic insulators. In mean field (molecular field) approximation, the power series expansion of the Brillouin function (eq. (5.6)) gives the equation, which leads to the Curie-Weiss law:

$$\chi = \frac{\mu^2 S(S+1)}{k_{\rm B}} \frac{1}{T - T_{\rm C}}. \tag{5.8}$$

In the region $T < T_{\rm C}$, the solutions of $M \neq 0$ exists for $B = 0$, i.e., the **spontaneous magnetization** appears. In the vicinity of $T_{\rm C}$, the term of M^3 in eq. (5.6) is included to give the spontaneous magnetization as

$$M = \mu \sqrt{\frac{10}{3}} \frac{S(S+1)}{\sqrt{(S+1)^2 + S^2}} \sqrt{1 - \frac{T}{T_{\rm C}}}. \tag{5.9}$$

On the other hand, at $T \ll T_{\rm C}$, we use the asymptotic expression

$$B_S(x) \sim 1 - \frac{1}{S} \exp\left(-\frac{x}{S}\right) + \left[\frac{2S+1}{S} \exp\left(-\frac{2S+1}{S} x\right)\right] \tag{5.10}$$

for $x \gg 1$. The first two leading terms give

$$M = \mu \left[S - \exp\left(-\frac{3}{S+1} \frac{T_{\rm C}}{T}\right)\right], \tag{5.11}$$

which approaches the perfect magnetization μS with $T \to 0$. The temperature dependences of χ and M obtained above are summarized schematically in Fig. 5.1.

5.2 Phenomenology of ferromagnetic transition: the GL theory

The above simple results still contains characteristic features of **cooperative phenomena**. For example, in eq. (5.8), $T \approx T_{\rm C}$, we can write

$$\chi \propto \frac{1}{1 - (T_{\rm C}/T)} = 1 + \frac{T_{\rm C}}{T} + \left(\frac{T_{\rm C}}{T}\right)^2 + \left(\frac{T_{\rm C}}{T}\right)^3 + \cdots,$$

which expresses the following process: the effective field by the neighboring sites gives the excess polarization proportional to $T_{\rm C}/T$, while the neighboring sites get the same excess polarizations that give the feedback of $(T_{\rm C}/T)^2$. This series continues infinitely. The series reaches the radius of convergence at $T = T_{\rm C}$ and the spontaneous magnetization appears there.

We know that even such a simple model includes a mechanism of the appearance of ferromagnetism. Then, here, we have a look on a very general properties of phase transitions and try to find the correspondence with the mean field approximation.

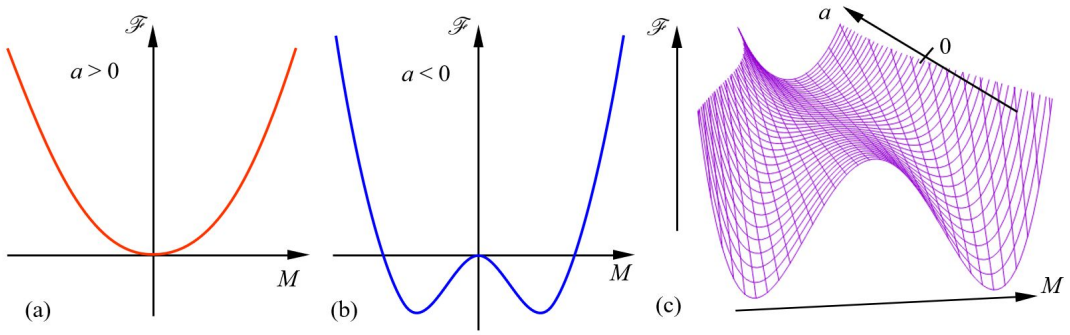

Fig. 5.2 Illustration of power expansion formula for the free energy $\mathscr{F}$ by M eq. (5.14). (a) Case $a \geq 0$. (b) case $a < 0$. In (c), a varies continuously through 0, and $\mathscr{F}$ is plotted in a wireframe.

5.2.1 Free energy

Here we introduce the **Ginzburg-Landau (GL)** theory of phase transition[1, 2]. This was constructed to understand superconductivity and superconducting transition phenomenologically. The GL theory, however, can be applied to a wide range of phase transition phenomena, and naturally have hugely been affecting the study of critical phenomena[3, 4]. In the theory, the free energy of the system is a function of physical quantities. In an equilibrium, the free energy should be at a minimum for the parameters "adjustable" by the system such as magnetization. In other words, the parameters take the values that make the free energy take a minimum. Let $\mathscr{F}$ be the free energy per spin, then we consider the functional form of $\mathscr{F}(M)$, where M is the magnetization per spin.

In order to consider the symmetry of the system, we turn off the magnetic field in the Hamiltonian in eq. (5.1), which reduces the symmetry. Now we perform a kind of symmetry operation of spin inversion on all sites, namely

$$\forall i \;\; \boldsymbol{S}_i \to -\boldsymbol{S}_i.$$

For this operation, the Hamiltonian in eq. (.1) with $\boldsymbol{B} = 0$ is invariant. Accordingly $\mathscr{F}$ is unchanged. On the other hand, from the definition,

$$\boldsymbol{M} = \langle \boldsymbol{S}_i \rangle \to \langle -\boldsymbol{S}_i \rangle = -\boldsymbol{M}, \tag{5.12}$$

that is the parameter M is inverted. The above inference leads to

$$\mathscr{F}(M) = \mathscr{F}(-M), \tag{5.13}$$

namely $\mathscr{F}$ is an even function of M. Therefore we can expand $\mathscr{F}$ to the power series of small M (hence close to the transition) to the forth order as

$$\mathscr{F}(M) = \mathscr{F}_0 + aM^2 + bM^4. \tag{5.14}$$

First in eq. (5.14), to have a stable point of $\mathscr{F}$ at finite M, b should be positive ($b > 0$). Under this condition, a positive a ($a \geq 0$) always gives $M = 0$ as the stable point of $\mathscr{F}$ as in Fig. 5.2(a). For $a < 0$, two finite values of M give energy minima, hence are stable points, lower than the energy for $M = 0$ as in Fig. 5.2(b). The equation which gives the stable points is

$$\frac{\partial \mathscr{F}}{\partial M} = 0 = 2aM + 4bM^3 = 2M(2bM^2 + a), \tag{5.15}$$

which is in the same form as in eq. (5.6), thus is the same equation. This is sometimes called "magnetic equation of state." As in Fig. 5.2, the system is paramagnetic for (a) $a \geq 0$, and ferromagnetic for (b) $a < 0$. We now find that a is a parameter: i) which determines $\mathscr{F}(M)$; ii) which has no anomaly at zero, the transition point of M. Therefore a is a "relevant" parameter for the transition (in a sense, a parameter that drives the transition). a must vary in the first order for

thermodynamic parameters like temperature, pressure, etc. Figure 5.2(c) shows such continuous change in $\mathscr{F}(M)$ with the variation of a, and the appearance of stable points other than $M = 0$ at the transition point $a = 0$. This indicates that we are considering a second order phase transition, which does not have latent heat at the ferromagnetic transition. If we take temperature T as the relevant parameter of the transition, a should be in the first order of T. As the expression of a, which is zero at the transition point and in the first order in T, we can write $a = k(T_{\rm C} - T)/T_{\rm C}$. Then a finite solution of M_0 for eq. (5.15) is given by

$$M_0 = \sqrt{-\frac{a}{2b}} = \sqrt{\frac{k(T_{\rm C} - T)}{2bT_{\rm C}}}. \tag{5.16}$$

5.2.2 Spontaneous symmetry breaking

In the region $T \leq T_{\rm C}$, $\mathscr{F}(\pm M_0)$ are the thermodynamically stable solutions, in which $\langle M \rangle = M_0$ or $-M_0$. These correspond to the **spontaneous magnetization** of ferromagnets, which was introduced in the first lecture [*1]. For the expansion of eq. (5.14), we have used the symmetry of free energy (5.13) deduced from the symmetry of Hamiltonian (5.1) for the symmetry operation $\forall i : \boldsymbol{S}_i \to -\boldsymbol{S}_i$. In the region $T < T_{\rm C}$, $M = 0$ is unstable and one of stable solutions $\pm M_0$ is realized. Due to (5.13), the symmetry operation does not change the free energy, but now M is the parameter determining the state of the system. That means the operation changes the state. The situation is summarized that the symmetry of realized state is broken while that of the system (Hamiltonian) is kept. Such a phenomenon is called **spontaneous symmetry breaking**. The concept was introduced by Yoichiro Nambu[5, 6, 7] from the analogy of the BCS theory (and the Bogoliubov theory) for superconductivity and the mechanism for the appearance of particle mass. It is one of the basic concepts in physics, has been widely applied to a variety of phenomena under active research. There are many textbooks including the one for general public written by Nambu himself[8, 9, 10, 11].

The continuous spatial symmetry in the original system with random direction of spins is broken in the state with spontaneous magnetization M_0, in which the spins are in order pointing a single point in space. The parameter that appears at the critical point and represents the order of the state is called **order parameter**.

5.3 Critical exponent

$\mathscr{F}$ in the presence of spontaneous magnetization M_0 is given as a function of temperature as

$$\mathscr{F}(T) = \mathscr{F}_0 + aM_0^2 + bM_0^4 = \mathscr{F}_0 - \frac{a^2}{4b} = \mathscr{F}_0 - \frac{k^2(T_{\rm C} - T)^2}{4bT_{\rm C}^2}. \tag{5.17}$$

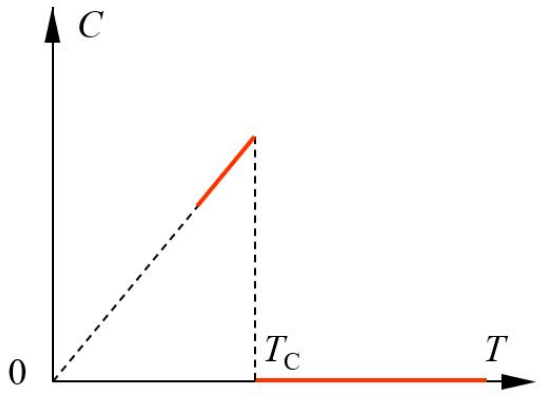

Then in $T \leq T_{\rm C}$, the specific heat C is given by

$$C = -T\frac{\partial^2 \mathscr{F}}{\partial T^2} = \frac{k^2 T}{2bT_{\rm C}^2}. \tag{5.18}$$

On the other hand in $T \geq T_{\rm C}$, $C = 0$ because $M_0 = 0$ and $\mathscr{F}(T) = \mathscr{F}_0$. Then the specific heat has a jump of

$$\Delta C = \frac{k^2}{2bT_{\rm C}}, \tag{5.19}$$

at $T = T_{\rm C}$ which is illustrated in the left.

Now when a small magnetic field is introduced, in the lowest order approximation, we can replace the term of external

[*1] As also introduced in the lecture, in practice, with zero-field cooling from above the Curie temperature, we cannot observe macroscopic spontaneous magnetization due to the formation of magnetic domains, which build up magnetic circuit and confine the magnetic flux inside.

field in Hamiltonian (5.1) with $-BM$, where M is the magnetization. That is we add the first order term as

$$\mathscr{F}(M) = \mathscr{F}_0 + aM^2 + bM^4 - BM. \tag{5.20}$$

Then from

$$\frac{\partial \mathscr{F}}{\partial M} = 0 = 2aM + 4bM^3 - B, \tag{5.21}$$

we get $M^3 \propto B$ just at the critical point $T = T_{\mathrm{C}}$ because $a = 0$.

So far we have obtained the expressions for magnetization M, susceptibility χ and specific heat C in the forms of

$$M \propto \begin{cases} B^{1/\delta} & (T = T_{\mathrm{C}}), \\ (T_{\mathrm{C}} - T)^{\beta} & (T < T_{\mathrm{C}}), \end{cases} \tag{5.22a}$$

$$\chi \propto \begin{cases} (T - T_{\mathrm{C}})^{-\gamma} & (T > T_{\mathrm{C}}), \\ (T_{\mathrm{C}} - T)^{-\gamma'} & (T < T_{\mathrm{C}}), \end{cases} \tag{5.22b}$$

$$C \propto \begin{cases} (T - T_{\mathrm{C}})^{-\alpha} & (T > T_{\mathrm{C}}), \\ (T_{\mathrm{C}} - T)^{-\alpha'} & (T < T_{\mathrm{C}}). \end{cases} \tag{5.22c}$$

As above, we pick up a relevant parameter, which drives a phase transition in the system, and consider the shift from the critical value. The power indices of the "shift" in the functional expressions of physical quantities are called **critical exponents**. This is particularly important concept in the second order phase transitions. The above symbols α, β, γ, δ, $\cdots$ are habitually used in the field of magnetism and statistical physics. There is an anomaly of jump for the specific heat in eq. (5.22c), we apply the forms of critical exponent separately for $T < T_{\mathrm{C}}$ and for $T_{\mathrm{C}} < T$. In both cases the main term is a constant in the expression of $T - T_{\mathrm{C}}$, hence $\alpha = \alpha' = 0$.

The critical exponents depend on symmetry, dimension, range of interaction, way of approximation, etc. of the model. On the other hand, the variations in the system parameters do not change the exponents. The property is expressed as the critical exponents have **universality**. Further, we can classify the theoretical models (including approximations) of phase transitions with the set of the values of critical exponents. This classification called **universality class**, depends, as we saw in the introduction of the GL theory, often symmetry of the system. The universality class is also determined by general properties of the system such as the spatial dimension, the range of interaction. The next table summarizes the values of critical exponents in the mean field theory.

Critical exponent	α	β	γ	δ
Mean field approximation	0	1/2	1	3

Though we have introduced the concept of universality class, the model examined is only the mean field theory of Heisenberg model. We would like to have a short look at the other models.

5.4 Theoretical models of ferromagnet (localized spins)

The theoretical models of magnetic materials are the big stage for statistical physics. In the above we consider the Heisenberg model as ferromagnetic insulators. In the Heisenberg model, the spin variable has three components $\boldsymbol{S}_i = (S_i^x, S_i^y, S_i^z)$. In the **XY model**, the spin components are limited to two, that is $\boldsymbol{S}_i = (S_i^x, S_i^y)$. In the **Ising model**, the spin has a single component. In the Heisenberg model and the XY model, the spin degree of freedom takes a continuous value while in the Ising model it is quantized to the two values.

5.4.1 XY model

First we pick up a direction for "angle zero," then because the spins in this model are in the two-dimensional plane, we can assign an angle ϕ_i for each site i measured from the angle zero. Then the angle between the spins at sites i and j is $\phi_i - \phi_j$. Accordingly the Hamiltonian of the XY model can be written as

$$\mathscr{H} = -J \sum_{\langle i,j \rangle} \cos(\phi_i - \phi_j). \tag{5.23}$$

In the two dimensional XY model, there is no long range order due to the Mermin-Wagner theorem though it has another type of phase transition, in which the order parameter decreases not with exponential damping but with power of distance damping. The transition is called Berezinskii-Kosterlitz-Thouless (BKT) transition[12]. The BKT transition is caused by excitations called vortices, in which the spins form rotation structures. They have two possible directions of rotation, and we distinguish them with the naming vortex and anti-vortex. An attractive force works between a vortex and an anti-vortex, which form a vortex pair bound state. The bound states are more stable than free unbound vortices. In the low temperature phase all vortices are bound into pairs. With increasing temperature the number of vortex pairs increases and at the transition point free unbound vortices appear due to the weakening of attractive force by screening. This can be taken as a two-dimensional melting transition.

It is easier to realize the XY model (5.23) in superconducting Josephson networks than in spin systems[13]. A Josephson network is an arrangement of superconducting islands and junctions connecting them. They can be prepared by e.g., lithography, or growth of granular films. We can write the phase of superconducting order parameter on each plaquette (island) i as ϕ_i[*2]. Then the summation of Josephson energy is written in the form of (5.23). Also two-dimensional vortices mentioned above appear in a thin film of superfluid on a plate (the film flow effect). Hence observation of the BKT transition has been reported in such systems.

5.4.2 Ising model

The name of the Ising model comes from Ernst Ising, who showed the solution of this model in the case of nearest neighbor interaction[14]. It can be expressed by the Hamiltonian:

$$\mathscr{H} = -J \sum_{\langle i,j \rangle} S_i S_j - h \sum_i S_i, \tag{5.24}$$

where i, j are indices of the lattice. S_i is the Ising spin on i, which takes values ± 1. In the second term μB is written as h for simplicity. The Ising model may be the most known model of magnetic materials. The model is so simple, and overall, not only the solution by Ernst Ising for one-dimensional model, but also the rigorous solution of two-dimensional model in the absence of magnetic field[15] are the base of study for various physics in this system.

The critical exponents of these models are listed in the following table[16]. What is written using the decimal point is the value obtained by the computation with the Monte Carlo method.

Model (Universality class)	α	β	γ	δ
2D Ising	0	1/8	7/4	15
3D Ising	0.115	0.324	1.239	4.82
3D XY	-0.01	0.34	1.32	4.9
3D Heisenberg	-0.11	0.36	1.39	4.9
Mean field approximation	0	1/2	1	3

[*2] This quantity is not gauge invariant, not an observable. However the phase difference appears in the Hamiltonian is a gauge invariant observable.

5.5 Anti-ferromagnetic Heisenberg model

Next we consider the case when the interaction is anti-ferromagnetic ($J < 0$) in the Heisenberg model:

$$\mathscr{H} = -2J \sum_{\langle i,j \rangle} \boldsymbol{S}_i \cdot \boldsymbol{S}_j - \mu \sum_i \boldsymbol{B} \cdot \boldsymbol{S}_i. \tag{5.1}$$

We consider a two dimensional square lattice with nearest neighbor interaction. When the system is in the anti-ferromagnetic order, the classical ground state of two-dimensional square lattice Heisenberg model is a Néel ordering state, in which the neighboring spins are in anti-parallel order. We divide the entire crystal lattice into A and B sublattices, and consider a state in which the spins are parallel in each lattice. In the treatment of ferromagnetic Heisenberg model, we first applied an external magnetic field to give direction to the isotropic space[*3]. In the anti-ferromagnetic case, we take a similar method. This time as in the right panel of Fig. 5.3, we need to prepare the field that changes the direction alternatively with site[17]. Anyway the alternative field will be set to zero in the ordered state. We consider the starting state as the moments are alternatively aligned with the alternative field with oblique angle due to the external magnetic field as illustrated in the right panel of Fig. 5.3.

Let $\boldsymbol{B}_{\mathrm{u}}$ be the external constant field, $\pm\boldsymbol{B}_{\mathrm{s}}$ be the site-alternative field. The fields on the two kinds of sites are

$$\left.\begin{aligned} \boldsymbol{B}_{\mathrm{A}} &= \boldsymbol{B}_{\mathrm{u}} + \boldsymbol{B}_{\mathrm{s}}, \\ \boldsymbol{B}_{\mathrm{B}} &= \boldsymbol{B}_{\mathrm{u}} - \boldsymbol{B}_{\mathrm{s}}. \end{aligned}\right\} \tag{5.25}$$

The effective Hamiltonian of the molecular field approximation is

$$\mathscr{H}_{\mathrm{eff}}(i) = -2J \sum_{\delta} \langle \boldsymbol{S}_{i+\delta} \rangle \cdot \boldsymbol{S}_i - \mu \boldsymbol{B}_{\mathrm{A}} \cdot \boldsymbol{S}_i \quad (i \in \mathrm{A}), \tag{5.26a}$$

$$\mathscr{H}_{\mathrm{eff}}(j) = -2J \sum_{\delta} \langle \boldsymbol{S}_{j+\delta} \rangle \cdot \boldsymbol{S}_j - \mu \boldsymbol{B}_{\mathrm{B}} \cdot \boldsymbol{S}_j \quad (j \in \mathrm{B}). \tag{5.26b}$$

The averaged magnetic moments at the two sites are

$$\left.\begin{aligned} \boldsymbol{M}_{\mathrm{A}} &= \mu \langle \boldsymbol{S}_i \rangle = \boldsymbol{M}_{\mathrm{u}} + \boldsymbol{M}_{\mathrm{s}} \\ \boldsymbol{M}_{\mathrm{B}} &= \mu \langle \boldsymbol{S}_j \rangle = \boldsymbol{M}_{\mathrm{u}} - \boldsymbol{M}_{\mathrm{s}} \end{aligned}\right\}. \tag{5.27}$$

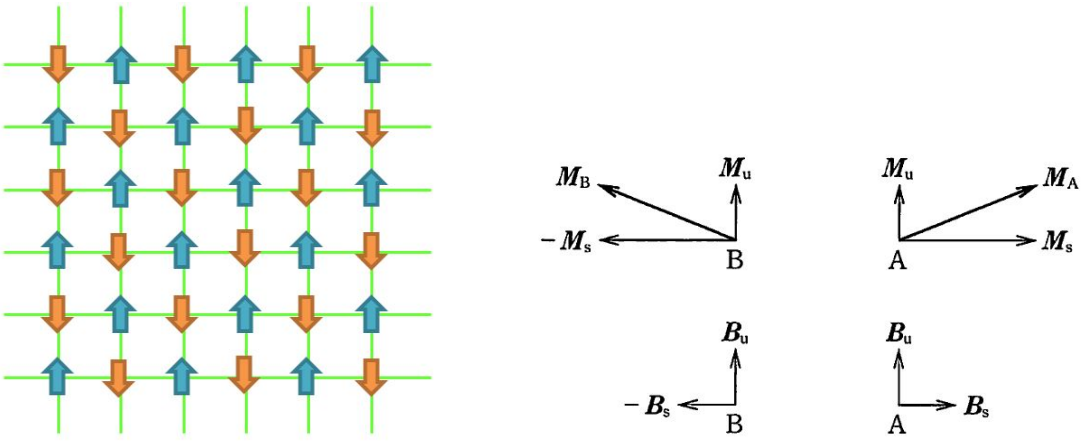

Fig. 5.3 Left: Illustration of Néel anti-ferromagnetic order. Right: Drawing of "seeds field" to set the spins around the anti-ferromagnetic order. From [17].

[*3] In theories, without such "seeds" field, the system continues to take the unstable solution.

We here define the Brillouin "vector" function as

$$\vec{B}_S(\boldsymbol{x}) = B_S(x)\frac{\boldsymbol{x}}{x}. \tag{5.28}$$

Then the self-consistent equation is written as [*4],

$$\boldsymbol{M}_{\rm u} + \boldsymbol{M}_{\rm s} = \mu S \vec{B}_S \left\{ \frac{\mu S}{k_{\rm B}T} \left[\boldsymbol{B}_{\rm u} + \boldsymbol{B}_{\rm s} + \frac{2\alpha_z J}{\mu^2}(\boldsymbol{M}_{\rm u} - \boldsymbol{M}_{\rm s}) \right] \right\}. \tag{5.29}$$

Above the critical temperature $T > T_{\rm N}$, from $\vec{B}_S(\boldsymbol{x}) \sim (S+1)\boldsymbol{x}/3S$, we write

$$\boldsymbol{M}_{\rm u} + \boldsymbol{M}_{\rm s} = \chi_0 \left[\boldsymbol{B}_{\rm u} + \boldsymbol{B}_{\rm s} + \frac{2\alpha_z J}{\mu^2}(\boldsymbol{M}_{\rm u} - \boldsymbol{M}_{\rm s}) \right]. \tag{5.30}$$

The definition of χ_0 is in eq. (5.6).

Then **uniform susceptibility** $\chi_{\rm u}$, and **sublattice susceptibility** $\chi_{\rm s}$ are given by

$$\chi_{\rm u} = \lim_{B_{\rm u}\to 0} \frac{M_{\rm u}}{B_{\rm u}} = \chi_0 \left(1 - \frac{2\alpha_z J}{\mu^2}\chi_0 \right)^{-1}, \tag{5.31a}$$

$$\chi_{\rm s} = \lim_{B_{\rm s}\to 0} \frac{M_{\rm s}}{B_{\rm s}} = \chi_0 \left(1 + \frac{2\alpha_z J}{\mu^2}\chi_0 \right)^{-1}. \tag{5.31b}$$

Because $J < 0$, $\chi_{\rm u}$ does not diverge. On the other hand $\chi_{\rm s}$ diverges at **Néel temperature**

$$k_{\rm B}T_{\rm N} = \frac{2}{3}S(S+1)\alpha_z|J|. \tag{5.32}$$

Hence with $\boldsymbol{B}_{\rm s} \to 0$, we have **sublattice spontaneous magnetization** $\boldsymbol{M}_{\rm s}$.

From the expansion around the spontaneous magnetization $\boldsymbol{M}_{\rm s}$,

$$\boldsymbol{M}_{\rm u} + \boldsymbol{M}_{\rm s} = \mu S \left[\vec{B}_S \left(\frac{\mu S}{k_{\rm B}T} \frac{-2\alpha_z J}{\mu^2} \boldsymbol{M}_{\rm s} \right) + \frac{d}{dM_{\rm s}} B_S \left(\frac{\mu S}{k_{\rm B}T} \frac{-2\alpha_z J}{\mu^2} \boldsymbol{M}_{\rm s} \right) \left(-\boldsymbol{M}_{\rm u} - \frac{\mu^2}{2\alpha_z J}\boldsymbol{B}_{\rm u} \right) \right]. \tag{5.33}$$

From the first term in the rhs, we obtain the self-consistent equation for $M_{\rm s}$ as

$$M_{\rm s} = \mu S B_S \left(\frac{\mu S}{k_{\rm B}T} \frac{-2\alpha_z J}{\mu^2} M_{\rm s} \right). \tag{5.34}$$

By taking derivative of both sides with $M_{\rm s}$ we know

$$1 = \mu S \frac{d}{dM_{\rm s}} B_S \left(\frac{\mu S}{k_{\rm B}T} \frac{-2\alpha_z J}{\mu^2} M_{\rm s} \right).$$

Then from the second term in the rhs of eq. (5.33), we obtain

$$\boldsymbol{M}_{\rm u} = -\boldsymbol{M}_{\rm u} - \frac{\mu^2}{2\alpha_z J}\boldsymbol{B}_{\rm u}. \tag{5.35}$$

And from $\boldsymbol{M}_{\rm u} = -\mu^2 \boldsymbol{B}_{\rm u}/4\alpha_z J$, the uniform susceptibility is obtained as

$$\chi_{\rm u} = \lim_{B_{\rm u}\to 0} \frac{M_{\rm u}}{B_{\rm u}} = -\frac{\mu^2}{-4\alpha_z J}. \tag{5.36}$$

The above results are illustrated in Fig. 5.4.

[*4] $\alpha_z = 4$ in the present case

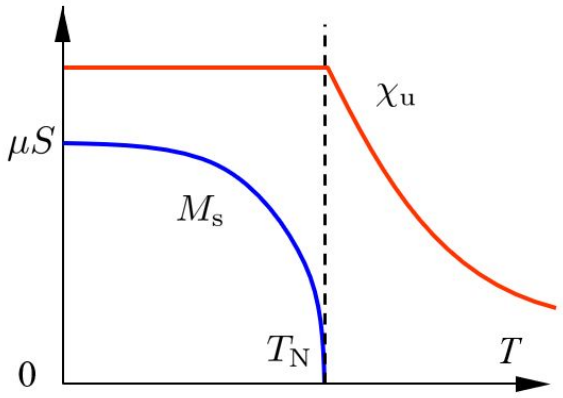

Fig. 5.4 Illustration of (uniform) susceptibility and sublattice spontaneous magnetization in anti-ferromagnetic Heisenberg model.

References

[1] V.L. Ginzburg and L.D. Landau. *Zh. Eksp. Teor. Fiz.*, Vol. 20, p. 1064, 1950.

[2] Vitaly L. Ginzburg. On superconductivity and superfluidity (what i have and have not managed to do), as well as on the'physical minimum' at the beginning of the 21st century. *ChemPhysChem*, Vol. 5, No. 7, pp. 930–945, July 2004.

[3] Shang-keng Ma. *Modern Theory Of Critical Phenomena (Advanced Books Classics)*. Routledge, 5 2018.

[4] 西森秀稔. 相転移・臨界現象の統計物理学 新物理学シリーズ. 培風館, 11 2005.

[5] Yoichiro Nambu. Quasi-particles and gauge invariance in the theory of superconductivity. *Phys. Rev.*, Vol. 117, pp. 648–663, Feb 1960.

[6] Y. Nambu and G. Jona-Lasinio. Dynamical model of elementary particles based on an analogy with superconductivity. i. *Phys. Rev.*, Vol. 122, pp. 345–358, Apr 1961.

[7] Y. Nambu and G. Jona-Lasinio. Dynamical model of elementary particles based on an analogy with superconductivity. ii. *Phys. Rev.*, Vol. 124, pp. 246–254, Oct 1961.

[8] 南部陽一郎. クォーク第 2 版: 素粒子物理はどこまで進んできたか (ブルーバックス). 講談社, 2 1998.

[9] 南部陽一郎. 素粒子論研究 (わが研究の思い出) (〈 特集 〉 日本物理学会のあゆみ). 日本物理学会誌, Vol. 32, No. 10, pp. 773–778, 1977.

[10] Y. Nambu. *Broken Symmetry: Selected Papers of Y. Nambu (World Scientific Series in 20th Century Physics)*. World Scientific Pub Co Inc, 10 1995.

[11] PHILIP W. ANDERSON. *BASIC NOTIONS OF CONDENSED MATTER PHYSIC*. TAYLOR & FRANCIS, 2 2019.

[12] V N Ryzhov, E E Tareyeva, Yu D Fomin, and E N Tsiok. Berezinskii – kosterlitz – thouless transition and two-dimensional melting. *Physics-Uspekhi*, Vol. 60, No. 9, pp. 857–885, September 2017.

[13] Shingo Katsumoto. Single-electron tunneling and phase transitions in granular films. *Journal of Low Temperature Physics*, Vol. 98, No. 5-6, pp. 287–349, March 1995.

[14] Ernst Ising. Beitrag zur theorie des ferromagnetismus. *Zeitschrift für Physik*, Vol. 31, No. 1, pp. 253–258, February 1925.

[15] Lars Onsager. Crystal statistics. i. a two-dimensional model with an order-disorder transition. *Phys. Rev.*, Vol. 65, pp. 117–149, Feb 1944.

[16] H W J Blöte, E Luijten, and J R Heringa. Ising universality in three dimensions: a monte carlo study. *Journal of Physics A: Mathematical and General*, Vol. 28, No. 22, pp. 6289–6313, nov 1995.

[17] 上田和夫. 磁性入門 (物性科学入門シリーズ). 裳華房, 単行本, 9 2011.

Lecture note Magnetism (9)

8th June (2022) Shingo Katsumoto, Institute for Solid State Physics, University of Tokyo

In the last lecture, we stopped at the molecular field approximation of anti-ferromagnetic Heisenberg model. The lecture note was at the beginning of ferrimagnetism. I would like to add the treatment of parallel magnetic field to spontaneous (internal) magnetization of an anti-ferromagnetic state. And would like to change some notations in the ferrimagnetic part. Hence, here, I would like to rewrite the ferrimagnetic part.

5.5.1 Parallel susceptibility

Next we consider the case that the external magnetic field is parallel or anti-parallel (collinear) to the spontaneous magnetizations of sublattices. The Heisenberg model is completely isotropic. If we assume that the system always takes the lowest energy state, then the magnetization should rotate to be perpendicular to the external magnetic field. However real materials usually have some magnetic anisotropies that lock the directions of moment. We thus consider the case the external field is collinear to the spontaneous magnetization. The effective fields in A and B sublattices are written as

$$B_{\mathrm{eff}}(\mathrm{A}) = B + B_{\mathrm{sub}}(\mathrm{A}), \tag{5.37a}$$
$$B_{\mathrm{eff}}(\mathrm{B}) = B + B_{\mathrm{sub}}(\mathrm{B}). \tag{5.37b}$$

Because the vectors are collinear, we do not use vector symbols here. Then as is due course, we write down a set of self-consistent equations for magnetizations as

$$\begin{aligned} \langle M_{\mathrm{A}} \rangle &= \mu S \mathcal{B}_S \left[\frac{\mu S}{k_{\mathrm{B}} T} \left(B + \frac{2\alpha_z J}{\mu^2} \langle M_{\mathrm{B}} \rangle \right) \right], \\ \langle M_{\mathrm{B}} \rangle &= \mu S \mathcal{B}_S \left[\frac{\mu S}{k_{\mathrm{B}} T} \left(B + \frac{2\alpha_z J}{\mu^2} \langle M_{\mathrm{A}} \rangle \right) \right], \end{aligned} \tag{5.38}$$

where $\mathcal{B}_S(x)$ is the Brillouin function. With solving the above and from the relation [*1] ,

$$\chi_{\parallel} = \lim_{B \to 0} \frac{M_A + M_B}{B}, \tag{5.39}$$

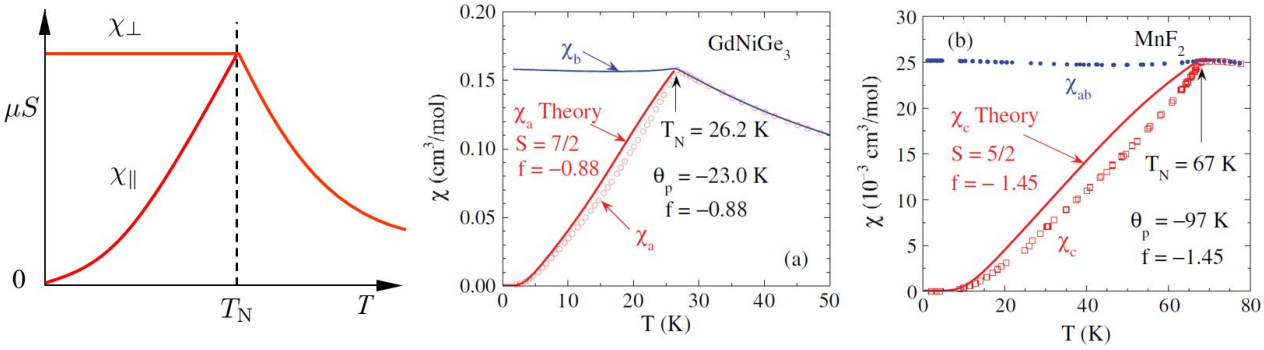

Fig. 5.1 Left panel: Schematic diagram of temperature dependent susceptibility in the molecular field approximation of the anti-ferromagnetic Heisenberg model. The susceptibilities for magnetic field perpendicular ($\chi_\perp$) and parallel ($\chi_\parallel$) to the spin polarization. Measured susceptibilities of (a) $GdNiGe_3$, (b) MnF_2. From [1].

[*1] As is the case of spontaneous ferromagnetic magnetization, we need to solve the equation numerically.

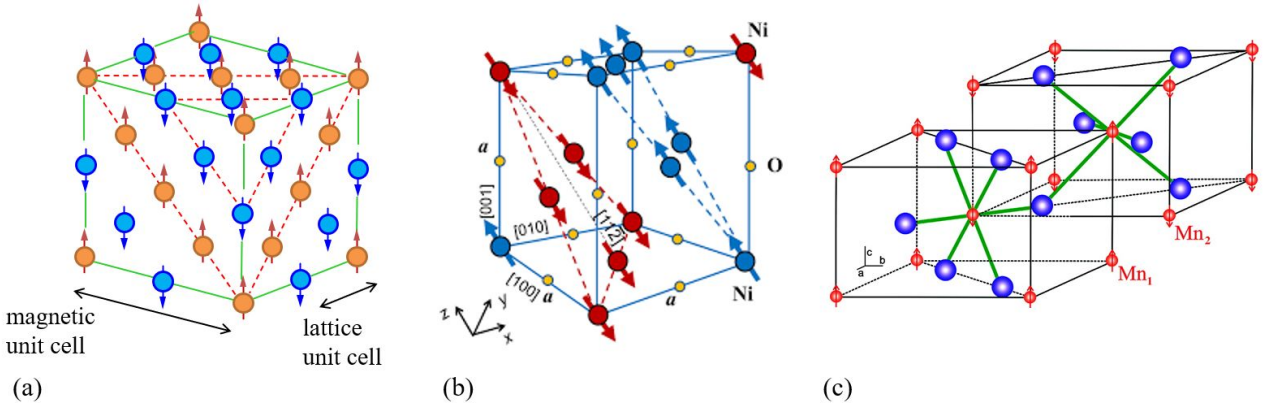

Fig. 5.2 Examples of spin configurations in metal oxides, fluorides. (a) and (b) shows the spin-directions at magnetic ions. (c) also shows the positions of F-atoms. (a) MnO. From [2]. Red broken lines show the sheets of aligned spins. (b) NiO. From [3]. (c) MnF_2. From [4].

we obtain the parallel magnetization.

From eq. (5.38), in the limit of $T \to 0$, $M_{\rm A} = -M_{\rm B} = \mu S$ as in the case of ferromagnetism, $\chi_\parallel \to 0$. On the other hand, $\chi_\parallel = \chi_\perp$ at $T = T_{\rm N}$ The susceptibility, thus has a large anisotropy below $T_{\rm N}$ as shown in the left panel of Fig. 5.1. Though the situation of perpendicular field to the sublattice magnetization cannot be realized in the Heisenberg model, a small anisotropy may enable it. In many anti-ferromagnets, such properties have been really observed. Figure 5.1(a), (b) show examples of $GdNiGe_3$, MnF_2, which are claimed to be close to the anti-ferromagnetic Heisenberg model.

5.5.2 Antiferromagnetic insulators

So far, we have discussed the magnetic susceptibility of antiferromagnetic materials with a very simple two-dimensional Heisenberg model. As mentioned in the section on superexchange interactions, oxides and fluorides of magnetic metals are often antiferromagnetic. Figure 5.2 shows examples of spin configurations in anti-ferromagnetic insulators. As in the Heisenberg model, neighboring (though with intermediate negative ions) spins at magnetic ions have opposite directions. As can be seen in the figure, actual "sublattices" can be taken as two-dimensional spin-aligned sheets. In such a case, the structure is a kind of magnetic superlattice.

In an anti-ferromagnetic ordered state, the spins have a periodic structure with a larger volume than that of lattice (unit cell). This is sometimes called a spin-superlattice. For this situation, we can apply a concept called **magnetic unit cell**, which is the unit of periodicity including the spin configuration. These two kinds of unit cell lengths are indicated in Fig. 5.2(a).

$\chi_{\rm u}$ in eq. (5.31a) does not diverge because $J < 0$. Instead it shows the temperature dependence

$$\chi_{\rm u} \propto \frac{1}{T+\theta}, \tag{5.40}$$

which is different from the Curie law. This θ is called **Weiss temperature**.

The Néel temperatures and the Weiss temperatures of typical anti-ferromagnets are liste in Tab. 5.1. From eqs. (5.31,32), these two kinds of temperatures should be symmetric to 0 K. Of course, a simple model even without anisotropy should give results far different from the reality. However, there is some rough correlation between them.

Material	Lattice-type of magnetic ions	Néel temperature (K)	Weiss temperature (K)
MnO	fcc	116	610
MnS	fcc	160	528
MnTe	hexagonal	307	690
MnF_2	bct	67	82
FeF_2	bct	79	117
$FeCl_2$	hexagonal	24	48
FeO	fcc	198	570
$CoCl_2$	hexagonal	25	38
CoO	fcc	291	330
$NiCl_2$	hexagonal	50	62
NiO	fcc	525	~ 2000
Cr	fcc	308	

Tab. 5.1 Néel temperatures and Weiss temperatures of typical anti-ferromagnets.

5.5.3 Spin flop transition and metamagnetism

Consider a general material with susceptibility χ. With increasing the external magnetic field, the energy gain due to the magnetization is

$$E_{\mathrm{m}} = -\int_0^B \frac{M(B')}{\mu_0}\frac{dB'}{\mu_0} = -\chi\int_0^B \frac{B'}{\mu_0}\frac{dB'}{\mu_0} = -\frac{\chi}{2\mu_0^2}B^2. \tag{5.41}$$

In the region $T < T_{\mathrm{N}}$, $\chi_\perp > \chi_\parallel$ as shown in Fig. 5.1, hence the energy is lower for the magnetic field perpendicular to the sublattice magnetization. As mentioned in the beginning of "parallel susceptibility," with increasing a parallel field, the energy difference overcomes the anisotropic energy K at a certain point, at which the sublattice magnetizations rotate to the direction perpendicular to the magnetic field. This is called **spin flop transition**. The critical field is obtained from

$$\frac{\chi_\perp - \chi_\parallel}{2\mu_0^2}B_{\mathrm{c}}^2 = K, \tag{5.42}$$

as

$$B_{\mathrm{c}} = \mu_0\sqrt{\frac{2K}{\chi_\perp - \chi_\parallel}}. \tag{5.43}$$

After the transition, the field also gives an oblique angle to sublattice magnetizations as shown in Fig. 5.3(a). In the process of increasing field, the total magnetization increases with the field proportionally and saturates at the field of complete polarization.

In conventional anti-ferromagnets, this critical field is too large to reach in many of laboratories. Recently, however, there have been many reports on the spin flop transition in nano-ferromagnets or in molecular ferromagnets. Figure 5.3(b) shows such an example of a crystal composed of a polymer $\{[\mathrm{Mn_2(bpdo)(H_2O)_4}][\mathrm{Nb(CN)_8}]\cdot 6\mathrm{H_2O}\}_n$. It has Néel point at T_{N}=15 K, which is comparatively low. We observe a clear spin flop transition at around 0.6 T at 1.8 K.

So far we have considered the case of nearest-neighbor-only exchange interaction. That is, only inter-sublattice interaction is considered and intra-sublattice interaction is ignored. In reality, the super-exchange interaction often works between spins in a sublattice (intra-sublattice interaction). In some cases, an anti-ferromagnetism at zero field is realized by a small difference in inter-sublattice anti-ferromagnetic interaction and intra-sublattice ferromagnetic interaction. In such a case, increasing the external field lowers the energy of magnetic moments parallel to the field. And at a certain

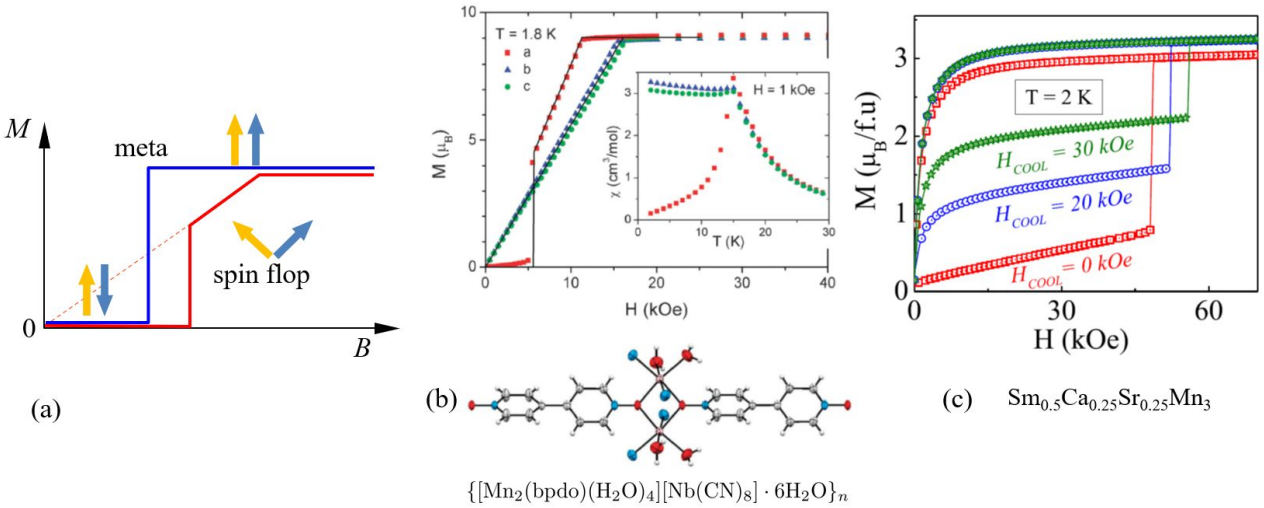

Fig. 5.3 (a) Illustration of spin flop transition (red line) and metamagnetism (blue line). (b) Spin flop transition appeared in a polymer anti-ferromagnet $\{[Mn_2(bpdo)(H_2O)_4][Nb(CN)_8]\cdot 6H_2O\}_n$. The inset shows the susceptibility at a low (0.1 T) field. It is an anti-ferromagnet with T_N=15 K, with the spin-easy axis along a-axis. From [5]. Lower panel shows the molecular structure with axes b (pointing up), c (pointing left), a (coming up from this paper). (c) Examples of metamagnetic transition in a Mott insulator $Sm_{0.5}Ca_{0.25}Sr_{0.25}MnO_3$[6].

field, the whole system goes to a ferromagnetic, which phenomenon appears as a sudden or steep increase in magnetization up to the saturation. This is called **meta-magnetism**[6]. An example is shown in Fig. 5.3(c). Meta-magnetism often has strong temperature dependence. If we fix the magnetic field close to the critical field, the temperature also drives a meta magnetic transition, which gives a very large $(\partial M/\partial T)_B$. From eq. (2.114), this is very advantageous for magnetic refrigeration. And now the application of meta-magnetism to high-efficiency magnetic refrigeration is active([7] is an example from a helimagnetism).

5.6 Ferrimagnetism

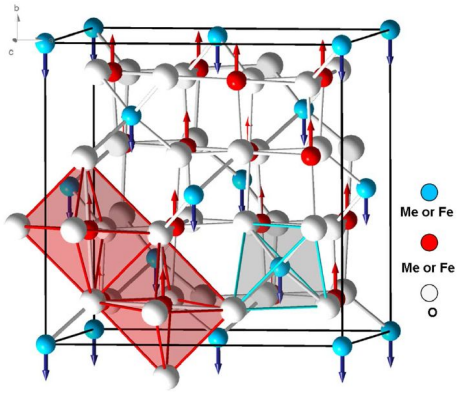

The most typical material of magnetic insulators is ferrite, which I mentioned in the beginning of this chapter.

5.6.1 Magnetism in ferrite

In the ferromagnetism of ferrite (AFe_2O_4, A=Mn, Co, Ni, Cu, Zn, $\cdots$), the spin-alignment is a mixture of anti-ferro and ferro types. Because the sublattices have different magnetic moments, they do not cancel out. As a result a total finite spontaneous magnetization appears. Such magnetism is named **ferrimagnetism** after ferrite.

In the unit cell of spinel-type ferrite, there are 16 Fe^{3+}, 8 M^{2+}, 32 O^{2-}. Spin magnetic moments at Fe ions are mostly cancelled by anti-ferromagnetic interaction, and spins at M^{2+} survive, causing the ferrimagnetism. The expected magnetic moments of ferrite and experimental values along with this statement are listed below showing a good agreement.

Materials	$MnFe_2O_4$	$FeFe_2O_4$	$CoFe_2O_4$	$NiFe_2O_4$	$CuFe_2O_4$
Moment (Theory)	$5\mu_B$	$4\mu_B$	$3\mu_B$	$2\mu_B$	$1\mu_B$
Moment (Exp.)	5.0	4.2	3.3	2.3	1.3
T_N (K)	783	848	793	863	728

A bit detailed discussions on the magnetism of ferrite can be found in ref. [8] (in Japanese), or in refs. [9, 10]. For the application of ferrite magnetism, refer to refs. [11, 12]. Ferrite is extremely important in industrial application. They show various magnetism depending on species of M, crystal types and shapes of samples. Even now, research is extremely active, and many review papers for each individual ferrite can be found even in the last few years.

5.6.2 Molecular field approximation of ferrimagnetism

We here use a Heisenberg model with unbalanced sublattices A and B.

$$B_A = \alpha M_A + (-\gamma)(-M_B) = \alpha M_A + \gamma M_B, \tag{5.44a}$$
$$B_B = \gamma M_A + \beta M_B, \tag{5.44b}$$

where we consider not only inter-sublattice exchange interaction but also intra-sublattice interaction. The imbalance is taken into account by the difference between α, β. The inter-sublattice interaction is γ (must be common).

5.6.3 Magnetization below the Néel temperature

The set of self-consistent equations for magnetizations M_A and M_B in sublattices is from molecular field approximation (5.44) as

$$M_A = \mu S_A \mathcal{B}_{S_A}\left[\frac{\mu S_A}{k_B T}(\alpha M_A + \gamma M_B)\right], \tag{5.45a}$$
$$M_B = \mu S_B \mathcal{B}_{S_B}\left[\frac{\mu S_B}{k_B T}(\gamma M_A + \beta M_B)\right], \tag{5.45b}$$

where the Brillouin function is written as $\mathcal{B}_S(x)$. Though $\mu = g\mu_B$ may be different for sublattices if g-factors are different, we here assume they are common for simplicity.

To obtain M_A, M_B, thus the total magnetization $M = M_A - M_B$, we need to solve eq. (5.45) numerically.

In such compensated ferrimagnetism, magnetizations show complicated temperature dependences below Néel temperature due to the differences between S_A and S_B, α and β. As an example, compensated ferrimagnetism is displayed in

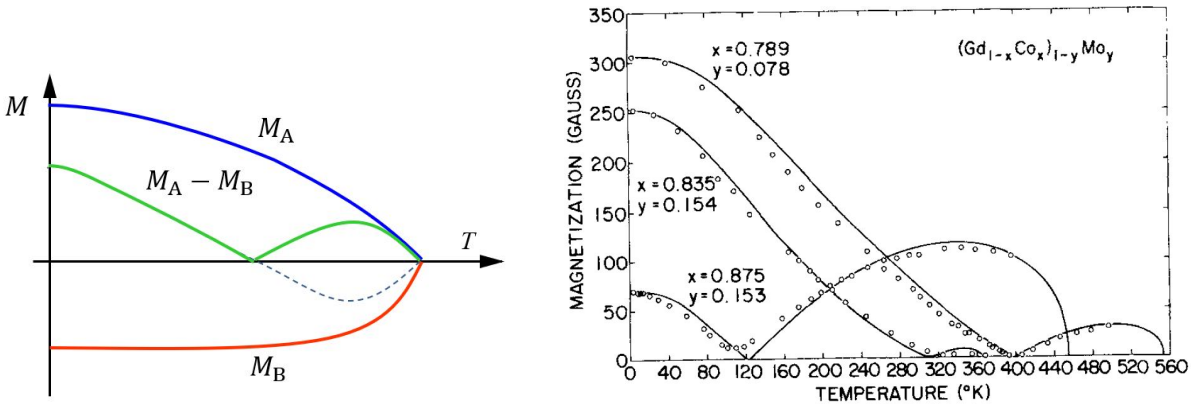

(a) (b)

Fig. 5.4 (a) Conceptual scheme of compensated ferrimagnetism. (b) Compensated ferrimagnetism appeared in the magnetization of amorphous alloy Gd-Co-Mn. From [13].

Fig. 5.4. In conceptual diagram in Fig. 5.4(a), A-sublattice has a larger lowest temperature magnetization ($S_{\mathrm{A}} > S_{\mathrm{B}}$). On the other hand, B-sublattice has a larger intra-sublattice interaction ($\beta < \alpha$), then the growth of magnetization M_{B} below Néel is faster with lowering the temperature. Hence in a certain temperature region lower than T_{N}, $M_{\mathrm{B}} > M_{\mathrm{A}}$ holds and as indicated by the broken line $M_{\mathrm{A}} - M_{\mathrm{B}}$ is negative though in the measurement, magnetization M parallel to the field always has lower energy and the green line is observed. With lowering of temperature, M_{A} increases and the total magnetization disappears at the point of $M_{\mathrm{A}} = M_{\mathrm{B}}$. But with further lowering of temperature, $M_{\mathrm{A}} > M_{\mathrm{B}}$ and the magnetization reappears. As a whole, it becomes a curious temperature dependence as shown by the green line. Figure 5.4(b) shows such a temperature dependence of an amorphous alloy Gd-Co-Mo[13]. In "complete compensation type" ferrimagnetism, there is a difference in intra-interaction but the sublattice magnetic moments are the same and the total magnetization disappears at lowest temperatures[14].

5.7 Helimagnetism

It is not alway possible to separate a spin system with anti-ferromagnetic interaction into a small numbers of magnetic sublattices. Also as considered in the previous section, ranges of interactions may span over more than single (magnetic) lattice constant. Let us consider **helimagnetism**, that appears in such a complex system in a Heisenberg model. It has a spiral-like spin configuration, which shows considerable difference from parallel/anti-parallel (collinear) configurations so far considered. In the treatment of anti-ferromagnetism, firstly the anti-ferromagnetic ground state (Néel ordered state) is given. Then the molecular field is considered based on the state. This time, we have a look on the process to find out the ground state[15].

5.7.1 Classical Heisenberg model

Here the exchange interaction potential J depends on the combination of sites (i, j) and a site-dependent magnetic field $\boldsymbol{B}_i$ is working on each site.

$$\mathscr{H} = -\sum_{\langle i,j \rangle} J_{ij} \boldsymbol{S}_i \cdot \boldsymbol{S}_j - \mu \sum_i \boldsymbol{B}_i \cdot \boldsymbol{S}_i. \tag{5.46}$$

However we put $\boldsymbol{B}_i = \boldsymbol{0}$ for a while. And in the first place, to see that a helical spin configuration can be stable, we consider a classical Heisenberg model, in that the spins are treated as classical vectors.

To look for an ordered stated, we assume an ordered state and perform Fourier expansion as

$$\langle \boldsymbol{S}_i \rangle = \frac{1}{\sqrt{N}} \sum_{\boldsymbol{q}} \langle \boldsymbol{S}_{\boldsymbol{q}} \rangle \exp(i\boldsymbol{q} \cdot \boldsymbol{r}_i). \tag{5.47}$$

Then

$$|\langle \boldsymbol{S}_i \rangle|^2 = S^2 = \frac{1}{N} \sum_{\boldsymbol{q},\boldsymbol{q}'} \langle \boldsymbol{S}_{\boldsymbol{q}} \rangle \cdot \langle \boldsymbol{S}_{\boldsymbol{q}'} \rangle \exp(i(\boldsymbol{q} + \boldsymbol{q}') \cdot \boldsymbol{r}_i) \tag{5.48}$$

Now the expectation value of Hamiltonian can be written as

$$\langle \mathscr{H} \rangle = -\sum_{\langle i,j \rangle} J_{ij} \langle \boldsymbol{S}_i \rangle \cdot \langle \boldsymbol{S}_j \rangle = -\sum_{\boldsymbol{q}} J_{\boldsymbol{q}} \langle \boldsymbol{S}_{\boldsymbol{q}} \rangle \cdot \langle \boldsymbol{S}_{-\boldsymbol{q}} \rangle, \tag{5.49}$$

where

$$J_{\boldsymbol{q}} = \sum_j J_{ij} \exp[-i\boldsymbol{q} \cdot (\boldsymbol{r}_i - \boldsymbol{r}_j)] \tag{5.50}$$

is the Fourier transform of the interaction potential. Taking the sum of both sides of eq. (5.48)on subscript i, the right hand side is

$$\frac{1}{N} \sum_i \sum_{\boldsymbol{q},\boldsymbol{q}'} \langle \boldsymbol{S}_{\boldsymbol{q}} \rangle \cdot \langle \boldsymbol{S}_{\boldsymbol{q}'} \rangle \exp(i(\boldsymbol{q} + \boldsymbol{q}') \cdot \boldsymbol{r}_i) = \sum_{\boldsymbol{q},\boldsymbol{q}'} \langle \boldsymbol{S}_{\boldsymbol{q}} \rangle \cdot \langle \boldsymbol{S}_{\boldsymbol{q}'} \rangle \delta_{\boldsymbol{q},-\boldsymbol{q}'}.$$

Then

$$NS^2 = \sum_{\boldsymbol{q}} \langle \boldsymbol{S}_{\boldsymbol{q}} \rangle \cdot \langle \boldsymbol{S}_{-\boldsymbol{q}} \rangle \,. \tag{5.51}$$

This works as a condition fulfilled by the classical solution.

In the Heisenberg model, $J_{ij} = J_{ji}$ and also is real, $J_{\boldsymbol{q}}$ should be an even function of $\boldsymbol{q}$. We then assume that $J_{\boldsymbol{q}}$ takes the maximum (i.e., has a repeating structure with a finite period), and let $\pm\boldsymbol{Q}$ be the wavenubers that give the maxima to $J_{\boldsymbol{q}}$. When $\boldsymbol{Q} = \boldsymbol{K} - \boldsymbol{Q}$ with an inverse lattice vector $\boldsymbol{K}$, the system is in classical anti-ferromagnetic state, and out of our scope here. Then though it is a bit bold, under the condition (5.51), we assume

$$\langle \boldsymbol{S}_{\boldsymbol{Q}} \rangle \neq 0, \quad \langle \boldsymbol{S}_{-\boldsymbol{Q}} \rangle \neq 0, \quad (\text{others}) = 0. \tag{5.52}$$

Then eq. (5.48) can be written as follows:

$$NS^2 = \langle \boldsymbol{S}_{\boldsymbol{Q}} \rangle \cdot \langle \boldsymbol{S}_{\boldsymbol{Q}} \rangle \exp(2i\boldsymbol{Q} \cdot \boldsymbol{r}_i) + \langle \boldsymbol{S}_{-\boldsymbol{Q}} \rangle \cdot \langle \boldsymbol{S}_{-\boldsymbol{Q}} \rangle \exp(-2i\boldsymbol{Q} \cdot \boldsymbol{r}_i) + 2 \langle \boldsymbol{S}_{\boldsymbol{Q}} \rangle \cdot \langle \boldsymbol{S}_{-\boldsymbol{Q}} \rangle \,. \tag{5.53}$$

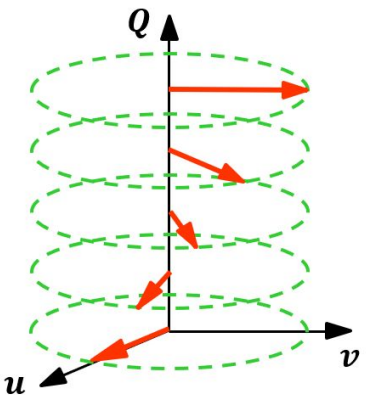

Because the sum in the rhs of eq. (5.51) should be taken for $\boldsymbol{q} = \pm\boldsymbol{Q}$, in the present case $2 \langle \boldsymbol{S}_{\boldsymbol{Q}} \rangle \cdot \langle \boldsymbol{S}_{-\boldsymbol{Q}} \rangle$, that just corresponds to the third term in eq. (5.53). From the above we get

$$\langle \boldsymbol{S}_{\boldsymbol{Q}} \rangle \cdot \langle \boldsymbol{S}_{\boldsymbol{Q}} \rangle = \langle \boldsymbol{S}_{-\boldsymbol{Q}} \rangle \cdot \langle \boldsymbol{S}_{-\boldsymbol{Q}} \rangle = 0. \tag{5.54}$$

This condition is, for example, for $\langle \boldsymbol{S}_{\boldsymbol{Q}} \rangle$,

$$\mathrm{Re}[\langle \boldsymbol{S}_{\boldsymbol{Q}} \rangle] = \boldsymbol{a}, \ \mathrm{Im}[\langle \boldsymbol{S}_{\boldsymbol{Q}} \rangle] = \boldsymbol{b} \longmapsto |\boldsymbol{a}|^2 - |\boldsymbol{b}|^2 = 0, \ \boldsymbol{a} \cdot \boldsymbol{b} = 0, \tag{5.55}$$

that is, the amplitude of the real and the imaginary parts are the same and they should be orthogonal. Then, we can write

$$\langle \boldsymbol{S}_{\boldsymbol{Q}} \rangle = \frac{\sqrt{N}}{2} S(\boldsymbol{u} - i\boldsymbol{v}), \tag{5.56}$$

where $\boldsymbol{u}$ and $\boldsymbol{v}$ are orthogonal unit vectors. This leads to the expectation value of spins in the ground state:

$$\langle \boldsymbol{S}_i \rangle = S[\boldsymbol{u} \cos(\boldsymbol{Q} \cdot \boldsymbol{r}_i) + \boldsymbol{v} \sin(\boldsymbol{Q} \cdot \boldsymbol{r}_i)]. \tag{5.57}$$

In this spin configuration, the spin rotates along and around $\boldsymbol{Q}$-axis in the plane stretched by $(\boldsymbol{u} and \boldsymbol{v})$. The configuration is called **helical spin structure**. Though the structure is affected by crystal anisotropy in real materials, the theoretical Heisenberg model is isotropic and the plane of $(\boldsymbol{u}, \boldsymbol{v})$ can be taken to any direction.

5.7.2 Molecular field approximation

Based on the classical ground state, we apply the molecular field approximation, by introducing the site-dependent magnetic field

$$\boldsymbol{B}_i = B_q[\boldsymbol{u} \cos(\boldsymbol{q} \cdot \boldsymbol{r}_i) + \boldsymbol{v} \sin(\boldsymbol{q} \cdot \boldsymbol{r}_i)] \tag{5.58}$$

into eq. (5.46). We write the averaged spin as

$$\langle \boldsymbol{S}_i \rangle = m_q[\boldsymbol{u} \cos(\boldsymbol{q} \cdot \boldsymbol{r}_i) + \boldsymbol{v} \sin(\boldsymbol{q} \cdot \boldsymbol{r}_i)]. \tag{5.59}$$

Then along with molecular field procedure, the effective Hamiltonian at site i is given by

$$\mathscr{H}_{\text{eff}}(i) = -(2m_q J_q + \mu B_q)[\boldsymbol{u} \cos(\boldsymbol{q} \cdot \boldsymbol{r}_i) + \boldsymbol{v} \sin(\boldsymbol{q} \cdot \boldsymbol{r}_i)] \cdot \boldsymbol{S}_i. \tag{5.60}$$

Then as is the course, a self-consistent equation is given by

$$m_q = S\mathcal{B}_S \left[\frac{S}{k_{\mathrm{B}}T} (2m_q J_q + \mu B_q) \right]. \tag{5.61}$$

This has a just same form as that in the ferromagnetism. If we define "helical magnetization" as μm_q, we obtain the helical magnetization in paramagnetic states as

$$\chi_q = \lim_{B_q \to 0} \frac{\mu m_q}{B_q} = \chi_0 \left(1 - \frac{2J_q}{\mu^2}\chi_0\right)^{-1}. \tag{5.62}$$

The critical temperature for the appearance of helical order $T_{\boldsymbol{Q}}$ is given by

$$k_{\mathrm{B}} T_{\boldsymbol{Q}} = \frac{2}{3} S(S+1) J_{\boldsymbol{Q}}. \tag{5.63}$$

5.7.3 Observation of helimagnetism, skyrmion excitations

In the above, a helimagnetism in a Heisenberg model is considered. In real materials, it is said that $NiBr_2$ or β-MnO_2 may have situations close to the model. There have been found many materials with helimagnetisms. Holmium (Ho) has a helimagnetism originated from the RKKY interaction. The Dyaloshinsky-Moriya (DM) interaction often causes helimagnetism.

Here I would like to introduce an experimental method called "Lorentz microscope" for observing real space image of magnetic structure, and observation of helimagnetism and related magnetic phenomena. One of the most powerful methods to observe spin configurations is the neutron diffraction. Actually one of the motivations for finding helimagnetism was an anomalous neutron spectrum of β-MnO_2, etc. Despite the powerfulness of neutron diffraction in detecting periodic structures, it has difficulties in catching local real space images. Lorentz transmission microscope is one of the methods to observe local images [*2].

Figure 5.5 shows the principle of Lorentz microscope, which utilizes the bending of electron beams by Lorentz force from the magnetic field in samples. Complete re-focusing of electrons, however, restore the bending resulting in no-

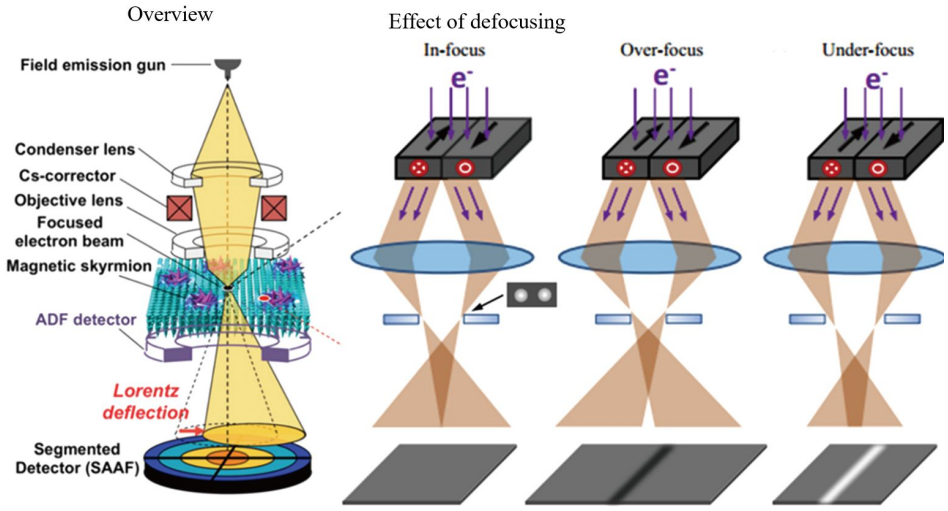

Fig. 5.5 Left panel: Illustration of electron beam lines in a Lorentz microscope. Focused electron beams go though a sample, and re-focused by electron lenses for forming an image on a screen. Three right panels: When the sample has inner magnetic field, the Lorentz force gives curving on the electron beams. Left in right: When the screen is just at the focal level, the bending are restored to have no contrast. Center in right: When the screen is a bit far, the over focusing results in a contrast. Right in right: When the screen is closer, the under focusing also results in a contrast. From Li-cong et al. Ch. Phys. B **27**, 066802 ('18).

[*2] There are many others like traditional observation of distribution of magnetic powders, micro MOKE with utilizing the Kerr rotation, magnetic force microscope, which detects magnetic field gradient, scanning SQUID, etc.

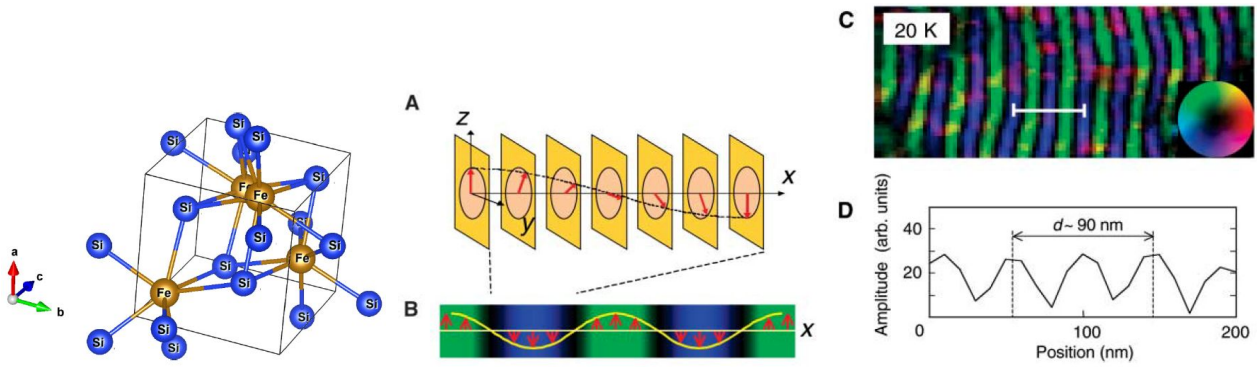

Fig. 5.6 Left: Cubic ϵ-FeSi (B20-type) structure without centrosymmetric point. A: Illustration of helimagnetism. B: Expected contrast in Lorentz micrograph for an observation in the angle of z-axis. C: False colored real space imaging of helimagnetism in $Fe_{1-x}Co_xSi$ at 20 K by a Lorentz microscope. D: Magnetic moment along z-axis deduced from the above[16].

contrast. Hence as illustrated in the right two panels in Fig. 5.5, the beams are a bit defocused to have a contrast, of which the intensity is reversed by the direction of defocusing.

Figure 5.6 shows an example of observing helimagnetism. The sample is $Fe_{1-x}Co_xSi$ in a non-centrosymmetric cubic ϵ-FeSi (B20) structure. Because of the lack of inversion symmetry, a term in similar form as an electric field appears in electric effective Hamiltonian and causes strong spin-orbit interaction. This leads to a strong DM interaction that creates the helimagnetism.

When one observes a helimagnetic spin ordered state in a side-view, as in Fig. 5.6A, B, the magnetization is modulated

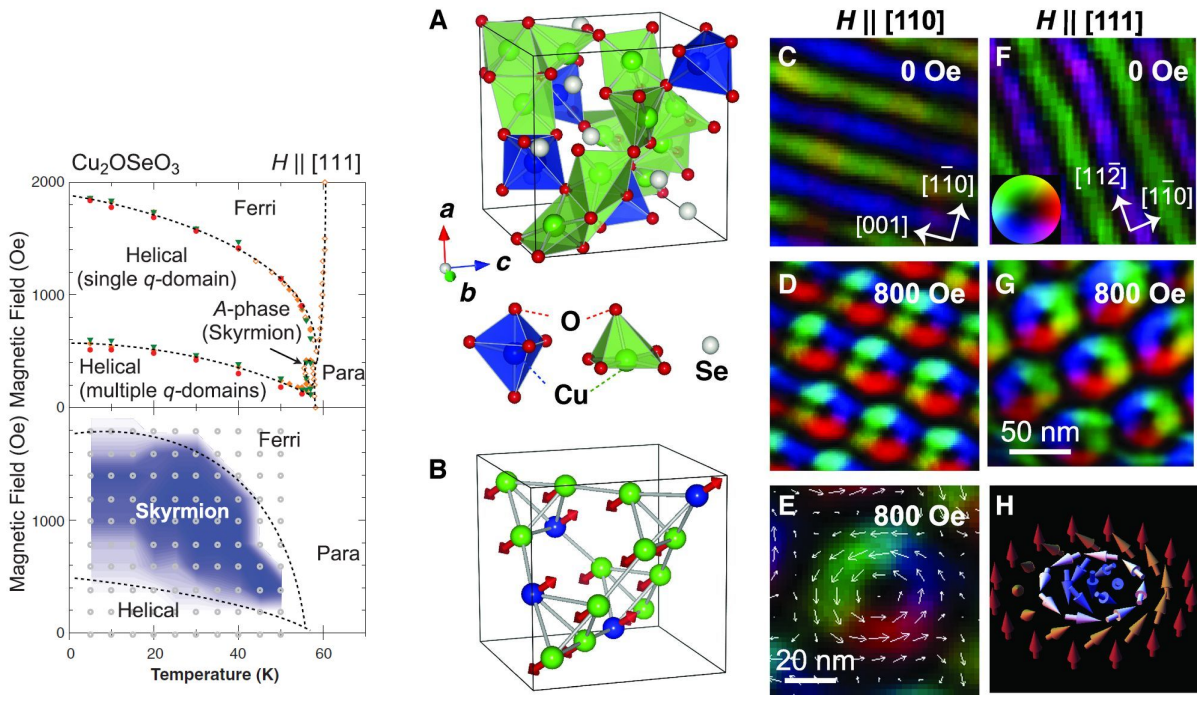

Fig. 5.7 Left: Experimentally obtained phase diagram of Cu_2OSeO_3. At low temperatures, low magnetic fields, it shows a helimagnetism, which is overtaken by a phase with skyrmion excitations with increasing the magnetic field. With further increase of the field, it changes to a ferrimagnetism. Right: A: Unit cell structure of Cu_2OSeO_3. B: Cu spin configuration in the ferrimagnetic phase. C $\sim$ G: Lorentz microscope images. At low magnetic field, a stripe due to helimagnetism, and at middle fields images of skyrmion are observed. H: shows schematic view of a skyrmion spin configuration. From ref. [17].

wavy in space. This corresponds to a Fresnel configuration of Lorentz microscope and actually in the image, a striping contrast is observed as in Fig. 5.6C.

Figure 5.7 shows skyrmion excitations observed with a Lorentz microscope. This is observed in Cu_2OSeO_3, which does not have inversion symmetry in lattice as shown in Fig. 5.7A, and the DM interaction causes a helimagnetism as in the phase diagram at low temperatures and at low magnetic fields. The helimagnetic phase is detected as stripe images by a Lorentz microscope as in C, F. With increasing the magnetic field, a phase with skyrmion excitation appears as in D, G, E. They are observed to be aligned periodically. Further increase in the field drives the system into a ferrimagnetic phase, of which spin configuration is shown in B.

5.8 Spin wave

The phase transitions with appearance of spontaneous magnetizations like ferromagnetic transition are an example of spontaneous symmetry breakings. They are also associated with the appearance of excited states called spin wave. Let us have a look on them.

5.8.1 Ferromagnetic spin wave

Here we need to consider dynamical properties of spins in ordered states. For that in ferromagnetic Heisenberg model (5.1), we consider the time evolution of operator $\boldsymbol{S}i$ by applying the Heisenberg equation of motion as

$$\hbar\frac{d\boldsymbol{S}_i}{dt} = \frac{1}{i}[\boldsymbol{S}_i, \mathscr{H}] = -2J\sum_{\delta}\boldsymbol{S}_{i+\delta}\times\boldsymbol{S}_i - \mu\boldsymbol{B}\times\boldsymbol{S}_i, \tag{5.64}$$

where δ is taken for the nearest neighbor of i. This calculation can be followed, with the use of commutation relation $[S^\alpha, S^\beta] = iS^\gamma$, $(\alpha,\beta,\gamma) = (x,y,z;$ cyclic), e.g., as

$$[S_i^x, S_i^xS_j^x + S_i^yS_j^y + S_i^zS_j^z] = [S_i^x, S_i^yS_j^y] + [S_i^x, S_i^zS_j^z] = i(S_i^zS_j^y - S_i^yS_j^z) = i(\boldsymbol{S}_j\times\boldsymbol{S}_i)_x.$$

Equation (5.64) is in the form of equation of motion for precession around the effective field (the external field plus the nearest neighbor interaction). Then we can foresee that the precessions are chained through the exchange interaction and forms a wave propagates over the spins. To see that we need to consider higher order approximation than the "averaged" field.

Then we consider the Fourier transform

$$\boldsymbol{S}_{\boldsymbol{q}} = \frac{1}{\sqrt{N}}\sum_i \boldsymbol{S}_i\exp(-i\boldsymbol{q}\cdot\boldsymbol{r}_i), \quad J_{\boldsymbol{q}} = \sum_{\delta} J\exp[-i\boldsymbol{q}\cdot(\boldsymbol{r}_i - \boldsymbol{r}_{i+\delta})], \tag{5.65}$$

and with substituting the inverse Fourier transformation into eq. (5.64), we represent (5.64) in the Fourier transformation as

$$\hbar\frac{d\boldsymbol{S}_{\boldsymbol{q}}}{dt} = -\frac{2}{\sqrt{N}}\sum_{\boldsymbol{q}'} J_{\boldsymbol{q}'}\boldsymbol{S}_{\boldsymbol{q}'}\times\boldsymbol{S}_{\boldsymbol{q}-\boldsymbol{q}'} - \mu\boldsymbol{B}\times\boldsymbol{S}_{\boldsymbol{q}}. \tag{5.66}$$

With the above, we extract a wave from the precessions of spins. By taking z-axis along magnetic field $\boldsymbol{B}$, $\langle\boldsymbol{S}_{\boldsymbol{0}}\rangle = \sqrt{N}S\boldsymbol{e}_z$ has by far the largest expectation value in a ferromagnetic state. Hence in the first term of rhs of (5.66), we ignore the terms other than $\langle\boldsymbol{S}_{\boldsymbol{0}}\rangle$ to obtain

$$\hbar\frac{d\boldsymbol{S}_{\boldsymbol{q}}}{dt} = -[2(J_{\boldsymbol{0}} - J_{\boldsymbol{q}})S + \mu B]\boldsymbol{e}_z\times\boldsymbol{S}_{\boldsymbol{q}}. \tag{5.67}$$

In each component

$$\left\{\begin{array}{l} \hbar\dfrac{dS_{\boldsymbol{q}x}}{dt} = \quad [2(J_{\boldsymbol{0}} - J_{\boldsymbol{q}})S + \mu B]S_{\boldsymbol{q}y}, \\ \hbar\dfrac{dS_{\boldsymbol{q}y}}{dt} = -[2(J_{\boldsymbol{0}} - J_{\boldsymbol{q}})S + \mu B]S_{\boldsymbol{q}x}, \\ \hbar\dfrac{dS_{\boldsymbol{q}z}}{dt} = 0. \end{array}\right. \tag{5.68}$$

For $S_{\boldsymbol{q}x}$ and $S_{\boldsymbol{q}y}$ these are harmonic oscillator equations. By comparison of this with

$$S_{\boldsymbol{q}x} + iS_{\boldsymbol{q}y} \propto \exp[-i\epsilon_{\boldsymbol{q}}t/\hbar], \tag{5.69}$$

we obtain the energy $\epsilon_{\boldsymbol{q}}$ of precession in $\boldsymbol{q}$ space as

$$\epsilon_{\boldsymbol{q}} = 2(J_{\boldsymbol{0}} - J_{\boldsymbol{q}})S + \mu B. \tag{5.70}$$

Because the precession is in $\boldsymbol{q}$-space, this represents a propagating wave in real space.

5.8.2 Holstein-Primakoff transformation

As is the case of Larmor precession, the equation of motion derived quantum mechanically has the same form as classical one. Then next we consider quantization of this wave. For a spin operator $\boldsymbol{S}$, we write an eigenfunction $|m\rangle$ of S_z with eigenvalue m ($m = -S, -S+1, \cdots, S-1, S$). The operation of up-down operators $S_\pm = S_x \pm S_y$ gives

$$\left.\begin{array}{l} S_+ |m\rangle = \sqrt{S(S+1) - m(m+1)}\, |m+1\rangle\,, \\ S_- |m\rangle = \sqrt{S(S+1) - m(m-1)}\, |m-1\rangle\,. \end{array}\right\} \tag{5.71}$$

Let us express a spin operator with creation and annihilation operators $a^\dagger$, a of bosons. For that we take the state $S_z = S$, i.e., $|S\rangle$ as the vacuum of boson, and $|S-n\rangle$ as n boson state. Namely,

$$a\,|S\rangle = 0, \quad |S-n\rangle = \frac{1}{\sqrt{n!}}(a^\dagger)^n\,|S\rangle\,. \tag{5.72}$$

Then with $\hat{n} = a^\dagger a$, we can formally write

$$\left.\begin{array}{l} S_z = S - \hat{n}, \\ S_+ = \sqrt{2S - \hat{n}}\; a, \\ S_- = a^\dagger\sqrt{2S - \hat{n}}. \end{array}\right\} \tag{5.73}$$

The above is called **Holstein-Primakoff transformation**.

Appendix 9A: Various “magnetism”

There are many ways to classify magnetisms and the classification itself is not very important. For example, as a macroscopic phenomena, there is “ferromagnetism”. However this contains a wide variety of magnetisms including “all-aligned” simple magnetism, ferrimagnetism, canted anti-ferromagnetism, etc. If we count for metastable configuration, the number of classes is huge, and the classification brings little knowledge. Here I would like to introduce some magnetisms to have smooth talks with experts on magnetism.

9A.1 Paramagnetism

So far we have seen the paramagnetism by local moments and that by itinerant electrons (Pauli paramagnetism). The Pauli paramagnetism usually have smaller contribution to the susceptibility and for the detection, a combination with other methods is usually required.

There are the cases that a finite number of spins form an ordered state, which does not spread over the system. Such a system generally shows paramagnetism with a huge magnetic moment, which is called **superparamagnetism**. The behavior of susceptibility resembles those of anti-ferromagnetism or spin-glass. Distinction of these is sometimes difficult.

9A.2 Diamagnetism

As we saw in the Landau diamagnetism in metals, usually diamagnetism originates from orbital motion of electrons. It sometimes becomes very large reflecting peculiar band structures as we saw in the section of graphite. Since water also has a large diamagnetism, various things including water cause magnetic levitation in a very large magnetic field. As a bit special example, the superconductors have perfect diamagnetism (the Meissner effect).

9A.3 Ferromagnetism

As mentioned at the beginning of this section, there can be various definitions of ”ferromagnetism.” It often refers to the case where itinerant electrons exist like metal and their spins become imbalanced to generate spontaneous magnetization. Also ferrimagnetism is often called ”ferromagnetism.”

9A.4 Anti-ferromagnetism

すでに見たように，磁気副格子内でスピンの向きが揃っているが，副格子のモーメントが互いに反転しているために全体としては自発磁化を持たないように見える (帯磁率が発散しない) ものを反強磁性と呼ぶ.

9A.5 Ferrimagnetism

As in anti-ferromagnets, neighboring moments have antiparallel alignment. However because there are unbalances in the size of moments or the numbers of magnetic sublattices, total spontaneous magnetization appears in ferrimagnetism. Oxide ferromagnets like ferrites, garnets are this type.

9A.6 Canted anti-ferromagnetism

This type also has anti-ferromagnetic interactions though the moments in magnetic sublattices are not completely inverted, but canted. Some of ferrite. Total spontaneous magnetization is generally small (weak ferromagnetism).

9A.7 Helimagnetism

The magnetic moments are arranged helically in space, and total spontaneous magnetization vanishes. On the other hand, ”chirality” occurs depending on the winding direction of the spiral, which causes various phenomena. In some cases, a topological excitation called “skyrmion” appears, and they form a lattice. This kinds of materials have been attracting attentions in these decades.

9A.8 Spin density wave

The state in which the spin density and direction are spatially distributed in a wavy manner is called the spin density wave (SDW). There are also anti-ferromagnetic SDW without total magnetization, and ferrimagnetic SDW with a total magnetization.

9A.9 Spin glass

When the localized magnetic moments exist randomly in space and the interaction between the moments is also random, the angles of the moments are randomly frozen, as in a glass state (amorphous state) in which atoms are randomly aggregated. This is called spin glass. It is found in dilute magnetic alloys containing magnetic atoms as impurities. In ferromagnetism and anti-ferromagnetism, there are only a few stable states of free energy, but in spin glass, there are a large number of metastable points. The Nishimori quantum annealing theory is built on the mathematical similarity between the relaxation from such metastable points to the true ground state by quantum tunneling (annealing) and a kind of optimization problem. This is the basics of modern quantum annealing computation[18]. The behavior of the magnetism is similar to that of anti-ferromagnetic materials. When cooling in a magnetic field, the temperature dependence becomes weaker on the lower temperature side than the spin glass transition point, and in zero magnetic field cooling, the magnetism disappears near zero degrees. As the temperature rises, the magnetization also rises and joins the cooling value in the magnetic field at the transition point.

References

[1] D. C. Johnston. Magnetic susceptibility of collinear and noncollinear heisenberg antiferromagnets. *Phys. Rev. Lett.*, Vol. 109, p. 077201, Aug 2012.

[2] W. L. Roth. Magnetic structures of mno, feo, coo, and nio. *Phys. Rev.*, Vol. 110, pp. 1333–1341, Jun 1958.

[3] Sergio M. Rezende, Antonio Azevedo, and Roberto L. Rodríguez-Suárez. Introduction to antiferromagnetic magnons. *Journal of Applied Physics*, Vol. 126, No. 15, p. 151101, October 2019.

[4] Z. Yamani, Z. Tun, and D. H. Ryan. Neutron scattering study of the classical antiferromagnet MnF_2: a perfect hands-on neutron scattering teaching courseSpecial issue on neutron scattering in canada. *Canadian Journal of Physics*, Vol. 88, No. 10, pp. 771–797, October 2010.

[5] Dawid Pinkowicz, Michał Rams, Wojciech Nitek, Bernard Czarnecki, and Barbara Sieklucka. Evidence for magnetic anisotropy of [NbIV(CN)8]4- in a pillared-layered mn2nb framework showing spin-flop transition. *Chemical Communications*, Vol. 48, No. 67, p. 8323, 2012.

[6] Sanjib Banik, Kalipada Das, Tapas Paramanik, Niranjan Prasad Lalla, Biswarup Satpati, Kalpataru Pradhan, and Indranil Das. Huge magnetoresistance and ultrasharp metamagnetic transition in polycrystalline $sm_{0.5}ca_{0.25}sr_{0.25}mno_3$. *NPG Asia Materials*, Vol. 10, No. 9, pp. 923–930, September 2018.

[7] Noriki Terada and Hiroaki Mamiya. High-efficiency magnetic refrigeration using holmium. *Nature Communications*, Vol. 12, No. 1, February 2021.

[8] 近角聡信. 強磁性体の物理 (上): 物質の磁性 (物理学選書 4). 裳華房, 単行本, 10 1978.

[9] A Broese van Groenou, P.F Bongers, and A.L Stuyts. Magnetism, microstructure and crystal chemistry of spinel ferrites. *Materials Science and Engineering*, Vol. 3, No. 6, pp. 317–392, February 1969.

[10] Chemistry310 at Penn State University. Chemistry libretexts; 8.7: Spinel, perovskite, and rutile structures, 2021. https://chem.libretexts.org/Bookshelves/Inorganic_Chemistry/Book%3A_

Introduction_to_Inorganic_Chemistry_%28Wikibook%29/08%3A_Ionic_and_Covalent_Solids_-_Structures/8.07%3A_Spinel_Perovskite_and_Rutile_Structures also https://en.wikibooks.org/wiki/Introduction_to_Inorganic_Chemistry/Ionic_and_Covalent_Solids_-_Structures#_8.6_Spinel,_perovskite,_and_rutile_structures.

[11] 電気学会マグネティックス技術委員会（編）. 磁気工学の基礎と応用. コロナ社, 10 2013.

[12] Alex Goldman. *Modern Ferrite Technology*. Van Nostrand Reinhold, 12 1990.

[13] R. Hasegawa, B. E. Argyle, and L-J. Tao. Temperature dependence of magnetization in amorphous gd-co-mo films. In *AIP Conference Proceedings*, Vol. 24, p. 110. AIP, 1975.

[14] Rolf Stinshoff, Ajaya K. Nayak, Gerhard H. Fecher, Benjamin Balke, Siham Ouardi, Yurii Skourski, Tetsuya Nakamura, and Claudia Felser. Completely compensated ferrimagnetism and sublattice spin crossing in the half-metallic heusler compound $\mathrm{mn}_{1.5}\,\mathrm{fev}_{0.5}\,\mathrm{Al}$. *Phys. Rev. B*, Vol. 95, p. 060410, Feb 2017.

[15] Akio Yoshimori. A new type of antiferromagnetic structure in the rutile type crystal. *Journal of the Physical Society of Japan*, Vol. 14, No. 6, pp. 807–821, June 1959.

[16] Masaya Uchida, Yoshinori Onose, Yoshio Matsui, and Yoshinori Tokura. Real-space observation of helical spin order. *Science*, Vol. 311, No. 5759, pp. 359–361, January 2006.

[17] S. Seki, X. Z. Yu, S. Ishiwata, and Y. Tokura. Observation of skyrmions in a multiferroic material. *Science*, Vol. 336, No. 6078, pp. 198–201, April 2012.

[18] 西森秀稔, 大関真之. 量子アニーリングの基礎 (基本法則から読み解く物理学最前線 18). 共立出版, 5 2018.

Lecture note Magnetism (10)

15th June (2022) Shingo Katsumoto, Institute for Solid State Physics, University of Tokyo

Last week, we have seen the Holstein-Primakoff transformation. However, we have skipped some elementary explanation on the classical view of the spin wave, and here I added some explanations in Appendix 10A.

Why we need to introduce the method of Holstein-Primakoff transformation? Because the variable in the Hamiltonian is now spin, which differs from the canonical variables in classical mechanics such as a spatial coordinate of an electron, and the ordinary general method of quantum field theory cannot be applied. Various problems in the Holtein-Primakoff way were pointed out, e.g., in [1]. A particularly problematic is the "extension" of functional space for n over $2S$ in the form of eq. (5.72). It is proven that the operators of physical quantities have no matrix element between the original functional space and the extended space[2]. However we need to be careful that the proof is for exact theories and some approximations may create some elements. We can escape the problem in treating small n cases.

In the quantization of the Heisenberg model by the Holstein-Primakoff method, the quantized bosons have mutual interaction due to the non-linear term in eq. (5.73). In order to ignore the interaction and to treat it as the sum of harmonic oscillators, we apply the following approximation. The expansions of eq. (5.73) with $\hat{n}$:

$$\left.\begin{aligned}\hat{S}_{j+} &= \sqrt{2S}\left(1-\frac{a_j^\dagger a_j}{4S}+\cdots\right)a_j,\\ \hat{S}_{j-} &= \sqrt{2S}a_j^\dagger\left(1-\frac{a_j^\dagger a_j}{4S}+\cdots\right),\end{aligned}\right\} \tag{5.74}$$

are substituted to the Heisenberg model, to get

$$\begin{aligned}\mathscr{H} &= -2\sum_{\langle i,j\rangle} J_{ij}\hat{\boldsymbol{S}}_i\cdot\hat{\boldsymbol{S}}_j = -2\sum_{\langle i,j\rangle} J_{ij}\{\hat{S}_{iz}\hat{S}_{jz}+(\hat{S}_{i+}\hat{S}_{j-}+\hat{S}_{i-}\hat{S}_{j+})/2\}\\ &= -2\sum_{\langle i,j\rangle} J_{ij}\left[S^2-S(\hat{n}_i+\hat{n}_j)+S(a_i^\dagger a_j+a_j^\dagger a_i)+\hat{n}_i\hat{n}_j-\frac{1}{4}a_i^\dagger a_j^\dagger a_j a_j-\frac{1}{4}a_j^\dagger a_j^\dagger a_j a_i+\cdots\right],\end{aligned} \tag{5.75}$$

where $\hat{n}_i = a_i^\dagger a_i$. We take the terms to quadratic of a_i, $a_i^\dagger$ to reach

$$\mathscr{H} = -2\sum_{\langle i,j\rangle} J_{ij}[S^2-S(\hat{n}_i+\hat{n}_j)+S(a_i^\dagger a_j+a_j^\dagger a_i)]. \tag{5.76}$$

The result is the same if we take the terms with S in them.

We define the Fourier transform of $a_j^\dagger$, a_j as

$$\left.\begin{aligned}a_{\boldsymbol{q}} &= \frac{1}{\sqrt{N}}\sum_j a_j\exp(i\boldsymbol{q}\cdot\boldsymbol{r}),\\ a_{\boldsymbol{q}}^\dagger &= \frac{1}{\sqrt{N}}\sum_j a_j\exp(-i\boldsymbol{q}\cdot\boldsymbol{r}).\end{aligned}\right\} \tag{5.77}$$

With substituting the above, the Hamiltonian is finally given by

$$\begin{aligned}\mathscr{H} &= -2\sum_{\langle i,j\rangle} J_{ij}S^2+2\sum_{\boldsymbol{q}}[J_{\boldsymbol{0}}-J_{\boldsymbol{q}}]Sa_{\boldsymbol{q}}^\dagger a_{\boldsymbol{q}}\\ &= E_0+\sum_{\boldsymbol{q}}\hbar\omega_{\boldsymbol{q}}a_{\boldsymbol{q}}^\dagger a_{\boldsymbol{q}},\end{aligned} \tag{5.78}$$

which is in the form of a set of spin waves without mutual interaction. In this way, we can take into account the interaction systematically with taking the higher order terms one by one. Such quantized spin waves as bosons are called **magnons**.

5.8.3 Magnon approximation of low energy excitations

As we saw in the derivation of eq. (5.76), the approximation of harmonic oscillators corresponds to the ignorance of the interaction between magnons. The approximation is not good for many-magnon excitation at high temperatures. We thus consider the contributions of magnons to physical quantities at low temperatures. With taking the magnetic field along z-axis, the magnetization is

$$M = \mu \left\langle \sum_i S_{iz} \right\rangle = \mu SN - \mu \sum_i \langle a_i^\dagger a_i \rangle = \mu SN - \mu \sum_{\boldsymbol{q}} n(\epsilon_{\boldsymbol{q}}), \tag{5.79}$$

where

$$n(\epsilon) = \left(\exp \frac{\epsilon}{k_{\rm B}T} - 1 \right)^{-1} \tag{5.80}$$

is the Bose distribution function. From eq. (5.78), $\hbar\epsilon_{\boldsymbol{q}} = 2S(J_{\boldsymbol{0}} - J_{\boldsymbol{q}}$. We assume the exchange interaction J works only between nearest neighbors. We here consider a square lattice. Let a be the distance of nearest neighbors and q vector be along a lattice direction. Then

$$\hbar\epsilon_{\boldsymbol{q}} = 2S(J_{\boldsymbol{0}} - J_{\boldsymbol{q}}) = 2SJ\{2 - [\exp(iqa) + \exp(-iqa)]\} \simeq 2SJ \left[2 - 2 \left(1 - \frac{(qa)^2}{2} \right) \right] = 2SJ(qa)^2. \tag{5.81}$$

From the above, with use of the low temperature asymptotic form of the Bose distribution function, M is given by

$$M = \mu N \left[S - \zeta \left(\frac{3}{2} \right) \left(\frac{k_{\rm B}T}{8\pi JS} \right)^{3/2} \right], \tag{5.82}$$

where $\zeta(x)$ is the Riemann's ζ-function and $\zeta(3/2) \approx 2.61$.

Next, we consider the specific heat at low temperatures. The internal energy is obtained from the low temperature asymptotic form of the Bose function and the dispersion relation as

$$U = E_0 + \sum_{\boldsymbol{q}} n(\epsilon_{\boldsymbol{q}}) = E_0 + 12\pi JSN\zeta \left(\frac{5}{2} \right) \left(\frac{k_{\rm B}T}{8\pi JS} \right)^{5/2}, \tag{5.83}$$

from which the specific heat is obtained as

$$C = \frac{\partial U}{\partial T} = \frac{15}{4} N k_{\rm B} \zeta \left(\frac{5}{2} \right) \left(\frac{k_{\rm B}T}{8\pi JS} \right)^{3/2}. \tag{5.84}$$

5.8.4 Anti-ferromagnetic spin wave

Next we proceed to the anti-ferromagnet. As in Sec. 5.5, we consider A and B sublattices with antiparallel magnetizations. We assume ferromagnetic Holstein-Primakoff transform can be applied to A-sublattice. Then a magnon propagation in A-sublattice affects spins in B-sublattice and causes propagation of precession around z-axis. However in B-sublattice the direction of the effective field is inverse and the direction of precession should be inverse. Consequently, the system can be described as coexistence of two-types of magnons with a mutual interaction. Then we need to consider another kind of bosons in B-sublattice. The vacuum should be the inverse of that in A-sublattice and $|0\rangle_{\rm B} = |-S\rangle$ Then for site j in B-sublattice j ($j \in {\rm B}$), we introduce the transform

$$\left.\begin{aligned} S_{jz} &= -S + b_j^\dagger b_j, \\ S_{j+} &= b_j^\dagger \sqrt{2S - b_j^\dagger b_j}, \\ S_{j-} &= \sqrt{2S - b_j^\dagger b_j}\, b_j. \end{aligned}\right\} \tag{5.85}$$

As in the case of ferromagnet, (5.73) and (5.85) are substituted into the anti-ferromagnetic Heisenberg model. Then taking to quadratic of boson operators,

$$\mathscr{H} = -\alpha_z |J| N S^2 + 2|J|S \sum_{\langle i,j \rangle} (a_i^\dagger a_i + b_j^\dagger b_j + a_i b_j + a_i^\dagger b_j^\dagger), \tag{5.86}$$

where $i \in \mathrm{A}$, $j \in \mathrm{B}$. Let the Fourier transform of a_i, b_j be written as

$$\left.\begin{aligned} a_i &= \sqrt{\frac{2}{N}} \sum_{\boldsymbol{q}} a_{\boldsymbol{q}} \exp(-i\boldsymbol{q}\cdot\boldsymbol{r}_i), \\ b_j &= \sqrt{\frac{2}{N}} \sum_{\boldsymbol{q}} b_{\boldsymbol{q}} \exp(-i\boldsymbol{q}\cdot\boldsymbol{r}_j), \end{aligned}\right\} \tag{5.87}$$

then the Hamiltonian is re-written as

$$\mathscr{H} = -\alpha_z |J| N S^2 + 2\alpha_z |J| S \sum_{\boldsymbol{q}} [a_{\boldsymbol{q}}^\dagger a_{\boldsymbol{q}} + b_{\boldsymbol{q}}^\dagger b_{\boldsymbol{q}} + \gamma(\boldsymbol{q})(a_{\boldsymbol{q}}^\dagger b_{\boldsymbol{q}}^\dagger + a_{\boldsymbol{q}} b_{\boldsymbol{q}})], \tag{5.88}$$

where $\gamma(\boldsymbol{q})$ is defined as

$$\gamma(\boldsymbol{q}) = \alpha_z^{-1} \sum_{\rho} \exp(-i\boldsymbol{q}\cdot\boldsymbol{\rho}) \tag{5.89}$$

with $\boldsymbol{\rho}$ a vector connecting interacting two spins.

For the diagonalization of the Hamiltonian, we introduce the **Bogoliubov transformation** $(a_{\boldsymbol{q}}, b_{\boldsymbol{q}}) \to (\alpha_{\boldsymbol{q}}, \beta_{\boldsymbol{q}})$ as

$$\left.\begin{aligned} a_{\boldsymbol{q}} &= \cosh\theta_{\boldsymbol{q}} \alpha_{\boldsymbol{q}} - \sinh\theta_{\boldsymbol{q}} \beta_{\boldsymbol{q}}^\dagger, \\ b_{\boldsymbol{q}} &= \cosh\theta_{\boldsymbol{q}} \beta_{\boldsymbol{q}} - \sinh\theta_{\boldsymbol{q}} \alpha_{\boldsymbol{q}}^\dagger. \end{aligned}\right\} \tag{5.90}$$

$(\alpha_{\boldsymbol{q}}, \beta_{\boldsymbol{q}})$ satisfy the following boson commutation relations,

$$[\alpha_{\boldsymbol{q}}, \alpha_{\boldsymbol{q}}^\dagger] = 1, \quad [\beta_{\boldsymbol{q}}, \beta_{\boldsymbol{q}}^\dagger] = 1, \quad [\alpha_{\boldsymbol{q}}, \beta_{\boldsymbol{q}}] = [\alpha_{\boldsymbol{q}}^\dagger, \beta_{\boldsymbol{q}}^\dagger] = 0. \tag{5.91}$$

The Hamiltonian reads

$$\begin{aligned} \mathscr{H} = -\alpha_z |J| N S^2 + 2\alpha_z |J| S \sum_{\boldsymbol{q}} [&(\cosh 2\theta_{\boldsymbol{q}} - \gamma(\boldsymbol{q}) \sinh\theta_{\boldsymbol{q}})(\alpha_{\boldsymbol{q}}^\dagger \alpha_{\boldsymbol{q}} + \beta_{\boldsymbol{q}}^\dagger \beta_{\boldsymbol{q}} + 1) \\ &- 1 - (\sinh 2\theta_{\boldsymbol{q}} - \gamma(\boldsymbol{q}) \cosh 2\theta_{\boldsymbol{q}})(\alpha_{\boldsymbol{q}} \beta_{\boldsymbol{q}} + \alpha_{\boldsymbol{q}}^\dagger \beta_{\boldsymbol{q}}^\dagger)]. \end{aligned} \tag{5.92}$$

For the last off-diagonal term to vanish, we should choose the parameter $\theta_{\boldsymbol{q}}$ as

$$\sinh 2\theta_{\boldsymbol{q}} / \cosh 2\theta_{\boldsymbol{q}} = \tanh 2\theta_{\boldsymbol{q}} = \gamma(\boldsymbol{q}). \tag{5.93}$$

Hence the diagonalized Hamiltonian is given by

$$\mathscr{H} = -\alpha_z |J| N S^2 + 2\alpha_z |J| S \sum_{\boldsymbol{q}} [(\sqrt{1-\gamma(\boldsymbol{q})^2} - 1) + \sqrt{1-\gamma(\boldsymbol{q})^2} (\alpha_{\boldsymbol{q}}^\dagger \alpha_{\boldsymbol{q}} + \beta_{\boldsymbol{q}}^\dagger \beta_{\boldsymbol{q}})]. \tag{5.94}$$

In eq. (5.94), the first two terms without operator represent the ground state energy. The first term is the energy of Néel ordered state. The second term can be interpreted as the zero-point motion energy of magnons. The classical Néel ordered state is not the quantum mechanical ground state unlike the ferromagnetic case. Namely the original $S_{jz} = S, S-1, \cdots, -S$ states are hybridized though the anti-ferromagnetic interaction and the perturbation decreases the ground state energy. Accordingly, the expectation value of spin size diminishes from the full-size of S. The amount of the decrease is

$$\langle S_{jz} \rangle = S - \frac{2}{N} \sum_{\boldsymbol{q}} \sinh\theta_{\boldsymbol{q}} = S - \frac{1}{N} \sum_{\boldsymbol{q}} \left(\frac{1}{\sqrt{1-\gamma(\boldsymbol{q})^2}} - 1 \right). \tag{5.95}$$

The table below shows the decreases in spin size ($\Delta = S - \langle S_{jz} \rangle$), and the variation in energy (ϵ is defined as $E_0 = N|J|\alpha_z S(S+\epsilon)$), calculated for some simple lattice structures[3].

Lattice	Square	Simple Cubic	Body Centered Cubic
Δ	0.917	0.078	0.0593
ϵ	0.158+0.0062S^{-1}	0.097+0.0024S^{-1}	0.073+0.0013S^{-1}

The anti-ferromagnetic magnons expressed by the last two terms, degenerate reflecting the equivalency of A- and B-sublattices. The dispersion relation is obtained from

$$\epsilon_{\boldsymbol{q}} = 2\alpha_z |J| S\sqrt{1-\gamma(\boldsymbol{q})^2}. \tag{5.96}$$

$\gamma(\boldsymbol{q})$ defined in eq. (5.89) can be calculated, e. g., for simple cubic lattice with a unit cell size a, the dispersion in the long wavelength limit is given by

$$\epsilon_{\boldsymbol{q}} = 2\sqrt{2\alpha_z}|J|Saq, \tag{5.97}$$

which is linear in q.

Specific heat is a quantity to be compared with experiments. As in the case of ferromagnet, we consider the internal energy which is given in the case of simple cubic lattice by

$$U = E_0 + \frac{\pi^2}{15} N \left(\frac{k_{\rm B}T}{2\sqrt{2\alpha_z}|J|S}\right)^3 k_{\rm B}T, \tag{5.98}$$

where E_0 is the ground state energy given by the first two terms in eq. (5.94). The calculated specific heats are summarized in the following table including the cases of 1D, 2D, etc.[3].

Lattice	1D Chain	2D Square Lattice	3D Simple Cubic
$-\dfrac{E_0}{\alpha_z\lvert J\rvert NS^2}$	1+0.363S^{-1}	1+0.158S^{-1}	1+0.097S^{-1}
$\dfrac{C}{Nk_{\rm B}}$	$\dfrac{2\pi}{3}\left(\dfrac{k_{\rm B}T}{2\alpha_z\lvert J\rvert S}\right)$	$\dfrac{14.42}{\pi}\left(\dfrac{k_{\rm B}T}{2\alpha_z\lvert J\rvert S}\right)^2$	$4\sqrt{3}\dfrac{\pi^2}{5}\left(\dfrac{k_{\rm B}T}{2\alpha_z\lvert J\rvert S}\right)^3$
ΔS	Diverge	0.197	0.078

The original purpose of considering magnons is to treat thermal fluctuation at low temperatures correctly. Particularly for anti-ferromagnets, there are real materials close to the theoretical models. Hence it is important whether the simple models can explain such experiments. Figure 5.8 shows the crystal structure and the measured specific heat of an organic

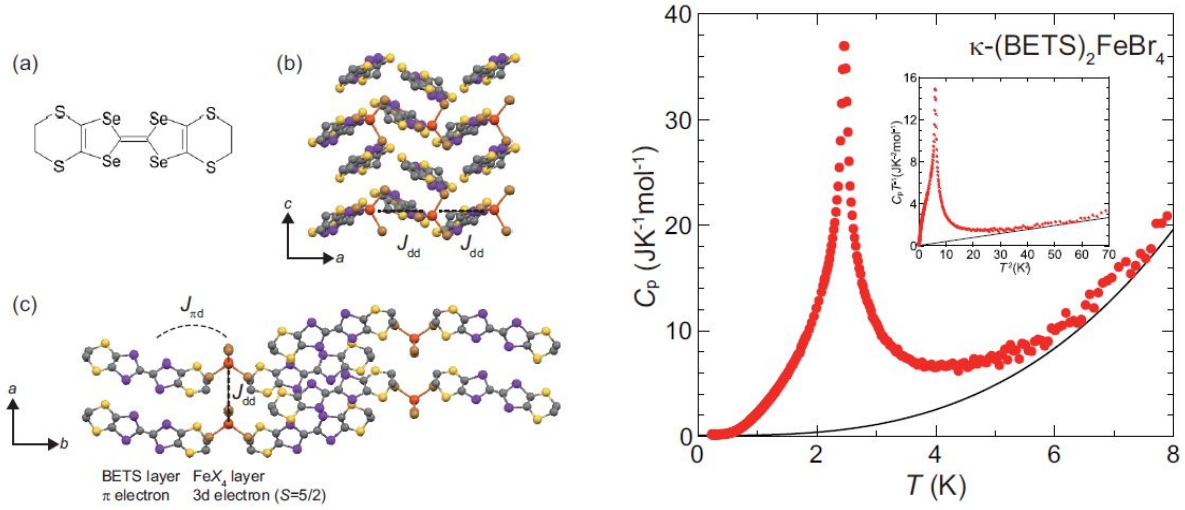

Fig. 5.8 Crystal structure and specific heat of κ-(BETS)$_2$FeX$_4$. Left: (a) Molecular structure of BETS. (b) Crystal structure viewed from b-axis. BETS molecules are in line with alternative oblique angles. (c) Crystal structure viewed from c-axis. Right: Low temperature specific heat of a sample with X=Br. The contribution from phonons with T^3 dependence is indicated by a black line. The inset shows $C_{\rm p}T^{-1}$ as a function of T^2[4].

anti-ferromagnet κ-(BETS)$_2$FeBr$_4$ (BETS = bis(ethylenedithio)tetraselenafulvalene)[4]. This material is not an insulator having metallic conductivity. At low temperatures, it undergoes an anti-ferromagnetic transition at $T_{\rm N}$ =2.47 K, and further, a superconducting transition at 1.1 K. The crystal shown in the left panel is composed of stacking of comparatively small molecules. Electrons in π-bonds spread over ab plane, which is stacked along c-axis. The anti-ferromagnetism originates from $3d$-electrons in Fe with S =5/2. There are J_{dd}, which is direct interaction between d's, and $J_{\pi d}$, which is mediated by π.

The right panel in Fig. 5.8 displays the measured specific heat, which shows very sharp increase at $T_{\rm N}$. This corresponds to the jump at $T_{\rm C}$ in the figure in Sec. 5.3. The inset shows $C_{\rm p}/T$ as a function of T^2. An ordinary metal has a specific heat $C_{\rm m} = AT + BT^3$ from an electron contribution ($\propto T$) and a lattice contribution ($\propto T^3$). This is written as $C_{\rm m}/T = A + BT^2$ and expressed as a line in this plot. The contribution of electrons is negligibly small as known from the fitting at high temperatures. The heat capacity shows T^2-like variation in the region lower than $T_{\rm N}$, as it shows a line. This seems to be in accordance with the result of 2D specific heat in the above table. In the paper, however, the authors claim that the results are in accordance with a theory on 1D anti-ferromagnetic chain.

5.8.5 Nambu-Goldstone theorem and spin wave

In the section of ferromagnetic transition in Heisenberg model, we have visited the concept of spontaneous symmetry breaking (SSB). In typical continuous phase transitions, a symmetry should be spontaneously broken and at the same time an order appears.

Nambu-Goldston theorem is summarized as follows:

Nambu-Goldstone theorem

When a symmetry of a physical system is spontaneously broken, there is an excitation with zero energy (gap) in the long wavelength limit.

Sometimes it is described as "excitation with zero-mass." From the still energy $E = mc^2$, the two descriptions are equivalent.

This can be intuitively understood in the case of ferromagnetic transition. In the phenomenology in Sec. 5.2, as (a)→(b) in Fig. 5.2, the SSB caused by appearance of two minima in the free energy $\mathscr{F}(M)$. For example, two-dimensional Heisenberg model is isotropic and in the SSB state, the free energy of the state $(M_0\cos\theta, M_0\sin\theta)$ does not depend on θ, in other words, the state can freely go around on the yellow line in the figure. The motion on the yellow line is **Nambu-Goldstone mode** (NG mode) in the present case. This corresponds to the rotation of macroscopic magnetization

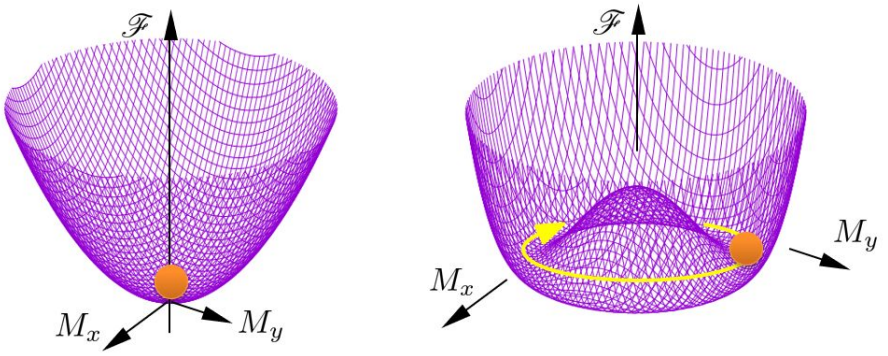

Fig. 5.9 Left: Free energy $\mathscr{F}$ of a system with rotational symmetry. The lowest $\mathscr{F}$ is obtained at M (magnetization)=0 on (M_x, M_y) plane. Right: A spontaneous symmetry breaking yields an order parameter (magnetization). The states with minimum $\mathscr{F}$ exist continuously, between which the system can transit without energy (Nambu-Goldstone mode).

and can be seen as the limit of long wavelength. Classically the magnon wavelength is determined by the phase shift of precessions between neighboring sites. In the long wavelength limit, the phase shift is zero, and the spins are rotating coherently. Hence we can say the magnon is the NG mode in the present case.

The dispersion relation of ferromagnetic magnon is quadratic in q as eq. (5.81). On the other hand in the anti-ferromagnetic magnons, the dispersion is linear as in eq. (5.96). Sometimes the latter is called type-A and the former is called type-B NG mode. On the other hand Nielsen-Chadha[5] called $\hbar\omega \propto k^{2n+1}$ as type-I, $\hbar\omega \propto k^{2n}$ as type-II.

As is well known, it originated from Yoichiro Nambu's idea for the acquisition of particle mass on the superconducting BCS theory as a model, and from there, the standard theory of elementary particles makes great progress. And also in the condensed matter theory, it is one of the central concepts as introduced by Anderson in the book "basic notions"[6]. Even though there are many open questions even in the basics of the NG mode. Surprisingly there are many important findings and progresses recently. Here I introduce an example. In the naíve NG theorem, the number of broken symmetries $N_{\rm BS}$ and that of NG modes $N_{\rm NG}$ should be the same($N_{\rm BS} = N_{\rm NG}$). However that does not hold in many simple examples. In the case of 3D ferromagnetic transition, the rotation symmetries of two axes are broken, hence $N_{\rm BS} = 2$ though simple ferromagnetic magnon NG mode number is one, i.e., $N_{\rm NG} = 1$.

For this problem, based on the pioneering works by Nielsen-Chadha[5] and by others, Watanabe-Murayama[7], and Hidaka[8] reached the satisfactory answer in 2012 independently. This can be viewed as a generalization of the NG theorem. To say it very short, let $N_{\rm I}$ and $N_{\rm II}$ be the number of type-I and type-II NG modes respectively, then

$$N_{\rm I} + 2N_{\rm II} = N_{\rm BS}.$$

For the detail see the review paper[9].

5.9 Experiments on magnons

As we saw in the above, magnons are elementary excitations from the ground state, considered to calculate macroscopic quantities of magnetic materials at finite temperatures. However recently, the concept of magnon goes beyond the framework. The researches are prosperous on the wave and the particle like manners, soliton physics or Bose-Einstein condensation in the high-density non-linear region where the original spin wave approximation does not hold. The birth is given to the word "magnonics" and application to quantum information processing is seriously considered[10]. You can find many reviews[11] and textbools[12].

Here I would like to introduce rather old results, which are now the basis of present studies, however.

5.9.1 Measurement of magnon dispersion relation by neutron scattering

Neutron scattering has long been used as a means of measuring microscopic magnetic structures. It can be said that it is still the most powerful reliable experimental method with atomic resolution. Inelastic scattering was used, in particular, for magnon dispersion measurements.

We write the interaction between the magnetic moment $\boldsymbol{\mu}_{\rm e}$ of electrons in an atom and that of a neutron as

$$\mathscr{H}_{\rm int} = -\boldsymbol{\mu}_{\rm e} \cdot \boldsymbol{B}_{\rm n}, \tag{5.99}$$

where

$$\boldsymbol{B}_{\rm n} = \mathrm{rot}\left(\boldsymbol{\mu}_{\rm n} \times \frac{\boldsymbol{r}}{r^3}\right) \tag{5.100}$$

is the magnetic field of neutron magnetic moment $\boldsymbol{\mu}_{\rm n}$, $\boldsymbol{r}$ is the vector connecting the atom and the neutron. When a neutron is scattered by such an interaction as

$$\hbar\boldsymbol{k} \longrightarrow \hbar(\boldsymbol{k} - \boldsymbol{q}), \tag{5.101}$$

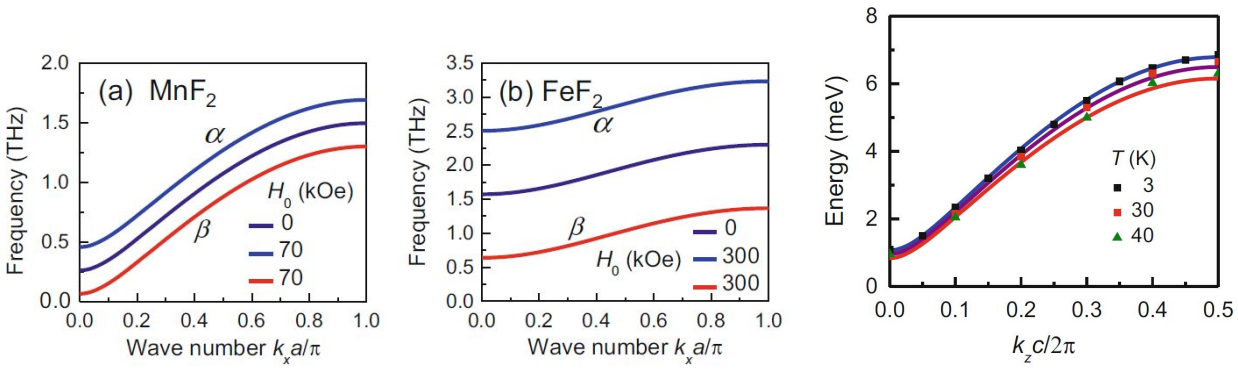

Fig. 5.10 (a), (b) Magnon dispersion relations calculated for MnF_2, FeF_2 incorporating anisotropic field[12]. Right panel: Magnon dispersion relation measured in MnF_2 by time of flight method of neutron scattering[13].

the variation in the energy is

$$\Delta E = \frac{\hbar^2}{2M}(-2\boldsymbol{k}\cdot\boldsymbol{q} + \boldsymbol{q}^2). \tag{5.102}$$

In very short, pulses of neutron with appropriate energy is applied to the sample, and the measurements of the energy (momentum) change and the scattering angle give certain information. This is (in the case of $\Delta E \neq 0$) the **inelastic scattering** of neutron. On the other hand in the case of elastic scattering ($\Delta E = 0$), the wave nature of neutrons the diffraction is important.

To obtain the dispersion relation of magnons, the inelastic scattering of neutron is mostly used. Figure 5.10 shows the magnon dispersion relation of MnF_2 obtained by neutron inelastic scattering. For the above information of (5.101) and (5.102), time-of-flight (TOF) method was utilized[13]. The result shows a good agreement with the result of molecular field approximation with the effect of anisotropy.

5.9.2 Bose-Einstein condensation of magnons

In the process of introducing magnons with creation/annihilation operators, we defined the vacuum $|0\rangle_{\rm F}$ as $|S\rangle$, i.e., the state of $S_z = S$, and $|n\rangle_{\rm F}$ as $|S-n\rangle$. As mentioned, while we do not have negative n state from the definition, repetitive operation of creation operator creates infinite number of n states. However in reality, S_z can take only down to $-S$. This physical space of function does not have any matrix element with the extended space as long as the theory is exact (no approximation). This means that the magnons, though their creation/annihilation operators satisfy bosonic commutation relations, the condition that "a single state can accommodate an infinite number of particles" is not fulfilled. In this sense, the statistics of magnon is not complete Bose statistics but a para-statistics[14].

A typical phenomenon appeared in the system of bosons is the **Bose-Einstein Condensation** (BEC). The BEC is very shortly introduced in Appendix 10B. Superfluidity of helium, BEC in laser-cooled neutral atomic gases are the representatives. Even for these phenomena, the interaction between the particles exists and they are not jus the same as the simple BEC described in the Appendix. Also, the superconductivity, in which weakly bound fermion pairs condensate is a similar phenomenon. Even in the case of magnons, though they obey para-statistics, they can be viewed as "bosons with hard cores" and there is a possibility that a similar phenomenon occurs. It is still difficult, though, for magnons to fulfill the basic condition of BEC that (averaged de Broglie wavelength)=(averaged particle distance) because the particle density decreases with lowering the temperature, as is guessed from the calculation of the magnetization in eq. (5.79). Then an experiment was carried out, in which a large number of magnons are excited by microwave and a non-equilibrium BEC took place[15]. They studied the Brillouin scattering of light by magnons and observed anomalous narrowing of the linewidth of the resonance.

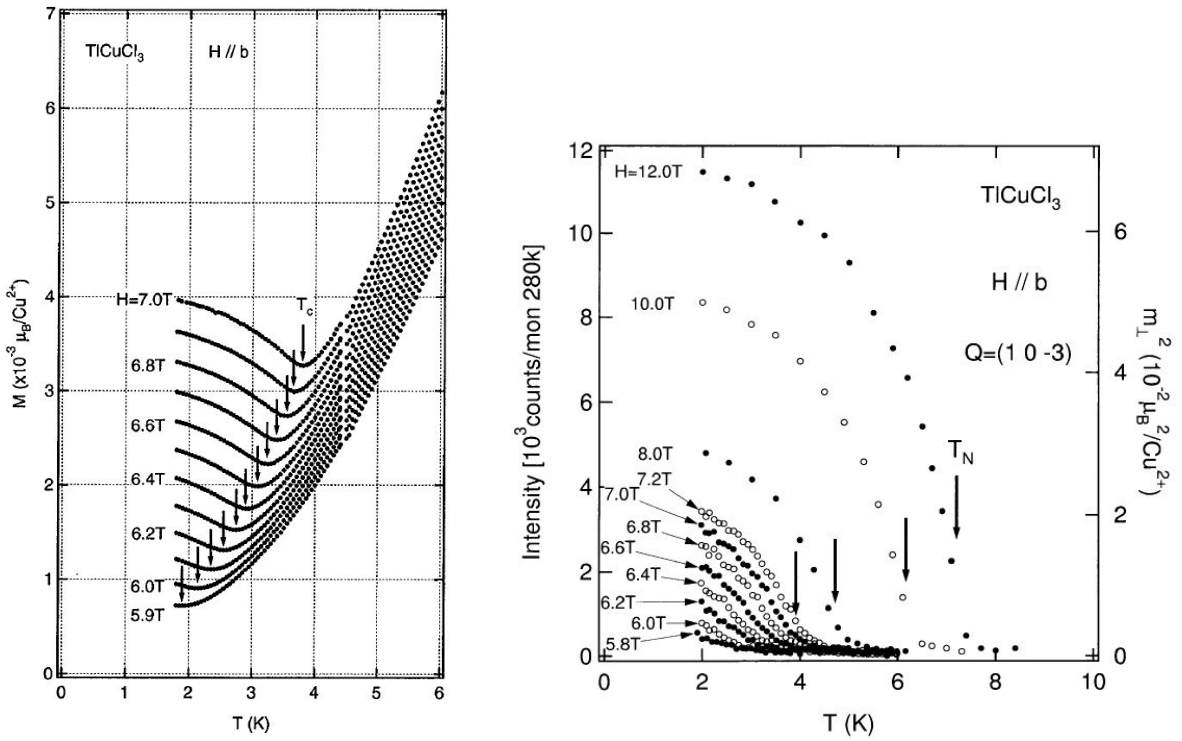

(a) (b)

Fig. 5.11 (a) Temperature dependent magnetization of $TlCuCl_3$ in magnetic fields[16], (b) Temperature variation of the intensity of Bragg reflection (1,0,−3) in neutron diffraction[17]. As indicated in the right axis, this is proportional to the square of vertical magnetic moment per site.

Let us see an experimental observation of BEC in thermal equilibrium[16, 17]. Due to the above restriction, the situation is rather special. The material is a compound of $TlCuCl_3$ in chemical formula. Two magnetic ions form pairs (dimer) with an antiferromagnetic coupling. There are singlet $|0,0\rangle$ and triplet $(|1,-1\rangle, |1,0\rangle, |1,1\rangle)$ as the states of the pair, in which the single is the ground state due to the antiferromagnetic coupling. There is an energy gap (spin gap) between the ground state and the first excited state. With applying magnetic field, the energy of $|1,1\rangle$ is lowered and the field driven phase transition takes place for the ferromagnetism to appear. In this system, the magnon appears when the energies of $|0,0\rangle$ and $|1,1\rangle$ are close as the propagation of $|1,1\rangle$ states to the neighboring sites. As known from this example, the propagation of magnons is the equivalent to that of spin angular momentum and that brings a **spin current**. For the behavior of magnetization in such a system without magnon BEC, a theory has been presented [18] and the high temperature behavior is well explained. It predicts for the the magnetization transverse to the spontaneous magnetization that it should be constant for temperature. However in the experiment, as in Fig. 5.11(a) the magnetization once decreases with decrease of temperature but the dependence is inverted around the transition point and increases. The magnon-BEC theory explains the experiment that an order grows in the mixture of $|0,0\rangle$ and $|1,1\rangle$ and the transverse magnetization appears as an average (does not cancel out)[16]. Furthermore as in Fig. 5.11(b) in neutron diffraction, it was confirmed that such an order actually grows[17]. From the above, the observation of magnon BEC is claimed.

Appendix 10A: Collective motion of spins

Because a macroscopic number of spins are bound to in a ferromagnetic state, the motion can be described as a collective motion. On the other hand, as lattice vibrations in lattice formation, a kind of collective motion from the magnetic ground state can exist and quantization as phonons is possible.

10A.1 Collective motion of magnetization

For a ferromagnetic total magnetization

$$\boldsymbol{S} = \sum_i \boldsymbol{S}_i, \tag{10A.1}$$

we apply Heisenberg equation of motion as

$$i\hbar \frac{\partial \boldsymbol{S}}{\partial t} = [\boldsymbol{S}, \mathscr{H}], \tag{10A.2}$$

which is formally the same as eq. (2.11) and represents the Larmor precession. A resonance experiment as EPR for a total magnetization is possible and called as **ferromagnetic resonance** (FMR). From FMR we get various information on the ferromagnetism and the spin wave.

Next we consider the case that the phase of the precession has a constant shift between neighboring spins. The above motion of the total magnetization can be considered as the long wavelength limit of this motion. The magnetization and the external field direction is taken to z. This situation is expressed as

$$S_{ix} = A\cos(\omega_0 t + \theta_i), \quad S_{iy} = A\sin(\omega_0 t + \theta_i), \tag{10A.3}$$

with a shift of θ_i with i. Let us use complex numbers for spins. And the Fourier transform and the inverse transform

$$S_{\boldsymbol{q}x} = \frac{1}{\sqrt{N}} \sum_j S_{jz} \exp(-i\boldsymbol{q}\cdot\boldsymbol{r}_j), \quad S_{jx} = \frac{1}{\sqrt{N}} \sum_{\boldsymbol{q}} S_{\boldsymbol{q}x} \exp(i\boldsymbol{q}\cdot\boldsymbol{r}_j) \tag{10A.4}$$

are introduced.

We apply (10A.2) to Heisenberg Hamiltonian $\mathscr{H} = -2J\sum_{\langle i,j\rangle} \hat{\boldsymbol{S}}_i \cdot \hat{\boldsymbol{S}}_j$ to obtain the following.

$$i\hbar \frac{\partial S_{\boldsymbol{q}x}}{\partial t} = \frac{4i}{\sqrt{N}} J \sum_{\langle i,j\rangle} S_{iy} S_{jz} \exp(-i\boldsymbol{q}\cdot\boldsymbol{r}_i)\{1 - \exp[i\boldsymbol{q}\cdot(\boldsymbol{r}_i - \boldsymbol{r}_j)]\} \tag{10A.5a}$$

$$i\hbar \frac{\partial S_{\boldsymbol{q}y}}{\partial t} = -\frac{4i}{\sqrt{N}} J \sum_{\langle i,j\rangle} S_{ix} S_{jz} \exp(-i\boldsymbol{q}\cdot\boldsymbol{r}_i)\{1 - \exp[i\boldsymbol{q}\cdot(\boldsymbol{r}_i - \boldsymbol{r}_j)]\}. \tag{10A.5b}$$

Fourier transform of J is written as

$$J_{\boldsymbol{q}} = \sum_j J \exp[i\boldsymbol{q}\cdot(\boldsymbol{r}_i - \boldsymbol{r}_j)]. \tag{10A.6}$$

In the above, the sum over j and i can be taken anywhere because the interaction only depends on $\boldsymbol{r}_i - \boldsymbol{r}_j$. Further, the sum only over the nearest neighbor because the interaction is assumed to work only for nearest neighbors. Here we approximate S_{jz} by S, which corresponds to small angle approximation. Then

$$\hbar \frac{\partial S_{\boldsymbol{q}x}}{\partial t} = 2[J_0 - J_{\boldsymbol{q}}] S S_{\boldsymbol{q}y}, \tag{10A.7a}$$

$$\hbar \frac{\partial S_{\boldsymbol{q}y}}{\partial t} = -2[J_0 - J_{\boldsymbol{q}}] S S_{\boldsymbol{q}x}. \tag{10A.7b}$$

This is the same as eq. (5.68) but with $B = 0$.

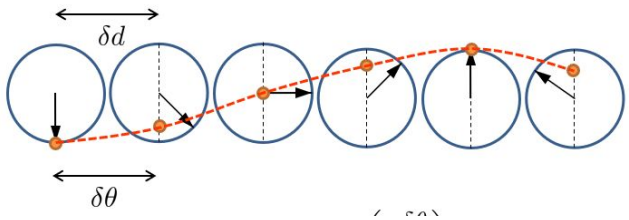

Fig. 10A.1 Schematic diagram showing a constant phase shift between neighboring spins.

Appendix 10B: Bose-Einstein condensation

The Bose-Einstein Condensation (BEC) [*1] is called a phase transitoin that is not due to the interaction between freedoms (quantum statistical phase transition). Though phase transitions caused by interaction beween some freedoms can be intuitively understood, there are different types of phase transitions, in which the transitions are caused as the results of competition between various factors. A representative is BEC.

In the case of bosonic systems, in spite of the absence of "force" betwen the particles, there exists the tendency for them to occupy the same quantum state originating from their statistical property. Let us see that for the case of two particles. We write a solution of the wave equation for two particles as $\psi(\boldsymbol{x}_1, \boldsymbol{x}_2)$. For the composition of wavefunctions of the system $\Psi(\boldsymbol{x}_1, \boldsymbol{x}_2)$ that reflects the statistical property of bosons, the symmetrization of ψ results in

$$\Psi(\boldsymbol{x}_1, \boldsymbol{x}_2) = \frac{1}{\sqrt{2}} \left[\psi(\boldsymbol{x}_1, \boldsymbol{x}_2) + \psi(\boldsymbol{x}_2, \boldsymbol{x}_1)\right]. \tag{10B.1}$$

Hence the probability of finding the system at $(\boldsymbol{x}_1, \boldsymbol{x}_2)$ is

$$|\Psi(\boldsymbol{x}_1, \boldsymbol{x}_2)|^2 = \frac{1}{2} \left[|\psi(\boldsymbol{x}_1, \boldsymbol{x}_2)|^2 + |\psi(\boldsymbol{x}_2, \boldsymbol{x}_1)|^2 + \psi(\boldsymbol{x}_1, \boldsymbol{x}_2)^* \psi(\boldsymbol{x}_2, \boldsymbol{x}_1) + \psi(\boldsymbol{x}_1, \boldsymbol{x}_2) \psi(\boldsymbol{x}_2, \boldsymbol{x}_1)^*\right]. \tag{10B.2}$$

This reveals that the last two interference terms intensify the probability of finding the system under the condition of $\boldsymbol{x}_1 = \boldsymbol{x}_2$. Let us write the de Broglie wavelength as λ and the averaged distance between the particles as l. Then at low temperatures $\lambda \sim l$, this tendency of bosons makes many of them to occupy the state of $k = 0$, which behavior leads to BEC. The above discusstion is expressed as

$$E_k = \frac{p^2}{2M} = k_{\mathrm{B}} T,$$

$$\begin{aligned} &\Delta p \sim \sqrt{M k_{\mathrm{B}} T} \\ &\therefore \lambda = \frac{h}{\Delta p} \sim \frac{h}{\sqrt{M k_{\mathrm{B}} T}}. \end{aligned} \tag{10B.3}$$

λ elongates as $1/\sqrt{T}$ with lowering the temperature. And with growing of the overlapp between the single particle wavefunctions makes them undistinguishable and the symmetrization of the wavefunction cause the condensation to the ground state in the phase space $(\boldsymbol{r}, \boldsymbol{p})$. The phase transition to the condensate at a certain temperature is BEC.

10B.1 Bose-Einstein condensation of ideal gas

Let us consider spin 0 ideal Bose gas. For the Bose distribution

$$f(\epsilon) = \frac{1}{e^{(\epsilon - \mu)\beta} - 1} \qquad (\beta \equiv (k_{\mathrm{B}} T)^{-1}) \tag{10B.4}$$

we define the point of $\mu = 0$ as follows. At $T = 0$, from (10B.4) all the particles fall into the ground state, there we define

$$\mu(T = 0) = 0. \tag{10B.5}$$

At finite temperatures, let N be the number of particles in the system:

$$N = \sum_i f(\epsilon_i).$$

[*1] The acronym of BEC is applied to both Bose-Einstein Condensation and Bose-Einstein Condensate. In actual use, the confution is not serious.

In the usual case we can write

$$N \to \int f(\epsilon)\mathcal{D}(\epsilon)d\epsilon. \tag{?}$$

Here the number of particle at the ground state N_0 should be

$$N_0 = \frac{1}{e^{-\mu\beta}-1} \sim \frac{1}{-\mu\beta} = -\frac{k_{\rm B}T}{\mu} \to \mu \sim -\frac{k_{\rm B}T}{N_0}. \tag{10B.6}$$

If we calculate the particle distribution on this line, for three dimensional ideal gas

$$\epsilon(k) = \frac{\hbar^2 k^2}{2m} \text{ then } \mathcal{D}(\epsilon) = \frac{m^{3/2}V}{\sqrt{2}\pi^2\hbar^3}\sqrt{\epsilon}. \tag{10B.7}$$

Therefore

$$N = \frac{Vm^{3/2}}{\sqrt{2}\pi^2\hbar^3}\int_0^\infty \frac{\sqrt{\epsilon}}{e^{(\epsilon-\mu)\beta}-1}d\epsilon = \frac{(mk_{\rm B}T)^{3/2}}{\sqrt{2}\pi^2\hbar^3}V\int_0^\infty \frac{\sqrt{x}}{e^{x-\alpha}-1}dx, \tag{10B.8}$$

where $x \equiv \epsilon\beta$ and $\alpha \equiv \mu\beta$. We write the definite integral term as $I(\alpha)$, then I is

$$I(0) = \int_0^\infty \frac{\sqrt{x}}{e^x-1}dx = \frac{\sqrt{\pi}}{2}\zeta\left(\frac{3}{2}\right) \sim 2.6, \tag{10B.9}$$

which decreases with increasing of the absolute value of $\alpha < 0$. Then, in this logic, with $T \to 0$ the maximum number of N determined from (10B.8) goes to zeo. It is apparent that we have dropped something from the counting. That is, of course, the macroscopic number of particles fall into the ground state.

From Eq. (10B.8),

$$I(\alpha) = \frac{\sqrt{2}\pi^2\hbar^3}{(mk_{\rm B}T)^{3/2}}\frac{N}{V}.$$

When this excessds (10B.9) at low temperatures the anomaly (increase in the particle number at the ground state.) occurs. This critical temperature T_c is

$$T < T_c \equiv \frac{2\pi\hbar^2}{mk_{\rm B}}\left[\frac{N}{\zeta(3/2)V}\right]^{2/3}. \tag{10B.10}$$

Here $l \equiv (V/N)^{1/3}$ is the average distance between the particles and Eq. (10B.10) is interpreted as

$$l = \frac{h}{\zeta(3/2)\sqrt{2\pi mk_{\rm B}T_c}} \sim \lambda(T = T_c). \tag{10B.11}$$

This confirms the statement that the BEC takes place when the average de Broglie wavelength is comparable with the average particel distance.

Below T_c, we add the number of ground state particles N_0 to Eq. (10B.8):

$$N = \frac{Vm^{3/2}}{\sqrt{2}\pi^2\hbar^3}\int_0^\infty \frac{\sqrt{\epsilon}}{e^{(\epsilon-\mu)\beta}-1}d\epsilon + N_0. \tag{10B.12}$$

From Eq. (10B.6), N_0 becomes a macroscopic number fro $T < T_c$, then $\mu = 0$. Therefore

$$N_0 = N - \frac{Vm^{3/2}}{\sqrt{2}\pi^2\hbar^3}\int_0^\infty \frac{\sqrt{\epsilon}}{e^{\epsilon\beta}-1}d\epsilon = N\left[1 - \frac{V}{N}\frac{(mk_{\rm B}T)^{3/2}}{\sqrt{2}\pi^2\hbar^3}I(0)\right] = N\left[1 - \left(\frac{T}{T_c}\right)^{3/2}\right]. \tag{10B.13}$$

This is just like a spontaneous magnetization rapidly grows to finite values below the critical temperature in the ferromagnetic transition.

The total energy of the system for $T < T_c$ is calculated as

$$E = \frac{Vm^{3/2}}{\sqrt{2}\pi^2\hbar^3}\int_0^\infty \frac{\epsilon^{3/2}}{e^{\beta\epsilon}-1}d\epsilon \tag{10B.14}$$

ここで $T < T_c$ では $\displaystyle\int_0^\infty \frac{x^{3/2}}{e^x-1}dx = \frac{3\sqrt{\pi}}{4}\zeta\left(\frac{5}{2}\right)$ より

$$E = \frac{3}{2}\zeta\left(\frac{5}{2}\right)\left(\frac{m}{2\pi\hbar^2}\right)^{3/2}V(k_{\rm B}T)^{5/2}. \tag{10B.15}$$

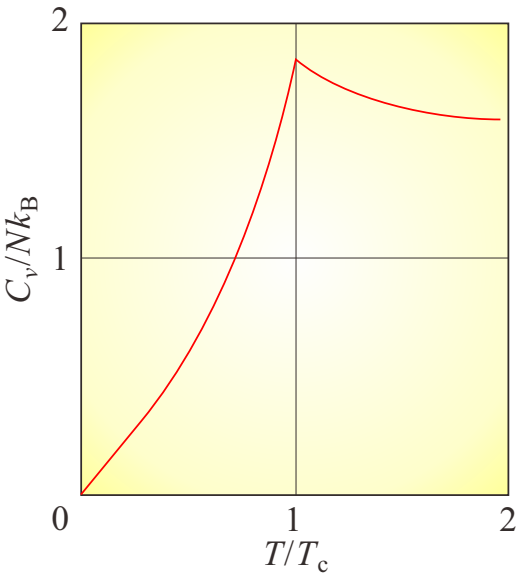

Fig. 10B.1 Specific heat at constant volume of three dimensional ideal Bose gas as a function of temperature. T_c is the critical temperature of the BEC.

Then the heat capacity at constant volume is calculated as

$$C_v = \frac{15}{4}\zeta\left(\frac{5}{2}\right)\left(\frac{m}{2\pi\hbar^2}\right)^{3/2} V k_{\mathrm{B}}^{5/2} T^{3/2}. \tag{10B.16}$$

C_v shows a cusp at T_c indicating that this is the phase transition.

10B.2 Bosonic stimulation

Here we have a look at **bosonic stimulation** for N particles, which is, though, essentially the same as what has been mentioned on the case of two particles in Sed. **??**. As we have seen, the bosonic stimulation works as if it is a driving force in BEC or laser oscillation. Let us consider a identical boson system the case a particle in state φ_{ini} gets perturbation and transitions to other single particel state φ_{fin}. Now the problem is the difference in the transition probabilities to the state occupied with N particles and to the empty state. We write the initial state as

$$\psi_+^{(i)}(\boldsymbol{r}_1, \cdots, \boldsymbol{r}_{N+1}) = \frac{1}{\sqrt{(N+1)N!\prod_l n_l!}} \prod_{m=1}^{N} \hat{R}_{m,N+1} \det{}^{(+)}\{\varphi_i(\boldsymbol{r}_j)\}\varphi_{\mathrm{ini}}(\boldsymbol{r}_{N+1}). \tag{10B.17}$$

The symbol $\det^{(+)}$ represents permanent, which is obtained by making the signs of all the terms into $+$. The final state $\psi_+^{(f)}$ is obtaned by exchanging φ_{ini} with φ_{fin}. Let the matrix elements of perturbation Hamiltonian be a, i.e. $\langle\varphi_{\mathrm{fin}}|\hat{H}_1|\varphi_{\mathrm{ini}}\rangle = a$.

Assuming that φ_i $(i \leq N)$ is orthogonal to φ_{fin}, among $\langle\psi_+^{(f)}|\hat{H}_1|\psi_+^{(i)}\rangle$, number of terms that give non-zero a is $(N+1)N!\prod_l n_l!$. This is equal to the sqare of the denominator in normalization constant. Then finally $\langle\psi_+^{(f)}|\hat{H}_1|\psi_+^{(i)}\rangle = a$.

On the other hand, assuming all of φ_i $(i \leq N)$ are φ_{fin}, we can write

$$\psi_+^{(i)} = \frac{1}{\sqrt{(N+1)}} \prod_{m=1}^{N} \hat{R}_{m,N+1}\varphi_{\mathrm{fin}}(\boldsymbol{r}_1)\cdots\varphi_{\mathrm{fin}}(\boldsymbol{r}_N)\varphi_{\mathrm{ini}}(\boldsymbol{r}_{N+1}). \tag{10B.18}$$

All of the $N!$ terms in $\det^{(+)}$ are $\varphi_{\mathrm{fin}}(\boldsymbol{r}_1)\cdots\varphi_{\mathrm{fin}}(\boldsymbol{r}_N)$ and devided by $N!$ in the denominator of normalization constant to 1. However the final state is

$$\psi_+^{(f)} = \varphi_{\mathrm{fin}}(\boldsymbol{r}_1)\cdots\varphi_{\mathrm{fin}}(\boldsymbol{r}_N)\varphi_{\mathrm{fin}}(\boldsymbol{r}_{N+1}). \tag{10B.19}$$

Then we get $\langle\varphi_{\mathrm{fin}}|\hat{H}_1|\varphi_{\mathrm{ini}}\rangle = a\sqrt{N+1}$, and from the Fermi's golden rule, the transition probability should be $N+1$ times larger.

References

[1] 高橋康. 物性研究者のための場の量子論 1 (新物理学シリーズ 16). 培風館, 10 1974.

[2] Silvia Viola Kusminskiy. *Quantum Magnetism, Spin Waves, and Optical Cavities (SpringerBriefs in Physics)*. Springer, 2 2019.

[3] Ryogo Kubo. The spin-wave theory of antiferromagnetics. *Phys. Rev.*, Vol. 87, pp. 568–580, Aug 1952.

[4] Shuhei Fukuoka, Satoshi Yamashita, Yasuhiro Nakazawa, Takashi Yamamoto, Hideki Fujiwara, Takashi Shirahata, and Kazuko Takahashi. Thermodynamic properties of antiferromagnetic ordered states of $\pi - d$ interacting systems of $\kappa - (\mathrm{BETS})_2\mathrm{Fe}X_4(x = \mathrm{Br},\ \mathrm{Cl})$. *Phys. Rev. B*, Vol. 93, p. 245136, Jun 2016.

[5] H.B. Nielsen and S. Chadha. On how to count goldstone bosons. *Nuclear Physics B*, Vol. 105, No. 3, pp. 445–453, March 1976.

[6] PHILIP W. ANDERSON. *BASIC NOTIONS OF CONDENSED MATTER PHYSIC*. TAYLOR & FRANCIS, 2 2019.

[7] Haruki Watanabe and Hitoshi Murayama. Unified description of nambu-goldstone bosons without lorentz invariance. *Phys. Rev. Lett.*, Vol. 108, p. 251602, Jun 2012.

[8] Yoshimasa Hidaka. Counting rule for nambu-goldstone modes in nonrelativistic systems. *Phys. Rev. Lett.*, Vol. 110, p. 091601, Feb 2013.

[9] Yoshimasa Hidaka and Yuki Minami. Spontaneous symmetry breaking and nambu–goldstone modes in open classical and quantum systems. *Progress of Theoretical and Experimental Physics*, Vol. 2020, No. 3, March 2020.

[10] H.Y. Yuan, Yunshan Cao, Akashdeep Kamra, Rembert A. Duine, and Peng Yan. Quantum magnonics: When magnon spintronics meets quantum information science. *Physics Reports*, Vol. 965, pp. 1–74, June 2022.

[11] Philipp Pirro, Vitaliy I. Vasyuchka, Alexander A. Serga, and Burkard Hillebrands. Advances in coherent magnonics. *Nature Reviews Materials*, Vol. 6, No. 12, pp. 1114–1135, July 2021.

[12] Sergio M. Rezende. *Fundamentals of Magnonics (Lecture Notes in Physics)*. Springer, 8 2020.

[13] G. G. Low, A. Okazaki, R. W. H. Stevenson, and K. C. Turberfield. A measurement of spin-wave dispersion in MnF_2 at 4.2 k. *Journal of Applied Physics*, Vol. 35, No. 3, pp. 998–999, March 1964.

[14] 高橋康. 物性研究者のための場の量子論 2 (新物理学シリーズ 17). 培風館, 4 1976.

[15] S. O. Demokritov, V. E. Demidov, O. Dzyapko, G. A. Melkov, A. A. Serga, B. Hillebrands, and A. N. Slavin. Bose-einstein condensation of quasi-equilibrium magnons at room temperature under pumping. *Nature*, Vol. 443, No. 7110, pp. 430–433, September 2006.

[16] T. Nikuni, M. Oshikawa, A. Oosawa, and H. Tanaka. Bose-einstein condensation of dilute magnons in tlcucl_3. *Phys. Rev. Lett.*, Vol. 84, pp. 5868–5871, Jun 2000.

[17] Hidekazu Tanaka, Akira Oosawa, Tetsuya Kato, Hidehiro Uekusa, Yuji Ohashi, Kazuhisa Kakurai, and Andreas Hoser. Observation of field-induced transverse néel ordering in the spin gap system $TlCuCl_3$. *Journal of the Physical Society of Japan*, Vol. 70, No. 4, pp. 939–942, April 2001.

[18] Masashi Tachiki and Takemi Yamada. Spin ordering and thermodynamical properties in spin-pair systems under magnetic fields. *Progress of Theoretical Physics Supplement*, Vol. 46, pp. 291–309, 1970.

Lecture note Magnetism (11)

22nd June (2022) Shingo Katsumoto, Institute for Solid State Physics, University of Tokyo

In the last week we saw an example of magnon BEC in thermal equilibrium observed in a bit special material [*1]. Here we would like to see an experiment on the BEC under quasi-equilibrium condition.

The experimental setup is shown in the left panel of Fig. 5.11[1]. A microwave pulse is applied to an YIG thin film for the generation of low energy ($\sim$ 100 mK) magnons through a parametric process. A photon of microwave has a very small momentum, with which the excitation of a single magnon is difficult. However as shown in the inset, it is possible to excite two magnons with the same momentums but in opposite directions. Therefore, the excited magnons have almost the half of the energy of applied microwave. The concentration and the energy distribution of magnons are measured by Brillouin scattering of a laser light. The right panel of Fig. 5.11 shows the results. With increasing the power of microwave from 4 W to 5.9 W, the number of magnons increased rapidly with keeping the width of distribution. The observed distribution is much broader than the actual one as demonstrated in (d), in which the result of measurement with a higher resolution is displayed. This is claimed as the observation of BEC.

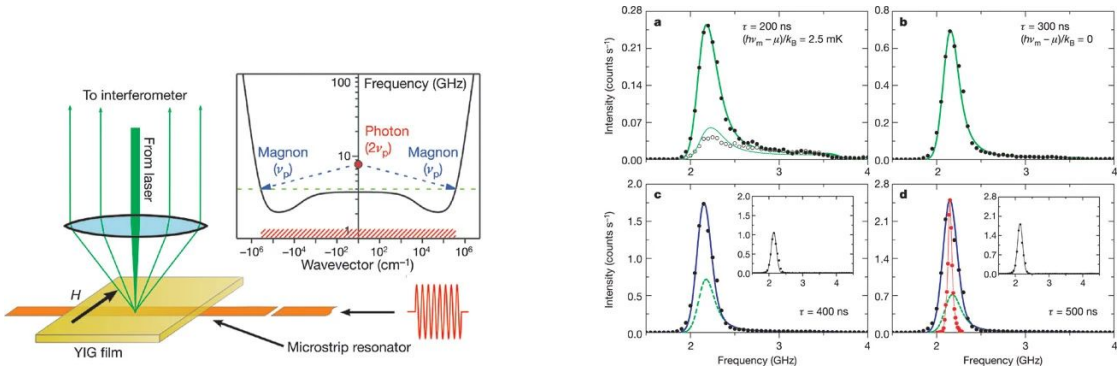

Fig. 5.11 Left: Experimental setup to observe a magnon BEC in quasi-equilibrium. A microwave is applied through a strip line. It excites a number of low energy magnons through a parametric process shown in the inset. A laser beam is applied for measurement of magnon distribution with the Brillouin scattering. Right: Time evolution of energy distribution of magnons after a microwave excitation pulse. Black closed dots are for 5.9 W of the power of microwave. Open ones are for 4 W. The red curve in (d) is with 50 MHz resolution measurement.

5.9.3 Ferromagnetic (Antiferromagnetic) resonance

As noted in Appendix 10A.1, **ferromagnetic resonance** (FMR) is a resonance absorption by the Larmor precession of a macroscopic magnetization. It can also be seen as the long wavelength limit of magnons. In an analysis of an experiment on a system with magnetic order, we need to consider complicated experimental details such as demagnetizing field, which was explained in the first lecture. Let us write the free energy of the system $\mathscr{F}$ as

$$\mathscr{F} = \sum_{\langle i,j \rangle} \lambda_{ij} \boldsymbol{M}_i \cdot \boldsymbol{M}_j - \sum_{i,j} \boldsymbol{M}_i \mathbf{K}_{i,j} \boldsymbol{M}_j - \sum_i \boldsymbol{M}_i \cdot \left(\boldsymbol{H} - \mathbf{N} \sum_j \boldsymbol{M}_j \right), \tag{5.103a}$$

$$= -\lambda \boldsymbol{M}^2 + \boldsymbol{M} \cdot \mathbf{K} \boldsymbol{M} - \boldsymbol{M} \cdot (\boldsymbol{H} - \mathbf{N} \boldsymbol{M}), \tag{5.103b}$$

[*1] Dimer magnetism is not so rare, but it often has a very high critical field of spin gap closing, that situation makes experiments difficult.

where eq. (5.103a) is for a paramagnetic case, and eq. (5.103b) is for a ferromagnetic case with macroscopic magnetization. Though we are mainly using $\boldsymbol{B}$, which is mostly used in experiments, here, we use $\boldsymbol{H}$ to avoid confusion due to existence of a spontaneous magnetization. In the rhs of eq. (5.103a), the first term is the exchange interaction, the second: magnetic anisotropy, the third: Zeeman with demagnetizing effect ($\mathbf{N}$ (tensor), Sec. 1.2.2). Then the effective magnetic field working on $\boldsymbol{M}$ other than $\boldsymbol{H}$ is

$$\boldsymbol{H}_{\text{eff}} = \lambda \boldsymbol{M} - (\boldsymbol{K} + \boldsymbol{N})\boldsymbol{M}, \tag{5.104}$$

in which $\lambda \boldsymbol{M}$ can be dropped from the equation of motion because it is always parallel to $\boldsymbol{M}$. Then the equation of motion is then given by

$$\frac{1}{\gamma}\frac{d\boldsymbol{M}}{dt} = \boldsymbol{M} \times (\boldsymbol{H} - \mathbf{K}\boldsymbol{M} - \mathbf{N}\boldsymbol{M}), \tag{5.105}$$

where γ is the gyromagnetic ratio. This becomes a very complicated form in general experiments. However, in case that the sample shape has an axis of rotational symmetry taken along the easy axis of magnetization, and the external field is also along the easy axis, the resonance frequency ω is given by

$$\omega = \gamma\sqrt{(H + (K_x - K_z + N_x - N_z)M)(H + (K_y - K_z + N_y - N_z)M)}, \tag{5.106}$$

where z-axis is taken along the field.

Also in antiferromagnets, ferrimagnets, similar resonances take place due to the Larmor precession of macroscopic magnetization. In order to treat the situation we consider the resonance conditions of magnetizations $\boldsymbol{M}_1$, $\boldsymbol{M}_2$ [*2] of magnetic sublattices. The effective fields $\boldsymbol{H}_{\text{eff1}}$, $\boldsymbol{H}_{\text{eff2}}$ for $\boldsymbol{M}_1$, $\boldsymbol{M}_2$ respectively, are

$$\boldsymbol{H}_{\text{eff1}} = -\lambda \boldsymbol{M}_2 + \mathbf{K}_{11}\boldsymbol{M}_1 + \mathbf{K}_{12}\boldsymbol{M}_2 + \mathbf{N}(\boldsymbol{M}_1 + \boldsymbol{M}_2) \tag{5.107a}$$

$$\boldsymbol{H}_{\text{eff2}} = -\lambda \boldsymbol{M}_1 + \mathbf{K}_{21}\boldsymbol{M}_1 + \mathbf{K}_{22}\boldsymbol{M}_2 + \mathbf{N}(\boldsymbol{M}_1 + \boldsymbol{M}_2). \tag{5.107b}$$

In antiferromagnetic case, because $\boldsymbol{M}_1 = -\boldsymbol{M}_2$, the last terms in the two equations of eq. (5.107) vanish. And in the tensor of anisotropy, the followings hold.

$$\mathbf{K}_{11} = \mathbf{K}_{22}, \quad \mathbf{K}_{12} = \mathbf{K}_{21}. \tag{5.108}$$

If the anisotropy is uniaxial, the anisotropic energy $\mathscr{F}_{\text{A}}$ is

$$\mathscr{F}_{\text{A}} = -\frac{K_1}{2}(\cos^2\theta_1 + \cos^2\theta_2), \tag{5.109}$$

where θ_i are the angles between the primary axis and the magnetization $\boldsymbol{M}_i$. The anisotropy tensor is

$$K_{zz} = -\frac{K_1}{|\boldsymbol{M}_1|}, \quad (\text{others}) = 0, \tag{5.110}$$

where the primary axis is taken to z. The resonance conditions, then, are given as follows[2].

$$\frac{\omega_\pm}{\gamma} = \sqrt{2\lambda K_1 + (K_1/|M_1|)^2} \pm H, \qquad H \le H_{\text{c}}, \tag{5.111a}$$

$$\frac{\omega_+}{\gamma} = \sqrt{B^2 - 2\lambda K_1} \qquad H > H_{\text{c}}. \tag{5.111b}$$

Here, $H_{\text{c}} = \sqrt{2\lambda K_1}$ is the critical field of the spin-flop transition. When the anisotropic field $K_1/|\boldsymbol{M}_1|$ is much smaller than the exchange field $\lambda|\boldsymbol{M}_1|$, we can write the condition as

$$\frac{\omega_\pm}{\gamma} = \sqrt{2\lambda K_1} \pm H, \quad H \le H_{\text{c}}. \tag{5.112}$$

In the case of ferrimagnet, the complexities are unavoidable. Refer to [3, 4], if necessary.

[*2] So far we have used $\boldsymbol{M}_{\text{A}}$, $\boldsymbol{M}_{\text{B}}$, which way makes the subscripts awkward. We will use 1, 2 instead, for a while.

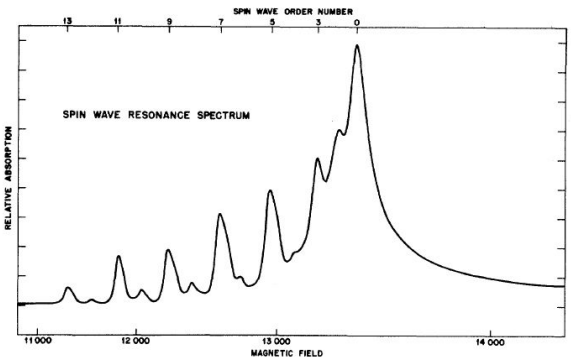

Fig. 5.12 Spin wave resonance (Walker mode) observed in a permalloy film with thickness of 560 nm. The horizontal axis is magnetic field in unit of Oe. The vertical axis is absorption strength for microwave of frequency 8.89 GHz. The boundary condition leaded to the observation of the odd number modes from n=7 to 13 in eq. (5.114). The absorption lines at higher fields were not counted by some reason. From [5].

5.9.4 Spin wave resonance

(A)FMR is a resonance of total magnetization and can be seen as the limit of long wavelength. For thin film samples, standing wave modes perpendicular to the films are expected. The spectra of such standing wave mode is discrete. Those modes are also called **Walker modes** [*3]. From the simplest dispersion relation (5.81) obtained in Secs.5.8.2, 5.8.3, the resonance frequency is

$$\omega_k = \gamma H + \frac{2SJ}{\hbar}(ka)^2. \tag{5.113}$$

Here γ is the gyromagnetic ratio defined for H- representation.

Now, we consider the case that spins are fixed at the surfaces due to some strong magnetic anisotropy. From the boundary condition that the surfaces should be the nodes, the condition of resonance is

$$k = \frac{n\pi}{L}, \quad n = 1, 2, \cdots, \tag{5.114}$$

where L is the film thickness[6]. In a comparatively simple case as the easy axis is perpendicular to the film, various information can be obtained by, e.g. changing the film thickness. This is called **spin wave resonance** (**magnon resonance**). Figure 5.12 shows an example of spectrum. In the era of theoretical proposal and experimental confirmation, the method was frequently used for direct measurement of exchange interaction coefficient J. In recent nano-sized magnets, various confinement shapes have been tested. In many cases, the analysis needs the help of numerical calculations[7].

A resonant motion of macroscopic magnetization can be viewed as a condensate of magnons and this can exists because they are bosons. The phenomenon is, however, different from the BEC, in which the boson system spontaneously condensates breaking the gauge symmetry. On the other hands, resultant phenomena are similar in that many quanta occupy a single quantum state and the condensate behaves as a classical wave. This is, for example, the same for electromagnetic waves, which we are using for communication in daily life. There is no problem in treating these as classical waves, but quantum mechanically, multiple photons are occupying a single quantum state and it is not too much to say they are forming (near) coherent states. This has long been pointed out, e.g., in introductory publications on quantum mechanics[8]. Accordingly, the fact that such condensates of magnons can be created at room temperatures with non-adiabatic methods, is not very surprising. But then, magnon condensate also shows quantum phenomena like quantum tunneling of macroscopic magnetization, or quantum entanglement with photons, and so on. This means we need to be aware of what phenomena we are observing in studying them.

In the lecture, we will see some examples of classical wavy manner in magnon condensates.

[*3] Because the wave equation has the form of Walker equation.

5.10 Renormalization group and scaling theory of phase transitions

Let us be back to general theory of phase transition. Magnetic phase transitions are the best subject for guessing the concept of scaling.

A huge number of review articles and books have been published on the renormalization group (RG), which is a major theme for physics as a whole. Anyone interested in this issue should read, after all, a bible review[9] in this area. As mentioned in the title of this paper, the original motive for developing the renormalization group theory is the Kondo effect discovered in dilute magnetic alloys and the Kondo problem (this is also a major subject for whole physics) raised by Kondo's theory. In that sense, the RG is closely related to the magnetism. I recommend as a basic textbook ref. [10, 11], as a standard for experts ref. [12] [*4]. Among the commentaries on the Internet, ref. [13] seems to be careful and easy to understand. Also a review ref. [14] can be taken in arXiv. In the lecture I would give a super digest explanation.

5.10.1 Correlation function

For the scaling and RG, an important concept is the correlation function. So far we considered the case the magnetization is uniform in space. Even the fluctuations, considered as magnons, have spatially uniform amplitude. However in reality, as we observed in the movie of numerical calculation of Ising model, with lowering the temperature, orderings in spins locally appear (spin **cluster**), the size of which grows on approaching the critical point. If we observe the phenomenon from the view point of spatial fluctuation and in the Fourier space, the characteristic wavelength of fluctuation grows to diverge at the critical point.

Let us treat the above process as follows. We consider a local magnetization density m, weakly depending on $\boldsymbol{r}$ as $m(\boldsymbol{r})$. Let m be a local **order parameter**. By the same logic in Sec. 5.2.1, the free energy density f at $\boldsymbol{r}$ is

$$f(m(\boldsymbol{r}, \nabla m(\boldsymbol{r})) = f_0 + \frac{a}{2}m^2 + \frac{b}{4}m^4 + c|\nabla m|^2 - hm, \tag{5.115}$$

where in the rhs, the argument $\boldsymbol{r}$ is omitted. h is the local field. Free energy $\mathscr{F}$ is represented in the functional form as

$$\mathscr{F}\{m(\boldsymbol{r})\} = \int_V d\boldsymbol{r}' f(m(\boldsymbol{r}'), \nabla' m(\boldsymbol{r}')). \tag{5.116}$$

The partition function is

$$Z = \int \mathcal{D}m(\boldsymbol{r}) \exp\left[-\frac{\mathscr{F}\{m(\boldsymbol{r})\}}{k_{\mathrm{B}}T}\right]. \tag{5.117}$$

Here $\mathcal{D}m(\boldsymbol{r})$ is a functional integral, which means taking the sum over all possible $m(\boldsymbol{r})$. This is a well known concept in the Feynman path integral[15, 16]. Because the probability density of realization of distribution $m(\boldsymbol{r})$ is

$$p\{m(\boldsymbol{r})\} = \frac{1}{Z}\exp\left[-\frac{\mathscr{F}\{m(\boldsymbol{r})\}}{k_{\mathrm{B}}T}\right], \tag{5.118}$$

the statistical average of a physical quantity A is given by

$$\langle A\rangle = \frac{1}{Z}\int \mathcal{D}m(\boldsymbol{r}) A \exp\left[-\frac{\mathscr{F}\{m(\boldsymbol{r})\}}{k_{\mathrm{B}}T}\right]. \tag{5.119}$$

Then as we did for eq/ (5.16), we assume the temperature dependences of a and b in eq. (5.115) as

$$a = \alpha(T - T_{\mathrm{C}}) \quad (\alpha > 0), \quad b = \text{const.}\ (> 0). \tag{5.120}$$

[*4] I recommend solving the problems. One of my friends in particle field solved all of these. I myself tried some, but felt difficult.

c is also assumed to be constant. We write the **correlation function** of fluctuation in the order parameter as

$$g(\boldsymbol{r}) = \langle (m(0) - \langle m(0) \rangle)(m(\boldsymbol{r}) - \langle m(\boldsymbol{r}) \rangle) \rangle = \langle m(0) m(\boldsymbol{r}) \rangle - \langle m(0) \rangle \langle m(\boldsymbol{r}) \rangle . \tag{5.121}$$

In the region $T > T_{\mathrm{C}}$, the average of the order parameter itself is zero, thus the second term is zero. The Fourier expansion representation of $m(\boldsymbol{r})$ is

$$m(\boldsymbol{r}) = \frac{1}{\sqrt{V}} \sum_{\boldsymbol{k}} m_{\boldsymbol{k}} \exp(i\boldsymbol{k} \cdot \boldsymbol{r}), \tag{5.122}$$

where V is the system volume. Because $m(\boldsymbol{r})$ is real, $m_{-\boldsymbol{k}} = m_{\boldsymbol{k}}^*$ should hold. In $\langle m(0) m(\boldsymbol{r}) \rangle$, the term $\exp(\pm i\boldsymbol{k} \cdot \boldsymbol{r})$ can be expressed as

$$(m_k + m_{-k})(m_k e^{ikr} + m_{-k} e^{-ikr}) = 2|m_k|^2 e^{-ikr} + 2|m_{-k}|^2 e^{ikr}.$$

By using this and from the translational symmetry of the system, we write

$$g(\boldsymbol{r}) = \frac{1}{V} \sum_{\boldsymbol{k}} \langle |m_{\boldsymbol{k}}|^2 \rangle \exp(-i\boldsymbol{k} \cdot \boldsymbol{r}). \tag{5.123}$$

Then we obtain

$$\mathscr{F} = V f_0 + \sum_{\boldsymbol{k}} |m_{\boldsymbol{k}}|^2 \left(\frac{a}{2} + ck^2 \right) + \frac{b}{4V} \sum_{\boldsymbol{k}_1 + \boldsymbol{k}_2 + \boldsymbol{k}_3 + \boldsymbol{k}_4 = \boldsymbol{0}} m_{\boldsymbol{k}_1} m_{\boldsymbol{k}_2} m_{\boldsymbol{k}_3} m_{\boldsymbol{k}_4}, \tag{5.124}$$

where we take the zero field limit $h \to 0$. In the region $T > T_{\mathrm{C}}$, we can ignore the last 4-th order term in (5.124). The weight function (5.118) now gives the Gaussian distribution

$$\frac{1}{Z} \exp \left[-\frac{2}{k_{\mathrm{B}} T} \sum_{\boldsymbol{k}}{}' \left(\frac{a}{2} + ck^2 \right) (m_{\boldsymbol{k}}^{(\mathrm{r})2} + m_{\boldsymbol{k}}^{(\mathrm{i})2}) \right], \tag{5.125}$$

where we drop the first constant term in eq. (5.124). In the last parentheses, the term $|m_{\boldsymbol{k}}|^2$ is written in a real-imaginary-separated form as

$$\mathrm{Re}[m_{\boldsymbol{k}}] = m_{\boldsymbol{k}}^{(\mathrm{r})}, \quad \mathrm{Im}[m_{\boldsymbol{k}}] = m_{\boldsymbol{k}}^{(\mathrm{i})}.$$

The symbol $\sum_{\boldsymbol{k}}'$ means taking the sum over independent $\boldsymbol{k}$, which give a half of the sum in (5.124). Hence the factor 2 is given. From the above we can write the average of $|m_{\boldsymbol{k}}|^2$ as

$$\langle |m_{\boldsymbol{k}}|^2 \rangle = \frac{k_{\mathrm{B}} T}{a + 2ck^2}. \tag{5.126}$$

Substituting the above into eq. (5.123), $g(\boldsymbol{r})$ is expressed as

$$g(\boldsymbol{r}) = \frac{1}{V} \sum_{\boldsymbol{k}}{}' \frac{k_{\mathrm{B}} T}{a + 2ck^2} e^{-i\boldsymbol{k} \cdot \boldsymbol{r}} = k_{\mathrm{B}} T \int_0^\infty \frac{e^{-i\boldsymbol{k} \cdot \boldsymbol{r}}}{2ck^2 + a} \frac{d^3 k}{(2\pi)^3} = \frac{k_{\mathrm{B}} T}{8\pi d} \frac{\exp(-r/\xi)}{r}, \quad \xi = \sqrt{\frac{2c}{a}}. \tag{5.127}$$

The result indicates that the correlation is damped exponentially on the distance in the region $T > T_{\mathrm{C}}$. ξ in eq. (5.127) is called **correlation length**. Considering the temperature dependence in eq. (5.120), the correlation length varies as $(T - T_{\mathrm{C}})^{1/2}$ in the vicinity of T_{C}. While ξ diverges at T_{C}, the correlation of fluctuation decrease with the distance as $g(r) \propto r^{-1}$.

In the region $T < T_{\mathrm{C}}$, a long range order appears resulting in the difference between the correlation of fluctuation (5.121) and that of the order parameter itself, that is

$$\tilde{g}(\boldsymbol{r}) = \langle m(0) m(\boldsymbol{r}) \rangle . \tag{5.128}$$

This $\tilde{g}(\boldsymbol{r})$ is thus finite for $r \to \infty$. This is equivalent with the appearance of **long range order**[17]. As for $g(\boldsymbol{r})$, it goes zero at $r \to \infty$.

5.10.2 Scaling relations

We introduced the concept of critical exponent in Sec. 5.3. In introducing the scaling relations, we review the "routine" notations. The relevant parameters are the temperature $t \equiv (T - T_{\rm C})/T_{\rm C}$, and the external magnetic field h. The behaviors in the critical region are

$$\begin{aligned} \text{Specific heat :} \quad & C \sim |t|^{-\alpha}, \\ \text{Magnetization (order parameter) :} \quad & m \sim |t|^{\beta} \quad (t < 0) \\ & m \sim h^{1/\delta} \quad (t = 0), \\ \text{Susceptibility :} \quad & \chi \sim |t|^{-\gamma}, \\ \text{Correlation length :} \quad & \xi \sim |t|^{-\nu}. \end{aligned}$$

As we saw in the previous subsection, these anomalous behaviors around the critical point $t = h = 0$, originate from the divergence of correlation length, namely the divergence of the size of clusters with a short range order.

The correlation function of fluctuation (5.121) of the system with spatial dimension of d is generally written as

$$g(\boldsymbol{r}) \sim \frac{\exp(-r/\xi)}{r^{d-2+\eta}}. \tag{5.129}$$

Here η is one of the critical exponents and in eq. (5.127) (i.e., the GL theory) $\eta = 0$. The GL theory also gives

$$\alpha = 0, \quad \beta = 1/2, \quad \gamma = 1, \quad \delta = 3, \quad \nu = 1/2, \quad \eta = 0. \tag{5.130}$$

The GL theory is a phenomenology. The critical exponents depend on the "universality" of the system as we already saw.

These critical exponents have the following relations.

$$\gamma = (2 - \eta)\nu, \tag{5.131a}$$
$$\alpha + 2\beta + \gamma = 2, \tag{5.131b}$$
$$\beta + \gamma = \beta\delta. \tag{5.131c}$$

Among them, eq. (5.131b) and eq. (5.131c) are called **scaling relation**, which can be derived from the **scaling ansatz** explained in the following. We have taken t and h as the relevant parameters of the transition, but the ansatz tells the behavior of the system in the vicinity of transition is determined by single relevant parameter $h/|t|^{\Delta}$. Here Δ is called **gap exponent**.

We assume that the anomalous part of the free energy f_s can be expressed with the use of a function $f_{\pm}(x)$

$$f_s \sim |t|^{2-\alpha} f_{\pm}\left(\frac{h}{|t|^{\Delta}}\right), \tag{5.132}$$

around the critical point. $\pm$ in $f_{\pm}$ correspond to $T \gtrless T_{\rm C}$. For $h = 0$, t can move without affecting $h/|t|^{\Delta}$. The factor $|t|^{2-\alpha}$ is then attached to have the consistency with the specific heat. Now the magnetization and the susceptibility are

$$m(h = 0) \sim -\frac{\partial f_s}{\partial h} \sim |t|^{2-\alpha-\Delta} f'_{\pm}(0) \sim |t|^{\beta} \quad (t < 0) \tag{5.133}$$
$$\chi \sim -\frac{\partial^2 f}{\partial h^2} \sim |t|^{2-\alpha-2\Delta} f''_{\pm}(0) \sim |t|^{-\gamma}. \tag{5.134}$$

These lead to the relations

$$\beta = 2 - \alpha - \Delta \tag{5.135}$$
$$-\gamma = 2 - \alpha - 2\Delta. \tag{5.136}$$

Then erasing

$$\Delta = \beta + \gamma \tag{5.137}$$

from the above, a scaling relation (5.131b) is obtained.

Next to see the behavior of magnetization at $t = 0$, we need to explore the asymptotic behavior of $f'_\pm$ for $h/t^\Delta \to \infty$. We assume the asymptotic form as

$$f'_\pm(x) \sim x^{\lambda_\pm} \quad (x \to \infty). \tag{5.138}$$

Then the asymptotic behavior of eq. (5.133) is

$$m \sim |t|^\beta f'_\pm \left(\frac{h}{|t|^\Delta} \right) \sim \frac{h^{\lambda_\pm}}{|t|^{\Delta\lambda_\pm - \beta}}. \tag{5.139}$$

For m to be finite for $t \to 0$,

$$\lambda_\pm = \frac{\beta}{\Delta} = \frac{\beta}{\beta + \gamma}. \tag{5.140}$$

From this relation and the relation and the definition of the critical exponent $m \sim h^{1/\delta}$,

$$\delta = \frac{\beta + \gamma}{\beta}, \tag{5.141}$$

which is eq. (5.131c). There is also a relation

$$2 - \alpha = d\nu, \tag{5.142}$$

with the spatial dimension d, and is called hyperscaling relation.

5.10.3 Renormalization group

As approaching the critical point, the correlation length of fluctuation ξ gets longer. Within the space of this length, some order is growing. Taking a distance x shorter than ξ ($1 < x \ll \xi$), we can assume that the system is uniform in a space with a size of x. We thus average physical quantities within the size x and then the unit of length is changed to x (i.e., $x \mapsto 1$). This is called coarse graining. With this operation, the correlation length is transformed to ξ/x and the system looks being drew apart from the critical point. Similarly, the parameters of the system get various modifications by this operation. This operation is called **renormalization group (RG) transformation** with scaling factor x.

Let $\mathcal{R}(x)$ be such an operation, then, e.g, the transform of $\mathscr{H} \to \mathscr{H}'$ can be written as

$$\mathscr{H}' = \mathcal{R}(x)\mathscr{H}. \tag{5.143}$$

Sequential operation of $\mathcal{R}(x)$ and $\mathcal{R}(x')$ is the same as a single RG transform with scaling factor of xx'. That is

$$\mathcal{R}(x')\mathcal{R}(x) = \mathcal{R}(x'x). \tag{5.144}$$

The RG transformation thus fulfils the associativity forming a semigroup. It is called then **renormalization group**. Generally there is no inverse transformation from once coarse-grained system to the original fine-grained system. Hence a set of such transformations is not a group but semigroup.

Figure 5.13(a) show an example of an Ising model on a two-dimensional square lattice, in which four spins are averaged into one as

$$s_q = \frac{1}{4} \sum_i s_{qi}. \tag{5.145}$$

Then a new lattice in Fig. 5.13(b) appears. The scaling factor is $\sqrt{4} = 2$. The averaging makes the spins to be able to take the value of ± 1, and the model is no longer an Ising model. Also the range of interaction is modified. Accordingly, with repetition of RG transformation, the system moves in the parameter(s) space. The invariants with RG transformation are the symmetry of the order parameter and the spatial dimension. The parameter(s) space is then characterized by them.

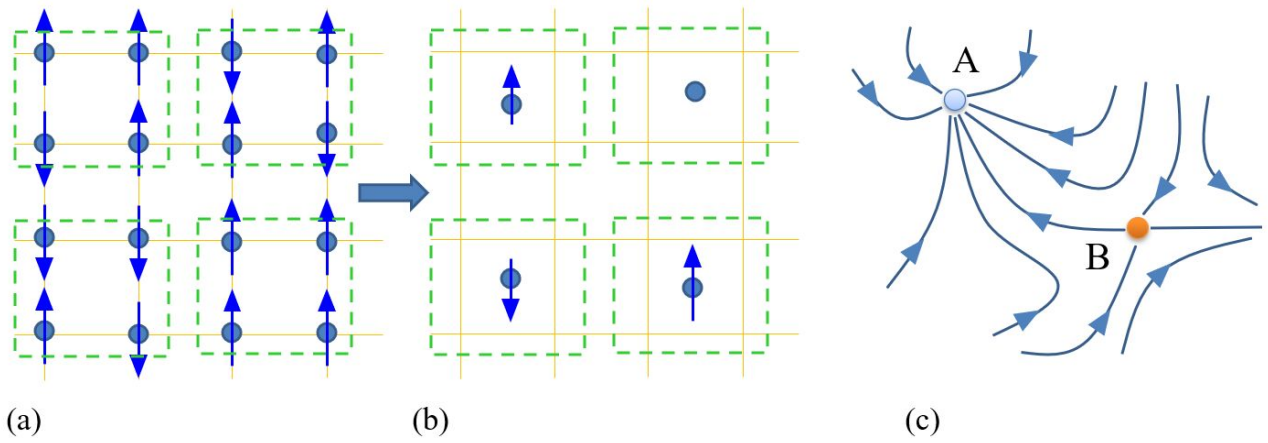

Fig. 5.13 (a) Illustration of an Ising model on two-dimensional square lattice. (b) Schematically shows a renormalization group transformation of averaging four spins in (a) as a single spin. (c) Schematic illustration of a flow diagram. A is a stable fixed point. B is an unstable fixed point.

Now we take the scaling factor as a continuous variable. Then the system transitions in the parameter space become continuous. Figure 5.13(c) shows an example of such continuous "flows" of system in parameter space by RG transformation. This kind of diagram is called **flow diagram**. If a system is in the high temperature side of the critical temperature at the starting point, the RG transformation drives it to the completely disordered state. If the starting point is in the opposite lower side of T_{C} ($t = 0$), it will transition to the perfectly ordered state. Perfectly ordered/disordered states are invariant for RG transformation, hence they form fixed points in the flow diagram as illustrated in Fig. 5.13(c). They are called stable fixed points, an example of which is indicated as A in Fig. 5.13(c). They collect the flow lines. On the other hand, just on the critical point, the correlation length of fluctuation diverges and the system on it does not change with RG transformation. Therefore the critical point is a fixed point. However, an infinitesimally small shift in the parameter causes repelling of flow lines from the critical point. Hence it is called unstable fixed point. In Fig. 5.13(c), B is an example of such an unstable fixed point.

5.10.4 Derivation of scaling ansatz

We again take t (temperature) and h (magnetic field) as the relevant parameters of transition. We write a RG transformation with a scale factor x as

$$t' = g_1^{(x)}(t, h), \tag{5.146a}$$
$$h' = g_2^{(x)}(t, h). \tag{5.146b}$$

In the vicinity of the fixed point $t = h = 0$ (critical point), we try to expand the above in the form

$$\begin{aligned} t' &\simeq \Lambda_{11}(x)t + \Lambda_{21}(x)h, \\ h' &\simeq \Lambda_{21}(x)t + \Lambda_{22}(x)h. \end{aligned} \tag{5.147}$$

There is no constant (0-th order) term because it is a fixed point. We further know that there is no linear coupling between t and h because the sign of h is reversed with reversing the sign of the order parameter while t does not change with that. Namely $\Lambda_{12}(x) = \Lambda_{21}(x) = 0$. Therefore the association law (5.144) gives

$$(\Lambda_{11}(x))^n = \Lambda_{11}(x^n), \quad (\Lambda_{22}(x))^n = \Lambda_{22}(x^n). \tag{5.148}$$

This should hold for any natural number n and any x (> 1). This means $\Lambda_{11}(x)$ and $\Lambda_{22}(x)$ are power functions of x.

$$\Lambda_{11}(x) = x^{\lambda_1}, \quad \Lambda_{22}(x) = x^{\lambda_2}. \tag{5.149}$$

Now we apply a RG transform with scaling factor x, n-times on a system that has the starting point at (t, h). We assume the final state temperature $t_0 = x^{n\lambda_1} t$ is far enough from the critical point. Because the correlation length of the fluctuation is

$$\frac{\xi(t)}{\xi(t_0)} = x^n = \left(\frac{t}{t_0}\right)^{-1/\lambda_1}, \tag{5.150}$$

and from the critical exponent definition $\xi \sim |t|^{-\nu}$, we obtaine $\nu = \lambda_1^{-1}$.

On the other hand in d-dimensional system, the free energy density $f(t, h)$ becomes x^d times by the RG transformation. Therefore

$$x^{nd} f(t, h) = f(x^{n\lambda_1} t, x^{n\lambda_2} h) = f(t_0, (t/t_0)^{-\lambda_2/\lambda_1} h). \tag{5.151}$$

We see t_0 as a constant, then with an appropriate function $f_\pm(x)$ we write

$$f(t, h) = t^{d/\lambda_1} f_\pm(t^{-\lambda_2/\lambda_1} h) = t^{d\nu} f_\pm\left(\frac{h}{t^\Delta}\right) \quad \Delta = \frac{\lambda_2}{\lambda_1}. \tag{5.152}$$

This is showing the scaling ansatz.

Chapter 6

Magnetism of itinerant electrons

The mechanism of ferromagnetism in common metals such as iron, cobalt, and nickel is thought to be significantly different from what we have seen so far.

References

[1] Evgeny Y. Tsymbal and Žutić Igor, editors. *Spintronics Handbook, Second Edition: Spin Transport and Magnetism: Volume One: Metallic Spintronics (Spintronics Handbook: Spin Transport and Magnetism Book 1) (English Edition)*. CRC Press, 5 2019.

[2] T. Nagamiya, K. Yosida, and R. Kubo. Antiferromagnetism. *Advances in Physics*, Vol. 4, No. 13, pp. 1–112, January 1955. Over 100 pages review.

[3] Roald K. Wangsness. Magnetic resonance in ferrimagnetics. *Phys. Rev.*, Vol. 93, pp. 68–71, Jan 1954.

[4] Roald K. Wangsness. Ferrimagnetic resonance and some related effects. *American Journal of Physics*, Vol. 24, No. 2, pp. 60–66, February 1956.

[5] M. H. Seavey and P. E. Tannenwald. Direct observation of spin-wave resonance. *Phys. Rev. Lett.*, Vol. 1, pp. 168–169, Sep 1958.

[6] C. Kittel and Conyers Herring. Effect of exchange interaction on ferromagnetic microwave resonance absorption. *Phys. Rev.*, Vol. 77, pp. 725–726, Mar 1950.

[7] Sergej O. Demokritov, editor. *Spin Wave Confinement: Propagating Waves, Second Edition (English Edition)*. Jenny Stanford Publishing, 9 2017.

[8] 中嶋貞雄. 量子の世界　新版 UP 選書. 東京大学出版会, 2 1975.

[9] Kenneth G. Wilson. The renormalization group: Critical phenomena and the kondo problem. *Rev. Mod. Phys.*, Vol. 47, pp. 773–840, Oct 1975.

[10] 西森秀稔. 相転移・臨界現象の統計物理学 新物理学シリーズ. 培風館, 11 2005.

[11] Hidetoshi Nishimori and Gerardo Ortiz. *Elements of Phase Transitions and Critical Phenomena (Oxford Graduate Texts) (English Edition)*. OUP Oxford, 12 2010.

[12] Daniel J. Amit and Victor Martin-mayor. *Field Theory, the Renormalization Group, And Critical Phenomena: Graphs To Computers*. World Scientific Pub Co Inc, 6 2005.

[13] 大谷聡. 統計力学 i –臨界現象と繰り込み群–, 2022. http://aries.phys.cst.nihon-u.ac.jp/~ohya/stat-mech/main.pdf.

[14] Andrea Pelissetto and Ettore Vicari. Critical phenomena and renormalization-group theory. *Physics Reports*, Vol. 368, No. 6, pp. 549–727, October 2002. available in arXiv: https://doi.org/10.48550/arXiv.cond-mat/0012164.

[15] Richard P. Feynman, Albert R. Hibbs, and Daniel F. Styer. *Quantum Mechanics and Path Integrals: Emended Edition (Dover Books on Physics)*. Dover Publications, 7 2010.

[16] Richard P. Feynman. *Statistical Mechanics: A Set Of Lectures (Frontiers in Physics)*. CRC Press, 3 1998.

[17] Tohru Koma and Hal Tasaki. Symmetry breaking and finite-size effects in quantum many-body systems. *Journal of Statistical Physics*, Vol. 76, No. 3-4, pp. 745–803, August 1994.

Chapter 6
Magnetism of Itinerant Electrons

In insulators, the following picture is expected to describe the magnetism: the spins localized at the lattice point cause magnetism through various spin-to-spin interactions. Common ferromagnetic metals like iron, cobalt, and nickel are supposed to have largely different mechanism from the above. Namely, electrons migrating in crystals (itinerant electrons) have their spins aligned partially due to the correlation effect, which phenomenon may generate the ferromagnetism. When the correlation effect is not very strong and the system is paramagnetic, such itinerant electron systems can be treated within the Landau's Fermi liquid theory[1] as mentioned in Ch. 3. On the other hand, the correlation is so strong that a ferromagnetism appears, the difficulties in theories increase largely. It was not easy for theoretical models to explain such types of ferromagnetism to the level in which the theories can be comparable with experiments. Including such difficulties, we would like to review the present understandings and open questions in the last three weeks.

6.1 Hartree-Fock approximation of electron gas

We would have a brief look at the difficulty to have a realistic ferromagnetism in the model of electron gas. We use the simplest Hartree-Fock approximation (not very simple actually) of electron correlation.

6.1.1 Hartree-Fock approximation

Though you are already familiar with **Hartee-Fock (HF) approximation**, we will shortly review it here (we will not use such details in analysis of electron gas here). We consider an N-particle system, in which the particles occupy single-particle wavefunctions

$$\varphi_{k_1}, \varphi_{k_2}, \cdots, \varphi_{k_N}. \tag{6.1}$$

The many body state of this N-body system can be expressed by the Slater determinant:

$$\Phi = \frac{1}{\sqrt{N!}} \begin{vmatrix} \varphi_{k_1}(x_1) & \cdots & \varphi_{k_N}(x_1) \\ \vdots & \ddots & \vdots \\ \varphi_{k_1}(x_N) & \cdots & \varphi_{k_N}(x_N) \end{vmatrix}, \tag{6.2}$$

which satisfies the ferminon particle exchange statistics. x_i is a general coordinate, which contains all of single particle freedoms. We write the Hamiltonian in the form

$$\mathscr{H} = \sum_{j=1}^{N} h(x_j) + \sum_{\langle i,j \rangle} v(x_i, x_j), \tag{6.3}$$

where h is a single-particle Hamiltonian, v is a two-body interaction. In the HF approximation, we calculate the expectation value

$$\mathcal{W} = \langle \Phi | \mathscr{H} | \Phi \rangle , \tag{6.4}$$

and look for the set $\{\varphi_{k_j}\}$ that minimize $\mathcal{W}$ with a variational method.

Here we use the ket representation $|k_j\rangle$ for φ_{k_j}. We assume the orthonormal basis condition:

$$\langle k_i | k_j \rangle = \delta_{ij}. \tag{6.5}$$

In this representation, $\mathcal{W}$ is written as

$$\mathcal{W} = \sum_{j=1}^{N} \langle k_j | h | k_j \rangle + \sum_{\langle i,j \rangle} [\langle k_i k_j | v | k_i k_j \rangle - \langle k_i k_j | v | k_j k_i \rangle]. \tag{6.6}$$

In the rhs, in the term $\langle k_i k_j | v | k_i k_j \rangle$, the two particles interact in the same order but in $\langle k_i k_j | v | k_j k_i \rangle$, the two particles exchange their positions during the interaction. The former is called the direct integral, the latter is called the exchange integral (exchange interaction). In the following, we adopt the Lagrange multiplier method to minimize the energy of the system (6.6) under the constraint of (6.5). That is, we consider the quantity

$$\mathcal{W} - \sum_{\langle i,j \rangle} \lambda_{ij} \langle k_i | k_j \rangle , \tag{6.7}$$

which should be minimized. In order for that, we consider the condition that the variations of the above quantity with $\{\varphi^*_{k_j}\}$ are zero, which can be expressed as

$$h\varphi_{k_j} + \sum_{i=1} [\langle k_i | v | k_i \rangle \varphi_{k_j} - \langle k_i | v | k_j \rangle \varphi_{k_i}] = \sum_{i=1}^{N} \lambda_{ij} \varphi_{k_i}. \tag{6.8}$$

Here we define a single-body density matrix as

$$\rho(x, x') = \sum_{i=1}^{N} \varphi^*_{k_i}(x) \varphi_{k_i}(x'), \tag{6.9}$$

with which we further define v_{eff} and A as

$$v_{\text{eff}}(x) = \int dx' v(x, x') \rho(x', x'), \quad A(x)\varphi(x) = \int dx' v(x, x') \varphi(x') \rho(x', x). \tag{6.10}$$

Then eq. (6.8) is written as

$$[h(x) + v_{\text{eff}}(x) - A(x)] \varphi_{k_j}(x) = \sum_{i=1}^{N} \lambda_{ij} \varphi_{k_i}(x). \tag{6.11}$$

In eq. (6.11), the Hermite operator given in $[\cdots]$ in the left hand side does not depend on the specific selection of k_j in the operand. Also the eigenfunctions are orthogonal to each other. Hence by taking φ_{k_j} as the eigenfunctions, we can write

$$[h(x) + v_{\text{eff}}(x) - A(x)] \varphi_{k_j}(x) = \epsilon_{k_j} \varphi_{k_j}(x). \tag{6.12}$$

Then we take N solutions in the ascending order from the lowest $\{\epsilon_{k_j}\}$. The Slater determinant of these N solutions is the ground state in the HF approximation. However, the operator in the $[\cdots]$ part also depends on $\{\epsilon_{k_j}\}$ (though not depends on specific selection of the operand), (6.12) should be solved self-consistently. Equation (6.12) is called **Hartree-Fock equation**. This is essentially the same as the self-consistent equation in the molecular field approximation of the Heisenberg model. To see how to proceed the calculation in more specific physical problems, or how to go beyond the HF approximation (e.g., taking the effect of higher order term into account), refer to textbooks on many-body problems (e.g., [2, 3, 4]).

6.1.2 Jellium model and ferromagnetism

Here we adopt **jellium model**, in which the lattice potential is approximated by a uniform background with a plus charge. And we consider a free electron system in the background. The ground state in the absence of electron mutual interaction is the state in which the Fermi sphere is filled up as

$$|\Psi\rangle = \prod_{E(\boldsymbol{k},\sigma)\le E_{\mathrm{F}}} c^\dagger_{\boldsymbol{k}\sigma}\,|0\rangle\,. \tag{6.13}$$

Next we write down the Hamiltonian in the presence of electron-electron interaction as

$$\mathscr{H} = \sum_{\boldsymbol{k},\sigma} \epsilon_{\boldsymbol{k}} c^\dagger_{\boldsymbol{k}\sigma} c_{\boldsymbol{k}\sigma} + \frac{1}{2V} \sum_{\boldsymbol{k},\boldsymbol{k}',\sigma,\sigma',\boldsymbol{q}\neq 0} v_{\boldsymbol{q}} c^\dagger_{\boldsymbol{k}+\boldsymbol{q},\sigma} c^\dagger_{\boldsymbol{k}'-\boldsymbol{q},\sigma'} c_{\boldsymbol{k}'\sigma} c_{\boldsymbol{k}\sigma}, \tag{6.14}$$

where V is the system volume, $\epsilon_{\boldsymbol{k}} = \hbar^2 k^2/2m$ and $v_{\boldsymbol{q}} = 4\pi e^2/q^2$. The Fermi wavenumber k_{F} is determined from the Fermi energy E_{F}, and the only parameter that characterizes the system is the averaged electron distance measured by Bohr radius a_{B}:

$$r_s \equiv \frac{1}{a_{\mathrm{B}}} \left[\frac{3}{4\pi(k_{\mathrm{F}}^3/3\pi^2)}\right]^{1/3}, \tag{6.15}$$

in the jellium model.

Because the system has spatially translational symmetry in the jellium model, plane waves are already the solutions of self-consistent HF equation (6.12), and then the residual procedure of the HF approximation is to minimize the energy of many-body state. The kinetic energy per single electron is

$$\epsilon_{\mathrm{ke}} = \frac{1}{N}\sum_{\boldsymbol{k}s} \epsilon_{\boldsymbol{k}} n_{\boldsymbol{k}s} = \frac{2V}{N}\int \frac{d^3k}{(2\pi)^3}\frac{\hbar^2k^2}{2m} n_k = \frac{3}{10}\frac{\hbar^2 k_{\mathrm{F}}^2}{m} = \frac{2.21}{r_s^2}\mathrm{Ry}, \tag{6.16}$$

where Ry=$\hbar^2/2ma_{\mathrm{B}}^2$=13.6 eV is the unit named "Rydberg," and is the binding energy of hydrogen atom. The Hartree term that corresponds to the direct integral is vanished by the charge neutral condition of jellium model. The exchange term, that is the expectation value of interaction between the states of exchanged particles. It is then

$$\epsilon_{\mathrm{ex}} = -\frac{1}{2NV}\sum_{\boldsymbol{k},\boldsymbol{q}\neq 0,s} v_{\boldsymbol{q}} \langle\psi| c_{\boldsymbol{k}+\boldsymbol{q},s} c_{\boldsymbol{k}+\boldsymbol{q},s} c^\dagger_{\boldsymbol{k}s} c_{\boldsymbol{k}s}|\psi\rangle = \frac{1}{2NV}\sum_{\boldsymbol{k}s} v_{\boldsymbol{q}} n_{\boldsymbol{k}+\boldsymbol{q}} n_{\boldsymbol{k}}, \tag{6.17}$$

per an electron. The summation can be carried out as an integral over $\boldsymbol{q}$ to be

$$\epsilon_{\mathrm{ex}} = -\frac{3e^2}{4}\frac{k_{\mathrm{F}}}{\pi} = -\frac{0.92}{r_s}\mathrm{Ry}. \tag{6.18}$$

Then the total Hartree-Fock energy is

$$\epsilon_{\mathrm{hf}} = \left(\frac{2.21}{r_s^2} - \frac{0.92}{r_s}\right)\mathrm{Ry}. \tag{6.19}$$

From eq. (6.16), the total kinetic energy of electrons per unit volume is

$$E_{\mathrm{ke}} = \frac{3}{10}\frac{\hbar^2 k_{\mathrm{F}}^2}{m}\frac{4\pi}{3}\left(\frac{k_{\mathrm{F}}}{2\pi}\right)^3 = \frac{\hbar^2 k_{\mathrm{F}}^5}{20\pi^2 m}. \tag{6.20}$$

Let $(k_{\mathrm{F}\uparrow}, n_\uparrow)$, $(k_{\mathrm{F}\downarrow}, n_\downarrow)$ be the Fermi wavenumber and the electron number of up and down spin states respectively. Then

$$E_{\mathrm{ke}}(p) = \frac{\hbar^2}{20\pi^2 m}(k_{\mathrm{F}\uparrow}^5 + k_{\mathrm{F}\downarrow}^5) = \frac{3(6\pi^2)^{2/3}\hbar^2}{10m}(n_\uparrow^{5/3} + n_\downarrow^{5/3}) = \frac{3(6\pi^2)^{2/3}\hbar^2}{10m}[p^{5/3} - (1-p)^{5/3}]n_0^{5/3}, \tag{6.21}$$

$$E_{\mathrm{ex}}(p) = -\frac{3e^2}{4}\left(\frac{6}{\pi}\right)^{1/3}(n_\uparrow^{4/3} + n_\downarrow^{4/3}) = -\frac{3e^2}{4}\left(\frac{6}{\pi}\right)^{1/3}[p^{4/3} - (1-p)^{4/3}]n_0^{4/3}. \tag{6.22}$$

Here because polarization $0.5 \leq p \leq 1$ is defined as $n_\uparrow = pn_0$, $n_\downarrow = (1-p)n_0$, $p = 1$ corresponds to perfect polarization, $p = 0.5$ corresponds to no polarization. Then let ΔE be

$$\Delta E = [E_{\mathrm{ke}}(1) + E_{\mathrm{ex}}(1)] - [E_{\mathrm{ke}}(0.5) + E_{\mathrm{ex}}(0.5)], \tag{6.23}$$

then if $\Delta E < 0$, the ground state is a spin-polarized ferromagnetic state. This condition can be calculated from the above and expressed with the average distance parameter defined in eq. (6.15), as

$$r_s > 5.4531. \tag{6.24}$$

However, we found several ordinary metals with $r_s \sim 5$. Hence the above criterion does not fit the reality.

6.1.3 Electron correlation

The above discrepancy should come from either overestimation of lowering in the Coulomb energy with avoiding each other between parallel spins, or that of the Coulomb repulsion energy between antiparallel spins. The latter seems to be more plausible because the itinerant electrons with antiparallel spins also should avoid each other to lower the Coulomb repulsion energy. That means, in the jellium model, the solution of antiparallel spins in HF (mean field) approximation is not good enough for discussion of ground state. We need to go for higher order approximation or to consider some different approximation. We here define **correlation energy** as the energy difference between the energy of true ground state and that of mean field approximation.

There exist various methods in the estimation of correlation energy. Figure 6.1 shows a phase diagram of charged fermion gas in the jellium model calculated by diffusion Monte-Carlo method[5]. The red line indicates spin-polarized gas and the ferromagnetism appears in the region that the red line lies below the blue broken line which indicates unpolarized gas. However as can be seen, r_s for the appearance of the ferromagnetism is around 70, which is too sparse for real metals. Around $r_s \sim 90$ the Wigner crystal state in which the electrons form a crystal and localize. This means if the correlation energy is correctly estimated, the ferromagnetism in common metallic ferromagnet like iron or nickel cannot be explained at all.

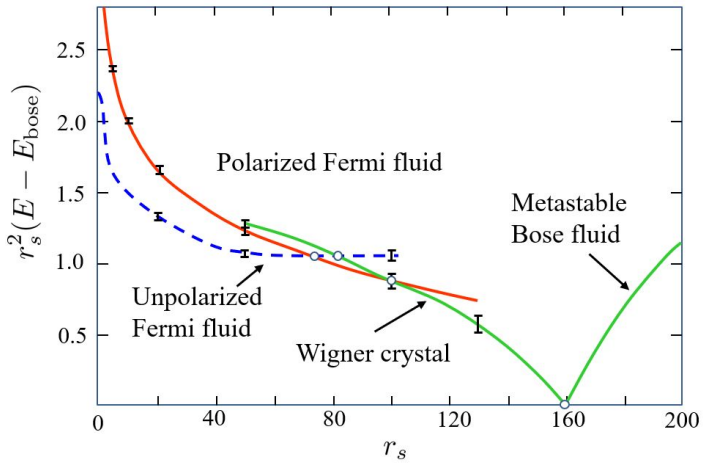

Fig. 6.1 Phase diagram of electron gas calculated by diffusion Monte-Carlo method. The energy origin (0) is taken to that of a bosonic system. The region where the red line lies lowest position should be ferromagnetic. From [5].

6.2 HF approximation in Hubbard model

The jellium model, not only in the mean field approximation, even with correct estimation of correlation energy, is far from the realistic explanation of ferromagnetism in metals. In the case of ferromagnets caused by double-exchange interaction, which we have seen in the previous chapter, the electrons hopping between local sites mediate ferromagnetic interaction between localized spins. Though the situation is different in the case of $3d$ transition metals, it can be a hint that the coexistence of localization and hopping can cause ferromagnetism in realistic conditions. Then we try to consider the Hubbard model introduced in Sec. 4.1.3.

6.2.1 Hubbard model for multiple site

We introduced two-site Hubbard model (sometimes referred to as Kanamori-Hubbard model) in Sec. 4.1.3. It is expected to describe from insulators, metals, ferromagnets and superconductors in spite of its compactness, and has been long used in theories. As we saw there, the long range part of the Coulomb interaction is ignored and the Coulomb repulsion only works between electrons in the same site (on-site interaction). On the other hand, the electrons hop between site i and site j with probability t_{ij}. The Hamiltonian for a general number of sites is

Hubbard Hamiltonian (1)

$$\mathscr{H} = \sum_{i,j,s} t_{ij} c_{is}^\dagger c_{js} + U \sum_i^N \hat{n}_{i\uparrow}\hat{n}_{i\downarrow}, \tag{6.25}$$

where s is the spin freedom. c_{is} satisfies the fermion commutation relation

$$\{c_{is}^\dagger, c_{is'}\} = \delta_{ij}\delta_{ss'}. \tag{6.26}$$

In the first hopping term, the annihilation operator c_{is} and hopping transition matrix element t_{ij} are Fourier-expanded as

$$c_{is} = \frac{1}{\sqrt{N}} \sum_{\boldsymbol{k}} e^{i\boldsymbol{R}_i\cdot\boldsymbol{k}} a_{\boldsymbol{k}s}, \quad t_{ij} = \frac{1}{N}\sum_{\boldsymbol{k}} \epsilon_{\boldsymbol{k}} e^{i\boldsymbol{k}\cdot(\boldsymbol{R}_i - \boldsymbol{R}_j)}. \tag{6.27}$$

$\boldsymbol{R}_i$ is the spatial coordinate of site i. With substituting these into the first term in the right hand side of (6.25), because

$$\sum_{\langle i,j\rangle,s} t_{ij} c_{is}^\dagger c_{js} = \sum_{i,j,s} \frac{2}{N^2} \sum_{\boldsymbol{k}_1,\boldsymbol{k}_2,\boldsymbol{k}_3} \epsilon_{\boldsymbol{k}_1} e^{i\boldsymbol{k}_1\cdot(\boldsymbol{R}_i-\boldsymbol{R}_j)} e^{-i\boldsymbol{k}_2\cdot\boldsymbol{R}_i} a_{\boldsymbol{k}_2 s}^\dagger e^{i\boldsymbol{k}_3\cdot\boldsymbol{R}_j} a_{\boldsymbol{k}_3 s} = \sum_{\boldsymbol{k},s} \epsilon_{\boldsymbol{k}} a_{\boldsymbol{k}s}^\dagger a_{\boldsymbol{k}s}, \tag{6.28}$$

we can view the hopping (1st) term as kinetic energy term of wide-spreading electrons. From this, (6.25) can be expressed as follows.

$$\mathscr{H} = \sum_{\boldsymbol{k},s} \epsilon_{\boldsymbol{k}} a_{\boldsymbol{k}s}^\dagger a_{\boldsymbol{k}s} + U\sum_i^N \hat{n}_{i\uparrow}\hat{n}_{i\downarrow}. \tag{6.29}$$

The Hubbard model is widely used in the study of many-body problem. Particularly it is practical to be applied to the ferromagnetism of $3d$ transition metals. In such systems, $4s$ and $3d$ electrons coexist in single band. $3d$ electrons are the origin of ferromagnetism and though the wavefunctions spread over the whole crystal (itinerant) they have high probabilities of existence at atomic positions, i.e. tendency to localize. On the other hand, $4s$ electrons tend to delocalize and screen the Coulomb interaction between $3d$ electrons. This property justifies the approximation of on-site short range Coulomb interaction.

6.2.2 HF approximation

We apply HF (mean field, molecular field) approximation to the Hubbard model. There is the same problem of overestimation as that in electron gas, but we will see what is different in the case of Hubbard model.

To estimate the ferromagnetic transition, we consider magnetization and electron number per site:

$$m = \langle n_\uparrow \rangle - \langle n_\downarrow \rangle , \quad n = \langle n_\uparrow \rangle + \langle n_\downarrow \rangle , \tag{6.30}$$

and compare the expectation values of energy for the states of $m = 0$ and $m \neq 0$. The magnetization is expressed in the unit of μ_{B} and g-factor is set to 2.

In the HF approximation of Hubbard model (6.25), the second term (interaction term) is simplified as

$$\begin{aligned} U \sum_i \hat{n}_{i\uparrow} \hat{n}_{i\downarrow} &= U \sum_i [\langle \hat{n}_\uparrow \rangle \hat{n}_{i\downarrow} + \langle \hat{n}_\downarrow \rangle \hat{n}_{i\uparrow} - \langle \hat{n}_\uparrow \rangle \langle \hat{n}_\downarrow \rangle + (\hat{n}_{i\uparrow} - \langle n_\uparrow \rangle)(\hat{n}_{i\downarrow} - \langle n_\downarrow \rangle)] \\ &\simeq U \sum_i (\langle \hat{n}_\uparrow \rangle \hat{n}_{i\downarrow} + \langle \hat{n}_\downarrow \rangle \hat{n}_{i\uparrow}) - NU \langle n_\uparrow \rangle \langle n_\downarrow \rangle \end{aligned} \tag{6.31}$$

$$\text{Take average } \rightarrow = \frac{NU}{4}(n^2 - m^2). \tag{6.32}$$

Namely, the second order term of fluctuation $(\hat{n}_{i\uparrow} - \langle n_\uparrow \rangle)(\hat{n}_{i\downarrow} - \langle n_\downarrow \rangle)$ is ignored. In this approximation, $\downarrow$-electrons work as an average on an $\uparrow$-electron, conversely, $\uparrow$-electrons work as an average on a $\downarrow$-electron. The last equation shows the expectation value for eigenstates.

We can rewrite eq. (6.31) with the Fourier expansions in (6.27), (6.28) to a Hamiltonian with the operators $\hat{n}_{\boldsymbol{k}s}$ as

$$\mathscr{H}_{\mathrm{HF}} = \sum_{\boldsymbol{k},s} (\epsilon_{\boldsymbol{k}} + U \langle n_{-s} \rangle) n_{\boldsymbol{k}s} - NU \langle n_\uparrow \rangle \langle n_\downarrow \rangle . \tag{6.33}$$

Here we assign $s = \pm 1$ to spin $\uparrow, \downarrow$, and use the relation

$$\langle n_s \rangle = \frac{1}{2}(n + sm), \tag{6.34}$$

to obtain

$$\begin{aligned} \mathscr{H}_{\mathrm{HF}} &= \sum_{\boldsymbol{k},s} \left(\epsilon_{\boldsymbol{k}} - \frac{sUm}{2} \right) \hat{n}_{\boldsymbol{k}s} + \frac{NU}{4}(n^2 + m^2) \\ &\equiv \sum_{\boldsymbol{k},s} \tilde{\epsilon}_{\boldsymbol{k}s} \hat{n}_{\boldsymbol{k}s} + \frac{NU}{4}(n^2 + m^2), \end{aligned} \tag{6.35}$$

where we take averages as $\sum_{\boldsymbol{k},s} \hat{n}_{\boldsymbol{k}s} \rightarrow N(\langle n_\uparrow \rangle + \langle n_\downarrow \rangle)$. That is, the appearance of the magnetization m shifts the single electron energy by $\Delta\mu = (-s)Um/2$. The directions of the shifts are opposite depending on spins. With packing the electrons into this band up to a common chemical potential μ, the total energy is given by

$$\begin{aligned} E &= \sum_{\tilde{\epsilon}_{\boldsymbol{k}s} \leq \mu} \left(\epsilon_{\boldsymbol{k}} - \frac{sUm}{2} \right) + \frac{NU}{4}(n^2 + m^2) \\ &= \sum_{\tilde{\epsilon}_{\boldsymbol{k}s} \leq \mu} \epsilon_{\boldsymbol{k}} + \frac{NU}{4}(n^2 - m^2). \end{aligned} \tag{6.36}$$

On the other hand, the spin-dependence of $\Delta\mu$ brings about the difference in the electron numbers in $\uparrow$ and $\downarrow$ states. And the difference should be equal to m. This is the **self-consistent condition**, which commonly appears in mean-field approximation. For simplicity, we assume that the density of states $\mathscr{D}(E_{\mathrm{F}})$ around E_{F} is constant for energy. Then from

$$m = 2\mathscr{D}(E_{\mathrm{F}})\Delta\mu = \mathscr{D}(E_{\mathrm{F}})Um, \tag{6.37}$$

the condition $m \neq 0$ gives the criterion of appearance of nonzero m as

$$U\mathscr{D}(E_{\rm F}) = 1. \tag{6.38}$$

We estimate the enhancement of kinetic energy by magnetization as we did in the electron gas. From the above condition we obtain

$$\mathscr{D}(E_{\rm F})(\Delta\mu)^2 = \frac{m^2}{4\mathscr{D}(E_{\rm F})}. \tag{6.39}$$

As in eq. (6.36), the decrease in the Coulomb repulsion energy by appearance of m is $-NUm^2/4$. Summing up of these gives

$$\Delta E = \frac{N}{4}\left[\frac{m^2}{\mathscr{D}(E_{\rm F})} - Um^2\right]. \tag{6.40}$$

The condition $\Delta E < 0$ is

$$U\mathscr{D}(E_{\rm F}) \geq 1, \tag{6.41}$$

which agrees with the criterion (6.38). This is called **Stoner condition**.

Roughly speaking, let $E_{\rm w}$ be the bandwidth and from $\mathscr{D}(E_{\rm F}) \sim E_{\rm w}^{-1}$, we can say that the Stoner condition means the ferromagnetism appears when the Coulomb interaction width U exceeds the bandwidth $E_{\rm w}$. Because it is still a HF approximation, as in the case of electron gas, we have the problem of overestimation the stability of ferromagnetic state.

6.2.3 Susceptibility

Before going into the problem, we see the magnetic susceptibility given in the HF approximation. The magnetization M is expressed as

$$M = \frac{g\mu_{\rm B}}{2}\sum_i[\langle n_{i\uparrow}\rangle - \langle n_{i\downarrow}\rangle]\frac{g\mu_{\rm B}}{2}\sum_i n_{i-}. \tag{6.42}$$

The susceptibility χ per an atom is

$$\chi = \frac{M}{NB} = \frac{g\mu_{\rm B}}{2}\frac{n_-}{B}. \tag{6.43}$$

Since the interaction energy of magnetic field and magnetic moment (Zeeman energy) is $-MB$, the energy of electrons in magnetic field is written as

$$E_B = E(0) + E_2 n_-^2 - N\frac{g\mu_{\rm B}}{2}Bn_-, \tag{6.44}$$

where n_- is small. And E_2 is

$$E_2 = \frac{1}{2}\frac{d^2(\Delta E)}{dn_-^2}, \tag{6.45}$$

where ΔE corresponds to ΔE in eq. (6.40).

In paramagnetic state, the coefficient of the term with the second order in M is positive in the GL theory. Then E_2 is also positive and n_- that minimizes E_B, gives the susceptibility. Namely,

$$\chi = \frac{(g\mu_{\rm B})^2 N}{4E_2}. \tag{6.46}$$

If we calculate E_2 from the HF approximation in eq. (6.40), we obtain

$$\chi = \left(\frac{g\mu_{\rm B}}{2}\right)^2 \frac{\mathscr{D}(E_{\rm F})}{1 - U\mathscr{D}(E_{\rm F})} = \frac{\chi_{\rm Pauli(a)}}{1 - U\mathscr{D}(E_{\rm F})}, \tag{6.47}$$

where $\chi_{\rm Pauli(a)}$ is the Pauli paramagnetic susceptibility in eq. (3.8) per an atom.

In the HF approximation, when the system does not fulfill the Stoner condition, it keeps paramagnetism though as in eq. (6.47), the susceptibility is enhanced from the Pauli paramagnetic susceptibility by the factor $[1 - U\mathscr{D}(E_{\rm F})]^{-1}$. This is called **Stoner factor**.

Here from the identity of temperature expansion of the chemical potential when the system is strongly Fermi degenerated:

$$\mu = \mu_0 \left[1 - \frac{\pi^2}{6} \frac{d \log \mathscr{D}(\mu_0)}{d \log \mu_0} \left(\frac{k_{\mathrm{B}} T}{\mu_0} \right)^2 + \cdots \right], \tag{6.48}$$

the temperature variation of chemical potential $\delta\mu$ is written as

$$\delta\mu = -\frac{\pi^2 \mathcal{D}'_{\mathrm{F}}}{6\mathcal{D}_{\mathrm{F}}} (k_{\mathrm{B}} T)^2. \tag{6.49}$$

For simpler expression, $d\mathscr{D}(E)/dE|_{E=E_{\mathrm{F}}}$ is simply written as $\mathcal{D}'_{\mathrm{F}}$. To add this to $\Delta\mu$ in eq. (6.37) as correction, taking the second derivative by the energy is required. Hence we write

$$A = \frac{\pi^2}{6} \left(\frac{(\mathcal{D}'_{\mathrm{F}})^2}{\mathcal{D}_{\mathrm{F}}} - \mathcal{D}''_{\mathrm{F}} \right), \tag{6.50}$$

and the temperature dependence of susceptibility is written as

$$\chi = \left(\frac{g\mu_{\mathrm{B}}}{2} \right)^2 \frac{\mathscr{D}(E_{\mathrm{F}})}{1 - U\mathscr{D}(E_{\mathrm{F}}) + UA(k_{\mathrm{B}}T)^2}. \tag{6.51}$$

The temperature that gives zero for the denominator is T_{C}, and by using this, we can write

$$\chi = \frac{C}{T^2 - T_{\mathrm{C}}^2}. \tag{6.52}$$

This does not agree with the Curie-Weiss law, which is also observed in $3d$ transition metals with ferromagnetism. This indicates that the HF approximation has problems other than the quantitative problem we will see in the second next section.

6.3 Ferromagnetism in 3d transition metals

Before going into more realistic theories, we would like to have a look on experimental facts on the ferromagnetism in $3d$ metals. Those should be also the target of more realistic theory. We also see "tuning" of the exchange parameter gives a qualitative understanding of the experiments even within the HF approximation.

In the table below, the bulk parameters of the three elemental ferromagnetic metals are listed[6].

	structure /density (kgm^{-3})	lattice parameters (pm)	T_{C} (K)	M_{S} (MAm^{-1})	K_1 (kJm^{-3})	λ_{S} (10^{-6})	α	P (%)
Fe	bcc 7874	287	1044	1.71	48	-7	1.6	45
Co	hcp 8836	251 407 (fcc)	1388	1.45	530	-62	8.0	42
Ni	fcc 8902	352	628	0.49	-5	-34		44

Tab. 6.1 Bulk properties related to the ferromagnetism in Fe, Co, Ni. K_1 is density of anisotropic energy; λ_{S} spin diffusion length; α damping factor of spin resonance; P spin polarization. P is measured by the Andreev reflection at 4.2 K. The others are measured at room temperature. From [6].

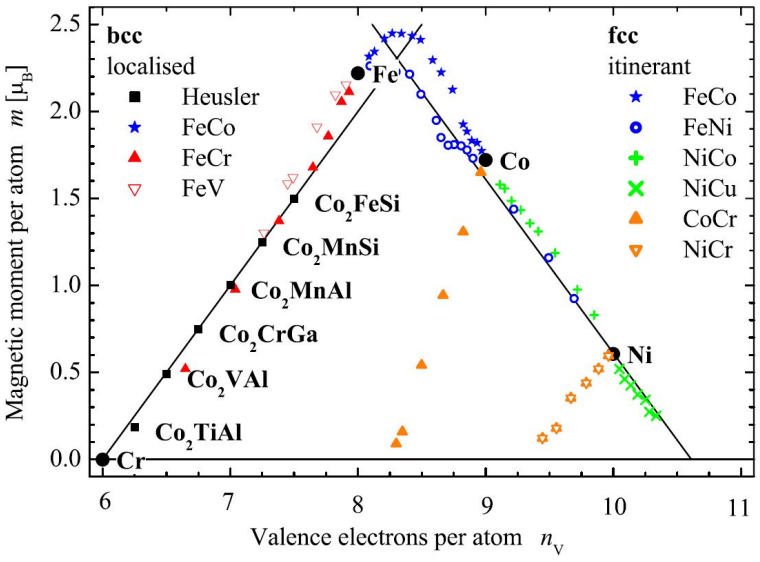

Fig. 6.2 Averaged spontaneous magnetic moment (in unit $\mu_{\rm B}$) is plotted as a function of averaged valence electron number (horizontal axis) for various $3d$ transition metals (elemental metals, and alloys). From [7]. Valence electron number 6 corresponds to Cr, 11 corresponds to Cu.

6.3.1 Slater-Pauling's curve

As shown above, among $3d$ transition metals, elemental metals that show ferromagnetism are Fe, Co, and Ni. The averaged valence electron numbers are 8, 9, 10 respectively. However, with making alloys with other $3d$ metals or Heusler alloys, which contains group III, or IV elements, we can synthesis metallic ferromagnets with the valence electron number from around 6 to about 10.5. Then we plot the spontaneous magnetization per an atom obtained from the saturated magnetization as a function of number of valence electrons. The data points align regularly as in Fig. 6.2. They are on the lines forming a triangle with Fe around the peak. And the edges of the triangle have gradients of ± 1. This curve is called **Slater-Pauling' curve**.

In Fig. 6.2 the alloys plotted in the left region than Fe are mainly Heusler alloys. For Heusler alloys, the following relation is reported to hold[8]:

$$m\text{matnetization per atom in unit of } \mu_{\rm B} \ = Z - 24. \tag{6.53}$$

Relation like eq. (6.53) is called **Slater-Pauling law**.

6.3.2 Spin-band structure in Ni

This relation should come from the number of $3d$ electron spins in the open shell. Here, however, the "open shells" form an energy band and the electrons in it are itinerant. Then numerically calculated band structures are often used for the explanation of Slater-Pauling's curve. The band structure must have spin-dependence, that means the electron mutual interaction should be taken into account in some way. Many of them are the HF approximation, which is known to overestimate the exchange energy gain. But still, qualitative explanation of Slater-Pauling's curve is possible as follows.

Nickel (Ni) has fcc structure and $T_{\rm C}$ is comparatively low among the three elemental ferromagnets. Figure 6.3(a) shows the spin-dependent density of states calculated by the APW method (Appendix 12A)[9]. The $4s$ electron band has a widely spread density of states with low amplitudes. Conversely, the $3d$ electron band has a comparatively narrow distribution and has several high sharp peaks. A single spin subband of $4s$ electrons can accommodate a single electron per atom while that of $3d$ electrons can accommodate 5 electrons per atom. The bottom of $4s$ band is lower than that of $3d$ band. The position of $E_{\rm F}$ shown in Fig. 6.3(a) indicates that the $4s$ band as 0.6 electron, the $3d\uparrow$ band (the upper side in the figure. the major spin subband) has 5 electrons, the $3d\downarrow$ band has 5.4 electrons. 10 valence electrons are

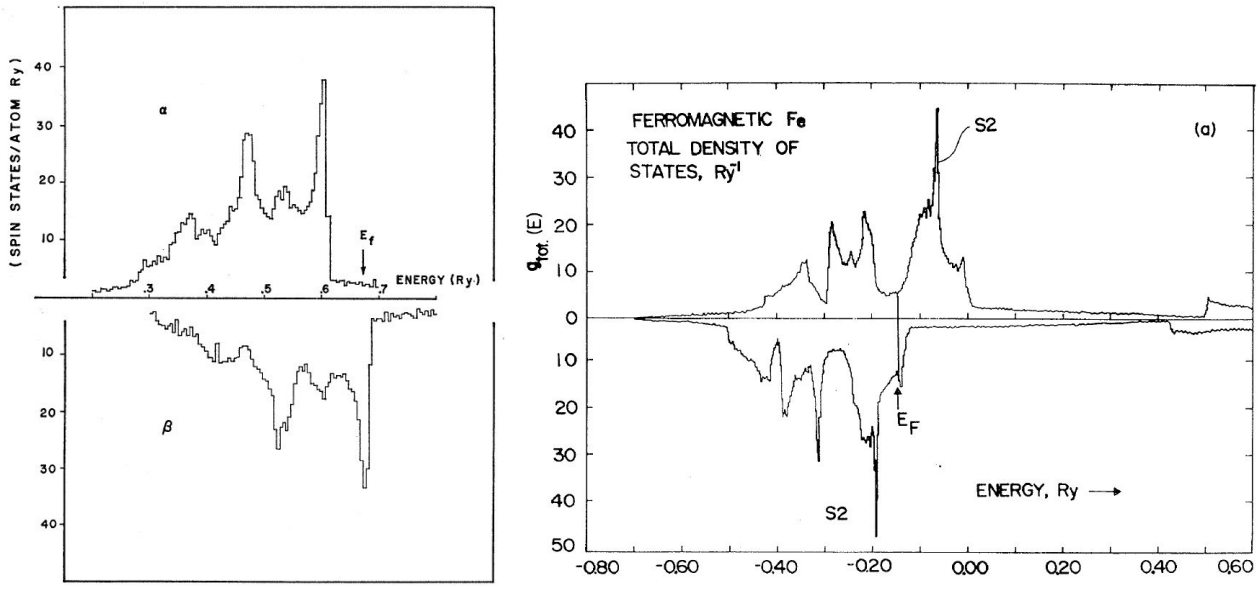

(a) (b)

Fig. 6.3 Spin-dependent density of states in (a) Ni, (b) Fe, calculated by the APW method. (a) is from [9]. (b) is from [10].

in an atom in total. In total, the total spin for 0.6 electron remains, which fact explains the appearance of spontaneous magnetic moment with $0.6\mu_{\rm B}$. As above, the non-integer spontaneous magnetic moment is explained by the coexistence of $4s$ band and $3d$ band and partial occupation of them by valence electrons.

In Ni-Cu alloys, the spontaneous magnetizations vanishes around 60% of Cu content. A Cu atom has 11 valence electrons, which is one more than Ni. Hence with increasing the Cu content, the extra one electron fills the vacant space of 0.6 electron in $3d\downarrow$ band. Just at 60%, the space is filled up and the spontaneous magnetization vanishes. Also, it is now clear that the gradient is -1 in Slater-Pauling's curve from Ni to Cu.

6.3.3 Spin band structure in Fe

Figure 6.3(b) shows the spin dependent density of states in bee Fe calculated by the APW method. Though the shape of density of states resembles to that of Ni, there is a large difference in the position of $E_{\rm F}$. The total electron number is 8 and the $4s$ band has 0.8 electron. Of the remaining 7.2 electrons, 4.7 electrons are in the major spin subband (the lower in the figure), 2.5 electrons are in the minor spin subband. The configuration brings about the spontaneous magnetization of $2.2\mu_{\rm B}$.

The reason why the major spin subband does not have full 5 electrons can be explained in Fig. 6.3(b). In the case of Ni, $E_{\rm F}$ places above the $3d$ major spin subband while in the case of Fe, $E_{\rm F}$ hits a valley of the minor spin subband. In such a situation, a variation of electron number in the minor spin subband causes a large shift in the relative $E_{\rm F}$ position. The position of $E_{\rm F}$ in fixed energy space does not move largely. That means actually the whole band should move largely. Summing up the discussion, once $E_{\rm F}$ hits a valley of density of states, change of electron number is mostly absorbed by other subbands and $E_{\rm F}$ is locked to the valley. This makes it hard to increase the space (hole) in the minor spin subband. And the major spin subband still has some hole in it.

Alloying with Co increases the number of electrons, with which we can test the above hypothesis. When the Co concentration is low, the increasing electrons fill the major spin band, and the spontaneous magnetic moment increases with the Co concentration. At 30% where the major spin band is completely filled ($5-4.7=0.3$), the increasing electrons work in the direction of filling the holes in the minor spin band, and the number starts to decrease. For the same reason,

the moment decreases due to alloying with Cr, which reduces the number of electrons.

Appendix 12A: An example of band calculation (APW)

Numerical calculations that exceed the HF approximation are still not vey common, and many theories used to explain the Slater-Pauling law are by (a bit-modified) HF approximation. Band calculation is often the basis for considering the electron correlation effect, so let us take a brief look at a type of calculation method here. Here we introduce APW (augmented plane wave) method, which is one of the techniques to find solutions of Kohn-Sham equation [*1], for the details, refer to [11, 12] and the references therein.

Let us consider the Schrödinger equation of the state $\phi(\boldsymbol{r})$ in potential $V(\boldsymbol{r})$:

$$\mathscr{H}\phi(\boldsymbol{r}) = \left[-\frac{\hbar^2}{2m}\nabla^2 + V(\boldsymbol{r})\right]\phi(\boldsymbol{r}) = E\phi(\boldsymbol{r}). \tag{12A.1}$$

As the potential, we consider one called Muffin-tin potential. Let r_{c} be the radius of Muffin-tins, which must be shorter than the half of the distance between neighboring atoms. Then the potential is described as(Fig. 12A.1)

$$V(\boldsymbol{r}) = \begin{cases} V_{\mathrm{a}}(r) \ \text{(spherical)} & (r < r_{\mathrm{c}}) \\ V_{\mathrm{o}} \ (= V_{\mathrm{a}}(r_{\mathrm{c}})\text{: const.}) & (r \geq r_{\mathrm{c}}). \end{cases} \tag{12A.2}$$

As $V(\boldsymbol{r})$, Hartree potential, which corresponds to the direct integral in eq. (6.6), is adopted. That is

$$V_{\mathrm{d}}(\boldsymbol{r}) = \sum_i \langle\phi_i(\boldsymbol{r}')| \frac{e^2}{|\boldsymbol{r}-\boldsymbol{r}'|} |\phi_i(\boldsymbol{r}')\rangle \,. \tag{12A.3}$$

And exchange potential which corresponds to the exchange integral is

$$V_{\mathrm{ex}\uparrow} = -3e^2\left(\frac{3}{4\pi}\right)^{1/3}\rho_\uparrow(\boldsymbol{r})^{1/3}. \tag{12A.4}$$

The above is from spin density function approximation. The above Hartree and exchange potentials are obtained from the eigen functions, which are the solutions of eq. (12A.1). Hence the equation constitutes the self-consistent equation.

Actual calculation is on the variational method. As the variation functions, we adopt

$$\Phi_{\mathrm{vr}}(\boldsymbol{r}) = \begin{cases} \sum_{l,m} A_{lm} R_l(r) Y_l^m(\theta,\varphi) & r < r_{\mathrm{c}}, \\ \sum_{n=0}^{N} B_n \exp[i(\boldsymbol{k}+\boldsymbol{K}_n)\cdot\boldsymbol{r}] & r > r_{\mathrm{c}}. \end{cases} \tag{12A.5}$$

That is, inside the muffin-cup, wavefunctions have the same form for an isolated atom potential, and outside, the superpositions of plane waves. $\boldsymbol{K}_n$ are inverse-lattice vectors.

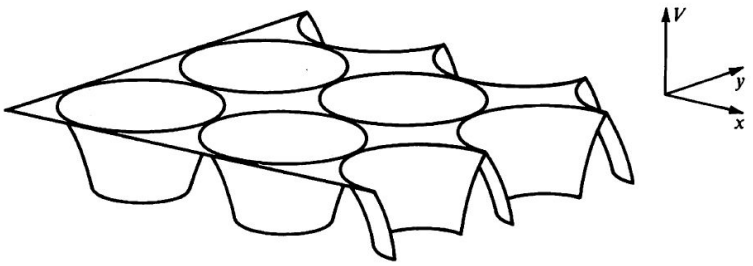

Fig. 12A.1 Schematic diagram of Muffin-tin potential. From [13].

[*1] Though APW method was invented long before the Kohn-Sham equation, now it can be placed at such a position in the present understandings.

The wavenumber k is fixed and the variation is taken under the boundary condition of wavefunction Φ connection at $r = r_c$. Actually, the coefficients $\{B_n\}$ is determined for $\langle\Phi|\mathscr{H}|\Phi\rangle$ to take the extremals. N cannot be taken to infinity and the calculation is done within a finite number. Thus obtained Φ is used to calculate the potential and the procedure is continued to reach conversion. Then k is varied and the same procedure is repeated to obtain the band structure as we have seen in Sec. 6.3.

Appendix 12B: MateriApps

MateriApps (https://ma.issp.u-tokyo.ac.jp/) is a portal site for material science simulations operated in cooperation with the Institute for Solid State Physics CMS and others, and has information and download links for many related applications.

Among them, Quantum Espresso (https://www.quantum-espresso.org/) is an application that performs a wide range of calculations such as ground state calculation, DFT calculation, and quantum transport, and is characterized by being able to run on a PC.

References

[1] A. A. Abrikosov. *Fundamentals of the Theory of Metals*. Dover Publications, 10 2017.

[2] Alexander L. Fetter and John Dirk Walecka. *Quantum Theory of Many-Particle Systems (Dover Books on Physics)*. Dover Publications, 6 2003.

[3] A. A. Abrikosov, L. P. Gorkov, and I. E. Dzyaloshinski. *Methods of Quantum Field Theory in Statistical Physics (Dover Books on Physics)*. Dover Publications, 10 1975.

[4] Henrik Bruus and Karsten Flensberg. *Many-body Quantum Theory In Condensed Matter Physics: An Introduction (Oxford Graduate Texts)*. Oxford Univ Pr, 11 2004.

[5] D. M. Ceperley and B. J. Alder. Ground state of the electron gas by a stochastic method. *Phys. Rev. Lett.*, Vol. 45, pp. 566–569, Aug 1980.

[6] J. M. D. Coey. Materials for spin electronics. In *Lecture Notes in Physics*, pp. 277–297. Springer Berlin Heidelberg.

[7] Benjamin Balke, Sabine Wurmehl, Gerhard H Fecher, Claudia Felser, and Jürgen Kübler. Rational design of new materials for spintronics: Co_2fez (z=al, ga, si, ge). *Science and Technology of Advanced Materials*, Vol. 9, No. 1, p. 014102, January 2008.

[8] I. Galanakis, P. H. Dederichs, and N. Papanikolaou. Slater-pauling behavior and origin of the half-metallicity of the full-heusler alloys. *Phys. Rev. B*, Vol. 66, p. 174429, Nov 2002.

[9] John W. D. Connolly. Energy bands in ferromagnetic nickel. *Phys. Rev.*, Vol. 159, pp. 415–426, Jul 1967.

[10] Rastko Maglic. Van hove singularity in the iron density of states. *Phys. Rev. Lett.*, Vol. 31, pp. 546–548, Aug 1973.

[11] 和子望月, 直鈴木. 固体の電子状態と磁性. 大学教育出版, 7 2003.

[12] Jorge Kohanoff. *Electronic Structure Calculations for Solids and Molecules*. Cambridge University Press, June 2006.

[13] Walter A. Harrison. *Solid State Theory (Dover Books on Physics) (English Edition)*. Dover Publications, 4 2012.

Lecture note Magnetism (13)

6th July (2022) Shingo Katsumoto, Institute for Solid State Physics, University of Tokyo

Last week, we saw that the HF approximation on the Hubbard model leads to the Stoner condition, which brings about an energy difference between the ↑-band and the ↓-band. This modeling and the approximation enable us to explain some experimental facts like Slater-Paulings' curve qualitatively. On the other hand, the approximation still has qualitative and quantitative problems naturally for such a simple approximation. In such situations, self-consistent renormalization (SCR) spin-fluctuation theory gave satisfactory results at least for the ground states. This week we would like to reach the entrance of SCR theory but before that we need a bit heavy preparation, to which most of the lecture time is devoted.

6.4 Dynamic susceptibility

So far we have seen responses of materials to static magnetic fields. Here we turn our attention to responses to vibrating external fields. In such a case, we need to use the linear response theory.

6.4.1 Linear response

Let $\mathscr{H}_{\rm ext}(t)$ be the Hamiltonian of time-dependent external field. The total Hamiltonian is expressed as $\mathscr{H}_0+\mathscr{H}_{\rm ext}(t)$. From the time dependence of density matrix ρ defined in the previous section in eq. (6.9) is,

$$i\hbar\frac{\partial\rho}{\partial t}=[\mathscr{H}_0+\mathscr{H}_{\rm ext}(t),\rho(t)], \tag{6.54}$$

where only time t is shown explicitly as a variable. The initial state, for time $t=-\infty$, is set to the thermal equilibrium state of $\mathscr{H}_0$, that is

$$\rho(-\infty)=\rho_{\rm eq}=\frac{1}{Z_0}\exp\left(-\frac{\mathscr{H}_0}{k_{\rm B}T}\right), \tag{6.55}$$

where $Z_0=\mathrm{Tr}[\exp(-\mathscr{H}_0/k_{\rm B}T)]$ is the partition function of unperturbed state.

As shown in Appendix 13A, the density matrix satisfies the following integral equation.

$$\rho(t)=\rho_{\rm eq}+\frac{1}{i\hbar}\int_{-\infty}^{t}dt'[U_0(t-t')\mathscr{H}_{\rm ext}(t')U_0^{-1}(t-t'),U_0(t-t')\rho(t')U_0^{-1}(t-t')] \tag{6.56}$$

$$=\rho_{\rm eq}+\frac{1}{i\hbar}\int_{-\infty}^{t}dt'U_0(t-t')[\mathscr{H}_{\rm ext}(t'),\rho(t')]U_0^{-1}(t-t'), \tag{6.57}$$

where also as in (13A.1),

$$U_0(t)\equiv\exp\left(\frac{\mathscr{H}_0}{i\hbar}t\right). \tag{6.58}$$

Since the commutation relation in the right hand side of eq. (6.57) is the response to an external field in addition to $\rho_{\rm eq}$, the lowest order in it is the first order of t. In the same way, $\mathscr{H}_{\rm ext}$ is a time-dependent part with no constant. As long as we consider the liner response, $\rho(t')$ in the commutation relation in eq. (6.57) can be replaced with time-independent $\rho_{\rm eq}$. $\rho_{\rm eq}$ commutes with Hamiltonian $\mathscr{H}_0$, being made from the eigenstates of it. Then we can write

$$\rho(t)\simeq\rho_{\rm eq}+\frac{1}{i\hbar}\int_{-\infty}^{t}dt'[U_0(t-t')\mathscr{H}_{\rm ext}(t')U_0^{-1}(t-t'),\rho_{\rm eq}]. \tag{6.59}$$

Now we assume the Hamiltonian of external field can be written in the form of

$$\mathscr{H}_{\rm ext}(t) = -PF(t), \tag{6.60}$$

where $F(t)$ is a quantity to represent the strength of the field and P is the operator corresponding to the field. With this density matrix, an expectation value of a general physical quantity Q can be obtained as $\mathrm{Tr}\{\rho(t)Q\}$[1, 2] in the following.

$$\langle Q(t)\rangle = \mathrm{Tr}\{\rho(t)Q\} = \langle Q_{\rm eq}\rangle + \frac{1}{i\hbar}\int_{-\infty}^{t} dt' \,\langle [P, Q(t-t')]\rangle \, F(t'). \tag{6.61}$$

Here $\langle Q_{\rm eq}\rangle$ and $Q(t)$ are defined as

$$\langle Q_{\rm eq}\rangle = \mathrm{Tr}\{\rho_{\rm eq}Q\}, \quad Q(t) = U_0(t)^{-1}QU_0(t). \tag{6.62}$$

From eq. (6.61), we know that the expectation value $\langle [P, Q(t-t')]\rangle$ is a pure imaginary.

Now we consider the external field of frequency ω and write

$$F(t) = F_0\cos(\omega t) = \mathrm{Re}[F_0 e^{-i\omega t}]. \tag{6.63}$$

We here define the susceptibility $\chi(\omega)$ as

$$\Delta Q(t) = \langle Q(t)\rangle - \langle Q_{\rm eq}\rangle = \mathrm{Re}[\chi(\omega)F_0 e^{-i\omega t}]. \tag{6.64}$$

On the other hand, from eq. (6.61)

$$\Delta Q(t) = \frac{1}{i\hbar}\int_{-\infty}^{t} dt' \,\langle [P, Q(t-t')]\rangle \,\mathrm{Re}[F_0 e^{-i\omega t'}]. \tag{6.65}$$

Now we know that the right-hand sides of eq. (6.64) equates eq. (6.65). The right hand side of (6.64) can be written as

$$\mathrm{Re}[\chi(\omega)F_0 e^{-i\omega t}] = \frac{F_0}{2}[\chi^*(\omega)e^{i\omega t} + \chi(\omega)e^{-i\omega t}]. \tag{6.66}$$

Similarly (6.65) is developed to

$$\frac{F_0}{2i\hbar}\left\{\left[\int_0^\infty d\tau \,\langle [P, Q(\tau)]\rangle \, e^{-i\omega\tau}\right] e^{i\omega t} + \left[\int_0^\infty d\tau \,\langle [P, Q(\tau)]\rangle \, e^{i\omega\tau}\right] e^{-i\omega t}\right\}, \tag{6.67}$$

where $\tau = t - t'$). By remembering $\langle [P, Q(\tau)]\rangle$ is a pure imaginary, we compare the above two to obtain the following.

Kubo formula

$$\chi_{QP}(\omega) = \frac{i}{\hbar}\int_0^\infty \langle [Q(\tau), P]\rangle \, e^{i\omega\tau} d\tau. \tag{6.68}$$

Here we add a subscript to χ, which shows the relation of response $P \to Q$. Equation (6.68) is one of the formulas called **Kubo formula**, which give linear response functions[3]. This can be viewed as a terminus ad quem of the linear response theory initiated by Nyquist and by others. The Kubo formula has been applied to a vast field of science with fruitful results. It should be used probably forever in science. On the other hand, there are various different formalisms in linear response. We need to select one of them according tot the character of the problem[2].

6.4.2 Fluctuation-dissipation theorem

Equation (6.68) is a Fourier transformation from (time) to (frequency). At the same time it is a response of a physical quantity Q to the external field in eq. (6.60). The correlation function $\langle [Q(\tau), P]\rangle$ represents transfer on time (τ) axis to

the susceptibility [*1]. Then we define a Green's function for physical quantity P, Q as

$$G^{\pm}_{QP}(t) = \mp\frac{i}{\hbar}\theta(\pm t)\left\langle [Q(t), P]\right\rangle, \tag{6.69}$$

in which we restore the symbol for time as $\tau \to t$. Here $\theta(t)$ is the Heaviside function defined as

$$\theta(t) = \begin{cases} 1 & (t \geq 0), \\ 0 & (t < 0). \end{cases} \tag{6.70}$$

We also call $G^{+}_{QP}(t)$ as a retarded Green's function, $G^{-}_{QP}(t)$ an advanced Green's function. Then eq. (6.68) is a Fourier transformation of $G^{+}_{QP}(t)$, and can be written in the form

$$\chi_{QP}(\omega) = -\mathcal{G}^{+}_{QP}(\omega) = -\mathscr{F}_{\omega}\{G^{+}_{QP}(t)\}, \tag{6.71}$$

where $\mathscr{F}_{\omega}\{\cdots\}$ expresses the Fourier transform of $\cdots$ to ω-space.

A Fourier transform of a correlation function of a perturbation and a response:

$$\mathcal{S}_{QP}(\omega) = \int_{-\infty}^{\infty} dt\, \langle Q(t), P\rangle\, e^{i\omega t} \tag{6.72}$$

is called a dynamical form factor. Here we can show the following as in Appendix 13B.

$$\mathcal{S}_{QP}(\omega) = \frac{i}{1 - e^{-\beta\hbar\omega}}[\mathcal{G}^{+}_{QP}(\omega) - \mathcal{G}^{-}_{QP}(\omega)], \tag{6.73}$$

where $\beta \equiv (k_{\mathrm{B}}T)^{-1}$. The left-hand side of eq. (6.73) is a Fourier transform of a correlation function and the right-hand side is a susceptibility of linear response. Such formulas that show linear relations between correlation functions and coefficients of linear responses are called **fluctuation dissipation theorem**. Of course fluctuations and energy-dissipations are different physical quantities. The theorems are not saying that they are the same but that fluctuations can be expressed by coefficients of linear response, which are parameters of energy dissipation.

Let $\{|n\rangle\}$ be a complete set of eigenfunctions of $\mathscr{H}$, then

$$\mathcal{G}^{+}_{QP}(\omega) = \sum_{n,m} \langle n|Q|m\rangle \langle m|P|n\rangle \frac{e^{-\beta E_n} - e^{-\beta E_m}}{E_n - E_m + \hbar\omega + i\eta}. \tag{6.74}$$

6.4.3 Random Phase Approximation (RPA)

We consider an external magnetic field

$$\boldsymbol{B}(\boldsymbol{r}, t) = \boldsymbol{B}(\boldsymbol{q}, \omega)e^{i(\boldsymbol{q}\cdot\boldsymbol{r} - \omega t)}, \tag{6.75}$$

applied on a Hubbard model

$$\mathscr{H} = \sum_{i,j,s} t_{ij} c^{\dagger}_{is} c_{js} + U\sum_{i}^{N} \hat{n}_{i\uparrow}\hat{n}_{i\downarrow}. \tag{6.25}$$

We write the local magnetization density in unit of $-g\mu_{\mathrm{B}}$ as

$$\boldsymbol{S}(\boldsymbol{r}) = \frac{1}{2}\sum_{i}\sum_{\alpha,\beta} \delta(\boldsymbol{r} - \boldsymbol{r}_i) c^{\dagger}_{i\alpha}\boldsymbol{\sigma}_{\alpha\beta} c_{i\beta}, \tag{6.76}$$

[*1] Green's function was invented by George Green (1973-1841). As you probably used in the electromagnetism, it is frequently used for finding solutions of differential equations. A Green's function generally expresses an effect of some local cause to an away point. It appears in various formalisms and the name "Green's function" is now also applied to general correlation (transfer) functions. I should note that according to ref. [4], the naming "Green's function" is strange and we should call it "Green function."

where $\boldsymbol{\sigma} = (\sigma_x, \sigma_y, \sigma_z)$ is a vector with Pauli matrices as elements. Accordingly, Hamiltonian(6.60) in the present case is

$$\mathscr{H}_{\rm ext}(t) = g\mu_{\rm B} \int \boldsymbol{B}(\boldsymbol{r},t)\cdot\boldsymbol{S}(\boldsymbol{r})d^3\boldsymbol{r} = g\mu_{\rm B}\boldsymbol{S}_{-\boldsymbol{q}}\cdot\boldsymbol{B}(\boldsymbol{q},\omega)e^{-i\omega t}. \tag{6.77}$$

Here Fourier-$\boldsymbol{q}$ components of magnetization $S_{\boldsymbol{q}}$ are defined as follows.

$$\left.\begin{aligned} S_{\boldsymbol{q}+} &= S_{\boldsymbol{q}x} + iS_{\boldsymbol{q}y} = \sum_{\boldsymbol{k}} a^\dagger_{\boldsymbol{k}\uparrow}a_{\boldsymbol{k}+\boldsymbol{q}\downarrow}, \\ S_{\boldsymbol{q}-} &= S_{\boldsymbol{q}x} - iS_{\boldsymbol{q}y} = \sum_{\boldsymbol{k}} a^\dagger_{\boldsymbol{k}\downarrow}a_{\boldsymbol{k}+\boldsymbol{q}\uparrow}, \\ S_{\boldsymbol{q}z} &= (1/2)\sum_{\boldsymbol{k}}(a^\dagger_{\boldsymbol{k}\uparrow}a_{\boldsymbol{k}+\boldsymbol{q}\uparrow} - a^\dagger_{\boldsymbol{k}\downarrow}a_{\boldsymbol{k}+\boldsymbol{q}\downarrow}). \end{aligned}\right\} \tag{6.78}$$

In comparison of eq. (6.77) and eq. (6.60), the quantity which corresponds to P is $g\mu_{\rm B}\boldsymbol{S}_{-\boldsymbol{q}}$. On the other hand, the response is also magnetization and in linear response, that is $g\mu_{\rm B}\boldsymbol{S}_{\boldsymbol{q}}$. Hence the z-component of dynamic susceptibility is

$$\chi_{zz}(\boldsymbol{q},\omega) = (g\mu_{\rm B})^2\frac{i}{\hbar}\int_0^\infty dt\,\langle[S_{\boldsymbol{q}z}(t), S_{-\boldsymbol{q}z}]\rangle\, e^{i\omega t}. \tag{6.79}$$

Similarly, considering non-zero part after taking correlation function, the transverse component is written as

$$\chi_{+-}(\boldsymbol{q},\omega) = (g\mu_{\rm B})^2\frac{i}{\hbar}\int_0^\infty dt\,\langle[S_{\boldsymbol{q}+}, S_{-\boldsymbol{q}-}]\rangle\, e^{i\omega t}. \tag{6.80}$$

Let us calculate $\chi_{+-}(\boldsymbol{q},\omega)$ in the following way. We take a $\boldsymbol{k}$ term in the expression of $S_{\boldsymbol{q}+}(t)$ in eq. (6.78). The corresponding Green's function is

$$G^+_{\boldsymbol{k}\boldsymbol{q}}(t) = -i\theta(t)\,\langle[a^\dagger_{\boldsymbol{k}\uparrow}(t)a_{\boldsymbol{k}+\boldsymbol{q}\downarrow}(t), S_{-\boldsymbol{q}-}]\rangle\,. \tag{6.81}$$

Henceforth we omit $+$ to specify "retarded." The time derivative of this Green's function (equation of motion) is

$$i\hbar\frac{\partial G_{\boldsymbol{k}\boldsymbol{q}}}{\partial t} = -i\theta(t)\,\langle[e^{i\mathscr{H}t/\hbar}[a^\dagger_{\boldsymbol{k}\uparrow}a_{\boldsymbol{k}+\boldsymbol{q}\downarrow},\mathscr{H}]e^{-i\mathscr{H}t/\hbar}, S_{-\boldsymbol{q}-}]\rangle + \delta(t)\hbar\,\langle[a^\dagger_{\boldsymbol{k}\uparrow}(t)a_{\boldsymbol{k}+\boldsymbol{q}\downarrow}(t), S_{-\boldsymbol{q}-}]\rangle\,. \tag{6.82}$$

We divide the Hubbard Hamiltonian into the kinetic energy term $\mathscr{H}_{\rm k}$ and the on-site interaction term $\mathscr{H}_{\rm int}$, and calculate the commutation relation in the right-hand side as follows.

$$\begin{aligned} [a^\dagger_{\boldsymbol{k}\uparrow}a_{\boldsymbol{k}+\boldsymbol{q}\downarrow}, S_{-\boldsymbol{q}-}] &= \sum_{\boldsymbol{k}'}[a^\dagger_{\boldsymbol{k}\uparrow}a_{\boldsymbol{k}+\boldsymbol{q}\downarrow}, a^\dagger_{\boldsymbol{k}'+\boldsymbol{q}\downarrow}a_{\boldsymbol{k}'\uparrow}] \\ &= a^\dagger_{\boldsymbol{k}\uparrow}a_{\boldsymbol{k}\uparrow} - a^\dagger_{\boldsymbol{k}+\boldsymbol{q}\downarrow}a_{\boldsymbol{k}+\boldsymbol{q}\downarrow}, && \text{(6.83a)} \\ [a^\dagger_{\boldsymbol{k}\uparrow}a_{\boldsymbol{k}+\boldsymbol{q}\downarrow}, \mathscr{H}_{\rm k}] &= (\epsilon_{\boldsymbol{k}+\boldsymbol{q}} - \epsilon_{\boldsymbol{k}})a^\dagger_{\boldsymbol{k}\uparrow}a_{\boldsymbol{k}+\boldsymbol{q}\downarrow}, && \text{(6.83b)} \\ [a^\dagger_{\boldsymbol{k}\uparrow}a_{\boldsymbol{k}+\boldsymbol{q}\downarrow}, \mathscr{H}_{\rm int}] &= (U/N)\sum_{\boldsymbol{k}_1,\boldsymbol{k}_2,\boldsymbol{p}}[a^\dagger_{\boldsymbol{k}\uparrow}a_{\boldsymbol{k}+\boldsymbol{q}\downarrow}, a^\dagger_{\boldsymbol{k}_1+\boldsymbol{p}\uparrow}a^\dagger_{\boldsymbol{k}_2-\boldsymbol{p}\downarrow}a_{\boldsymbol{k}_2\downarrow}a_{\boldsymbol{k}_1\uparrow}] \\ &= -(U/N)\left[\sum_{\boldsymbol{k}_1,\boldsymbol{p}} a^\dagger_{\boldsymbol{k}\uparrow}a^\dagger_{\boldsymbol{k}_1+\boldsymbol{p}\uparrow}a_{\boldsymbol{k}+\boldsymbol{q}+\boldsymbol{p}\downarrow}a_{\boldsymbol{k}_1\uparrow} + \sum_{\boldsymbol{k}_2,\boldsymbol{p}} a^\dagger_{\boldsymbol{k}+\boldsymbol{p}\uparrow}a^\dagger_{\boldsymbol{k}_2-\boldsymbol{q}\downarrow}a_{\boldsymbol{k}_2\downarrow}a_{\boldsymbol{k}+\boldsymbol{q}\downarrow}\right]. && \text{(6.83c)} \end{aligned}$$

There are terms with four (2+2) operators products term of annihilation-creation operators in eq. (6.83c) representing the interaction, to which we apply mean field approximation. That is, we replace two of the four operators with the average of them in $[\cdots]$ as

$$\begin{aligned} &-\sum_{\boldsymbol{p}} a^\dagger_{\boldsymbol{k}+\boldsymbol{p}\uparrow}a_{\boldsymbol{k}+\boldsymbol{q}+\boldsymbol{p}\downarrow}\,\langle a^\dagger_{\boldsymbol{k}\uparrow}a_{\boldsymbol{k}\uparrow}\rangle + \sum_{\boldsymbol{k}_1} a^\dagger_{\boldsymbol{k}\uparrow}a_{\boldsymbol{k}+\boldsymbol{q}\downarrow}\,\langle a^\dagger_{\boldsymbol{k}_1\uparrow}a_{\boldsymbol{k}_1\uparrow}\rangle \\ &\qquad - \sum_{\boldsymbol{k}_2} a^\dagger_{\boldsymbol{k}\uparrow}a_{\boldsymbol{k}+\boldsymbol{q}\downarrow}\,\langle a^\dagger_{\boldsymbol{k}_2\downarrow}a_{\boldsymbol{k}_2\downarrow}\rangle + \sum_{\boldsymbol{p}} a^\dagger_{\boldsymbol{k}+\boldsymbol{p}\uparrow}a_{\boldsymbol{k}+\boldsymbol{q}+\boldsymbol{p}\downarrow}\,\langle a^\dagger_{\boldsymbol{k}+\boldsymbol{q}\downarrow}a_{\boldsymbol{k}+\boldsymbol{q}\downarrow}\rangle\,. \end{aligned} \tag{6.84}$$

Mean field approximation to such dynamic quantity is generally called **Random Phase Approximation(RPA)**. The naming means a quantity with a phase factor ($\exp(i\theta)$) of randomized phase (θ) should vanish.

In eq. (6.84), a difference between an average on $\uparrow$ and that on $\downarrow$ is taken in the second and the thrid terms. In the paramagnetic states, they cancel each other, and the time derivative of Green's function in RPA (6.81)is

$$\begin{aligned} i\hbar\frac{\partial G_{\boldsymbol{kq}}}{\partial t} &= (\epsilon_{\boldsymbol{k}+\boldsymbol{q}} - \epsilon_{\boldsymbol{k}})G_{\boldsymbol{kq}}(t) \\ &\quad - (U/N)(\langle a^\dagger_{\boldsymbol{k}\uparrow}a_{\boldsymbol{k}\uparrow}\rangle - \langle a^\dagger_{\boldsymbol{k}+\boldsymbol{q}\downarrow}a_{\boldsymbol{k}+\boldsymbol{q}\downarrow}\rangle)\sum_{\boldsymbol{p}} G_{(\boldsymbol{k}+\boldsymbol{p})\boldsymbol{q}}(t) \\ &\quad + (\langle a^\dagger_{\boldsymbol{k}\uparrow}a_{\boldsymbol{k}\uparrow}\rangle - \langle a^\dagger_{\boldsymbol{k}+\boldsymbol{q}\downarrow}a_{\boldsymbol{k}+\boldsymbol{q}\downarrow}\rangle)\delta(t). \end{aligned} \tag{6.85}$$

Taking Fourier transformation of both side we get

$$\mathcal{G}_{\boldsymbol{kq}}(\omega) = \frac{f_{\boldsymbol{k}\uparrow} - f_{\boldsymbol{k}+\boldsymbol{q}\downarrow}}{\hbar\omega + \epsilon_{\boldsymbol{k}} - \epsilon_{\boldsymbol{k}+\boldsymbol{q}}}\left[1 - \frac{U}{N}\sum_{\boldsymbol{p}}\mathcal{G}_{\boldsymbol{pq}}(\omega)\right], \tag{6.86}$$

where $f_{\boldsymbol{k}s} = \langle a^\dagger_{\boldsymbol{k}s}a_{\boldsymbol{k}s}\rangle$ is the Fermi distribution function. Summation over $\boldsymbol{k}$ gives

$$\chi_{+-}(\boldsymbol{q},\omega) = N(g\mu_{\mathrm{B}})^2\frac{2\chi^{(0)}(\boldsymbol{q},\omega)}{1 - 2U\chi^{(0)}(\boldsymbol{q},\omega)}, \tag{6.87}$$

where

$$\chi^{(0)}(\boldsymbol{q},\omega) = \frac{1}{2N}\sum_{\boldsymbol{k}}\frac{f_{\boldsymbol{k}+\boldsymbol{q}\downarrow} - f_{\boldsymbol{k}\uparrow}}{\hbar\omega + \epsilon_{\boldsymbol{k}} - \epsilon_{\boldsymbol{k}+\boldsymbol{q}}} \tag{6.88}$$

is the susceptibility of non-interacting system per site normalized by $(g\mu_{\mathrm{B}})^2$.

For the calculation of above $\chi^{(0)}(\boldsymbol{q},\omega)$ we calculate the following. Here for clearness of expression, we adopt $\hbar \to 1$, the unit of wavenumber is taken to k_{F}, the unit of energy is taken to ϵ_{F}. With 3D Jacobian, the integral is written as

$$\begin{aligned} \frac{1}{2N}\sum_{\boldsymbol{k}}\frac{f_{\boldsymbol{k}}}{\omega + \epsilon_{\boldsymbol{k}-\boldsymbol{q}} - \epsilon_{\boldsymbol{k}}} &= \frac{1}{2}\rho(\epsilon_{\mathrm{F}})\int_0^1 k^2dk\int_{-1}^1\frac{d(\cos\theta)}{\omega + q^2 - 2kq\cos\theta} \\ &= \frac{1}{2}\rho(\epsilon_{\mathrm{F}})\int_0^1 k^2dk\frac{1}{2kq}\log\frac{\omega + q^2 + 2kq}{\omega + q^2 - 2kq}. \end{aligned} \tag{6.89}$$

From a mathematical identity

$$\int x\log(ax+b)dx = \frac{1}{2}\left[x^2 - \left(\frac{b}{a}\right)^2\right]\log(ax+b) - \frac{x^2}{4} + \frac{b}{2a}x,$$

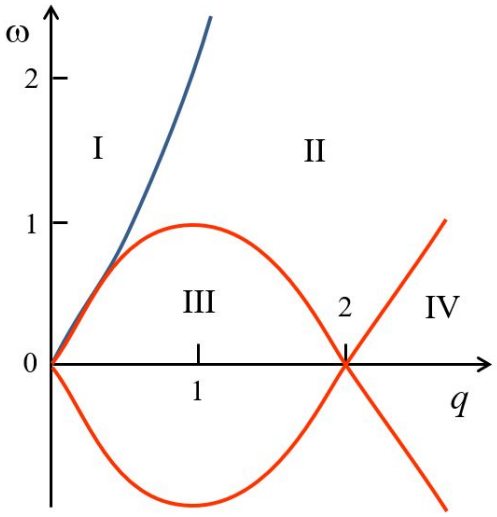

Fig. 6.4 Boundary lines of Kohn anomaly expressed in eq. (6.91), and four regions separated by them in the upper half of q-ω plane.

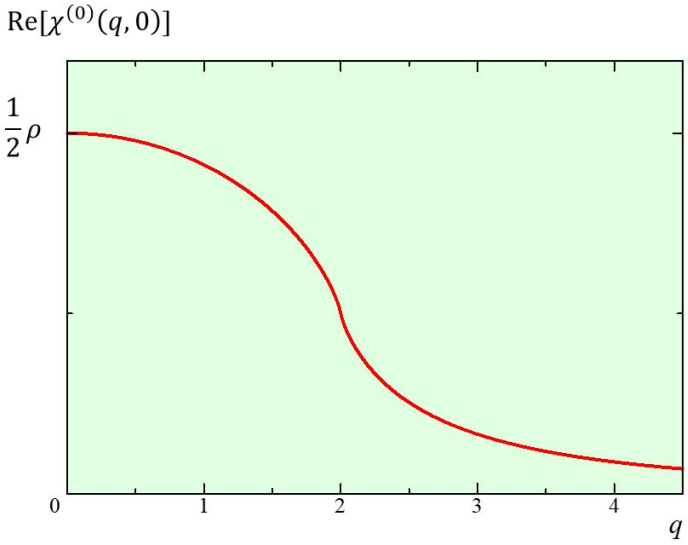

Fig. 6.5 Plot of the real part of $\chi^{(0)}(q,0)$ in eq. (6.93). The derivative diverges at $q=2$.

the integration can be performed as

$$\chi^{(0)}(q,\omega) = \frac{\rho(\epsilon_{\rm F})}{2}\frac{1}{2q}\left\{\frac{1}{2}\left[1-\left(\frac{\omega+q^2}{2q}\right)^2\right]\log\frac{\omega+q^2+2q}{\omega+q^2-2q}+\frac{\omega+q^2}{2q}\right.$$
$$\left.-\frac{1}{2}\left[1-\left(\frac{-\omega+q^2}{2q}\right)^2\right]\log\frac{-\omega+q^2-2q}{\omega+q^2+2q}+\frac{-\omega+q^2}{2q}\right\}. \tag{6.90}$$

In (6.90), when the arguments of log is negative, the susceptibility has a finite imaginary part that leads to damping. The boundary (Kohn anomaly boundary) is given by

$$\omega = \pm(q^2 \pm 2q). \tag{6.91}$$

Figure 6.4 shows these boundaries on $q-\omega$ plane. They divide the upper half plane to four regions I∼IV. In regions I and IV, the imaginary part is zero. In region III, the imaginary part is

$$\mathrm{Im}[\chi^{(0)}(q,\omega)] = \frac{\rho(\epsilon_{\rm F})}{2}\frac{\pi}{4}\frac{\omega}{q}. \tag{6.92}$$

The real part is for $\omega = 0$

$$\mathrm{Re}[\chi^{(0)}(q,0)] = \frac{\rho(\epsilon_{\rm F})}{2}\frac{1}{2q}\left\{\left(1-\frac{q^2}{4}\right)\log\left|\frac{2+q}{2-q}\right|+q\right\}. \tag{6.93}$$

This is plotted as a function of q in Fig. 6.5. At the Kohn anomaly boundary $q=2(k_{\rm F})$, the curve shows a divergence of derivative by q.

From eq. (6.87) the RPA on dynamical susceptibility of Hubbard model predicts appearance of magnetic order for

$$U\chi^{(0)}(\boldsymbol{q}_{\max},0) \geq \frac{1}{2}. \tag{6.94}$$

Here $\boldsymbol{q}_{\max}$ is the wavenumber that gives the maximum value of $\chi^{(0)}$. In the case of $\boldsymbol{q}_{\max}=0$, as can be seen in Fig. 6.5, $chi^{(0)}(\boldsymbol{q}_{\max}) \to \rho(\epsilon_{\rm F})/2$, then naturally this agrees with the Stoner condition. On the other hand, when $\boldsymbol{q}_{\max}\neq 0$, a magnetic order with finite wavenumber exists. This corresponds to **spin density wave (SDW)**.

6.5 Self-consistent renormalization spin fluctuation theory

As we have seen above, the mean field (HF approximation) theory based on the Hubbard model has various problems both in principle and in comparison with experiments. On the other hand, although parameter tuning may be included, it

explains some aspects of experiments such as the Slater-Pauling's curve. It is impossible to discuss trends of researches from a single point of view. However a way to view the flows of research on magnetism is that there were two ways to go after the HF approximation. One is to look for different ways from HFA by simplifying models, by considering extreme cases and the strong correlation is taken into account more seriously. The other is improvement of HFA to solve the difficulties. The former has produced many interesting results on mathematical physics and conversely experiments appeared aiming at realizing such mathematical models. A big success of the latter is **self-consistent renormalization (SCR) spin fluctuation** theory[5].

Since it is difficult to see the mathematical scientific direction in the remaining one lecture, I would like to briefly explain the SCR theory and finish it. Many textbooks on mathematical science directions and strongly correlated systems have been published during the last quarter century[6, 7, 8, 9]. If you are interested, please refer to them.

(To be continued)

Appendix 13A: Derivation of integral equation

We define the interaction representation of ρ ($\rho^{(\mathrm{I})}$) as

$$\rho(t) = e^{\mathscr{H}_0 t/(i\hbar)}\rho_{\mathrm{I}}(t)e^{-\mathscr{H}_0 t/(i\hbar)} = U_0(t)\rho_{\mathrm{I}}(t)U_0^{-1}(t), \quad U_0(t) \equiv \exp\left(\frac{\mathscr{H}_0}{i\hbar}t\right). \tag{13A.1}$$

Here, $\rho_{\mathrm{I}} = U_0^{-1}\rho U_0$, $[\mathscr{H}_0, U_0] = 0$. Also

$$\frac{\partial U_0}{\partial t} = \frac{\mathscr{H}_0}{i\hbar}U_0 = \frac{1}{i\hbar}U_0\mathscr{H}_0, \quad \frac{\partial U_0^{-1}}{\partial t} = -\frac{\mathscr{H}_0}{i\hbar}U_0^{-1} = -\frac{1}{i\hbar}U_0^{-1}\mathscr{H}_0, \quad U_0^{-1}(t) = U_0(-t).$$

Then from eq. (6.55), the equation of motion for $\rho_{\mathrm{I}}(t)$ is

$$\begin{aligned} i\hbar\frac{\partial\rho_{\mathrm{I}}}{\partial t} &= i\hbar\left(\frac{\partial U_0^{-1}}{\partial t}\rho U_0 + U_0^{-1}\frac{\partial\rho}{\partial t}U_0 + U_0^{-1}\rho\frac{\partial U_0}{\partial t}\right) \\ &= i\hbar\left(-\frac{\mathscr{H}_0}{i\hbar}U_0^{-1}\rho U_0 + \frac{1}{i\hbar}U_0^{-1}[\mathscr{H}_0 + \mathscr{H}_{\mathrm{ext}}, \rho]U_0 + U_0^{-1}\rho\frac{\mathscr{H}_0}{i\hbar}U_0\right) \\ &= U_0^{-1}(\mathscr{H}_{\mathrm{ext}}\rho - \rho\mathscr{H}_{\mathrm{ext}})U_0 \\ &= [U_0^{-1}\mathscr{H}_{\mathrm{ext}}U_0, \rho_{\mathrm{I}}]. \end{aligned} \tag{13A.2}$$

From the condition $\rho = \rho_{\mathrm{eq}}$ and $\mathscr{H}_{\mathrm{ext}} = 0$ for $t = -\infty$, by integrating both sides of eq. (13A.2) with $(-\infty, t]$,

$$\rho_{\mathrm{I}}(t) - \rho_{\mathrm{I}}(-\infty) = -\frac{1}{i\hbar}\int_{-\infty}^{t} dt'[U_0^{-1}(t')\mathscr{H}_{\mathrm{ext}}U_0(t'), \rho_{\mathrm{I}}(t')]. \tag{13A.3}$$

The we obtain

$$\begin{aligned} \rho(t) &= \rho(-\infty) + \frac{1}{i\hbar}U_0(t)\left\{\int_{-\infty}^{t} dt'[U_0^{-1}(t')\mathscr{H}_{\mathrm{ext}}U_0(t'), U_0^{-1}(t')\rho(t')U_0(t')]\right\}U_0^{-1}(t) \\ &= \rho_{\mathrm{eq}} + \frac{1}{i\hbar}\int_{-\infty}^{t} dt' U_0(t-t')[\mathscr{H}_{\mathrm{ext}}(t'), \rho(t')]U_0^{-1}(t-t'), \end{aligned} \tag{13A.4}$$

which is eq. (6.57).

Appendix 13B: Fluctuation-dissipation theorem

We change the order of Q and P in

$$\mathcal{S}_{QP}(\omega) = \int_{-\infty}^{\infty} dt\, \langle Q(t), P\rangle\, e^{i\omega t},$$

to write

$$\int_{-\infty}^{\infty} dt\, \langle PQ(t)\rangle\, e^{i\omega t} = \int_{-\infty}^{\infty} dt \frac{1}{Z} \mathrm{Tr}\{e^{-\beta\mathscr{H}} P e^{i\mathscr{H}t/\hbar} Q e^{-i\mathscr{H}t/\hbar}\} e^{i\omega t}. \tag{13B.1}$$

Now we use mathematical identity that for operators A, B, C, $\mathrm{Tr}\{ABC\}$ satisfies

$$\mathrm{Tr}\{ABC\} = \mathrm{Tr}\{CAB\} = \mathrm{Tr}\{BCA\}. \tag{13B.2}$$

Then

$$\begin{aligned}
\int_{-\infty}^{\infty} dt\, \langle PQ(t)\rangle\, e^{i\omega t} &= \int_{-\infty}^{\infty} dt \frac{1}{Z} \mathrm{Tr}\{e^{i\mathscr{H}t/\hbar} Q e^{-i\mathscr{H}t/\hbar} e^{-\beta\mathscr{H}} P\} e^{i\omega t} \\
&= \int_{-\infty}^{\infty} dt \frac{1}{Z} \mathrm{Tr}\{e^{-\beta\mathscr{H}} e^{(i/\hbar)\mathscr{H}(t-i\beta\hbar)} Q e^{-(i/\hbar)\mathscr{H}(t-i\beta\hbar)} P\} e^{i\omega(t-i\beta\hbar)} e^{-\beta\hbar\omega} \\
&= e^{-\beta\hbar\omega} \mathcal{S}_{QP}(\omega).
\end{aligned} \tag{13B.3}$$

Namely we reach

$$\mathcal{S}_{QP}(\omega) = \frac{1}{1-e^{-\beta\hbar\omega}} \int_{-\infty}^{\infty} dt\, \langle [Q(t), P]\rangle\, e^{i\omega t} = \frac{i}{1-e^{-\beta\hbar\omega}} [G^{+}_{QP}(\omega) - G^{-}_{QP}(\omega)]. \tag{13B.4}$$

References

[1] 川畑有郷. 電子相関 (パリティ物理学コース クローズアップ). 丸善, 3 1992.

[2] Giuseppe De Nittis. *Linear Response Theory: An Analytic-Algebraic Approach (SpringerBriefs in Mathematical Physics)*. Springer, 6 2017.

[3] Ryogo Kubo. Statistical-mechanical theory of irreversible processes. i. general theory and simple applications to magnetic and conduction problems. *Journal of the Physical Society of Japan*, Vol. 12, No. 6, pp. 570–586, June 1957.

[4] Philip Phillips. *Advanced Solid State Physics (English Edition)*. Cambridge University Press, 3 2012.

[5] Tôru Moriya. Theory of itinerant electron magnetism. *Journal of Magnetism and Magnetic Materials*, Vol. 100, No. 1-3, pp. 261–271, November 1991.

[6] 青木秀夫, 草部浩一. 強磁性 (多体電子論). 東京大学出版会, 12 1998.

[7] Adolfo Avella and Ferdinando Mancini, editors. *Strongly Correlated Systems: Theoretical Methods (Springer Series in Solid-State Sciences)*. Springer, 1 2014.

[8] 勝藤拓郎. 基礎から学ぶ強相関電子系 – 量子力学から固体物理、場の量子論まで (物質・材料テキストシリーズ). 内田老鶴圃, 6 2017.

[9] Daniel P. Arovas, Erez Berg, Steven A. Kivelson, and Srinivas Raghu. The hubbard model. *Annual Review of Condensed Matter Physics*, Vol. 13, No. 1, pp. 239–274, March 2022.

Lecture note Magnetism (14)

13th July (2022) Shingo Katsumoto, Institute for Solid State Physics, University of Tokyo

Let us go into **self-consistent renormalization** (SCR) **spin fluctuation** (SF) theory, the entrance of which we finally reached last week. As mentioned in the last lecture, SCR-SF theory approaches the problem with improving the approximation not taking completely different ways. The theory then gained great successes[1]. We have used two weeks to reach the entrance. It is impossible to introduce the details of the first paper[1] in a single lecture. Here I would like to introduce only the framework of the theory along with resumes like [2, 3].e Those who wish to know the details are requested to refer to monographs of this topic[4, 5, 6], and to original papers [*1].

6.5.1 Weak metallic ferromagnetism, paramagnonr

Kawabata, one of the founders of SCR-SP theory, says a strong motivation of the theory is the finding of weak metallic ferromagnetism like $ZrZn_2$, Sc_3In, Ni_3Al[2], Also in the textbook[4] by Moriya, who is synonymous with SCR-SF theory, paramagnon theory by Izuyama and Kubo[7] is introduced as a preliminary form of SCR-SF theory. Let us then consider paramagnons, which are spin waves in non-magnetically-ordered metals with strong effective interactions between spins. Such metals are considered to be marginal to ferromagnetism (anti-ferromagnetism). Palladium (Pd) tends to form ferromagnetic alloys with non-magnetic elements and is considered to be close to ferromagnetism[8]. Helium-3, which is not a metal but has a nuclear spin, can also be mentioned. It is long since the magnon (paramagnon) system of superfluid helium-3 was found to cause BEC[9, 10]. In high-T_C cuprates close to anti-ferromagnetic order[11], also in iron-based high-T_C superconductors[12], existences of paramagnons have been confirmed and the dispersion relations etc. have been determined.

We saw in the last lecture that in RPA, which is the mean field approximation on dynamic susceptibility, magnon states may be magnetically ordered ground states. This suggests that spin-fluctuations may be considered as excited states in the magnon-system picture even when the ground state is paramagnetic. It also suggests that the existence of such collective excitations may greatly lower the energy of excited states compared with those in static HF approximations. In spite of such signs of improvement, the simple RPA does not solve the problems of mean field theory in temperature dependence of susceptibility etc. This is probably due to ignoring spin fluctuation in finite temperature thermal equilibrium state. Then in the paramagnon theory we consider the spin fluctuation in paramagnetic state.

Hellmann-Feynman theorem

First we prove the following general theorem. We consider a Hamiltonian with parameter p

$$\mathscr{H}(p) = \mathscr{H}_0 + \mathscr{H}_1(p) \tag{6.95}$$

with normalized eigenstate $|p, n\rangle$ and the eigen energy $E_n(p)$. A change in an eigenstate due to an infinitesimally small change δp of p $\mathscr{H}(p + \delta p)$ is expressed as a linear sum of the original eigenstates as

$$|p + \delta p, n\rangle = |p, n\rangle + \sum_m C_m |p, m\rangle . \tag{6.96}$$

[*1] As far as I checked, most of textbooks written in English, do not even refer to the SCR-SF theory, whose logic is even difficult to be followed. They usually introduce the simple HF approximation, then shift to DFT or GGA, in which the approximation is improved. These ab initio calculation may doing similar improvement for the HF as SCR-SF though the details cannot be known.

If we assume linear approximation $C_m = c_m \delta p$, from

$$\langle p+\delta p, n|p+\delta p, n\rangle = |1+c_n\delta p|^2 \langle p, n|p, n\rangle + \sum_{m\neq n} |c_m|^2 |\delta p|^2 \langle p, m|p, m\rangle ,$$

the condition of normalization leads to $c_n = 0$, that is, within linear approximation in δp, $C_n = 0$. Namely, within linear approximation of δp,

$$\langle p+\delta p|\mathscr{H}(p)|p+\delta p\rangle = \langle p|\mathscr{H}(p)|p\rangle = E_n(p). \tag{6.97}$$

Then we can write the shift in the eigenenergy as

$$\begin{aligned} E_n(p+\delta p) &= \langle p+\delta p, n|\mathscr{H}(p+\delta p)|p+\delta p, n\rangle \\ &= \left\langle p+\delta p, n \left| \mathscr{H}(p) + \delta p \frac{\partial \mathscr{H}(p)}{\partial p} \right| p+\delta p, n \right\rangle \\ &= E_n(p) + \delta p \left\langle p, n \left| \frac{\partial \mathscr{H}(p)}{\partial p} \right| p, n \right\rangle . \end{aligned} \tag{6.98}$$

We can thus conclude

$$\frac{dE_n(p)}{dp} = \left\langle p, n \left| \frac{\partial \mathscr{H}_1(p)}{\partial p} \right| p, n \right\rangle . \tag{6.99}$$

This is called **Hellmann-Feynman theorem**.

From this theorem, e.g., the free energy $F(p)$ of the system of Hamiltonian $\mathscr{H}(p)$ can be written as

$$\frac{\partial F(p)}{\partial p} = \frac{1}{Z}\sum_n \exp\left[\frac{-E_n(p)}{k_{\mathrm{B}}T}\right] \frac{\partial E_n(p)}{\partial p}. \tag{6.100}$$

In eq. (6.95), $\mathscr{H}_1(p)$ can be an interaction Hamiltonian $\mathscr{H}_I$ of interaction constant I. From Hellmann-Feynman theorem, we can introduce the interaction with varying the interaction constant as $I : 0 \to I$. The correction term for free energy is given as a function of I by

$$F(I) = F(0) + \int_0^I \left\langle \frac{\partial \mathscr{H}_{I'}}{\partial I'} \right\rangle dI'. \tag{6.101}$$

From the above, we consider the contribution of spin fluctuation to the specific heat. Here Hubbard model in eq. (6.29) can be written as

$$\mathscr{H} = \sum_{\boldsymbol{k},s} \epsilon_{\boldsymbol{k}} a^\dagger_{\boldsymbol{k}s} a_{\boldsymbol{k}s} + U\sum_i^N \hat{n}_{i\uparrow}\hat{n}_{i\downarrow} = \mathscr{H}_0 + \mathscr{H}_I. \tag{6.102}$$

As in the transform of first term, an operator at lattice point $\boldsymbol{R}_i$ is Fourier-expanded as

$$c_{is} = \frac{1}{\sqrt{N}}\sum_{\boldsymbol{k}} e^{i\boldsymbol{R}_i\cdot\boldsymbol{k}} a_{\boldsymbol{k}s}. \tag{6.103}$$

And as in eq. (6.83c), we write $\mathscr{H}_I$ as

$$\mathscr{H}_I = \frac{U}{N}\sum_{\boldsymbol{k},\boldsymbol{k}',\boldsymbol{q}} a^\dagger_{\boldsymbol{k}+\boldsymbol{q}\uparrow} a_{\boldsymbol{k}\uparrow} a^\dagger_{\boldsymbol{k}'-\boldsymbol{q}\downarrow} a_{\boldsymbol{k}'\downarrow}, \tag{6.104}$$

where the interaction parameter is $I = U/N$. We also change the notation in eq. (6.78) a bit to

$$\left.\begin{aligned} S_+(\boldsymbol{q}) &= \sum_{\boldsymbol{k}} a^\dagger_{\boldsymbol{k}\uparrow} a_{\boldsymbol{k}+\boldsymbol{q}\downarrow}, \\ S_-(\boldsymbol{q}) &= \sum_{\boldsymbol{k}} a^\dagger_{\boldsymbol{k}\downarrow} a_{\boldsymbol{k}+\boldsymbol{q}\uparrow}. \end{aligned}\right\} \tag{6.78}$$

From fermionic commutation relation, with exchanging the last two operators in the sum in right-hand side, eq. (6.104) is developed to

$$\begin{aligned}\mathscr{H}_I &= I \sum_{\boldsymbol{k},\boldsymbol{k}',\boldsymbol{q}} a^\dagger_{\boldsymbol{k}+\boldsymbol{q}\uparrow} a_{\boldsymbol{k}\uparrow} (\delta_{\boldsymbol{k}',\boldsymbol{k}'-\boldsymbol{q}} - a_{\boldsymbol{k}'\downarrow} a^\dagger_{\boldsymbol{k}'-\boldsymbol{q}\downarrow}) \\ &= I \left[\sum_{\boldsymbol{k},\boldsymbol{k}'} a^\dagger_{\boldsymbol{k}\uparrow} a_{\boldsymbol{k}\uparrow} - \sum_{\boldsymbol{k},\boldsymbol{k}',\boldsymbol{q}} a^\dagger_{\boldsymbol{k}+\boldsymbol{q}\uparrow} a_{\boldsymbol{k}'\downarrow} a^\dagger_{\boldsymbol{k}-\boldsymbol{q}\downarrow} a_{\boldsymbol{k}\uparrow} \right]. \end{aligned} \tag{6.105}$$

Wavenumber $\boldsymbol{q}$, over which the sum is taken, transform $\boldsymbol{q} \to -\boldsymbol{q} + \boldsymbol{k}' - \boldsymbol{k}$ results in $\boldsymbol{k} + \boldsymbol{q} \to \boldsymbol{k} - \boldsymbol{q} + \boldsymbol{k}' - \boldsymbol{k} = \boldsymbol{k}' - \boldsymbol{q}$, and similarly $\boldsymbol{k}' - \boldsymbol{q} \to \boldsymbol{k} + \boldsymbol{q}$. Then from eq. (6.78), we can write

$$\begin{aligned}\mathscr{H}_I &= I \left[\sum_{\boldsymbol{k},\boldsymbol{k}'} a^\dagger_{\boldsymbol{k}\uparrow} a_{\boldsymbol{k}\uparrow} - \sum_{\boldsymbol{k},\boldsymbol{k}',\boldsymbol{q}} a^\dagger_{\boldsymbol{k}'-\boldsymbol{q}\uparrow} a_{\boldsymbol{k}'\downarrow} a^\dagger_{\boldsymbol{k}+\boldsymbol{q}\downarrow} a_{\boldsymbol{k}\uparrow} \right] \\ &= I \left[\sum_{\boldsymbol{k},\boldsymbol{k}'} a^\dagger_{\boldsymbol{k}\uparrow} a_{\boldsymbol{k}\uparrow} - \sum_{\boldsymbol{q}} S_+(-\boldsymbol{q}) S_-(\boldsymbol{q}) \right] = I \left[\sum_{\boldsymbol{k},\boldsymbol{k}'} a^\dagger_{\boldsymbol{k}\uparrow} a_{\boldsymbol{k}\uparrow} - \sum_{\boldsymbol{q}} S_+(\boldsymbol{q}) S_-(-\boldsymbol{q}) \right]. \end{aligned} \tag{6.106}$$

Next, in paramagnetic states, $\mathscr{H}_I$ does not change with spin inversion, thus, we add the expression of $\uparrow \leftrightarrow \downarrow$ and divide by two to obtain

$$\mathscr{H}_I = \frac{N_e U}{2} - \frac{I}{2} \sum_{\boldsymbol{q}} \{S_+(\boldsymbol{q}), S_-(-\boldsymbol{q})\}_+, \tag{6.107}$$

where N_e is the number of electrons, $\{A, B\}_+ = AB + BA$ represents anti-commutation relation. In eq. (6.106), sums over $\boldsymbol{k}$, $\boldsymbol{k}'$ produce N_e and N respectively. The latter is because the sum comes from that over $\boldsymbol{R}_i$. Accordingly, the variation in the free energy due to introduction of interaction is given by

$$\Delta F = \frac{N_e U}{2} - \frac{1}{2} \sum_{\boldsymbol{q}} \int_0^I dI' \, \langle \{S_+(\boldsymbol{q}), S_-(-\boldsymbol{q})\}_+ \rangle \,. \tag{6.108}$$

For usage of fluctuation-dissipation theorem, remember eq. (6.74):

$$\mathcal{G}^+_{QP}(\omega) = \sum_{n,m} \langle n|Q|m\rangle \langle m|P|n\rangle \frac{e^{-\beta E_n} - e^{-\beta E_m}}{E_n - E_m + \hbar\omega + i\eta}. \tag{6.74}$$

If we use the lower half of complex plane by replacing $\eta \to -\eta$, we obtain a parallel representation for $\mathcal{G}^-_{QP}(\omega)$. From these two, we can write

$$\mathcal{G}^+_{QP}(\omega) - \mathcal{G}^-_{QP}(\omega) = -2i\mathrm{Im}[\chi_{QP}(\omega)],$$

to further obtain

$$\mathcal{S}_{QP}(\omega) = \frac{2}{1 - e^{-\beta\hbar\omega}} \mathrm{Im}[\chi_{QP}(\omega)]. \tag{6.109}$$

We also rewrite eq. (6.80) as

$$\chi_{+-}(\boldsymbol{q}, \omega) = -(g\mu_\mathrm{B})^2 \frac{i}{\hbar} \int_0^\infty dt \, \langle [S_-(-\boldsymbol{q}), S_+(\boldsymbol{q}, t)] \rangle \, e^{i\omega t}. \tag{6.110}$$

Let $|n\rangle$ and E_n be a many-body eigenstate and its eigenenergy of Hamiltonian in eq. (6.102), then the imaginary part of $\chi_{+-}(\boldsymbol{q}, \omega)$ is given by

$$\mathrm{Im}[\chi_{+-}(\boldsymbol{q}, \omega)] = \frac{\pi(g\mu_\mathrm{B})^2}{\hbar} \sum_{m,n} (\rho_m - \rho_n) \delta(\omega - \Delta E_{mn}/\hbar) \, \langle n|S_-(-\boldsymbol{q})|m\rangle \langle m|S_+(\boldsymbol{q})|n\rangle \,, \tag{6.111}$$

where

$$\text{Boltzmann factor: } \rho_n = \frac{1}{Z} \exp\left[-\frac{E_n}{k_\mathrm{B} T}\right], \quad \Delta E_{mn} = E_m - E_n.$$

Multiply both sides of eq. (6.111) by $\coth(\beta\omega\hbar/2)$, and integrate over ω to obtain

$$\begin{aligned}
&\int_{-\infty}^{\infty} d\omega \mathrm{Im}\chi_{+-}(\boldsymbol{q},\omega)\coth\left(\frac{\hbar\omega}{2k_{\mathrm{B}}T}\right) \\
&\quad = \frac{\pi(g\mu_{\mathrm{B}})^2}{\hbar}\sum_{m,n}(\rho_m-\rho_n)\coth\left(\frac{\Delta E_{nm}}{k_{\mathrm{B}}T}\right)\langle n|S_-(-\boldsymbol{q})|m\rangle\langle m|S_+(\boldsymbol{q})|n\rangle \\
&\quad = \frac{\pi(g\mu_{\mathrm{B}})^2}{\hbar}\langle\{S_-(-\boldsymbol{q}),S_+(\boldsymbol{q})\}_+\rangle\,. \qquad (6.112)
\end{aligned}$$

Then we can write the variation of free energy in eq. (6.108) as

$$\Delta F = \frac{N_e U}{2} - \sum_{\boldsymbol{q}}\int_0^I dI'\frac{1}{2\pi}\int_{-\infty}^{\infty} d\omega\coth\left(\frac{\hbar\omega}{2k_{\mathrm{B}}T}\right)\mathrm{Im}[\chi_{+-}(\boldsymbol{q},\omega)]. \qquad (6.113)$$

By applying the RPA formula in eq. (6.87), the above is approximated as

$$\Delta F = \frac{N_e U}{2} + \sum_{\boldsymbol{q}}\frac{1}{\pi}\int_0^{\infty} d\omega\coth\left(\frac{\hbar\omega}{k_{\mathrm{B}}T}\right)\mathrm{Im}\{\log[1-2U\chi^{(0)}(\boldsymbol{q},\omega)]\}. \qquad (6.114)$$

For calculation of specific heat, only temperature-dependent parts in ΔF are necessary.

$$\coth\frac{\hbar\omega}{k_{\mathrm{B}}T} = 1 + \frac{2}{e^{\hbar\omega/k_{\mathrm{B}}T}-1}. \qquad (6.115)$$

In the above, the first term "1" in the right hand side is the zero-point motion of paramagnons and ignored in the calculation of specific heat. In eq. (6.114), we need to consider the contribution of $\chi^{(0)}(q,\omega)$, susceptibility of non-interacting system. In (q,ω)-plane shown in Fig. 6.4, the largest contribution is given in region-III, in which we can expand $\chi^{(0)}(q,\omega)$ as

$$\chi^{(0)}(q,\omega) = \frac{1}{2}\rho(\epsilon_{\mathrm{F}})\left[1 - A_0\left(\frac{q}{k_{\mathrm{F}}}\right)^2 + iC_0\frac{\hbar\omega}{\epsilon_{\mathrm{F}}}\frac{k_{\mathrm{F}}}{q}\right]. \qquad (6.116)$$

Here the expansion coefficients are

$$A_0 = \frac{1}{12}, \quad C_0 = \frac{\pi}{4}. \qquad (6.117)$$

For the simplest approximation we use this expression of $\chi^{(0)}(q,\omega)$. Let $\alpha \equiv U\rho(\epsilon_{\mathrm{F}})$ be the interaction constant, we reach

$$\begin{aligned}
\Delta F(T) &= \frac{N}{2}\rho(\epsilon_{\mathrm{F}})\epsilon_{\mathrm{F}}^2\int_0^{q_{\mathrm{c}}} q^2dq\int_0^{\infty} d\omega\frac{2}{e^{\beta\omega}-1}\mathrm{Im}\left[\log\left(1-\alpha+\alpha A_0q^2 - i\alpha C_0\frac{\omega}{q}\right)\right] \\
&= -\frac{N}{2}\rho(\epsilon_{\mathrm{F}})\epsilon_{\mathrm{F}}^2\int_0^{q_{\mathrm{c}}} q^2dq\int_0^{\infty} d\omega\frac{2}{e^{\beta\omega}-1}\arctan\left[\frac{\omega}{q}\frac{C_0}{K_0^2+A_0q^2}\right]. \qquad (6.118)
\end{aligned}$$

As before, for simplicity of representation, unit of wavenumber q is taken as k_{F}, $\hbar = 1$, unit of energy ω is taken as ϵ_{F}. q_{c} is a cutoff of wavenumber. Here expansion in region-III is effective only for finite q and the cutoff is indispensable and is around 1 (k_{F}). And K_0 is

$$K_0^2 = \frac{1-\alpha}{\alpha}. \qquad (6.119)$$

We further apply low temperature approximation $\omega \ll 1$ and $\arctan x \sim x$ to obtain

$$\frac{\Delta F(T)}{N} = -\frac{2\pi^2}{3}\rho(\epsilon_{\mathrm{F}})(k_{\mathrm{B}}T)^2\frac{C_0}{2\pi A_0}\log\frac{K_0^2+A_0q_{\mathrm{c}}^2}{K_0^2}, \qquad (6.120)$$

from which we know the spin-fluctuation contribution to low temperature specific heat is proportional to T. Then if we write

$$C = \gamma T, \quad \gamma_0 \equiv \frac{2\pi^2}{3}k_{\mathrm{B}}^2\rho(\epsilon_{\mathrm{F}}), \qquad (6.121)$$

then the coefficient γ is

$$\gamma = \gamma_0 \left(1 + \frac{C_0}{\pi A_0} \log \frac{K_0^2 + A_0 q_c^2}{K_0^2}\right), \tag{6.122}$$

where γ_0 is the temperature coefficient of specific heat of electron systems without contribution from spin fluctuation. Equation (6.122) tells that the temperature coefficient of specific heat logarithmically diverges as the condition approaches Stoner ferromagnetic criterion $\alpha \to 1$, $K_0 \to 0$.

6.5.2 SCR spin-fluctuation theory

So far, Hellmann-Feynman theorem and fluctuation-dissipation theorem are used to obtain the expression for free energy of thermal equilibrium with dynamic susceptibility. By applying RPA to dynamic susceptibility, the effect of spin-fluctuation is included. However, at this stage the theory just describes low-temperature approximation of paramagnetic states. A problem here is, as is always the case of many-body problem, the effect of spin-fluctuation should be reflected on the spin-fluctuation. Hence this simply cannot be applied to ferromagnetic state with spontaneous magnetization. For that we need to consider self-consistent equation as in the case of Heisenberg model.

Then, here, we consider the free energy in the presence of magnetization M. The free energy is given as the sum of free energy $F_0(M,T)$ of non-interacting system and the quantity in eq. (6.113) by

$$F(M,T) = F_0(M,T) + \frac{N_e U}{2} - bM - \sum_{\boldsymbol{q}} \int_0^I dI' \frac{1}{2\pi} \int d\omega \coth \frac{\hbar\omega}{2k_B T} \mathrm{Im}[\chi_{+-}(M, I'; \boldsymbol{q}, \omega)]. \tag{6.123}$$

$-bM$ is the Zeeman term. Here, as a notation, the magnetization M and the interaction parameter I are specified in the dynamic susceptibility χ_{+-}.

As we saw in the GL theory static spontaneous magnetization M is given by extremum condition of F as

$$\frac{\partial F(M,T)}{\partial M} = 0. \tag{6.124}$$

This can be viewed as **magnetic equation of state**.

We restart with eq. (6.113), which does not contain any approximation. In HF mean-field approximation, integrand of the second term in right-hand side is replaced with the one without interaction ($I = 0$), thus the integration with dI' over region $[0, I]$ is replaced with simple product of I.

$$\Delta F_{\mathrm{HF}} = \frac{N_e U}{2} - I \sum_{\boldsymbol{q}} \frac{1}{2\pi} \int_{-\infty}^{\infty} d\omega \coth \left(\frac{\hbar\omega}{2k_B T}\right) \mathrm{Im}[\chi_{+-}(M, 0; \boldsymbol{q}, \omega)]. \tag{6.125}$$

From the Hubbard model in eq. (6.102), we consider the quantity:

$$\begin{aligned} \left\langle \frac{\partial \mathscr{H}}{\partial I} \right\rangle_{I=0} &= N \sum_i^N \langle n_{i\uparrow} n_{i\downarrow} \rangle_{I=0} = N \sum_i^N \langle n_{i\uparrow} \rangle \langle n_{i\downarrow} \rangle \\ &= \frac{N^2}{4}(n_+^2 - n_-^2) = \frac{N^2}{4}[n^2 - (2m)^2] = \frac{N_e^2}{4} - M^2. \end{aligned} \tag{6.126}$$

In the above, small characters n, m are the numbers per sites, and

$$n_+ = n_\uparrow + n_\downarrow, \quad n_- = n_\uparrow - n_\downarrow, \quad m = \frac{n_-}{2},$$

where the unit of magnetization is taken as $g\mu_B$, the spin is 1/2. We take eq. (6.126) multiplied by I as the I-proportional term in (6.125). Then we can write formally

$$\begin{aligned} F(M,T) = F_0(M,T) + I\left(\frac{N_e^2}{4} - M^2\right) - bM & \quad : \text{HF Approximation} \\ - \sum_{\boldsymbol{q}} \int_0^I dI' \frac{1}{2\pi} \int_{-\infty}^{\infty} d\omega \coth \frac{\hbar\omega}{k_B T} \mathrm{Im}[\chi_{+-}(M, I'; \boldsymbol{q}, \omega) - \chi_{+-}(M, 0; \boldsymbol{q}, \omega)] & \quad : \text{Correction.} \end{aligned} \tag{6.127}$$

As is in paramagnon theory, we apply RPA(eq. (6.87)) to $\chi_{+-}(M, I'; \boldsymbol{q}, \omega)$. Then the integration with I' can be performed and the result is

$$F(M,T) = F_0(M,T) + I\left(\frac{N_e^2}{4} - M^2\right) - bM \\ - \sum_{\boldsymbol{q}} \frac{1}{2\pi}\int_{-\infty}^{\infty} d\omega \coth\frac{\hbar\omega}{k_{\mathrm{B}}T}\mathrm{Im}[\log\{1 - 2U\chi^{(0)}(M;\boldsymbol{q},\omega)\} + 2U\chi^{(0)}(M;\boldsymbol{q},\omega)], \tag{6.128}$$

where we write

$$\chi^{(0)}(M;\boldsymbol{q},\omega) = \frac{1}{2N}\chi_{+-}(M,0;\boldsymbol{q},\omega). \tag{6.129}$$

We obtain the following magnetic equation of state by calculating magnetization-derivative of eq. (6.124) in eq. (6.128).

$$\frac{\partial F_0}{N\partial m} - 2Um - b - \frac{1}{N}\sum_{\boldsymbol{q}}\frac{1}{2\pi}\int_{-\infty}^{\infty} d\omega \coth\frac{\hbar\omega}{2k_{\mathrm{B}}T}\mathrm{Im}\left[\frac{2U\chi^{(0)}(M;\boldsymbol{q},\omega)}{1-2U\chi^{(0)}(M;\boldsymbol{q},\omega)}2U\frac{\partial\chi^{(0)}(M;\boldsymbol{q},\omega)}{\partial m}\right] = 0, \tag{6.130}$$

which is given as an equation for magnetization per site $m = M/N$.

Here we formally define magnetization per site in paramagnetic states as

$$\chi = \frac{\partial m}{\partial b}, \quad \frac{1}{\chi} = \frac{\partial b}{\partial m}. \tag{6.131}$$

We also write susceptibility per site for non-interacting system as χ_0. Free energy of the system with Zeeman term $F_0 - bm$ gives a magnetic equation of state as

$$\frac{\partial F_0}{N\partial m} - b = 0. \tag{6.132}$$

By applying eq. (6.124) to the above with transposition of b, we obtain

$$\frac{\partial^2 F_0}{N\partial m^2} = \frac{1}{\chi_0}. \tag{6.133}$$

Then in eq. (6.130) for the case of paramagnetic state, substituting the above gives

$$\frac{1}{\chi} = \frac{1}{\chi_0} - 2U \\ - \frac{1}{N}\sum_{\boldsymbol{q}}\frac{1}{2\pi}\int_{-\infty}^{\infty} d\omega \coth\frac{\hbar\omega}{2k_{\mathrm{B}}T}(2U)^2 \\ \times \mathrm{Im}\left[\chi(\boldsymbol{q},\omega)\left.\frac{\partial^2\chi^{(0)}(\boldsymbol{q},\omega)}{\partial m^2}\right|_{m=0} + \chi^2(\boldsymbol{q},\omega)\left\{\frac{1}{\chi^{(0)}}(\boldsymbol{q},\omega)\left.\frac{\partial\chi^{(0)}(\boldsymbol{q},\omega)}{\partial m}\right|_{m=0}\right\}^2\right], \tag{6.134}$$

the last part of which is calculated as follows. Equation (6.87) of RPA and eq. (6.129) lead to

$$\chi_(\boldsymbol{q},\omega) = \frac{\chi^{(0)}(\boldsymbol{q},\omega)}{1-2U\chi^{(0)}(\boldsymbol{q},\omega)}. \tag{6.135}$$

We then apply this to obtain

$$\frac{\partial\chi}{\partial m} = \frac{\partial\chi}{\partial\chi^{(0)}}\frac{\partial\chi^{(0)}}{\partial m} = \frac{1}{(1-2U\chi^{(0)})^2}\frac{\partial\chi^{(0)}}{\partial m} = \chi^2\frac{1}{\chi^{(0)2}}\frac{\partial\chi^{(0)}}{\partial m}.$$

Equation (6.134) tells the existence of correction, which is expressed as an integral with ω, to the susceptibility from the term indicated as "Correction" in eq. (6.127). In the correction, inside $\mathrm{Im}[\cdots]$, within two terms in $\cdots$, the first term is linear in spin-fluctuation, the second is in the second order. Here we only consider the linear term. We further approximate the first term by replacing $\partial^2\chi^{(0)}/\partial m^2|_{m=0}$ with the value for $q = 0, \omega = 0$.h Then by writing that

$$g = -(2U)^2\chi_0\left.\frac{\partial^2\chi^{(0)}(\boldsymbol{q},\omega)}{\partial m^2}\right|_{m=0,q=0,\omega=0}, \tag{6.136}$$

we obtain the following.

$$\frac{\chi_0}{\chi} = 1 - 2U\chi_0 + \frac{g}{N}\sum_{\boldsymbol{q}} \frac{1}{2\pi}\int_{-\infty}^{\infty} d\omega \coth\frac{\hbar\omega}{2k_{\mathrm{B}}T}\mathrm{Im}[\chi(\boldsymbol{q},\omega)]. \tag{6.137}$$

We further ignore the temperature dependence of susceptibility of non-interacting system χ_0. This should be taken into account, e.g., in comparison with experiments etc., though here our purpose is to see the essential structure of SCR-SF theory. However, we still have the problem of inconsistency in that application of RPA (eq. (6.135)) to the result of (6.137) results in a disagreement of the divergent point of dynamic susceptibility $\omega \neq 0$ and that of static one ($\omega = 0$). In spite of the progress of approximation, a simple RPA still cannot satisfy the self-consistent condition.

The difficulty is avoided in the SCR-SF theory in the following way. We write the susceptibility at absolute zero as

$$\frac{\chi_0}{\chi(T=0)} = 1 - 2U\chi_0 + \frac{g}{N}\sum_{\boldsymbol{q}} \frac{1}{\pi}\int_{0}^{\infty} d\omega \mathrm{Im}[\chi(\boldsymbol{q},\omega)]_{T=0}. \tag{6.138}$$

The third term in the rhs represents the contribution of spin-fluctuation with $q \neq 0$ at absolute zero, namely the zero-point motion. As can be seen here, the effect of spin-fluctuation enters into the denominator of RPA representation making the condition of ferromagnetism difficult to be satisfied.

We take this as an RPA modified in the simplest way by the effect of spin-fluctuation. As is in the case of eq. (6.115), we again ignore the temperature dependence of zero-point motion in magnon spectrum and take the difference between eq. (6.137) and eq. (6.138). The approximation gives

$$\frac{\chi_0}{\chi} = \frac{\chi_0}{\chi(T=0)} + \frac{g}{N}\sum_{\boldsymbol{q}} \frac{1}{\pi}\int_{0}^{\infty} d\omega \frac{2}{e^{\hbar\omega\beta}-1}\mathrm{Im}[\chi(\boldsymbol{q},\omega)]. \tag{6.139}$$

Here an expansion of $\chi^{-1}(\boldsymbol{q},\omega)$ around $(q,\omega) = (0,0)$ is possible as in eq. (6.116). The functional form is

$$\frac{\chi_0}{\chi(\boldsymbol{q},\omega)} = \frac{\chi_0}{\chi(+0,+0)} + A\left(\frac{q}{k_{\mathrm{F}}}\right)^2 - iC\frac{\omega}{\epsilon_{\mathrm{F}}}\frac{k_{\mathrm{F}}}{q}. \tag{6.140}$$

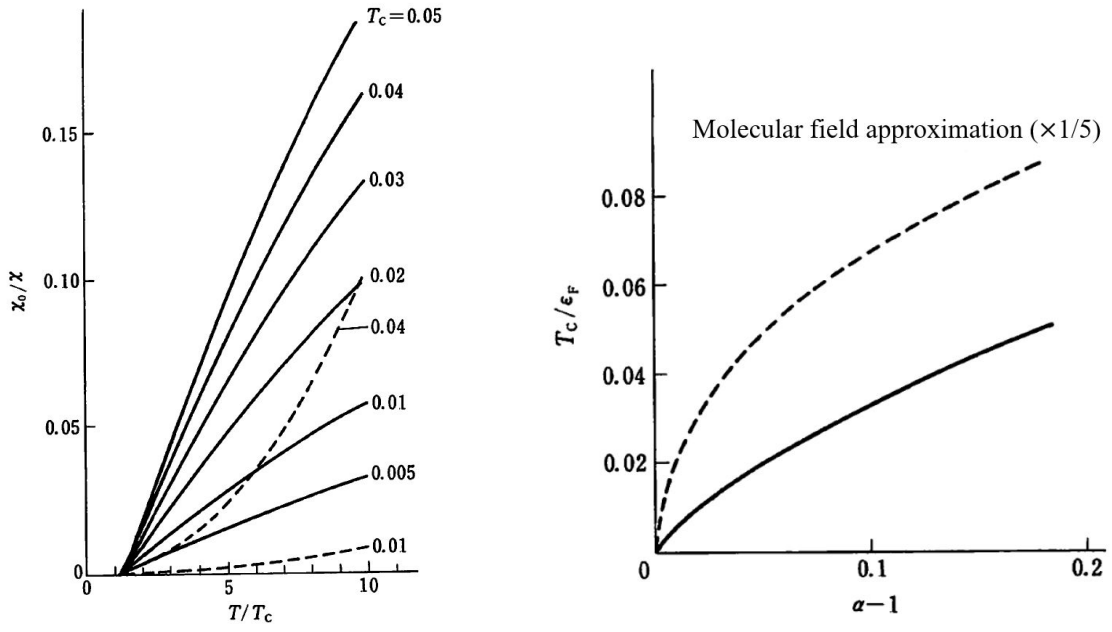

(a) (b)

Fig. 6.6 (a) Temperature dependence of susceptibility in a ferromagnet calculated in the SCR-SF theory. The parameter here is the interaction parameter, which determines T_{C}. The broken lines are by the simple molecular field theory. (b) Critical temperature as a function of Stoner parameter $\alpha = I\mathscr{D}(\epsilon_{\mathrm{F}})$ calculated by the SCR-SF theory. The broken line is 1/5 of the result in the simple molecular field theory. From [1].

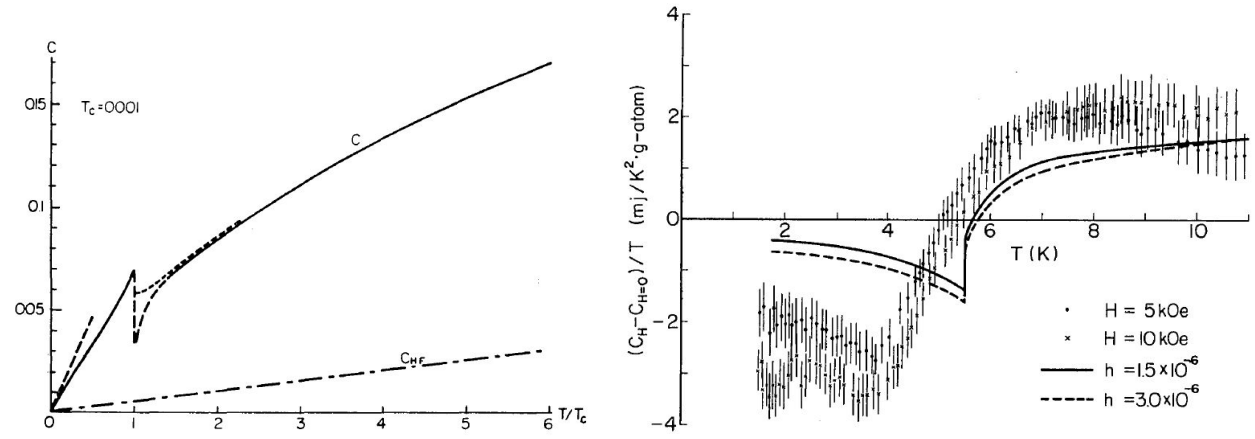

(a) (b)

Fig. 6.7 (a) Specific heat in the vicinity of ferromagnetic transition point calculated with the SCR-SF theory. From [13]. (b) Specific heat of itinerant electron weak ferromagnet Sc_3In under magnetic field around T_C. The measured values in zero-magnetic field is subtracted. Solid and broken lines are results of numerical calculation. From [14].

This form requires agreement of $\chi(\boldsymbol{q},\omega)$ with the static susceptibility for $q \to +0, \omega \to +0$.

In summary, calculation of $\chi(\boldsymbol{q},\omega)$ from (6.139) and (**??**) results in a self-consistent solution. The above is the essential framework of the SCR-SF theory though realistic calculations are far more complicated even for simplified band structure with many expansion coefficients[1].

In Fig. 6.6, we show the temperature dependence of susceptibility calculated with the SCR-SF theory for a simple parabolic band structure and the critical temperature T_C as a function of interaction strength $\alpha = I\mathscr{D}(\epsilon_F)$ (Stoner parameter) [1]. In Fig. 6.6(a), compared with the simplest molecular field theory (broken lines), the SCR-SF theory gives much better linearity in a wide temperature range, which indicates the Curie-Weiss law. Also as in Fig. 6.6(b), the energy of paramagnetic state largely lowers due to the contribution of spin-fluctuation in thermal equilibrium, leading to correction of overestimation in stability of ferromagnetic state. As a result, T_C largely lowers from the results of the molecular field theory.

On the other hand, there still exist many problems and open questions. As shown in Fig. 6.7, there is a large difference between the calculated behavior of specific heat and those in experiments. Studies on these points have long history and they are summarized e.g., in [5].

Appendix 14A: Calculation in (6.111)

The calculation shown in the following, very often appears, e.g, in usage of Green's function (calculation of (6.74) is almost the same). For your convenience, I would like to show a little of calculation in (6.111). It is probably enough to see

$$\frac{i}{\hbar}\int_0^\infty dt\,\langle S_+(\boldsymbol{q},t)S_-(\boldsymbol{q})\rangle\, e^{i\omega t} = (**).$$

This is calculated as follows.

$$\begin{aligned}(**) &= \frac{i}{\hbar Z}\int_0^\infty dt \mathrm{Tr}\left[e^{-\beta\mathscr{H}}e^{(i/\hbar)\mathscr{H}t}S_+(\boldsymbol{q})e^{-(i/\hbar)\mathscr{H}t}S_-(\boldsymbol{q})\right]e^{i\omega t}\\ &= \frac{i}{\hbar Z}\int_0^\infty dt\sum_{n,m}\langle n|\, e^{-\beta\mathscr{H}+(i/\hbar)\mathscr{H}t}S_+(\boldsymbol{q})\,|m\rangle\,\langle m|\, e^{-(i/\hbar)\mathscr{H}t}S_-(\boldsymbol{q})\,|n\rangle\, e^{i\omega t}\\ &= \frac{i}{\hbar Z}\int_0^\infty dt\sum_{n,m} e^{(-\beta+(i/\hbar)t)E_n}\,\langle n|\, S_+(\boldsymbol{q})\,|m\rangle\,\langle m|\, S_-(-\boldsymbol{q})\,|n\rangle\, e^{-(i/\hbar)E_m t}e^{i\omega t}. \qquad (14A.1)\end{aligned}$$

Here we add a infinitesimal real part to the pure imaginary argument of exponential function, which is a trick often appears in Fourier integration over half-infinite region. Rigorous proof is of course possible with ϵ-δ logics. Below, we omit to write but η implicitly means taking the limit $\eta \to +0$.

$$
\begin{aligned}
(**) &= \sum_{n,m} \langle n| S_+(\boldsymbol{q}) |m\rangle \langle m| S_-(-\boldsymbol{q}) |n\rangle \frac{ie^{-\beta E_n}}{\hbar Z} \int_0^\infty dt e^{(i/\hbar)(E_n - E_m + \hbar\omega + i\eta)t} \\
&= \sum_{n,m} \langle n| S_+(\boldsymbol{q}) |m\rangle \langle m| S_-(-\boldsymbol{q}) |n\rangle \rho_n \left[\frac{e^{(i/\hbar)(\hbar\omega - \Delta E_{mn} + i\eta)t}}{\hbar\omega - \Delta E_{mn} + i\eta} \right]_0^\infty \\
&= \sum_{n,m} \langle n| S_+(\boldsymbol{q}) |m\rangle \langle m| S_-(-\boldsymbol{q}) |n\rangle \frac{-\rho_n}{\hbar} \frac{1}{\omega - \Delta E_{mn}/\hbar + i\eta} \\
&= \sum_{n,m} \langle n| S_+(\boldsymbol{q}) |m\rangle \langle m| S_-(-\boldsymbol{q}) |n\rangle \frac{-\rho_n}{\hbar} \left[\frac{1}{\omega - \Delta E_{mn}/\hbar} - i\pi\delta(\omega - \Delta E_{mn}/\hbar) \right].
\end{aligned}
\tag{14A.2}
$$

Then eq. (6.111) is obtained. Here in the last part we have used

$$
\lim_{\eta \to +0} \frac{1}{x \pm i\eta} = \frac{1}{x} \mp i\pi\delta(x). \tag{14A.3}
$$

This equation can be shown from an expression of δ-function as a limit of function:

$$
\lim_{\eta \to +0} \frac{1}{\pi} \frac{\eta}{x^2 - \eta^2} = \delta(x).
$$

References

[1] Tôru Moriya and Arisato Kawabata. Effect of spin fluctuations on itinerant electron ferromagnetism. *Journal of the Physical Society of Japan*, Vol. 34, No. 3, pp. 639–651, March 1973.

[2] 川畑有郷. 電子相関 (パリティ物理学コース クローズアップ). 丸善, 3 1992.

[3] 上田和夫. 磁性入門 (物性科学入門シリーズ). 裳華房, 9 2011.

[4] Toru Moriya. *Spin Fluctuations in Itinerant Electron Magnetism (Springer Series in Solid-State Sciences, 56)*. Springer, 10 2012.

[5] 高橋慶紀, 吉村一良. 遍歴磁性とスピンゆらぎ. 内田老鶴圃, 単行本, 4 2012.

[6] Yoshinori Takahashi. *Spin Fluctuation Theory of Itinerant Electron Magnetism (Springer Tracts in Modern Physics)*. Springer, 5 2015.

[7] Takeo Izuyama and Ryogo Kubo. Some considerations on the magnetic carriers in ferromagnetic transition metals. *Journal of Applied Physics*, Vol. 35, No. 3, pp. 1074–1081, 1964.

[8] R. Doubble, S. M. Hayden, Pengcheng Dai, H. A. Mook, J. R. Thompson, and C. D. Frost. Direct observation of paramagnons in palladium. *Phys. Rev. Lett.*, Vol. 105, p. 027207, Jul 2010.

[9] A. S. Borovik-Romanov, Y. M. Bunkov, V. V. Dmitriev, and Y. M. Mukharskiy. *JETP Lett.*, Vol. 40, p. 1033, 1984.

[10] G. E. Volovik. Twenty years of magnon bose condensation and spin current superfluidity in 3he-b. *Journal of Low Temperature Physics*, Vol. 153, No. 5-6, pp. 266–284, October 2008.

[11] Jagat Lamsal and Wouter Montfrooij. Extracting paramagnon excitations from resonant inelastic x-ray scattering experiments. *Phys. Rev. B*, Vol. 93, p. 214513, Jun 2016.

[12] M. C. Rahn, K. Kummer, N. B. Brookes, A. A. Haghighirad, K. Gilmore, and A. T. Boothroyd. Paramagnon dispersion in β-fese observed by fe l-edge resonant inelastic x-ray scattering. *Phys. Rev. B*, Vol. 99, p. 014505, Jan 2019.

[13] Kenji Makoshi and Tôru Moriya. Effect of spin fluctuations on the specific heat of weakly and nearly ferromagnetic metals. *Journal of the Physical Society of Japan*, Vol. 38, No. 1, pp. 10–20, 1975.

[14] Jun Takeuchi and Yoshika Masuda. Low temperature specific heat of itinerant electron ferromagnet sc3in. *Journal of the Physical Society of Japan*, Vol. 46, No. 2, pp. 468–474, 1979.